



TECHNISCHE
UNIVERSITÄT
WIEN

Dissertation

Advances in Bioprocess Monitoring by Mid-Infrared Spectroscopy

ausgeführt zum Zwecke der Erlangung des akademischen Grades einer
Doktorin der technischen Wissenschaften unter der Leitung von

Prof. DI Dr. Bernhard Lendl

E164

Institut für Chemische Technologien und Analytik

eingereicht an der Technischen Universität Wien

Fakultät für Technische Chemie

von

Cosima Koch

Matrikelnummer 0025132

Mostgasse 14/6

1040 Wien

Wien, am

“I love deadlines. I love the whooshing noise they make as they go by.”

-Douglas Adams

KURZFASSUNG

Im Rahmen dieser Dissertation wurde ein neues Messverfahren zur selektiven Aufnahme von Spektren von biologischen Zellen in Suspension im mittleren Infrarot (MIR) entwickelt. MIR Messungen mittels abgeschwächter Totalreflexion (ATR) wurden dazu mit Ultraschall-Partikel-Manipulation kombiniert. Ein Ultraschall-Aufsatz wurde entworfen, ein Prototyp gefertigt und mit einer speziell angefertigten ATR Sonde kombiniert. Mit dieser ultraschall-gestützten ATR Sonde konnten Spektren von *Saccharomyces cerevisiae* in Suspension erfolgreich off-line aufgenommen werden. Mit den gewonnen Erkenntnissen wurde ein weiterer Prototyp entworfen und gefertigt, der zum Einsatz in situ in einem Bioreaktor geeignet war. Dieser wurde mit einem kommerziellen Prozessspektrometer kombiniert welches mit einer faser-optischen in-line ATR Sonde ausgestattet war. Mit diesem Aufbau konnten, nach bestem Wissen der Autorin, zum ersten Mal Spektren von Zellen in einem gerührten, begasten Bioreaktor aufgenommen werden.

Die Änderung der Polysaccharidzusammensetzung von *S. cerevisiae* konnte off-line quantifiziert werden. Durch eine gezielt herbeigeführte Stickstoff-Limitation akkumulierten die Zellen Trehalose und Glykogen. MIR Spektren von gewaschenen, getrockneten Zell-Proben wurden mit einem Infrarotmikroskop aufgenommen, diese konnten mittels Partial Least Squares Regression (PLS-R) auf Referenzwerte aus nasschemischen Verfahren und High Pressure Liquid Chromatography kalibriert werden (root-mean-square Kreuzvalidierungsfehler: 0.33 % Trockengewicht (%DW) für Trehalose, 0.55 %DW für Glykogen und 1.17 %DW für Mannan). Mit der neu-entwickelten ultraschall-gestützten faser-optischen ATR Sonde und Hauptkomponentenanalyse konnten ähnliche Änderungen in den Spektren der Zellen in der Fermentationsbrühe in-line verfolgt werden. Durch die simultane Änderung der Biomassekonzentration und des Polysaccharidgehalts der Zellen war eine quantitative Bestimmung der Analyten aus in-line Spektren nicht möglich.

Darüber hinaus wurde die Eignung von Stand-der-Technik-MIR-Instrumentierung für die in-line Quantifizierung von im Medium gelösten Stoffen untersucht. Am Beispiel von *Penicillium chrysogenum* Fermentationen wurden PLS-R und multivariate curve resolution – alternating least squares (MCR-ALS) für die quantitative Bestimmung von Phenoxyessigsäure und Penicillin V verwendet. Die beiden Methoden ergaben vergleichbare Kalibrationsmodelle mit Detektionsschwellen im niedrigen g L⁻¹ Bereich. Für

MCR-ALS Modelle benötigt man mehr Wissen über den Prozess als für PLS-R, die Selektivität der MCR-ALS Modelle kann jedoch durch den Vergleich der errechneten “pure component” Spektren mit gemessenen Referenzspektren leichter überprüft werden. Im gleichen biologischen System wurden eine faser-optische und eine Sonde mit einem optischen Conduit simultan verwendet um Spektren in-line aufzunehmen. Die PLS-R Modelle für die beiden oben erwähnten Analyten waren von vergleichbarer Qualität, die Conduit-Sonde wies jedoch eine höhere Stabilität (Spektrum-zu-Spektrum-Änderungen) und ein besseres Signal-Rausch-Verhältnis auf.

ABSTRACT

In this thesis two techniques, attenuated total reflection (ATR) mid-infrared (mid-IR) spectroscopy and ultrasonic particle manipulation, were successfully combined for the acquisition of mid-IR spectra of cells in suspension. A prototype ultrasound accessory was designed, realized and combined with a custom fiber optic ATR probe. The working principle was successfully tested off-line with suspensions of *Saccharomyces cerevisiae*. A second prototype fit for use in a semi-industrial bioprocess environment was designed and built. It comprised the optimized ultrasound accessory and a commercial process spectrometer equipped with an in-line fiber optic ATR probe. Using this instrumental development, to the best of the author's knowledge, mid-IR spectra of cells inside a stirred, aerated bioreactor could be successfully recorded for the first time.

Changes of the carbohydrate content of *S. cerevisiae* undergoing nitrogen-limited growth, i.e. the accumulation of trehalose and glycogen, could be followed quantitatively off-line. Mid-IR spectra of washed, dried cells were recorded and analyzed by partial least squares regression (PLS-R) with reference values obtained by wet chemistry and liquid chromatography (root-mean-square error of cross validation: 0.33 % dry weight (%DW) for trehalose, 0.55 %DW for glycogen, and 1.17 %DW for mannan). Similar spectral changes could also be observed in-line using the novel ultrasound enhanced fiber optic ATR probe and principal components analysis of spectra of cells present in the fermentation broth. Quantification of the analytes proved to be difficult because changes in biomass and in the carbohydrate content occurred simultaneously, and this correlation could not be broken.

Complimentary, the applicability of state-of-the-art mid-IR technology for quantitative analysis of solutes in-line was explored. On the example of *Penicillium chrysogenum* fermentations, PLS-R and multivariate curve resolution-alternating least squares (MCR-ALS) were applied for the simultaneous determination of penicillin V and phenoxyacetic acid. The obtained results show that models are of comparable quality with LODs in the low gL⁻¹ range. MCR-ALS requires more process knowledge than PLS-R, but provides an objective assessment for model validity by comparison of the calculated pure component with the respective reference spectra. Using the same biological system, a fiber optic and a conduit ATR probe were simultaneously applied in-line. No significant difference in performance for quantification of the two analytes by PLS-R could be found. However, higher spectrum-to-spectrum stability and better signal-to-noise were found for the optical conduit set-up.

ACKNOWLEDGEMENTS

I want take the opportunity to express my gratitude to all the people who have in so many different ways supported me along the way to completion of this PhD thesis:

First and foremost I want to thank my supervisor, Bernhard Lendl, for giving me the opportunity (and the funding) to do research in this exiting field. You have always been supportive, open for discussion and very generous with opportunities to attend and present at international conferences. I greatly appreciate your tips and suggestions on how to tell a good story in presentations and publications and the extension of our discussions to more philosophical levels. Stefan Radel, whose enthusiasm for ultrasonic manipulation of cells lured me into this field a long time ago. You have sparked my curiosity during my Master's thesis under your supervision and have become a close friend over the years. Your continuing support, interest and belief in the project (and in my abilities) have made our collaboration productive, fun and easy-going. To many more discussions over coffee at George's! This thesis would not have been possible without our collaboration partner Christoph Herwig. Thank you for sharing your knowledge on bioprocess engineering, development, and analysis, for providing lab space, equipment, and, most importantly, knowledgeable colleagues for planning and performing the fermentations (thank you Betti Lorantfy, Andreas Posch, and Patrick Wechselberger!), and for continuously supporting the development of the ultrasound enhanced in-line ATR probe.

Thanks go out to all current and former members of the CAVS workgroup who have made the university a second home to me: Alison Hobro, Andreas Genner, Andreas Schwaighofer, Anna Balbekova, Bernhard Zachhuber, Christian Kristament, Christoph Gasser, Christoph Reidl-Leuthner, Christoph Wagner, Engelene Chrysostom, Eric Gonzalez Garcia, Eva Aguilera, Georg Ramer, Harald Moser, Ionela Stancu, Johannes Ofner, Julia Kuligowski, Karin Wieland, Marek Helmann, Markus Brandstetter, Marwa el-Zahry, Nani Caballero, Paul Wacławek, Quela Alcaraz, Reyes Plata Torres, Stefan Tauber and Volker Bauer. Special props go out to: Markus, my long-term office mate and work husband, thank you for always being there to help, listen, and discuss both work and private matters. I will never forget the incredible productiveness that always followed our decisions to have a coffee break. Engelene, thank you for sharing your knowledge and experience with me, both scientific and concerning life in general; I greatly admire your humbleness and determination and I am glad to count you as a friend. Reyes, without you I would never have been able to master

the extensive reference analyses - thank you for sharing your expertise on HPLC and all the wet chemical methods with me. My first contact with FT-IR microspectroscopy of cells and chemometrics goes back to my first days here: Julia, I really appreciate your patience when first explaining it all to me – I couldn't have wished for a better start – and thank you for the friendship that has since developed Christoph, thank you for being a friend - and the unforgettable trips to Graz and Bozen. Allie, thank you sharing your knowledge on Raman spectroscopy with me, for explaining the LabRAM - the piggy bank and the ferris wheel – and your friendship. Work isn't everything, from time to time you have to relax and party. Thanks to the party posse - Christoph "Guessy" Gasser, George "Jorge" Ramer, Harald "Harry - Was-soll-sein" Moser, Markus "Brandy" Brandstetter, Paul "Pauli" Waclawek, Stefan "little Guessy" Tauber – this part of life wasn't neglected. Quela, thank you for our fun "work outings". Andreas, my "new" office and lunch break mate, thank you for the chocolate croissants (and ICAVS in general) and the concerts (whether we went together or not). And special thanks go out to the circle of trust for always talking honestly about everything.

All the project, Bachelor and Master students who I have had the opportunity and honor to supervise and whose support of this thesis and other projects is greatly appreciated: Bernhard Seyer, Clemens Ditterstorfer, Felix Horak, Gerhard Fritsch, Geza Horvath, Karin Wieland, Lukas Strobl – twice, Max Dirnbacher, Pietro Palmesi.

Furthermore, I want to thank the whole third floor, especially Magda Kistler, for being a great office mate, and Hans Lohninger, for taking a lot of time to explain and discuss chemometrics. Hans, I really appreciate your professional and personal advice and enjoyed our "Kaffeehaus-conversations" about holidays, life and all the rest.

Andreas Limbeck, thank you for the collaboration on ultrasonic filtering of nanoparticles for ICP-OES. Héctor Goicoechea, thank you for the introduction to MCR-ALS and the fruitful collaboration. Johannes Frank, thank you for sharing your knowledge and experience in engineering and construction. Wolfgang Tomischko, thank you for helpful advice on soldering and electronics.

My friends outside the university universe: for putting up with my complaints when something was not working, helping me take my mind off it and being there; especially die Mädels, fabs, Konny und Moni, and mi chica Almu.

Last but not least I want to thank my parents, Sissi and Meinhard, for always believing in me, supporting me, and being there for me from near and far.

Content

KURZFASSUNG	I
ABSTRACT	III
ACKNOWLEDGEMENTS	V
TABLE OF CONTENTS	VII
ABBREVIATIONS	XI
1 INTRODUCTION	1
1.1 AIM AND SCOPE OF THIS THESIS	1
1.2 PROCESS ANALYTICAL TECHNOLOGY – PAT	2
1.3 MID-INFRARED SPECTROSCOPY	6
1.3.1 INFRARED SPECTROSCOPIC MEASUREMENT PRINCIPLES FOR CONDENSED PHASE SAMPLES	9
1.3.2 IN-LINE ATR PROBES – CONDUIT VS. FIBER OPTIC COUPLING	15
1.4 MULTIVARIATE DATA ANALYSIS	16
1.4.1 PRINCIPAL COMPONENT ANALYSIS (PCA)	17
1.4.2 PARTIAL LEAST SQUARES REGRESSION (PLS-R)	19
1.4.3 MULTIVARIATE CURVE RESOLUTION – ALTERNATING LEAST SQUARES (MCR-ALS)	21
1.5 ACOUSTIC PARTICLE MANIPULATION - ACOUSTOPHORESIS	23
1.5.1 POTENTIAL BIOEFFECTS OF ULTRASOUND	26
1.6 MICROORGANISMS STUDIED	29
1.6.1 <i>SACCHAROMYCES CEREVISIAE</i>	29
1.6.1.1 Storage carbohydrates	30
1.6.2 <i>PENICILLIUM CHRYSOGENUM</i>	30
2 STATE OF THE ART	33
2.1 MID-IR SPECTROSCOPY FOR BIOPROCESS MONITORING	33
2.2 MID-IR SPECTROSCOPY OF MICROORGANISMS	40
2.3 ACOUSTIC PARTICLE MANIPULATION OF CELLS	44

3	ULTRASOUND ENHANCED IN-LINE ATR PROBE	47
3.1	ACOUSTIC PARTICLE MANIPULATION AND ATR SPECTROSCOPY.....	47
3.2	DESIGN REQUIREMENTS	48
3.2.1	RESONATOR CONSTRUCTION.....	49
3.2.2	ATR PROBE	50
3.2.3	BIOPROCESSING EQUIPMENT REQUIREMENTS	50
3.3	PROTOTYPE 1	51
3.4	PROTOTYPE 2	54
4	PERFORMANCE	59
4.1	BRUKER HYPERION 3000 COUPLED TO TENSOR 37.....	60
4.2	BRUKER TENSOR 37 EQUIPPED WITH PLATINUM ATR.....	60
4.3	PROTOTYPE 1: BRUKER MATRIX & PROTOTYPE ATR PROBE	61
4.4	PROTOTYPE 2: METTLER TOLEDO REACTIR 15 & FIBER OPTIC DS DiCOMP PROBE.....	63
4.5	METTLER TOLEDO REACTIR 45 & OPTICAL CONDUIT K4 PROBE.....	64
5	INTRODUCTION TO PUBLICATIONS	67
	PUBLICATION I	67
	PUBLICATION II.....	68
	PUBLICATION III	70
	PUBLICATION IV	71
	PUBLICATION V	72
6	CONCLUSIONS AND OUTLOOK	73
7	BIBLIOGRAPHY	77
8	SCIENTIFIC PUBLICATIONS	87
	PUBLICATION I	87
	PUBLICATION II.....	97
	PUBLICATION III	109
	PUBLICATION IV	119

Table of Contents	ix
PUBLICATION V	129
9 APPENDIX	147
APPENDIX A.....	147
APPENDIX B.....	163
APPENDIX C	173
APPENDIX D.....	177

ABBREVIATIONS

AgX	Silver Halogenide
ANN	Artificial Neural Networks
ASME	American Society of Mechanical Engineers
ATR	Attenuated Total Reflection
BPE	Bioprocessing Equipment
CaF ₂	Calcium Fluoride
<i>C. beijerinckii</i>	<i>Clostridium beijerinckii</i>
CLS	Classical Least Squares
CVA	Canonical Variance Analysis
DTGS	Deuterated Tri Glycine Sulfate
DW	Dry Weight
<i>E. coli</i>	<i>Escherichia coli</i>
EFA	Evolving Factor Analysis
EMA	European Medicines Agency
FDA	Food and Drug Administration
FT-IR	Fourier-transform infrared
Ge	Germanium
<i>G. xylinus</i>	<i>Gluconacetobacter xylinus</i>
HCA	Hierarchical Cluster Analysis
HPLC	High Pressure Liquid Chromatography
HTS-XT	High-Throughput Screening extension
I/O	Input/Output
KBr	Potassium Bromide

<i>L. bulgaricus</i>	<i>Lactobacillus bulgaricus</i>
MCR-ALS	Multivariate Curve Resolution – Alternating Least Squares
MCT	Mercury Cadmium Telluride
mid-IR	mid-Infrared
MLR	Multiple Linear Regression
NA	Numerical Aperture
NIR	Near-Infrared
OD ₆₀₀	Optical Density at 600 nm
PAT	Process Analytical Technology
<i>P. chrysogenum</i>	<i>Penicillium chrysogenum</i>
PCA	Principal Component Analysis
PCI	Peripheral Component Interconnect
PCR	Principal Component Regression
PLS-R	Partial Least Squares – Regression
PLS-DA	Partial Least Squares-Discriminant Analysis
<i>P. pastoris</i>	<i>Pichia pastoris</i>
<i>P. aeruginosa</i>	<i>Pseudomonas aeruginosa</i>
PTFE	Polytetrafluoroethylene (Teflon)
PZT	Lead Zirconate Titante
QCL	Quantum Cascade Laser
RBCs	Red Blood Cells
RI	Refractive Index
RMSE	Root Mean Square Error
RMSECV	Root Mean Square Error of Cross-Validation
RMSEP	Root Mean Square Error of Prediction
<i>S. cerevisiae</i>	<i>Saccharomyces cerevisiae</i>
SIA	Sequential Injection Analysis
SIMCA	Soft Independent Modelling by Class Analogy
SIMPLISIMA	Simple to Use Interactive Self-Modeling Mixture Analysis

S. epidermidis *Staphylococcus epidermidis*

S. clavuligerus *Streptomyces clavuligerus*

UV Ultraviolet

Vis Visible

ZnSe Zinc Selenide

1 INTRODUCTION

1.1 Aim and scope of this thesis

The aim of this thesis was to explore and expand the potential of mid-infrared (mid-IR) spectroscopy for bioprocess monitoring. This included two major aspects: development and realization of an experimental strategy capable of measuring mid-IR spectra of cells in real time in-line and assessment of state-of-the-art technology for quantitative in-line analysis of solutes.

- **Combination of ultrasonic particle manipulation with mid-IR fiber optic probe (ultrasound enhanced ATR probe).** The combination of acoustic particle manipulation, a gentle, non-contact particle manipulation technique, and ATR (attenuated total reflection) spectroscopy was realized and investigated for its applicability to record mid-IR spectra of cells in suspension. A prototype ultrasound enhanced in-line ATR probe was successfully applied for selective acquisition of spectra of cells in a stirred suspension (**Publication I**).
- **Dedicated in-line ultrasound enhanced ATR probe.** Based on the expertise gained, a rugged in-line applicable ultrasound enhanced ATR probe was designed and realized. For this purpose, a small, robust, process spectrometer and fiber optic probe were combined with an in-house developed and optimized ultrasound accessory.
- **Investigation of quantification of cellular composition by mid-IR spectroscopy.** Mid-IR spectroscopy was investigated as a tool for identification of different cell constituents, on the example of different carbohydrates in *Saccharomyces cerevisiae* (trehalose, glycogen, mannan, glucose). For this purpose spectra of dried cells were recorded in transmission with a high-end laboratory mid-IR spectrometer for optimal signal-to-noise (**Publication II**).
- **Application of the ultrasound enhanced ATR probe for in-line cell monitoring.** Verification of the accessibility of the characteristic spectral changes in cell spectra

by the developed in-line measurement technology. Investigation of increased experimental difficulties due to measurement in water (high spectral background) and reduced signal-to-noise due to the demanding process environment (**Publication III**).

- **Assessment of state-of-the-art ATR probes & chemometrics:** The potential of in-line mid-IR spectroscopy for real-time quantification of precursor and product in monitoring was investigated using a fiber optic ATR probe and two chemometric methods, multivariate curve resolution – alternating least squares (MCR-ALS) and partial least squares – regression (PLS-R) for calibration (**Publication IV**). The performance of a fiber optic and an optical conduit ATR probe for bioprocess monitoring were compared (**Publication V**).

1.2 Process analytical technology – PAT

“Quality cannot be tested into products; quality should be built in by design”

- Food and Drug Administration (FDA), 2004¹

The following introduction to PAT (Process Analytical Technology) is based on the book chapter “Industrial Perspectives” by Kandelbauer et al. in “Part One: Process Control and Quality Assurance” of the Handbook of Biophotonics². They give a comprehensive introduction to the terminology and the motivation behind PAT, review the guidelines published by relevant regulatory authorities and describe PAT toolboxes for process understanding. They highlight the value of optical spectroscopy techniques as PAT tools, as they are applicable to a wide range of processes by choosing the respective appropriate wavelength regime and allow physical and chemical insight into the process.

The classic approach to quality control in (pharmaceutical) industrial manufacturing processes is to test randomly drawn samples of the final product for compliance with predefined quality criteria. The process itself is conducted according to a strict set of routine process parameters that have previously been approved by the authorities, e.g. the FDA or EMEA (European Medicines Agency). As most pharmaceutical and biotechnological products are produced in batch mode, a whole batch has to be discarded if compliance is not met. This is cost-intensive and inefficient, since the reason for the deviation in product quality cannot be identified by testing product quality only. Furthermore, innovation is

hindered by the current regulation that even minor changes to process parameters require re-approval of whole process.

In 2004 the FDA released its industrial guidance “PAT – A Framework for Innovative Pharmaceutical Development, Manufacturing and Quality Assurance”¹ as part of its PAT initiative. Here, PAT is defined as “... a system for *designing, analyzing, and controlling manufacturing* through *timely measurements* (i.e., during processing) of critical quality and performance attributes of raw and in-process materials and processes, with the goal of ensuring final product quality. It is important to note that the term *analytical* in PAT is viewed broadly to include *chemical, physical, microbiological, mathematical, and risk analysis* conducted in an integrated manner.” (Ref. 1, p. 4). The guidelines are aimed at encouraging industry to develop and use PAT tools for identification and monitoring of *critical process parameters* (i.e. parameters that have a strong influence on product quality). Through process analysis a greater understanding of the connection between the critical process parameters (the cause) and the quality parameters of the final product (the effect), i.e. causality, is sought. With this knowledge, the approval of rigid process parameters is no longer necessary; a wider parameter space can be defined. Within this parameter space, product quality can be assured by monitoring critical process parameters using suitable PAT tools. This is especially advantageous in processes where raw materials are subject to variation (e.g. lot-to-lot variability of natural products): knowing the connection between quality of the raw material(s) and the product, process parameters (e.g. the amount of raw material added, temperature, ...) can be selected that lead to the desired product quality.

In order to measure process parameters, a suitable mode of sampling from the process line/vessel has to be chosen. Measurements can be performed:

- **off-line:** A sample is withdrawn and analyzed using a laboratory analyzer (usually high selectivity and sensitivity, however limited robustnessⁱ) at a physical distance from the actual process environment. Therefore, results are only available after a delay and are of little to no use for process control. (They may still deliver valuable information for process analysis and process understanding.)

ⁱ Here robustness signifies the measurement's and the device's ability for tolerating perturbation induced by the potentially harsh process environment.

- **at-line:** A sample is withdrawn and analyzed in close proximity to the process line – the analyzers used have to be more rugged than laboratory analyzers (often at the cost of selectivity and sensitivity).
- **on-line:** A sample is automatically withdrawn from the process and transported to the analyzer. Analysis can be done in continuous mode or at tight time intervals. The measured sample is either fed back into the process (bypass system), or - if sample preparation, e.g. dilution, is necessary - discarded.
- **in-line** or **in situ:** A probe is introduced into the reactor vessel and brought in contact with the sample; measurements are performed inside the process vessel on the unaltered process liquid/gas/solid. The probe and the analyzer need to be robust regarding the process environment and cleaning-in-place (CIP) or steam-in-place (SIP)ⁱⁱ routines, especially when used for monitoring bioprocesses³.

The four different measurement types are illustrated in Figure 1. Since “timely measurements” are of major importance, in-line and on-line sampling are preferable to at-line and off-line sampling as PAT. Even though the FDA guidelines are aimed at pharmaceutical manufacturing, they can and should be applied to other chemical and biological processes, e.g. fermentations.

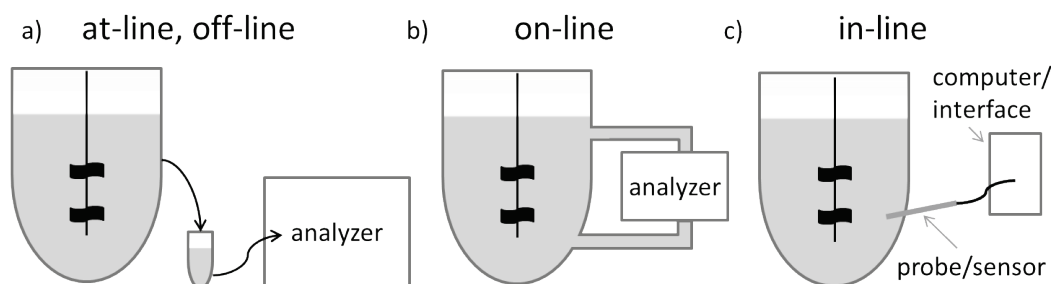


Figure 1: The different sampling strategies: Off-line (analyzer at a distance from the process in a laboratory environment) and at-line (analyzer in the process environment) (a), on-line (b), and in-line measurements (c).

The following paragraphs focus on the state-of-the-art of and the use of FT-IR (Fourier-transform infrared) spectroscopy as PAT for fermentation monitoring. A number of chemical and physical parameters are routinely monitored on- and in-line during

ⁱⁱ SIP is the process of sterilizing the process vessel/line usually achieved by subjecting it to high pressure saturated steam (commonly 121° to 130°C). Treatment with hot base or acid is often used for CIP.³

fermentations. These include pH, off-gas composition, pO_2 ⁱⁱⁱ, temperature, stirrer speed, volume, etc. Other chemical parameters, e.g. product concentration, substrate composition, and biological parameters like biomass, viability, and genetic and metabolic information, are typically measured at-line or off-line. One commonly employed at-line or on-line analysis method is UV/Vis (ultraviolet/visible) absorption spectroscopy (typically 200 – 700 nm), which is based on the measurement of electronic transitions in molecules. Standard applications are the determination of biomass by optical density measurements at 600 nm (OD_{600}), quantification of media components, e.g. glucose, ammonia, etc., by colorimetric analysis of enzymatic reactions, or determination of extracellular protein at 280 nm. Note that most of these analyses are not multivariate, i.e. only use a single wavelength of the spectrum. By observing chemical and biological parameters, conclusions about the state of the fermentation and thus the cells or microorganisms can be drawn. Obtaining such data often requires time-consuming sample preparation, furthermore, changes in the cellular environment caused by sampling can lead to changes in the biochemical composition due to fast metabolic responses. The interested reader is referred to Pohlscheidt et al.³ for a more detailed insight into routinely employed probes and sensors and the use of in-line and on-line acquired data for soft-sensors and first-principle models, e.g. by choosing appropriate constraints when building MCR-ALS models^{iv}.

The currently observed parameters and their use for process control are mainly based on experience and not on an understanding of the underlying principles. Hence, there is a need for the development of PAT tools aimed at obtaining biological and chemical information in real-time during fermentations. Optical spectroscopies are especially suitable as PAT tools for bioprocesses as they can give chemical and morphological information on the process. Depending on the wavelength range used, different properties can be investigated, often noninvasively and without the need for sample preparation. Vibrational spectroscopies, i.e. IR and Raman spectroscopy, give insight into the chemical composition of the sample under investigation by probing their vibrational energy levels. Different in-line probes are available and multivariate data analysis is commonly employed. Apart from the quantification of media components and desired products, these techniques cannot only

ⁱⁱⁱ Partial pressure of oxygen, also referred to as dissolved oxygen.

^{iv} A soft-sensor, abbreviation for software sensor, uses real-time data to estimate a parameter that cannot be measured directly. First-principle models use a priori knowledge about the process, i.e. fundamental laws like mass conservation and stoichiometric balances, to estimate performance parameters.

help to identify undesired by-products, but also to identify the reason for their production. In a second step this knowledge can be used to identify deviations from the planned process conditions before the by-product is produced by adjusting process parameters accordingly (feed forward instead of feed-back quality control).

This thesis focuses on FT-IR spectroscopy in the mid-IR range as a powerful PAT technology. Mid-IR spectroscopy gives molecular specific information on the sample under investigation, as each molecule leads to a specific, characteristic absorption pattern. It requires little to no sample preparation and allows for the fast, simultaneous, determination of several analytes given proper chemometric calibration methods. Mid-IR spectroscopy can be used for the determination of media components and extra-cellular products and analysis of the biochemical composition of the cells or microorganisms themselves (the state-of-the-art use of FT-IR spectroscopy for these purposes is given in chapters 2.1 and 2.2, pages 33 ff.). It is thus a method of great potential for bioprocess analysis that can be used in an at-line, on-line, and in-line mode.

1.3 Mid-Infrared Spectroscopy

The following brief introduction to vibrational spectroscopy, with a focus on mid-IR spectroscopy, is guided by the comprehensive introduction given by Peter R. Griffiths in the Handbook of Vibrational Spectroscopy⁴.

Vibrational spectroscopy is based on measuring the vibrational and rotational energy levels of molecules. The number of different ways that a molecule can vibrate (e.g. bending, stretching, scissoring of atoms), i.e. the number of vibrational modes, depends on the structure of the molecule and the number of atoms, N , in it. A linear molecule, e.g. CO_2 , has $3N-5$ degrees of vibrational freedom (or modes), while a non-linear molecule has $3N-6$ degrees of vibrational freedom^v. The vibrational energy levels range from relatively simple bands for two-atom molecules to complicated patterns for larger molecules.

The displacement of the atoms can be approximated as a harmonic oscillator: the atoms vibrate at a characteristic frequency ν_i at each mode i . The possible energy levels E_n of a single mode of a quantum-mechanical harmonic oscillator are described by Equation (1).

^v Every molecule has $3N$ degrees of freedom, here, the three (two for a linear molecule) degrees of freedom for translation along the x-, y-, and z-axis and for rotations around these axis are subtracted.

$$E_n = h\nu \left(n + \frac{1}{2} \right) \quad (1)$$

Here h is Planck's constant^{vi} and n is the vibrational quantum number (first-order approximation). This harmonic approximation is valid for lower vibrational quantum numbers and transitions are restricted to $\Delta n = \pm 1$; when higher states (i.e. energy levels) are reached and the displacement of the atoms becomes larger, an anharmonic potential like the Morse-potential describes the energy levels more accurately (second order approximation; Equation (2)).

$$E_n = h\nu \left(n + \frac{1}{2} \right) + h\nu\chi \left(n + \frac{1}{2} \right)^2 \quad (2)$$

Here, χ represents the anharmonicity constant. In the anharmonic case, transitions with $\Delta n = \pm 1, \pm 2, \pm 3, \dots$ are allowed, giving rise overtone bands and combination transitions.

A transition between two vibrational states can be induced by absorption of electromagnetic radiation, if the energy difference between these two states corresponds to the energy E of the incident radiation. The energy of an electromagnetic wave is dependent on its frequency ν multiplied by Planck's constant h (Equation (3)).

$$E = h\nu \quad (3)$$

The frequency ν is given in units of Hertz (Hz, s⁻¹); vibrational energies are usually given in wavenumbers $\tilde{\nu}$. Wavenumbers are wavelengths λ per unit length. In vibrational spectroscopy centimeters are usually the unit length, thus the units are given in cm⁻¹. Equation 3 can be rewritten as:

$$E = h \frac{c}{\lambda} = hc\tilde{\nu} \quad (4)$$

The energy difference of fundamental transitions, i.e. from ground state ($n = 0$) to the first excited state ($n = 1$), corresponds to electromagnetic radiation in the mid-IR range (4000 – 400 cm⁻¹ or 2.5 – 25 μm , i.e. 50 – 500 meV) for most vibrational modes. Overtone and combination bands correspond to energies in the near-infrared (NIR) spectrum (14000 – 4000 cm⁻¹ or 0.8 – 2.5 μm , i.e. 500 – 1500 meV) and are usually less intense than

^{vi} $h = 6.62607004 \times 10^{-34} \text{ J } (m^2 kg \text{ s}^{-1})$

fundamental transitions. Functional groups of molecules therefore have distinct, characteristic absorption bands in the mid-IR range, making identification of compounds and structure characterization of molecules possible.

For absorption of infrared light, the molecular vibration needs to lead to a change in dipole moment of the whole molecule; a permanent dipole is not a necessary prerequisite though. The second method vibrational spectroscopic method, Raman spectroscopy, also probes vibrational levels of molecular bonds, however, by inelastic scattering of higher-energy photons (from the UV to NIR). For Raman scattering, a change in the polarizability α of the molecule is necessary; a molecule's polarizability is a measure for the tendency of its electron cloud to distortion by external electrical fields. IR and Raman spectroscopy are complimentary, as under certain conditions, transitions that are forbidden in Raman scattering are allowed in IR absorption and vice versa. In practice, most transitions may be observed by both techniques, however, at different intensities.

Specific wavenumber regions in an IR absorption spectrum can be attributed to modes of specific functional groups in organic molecules (e.g. $-\text{OH}$, $-\text{CH}_2$, $\text{C}=\text{O}$, ...). These modes stem from large displacements of only a few atoms, while the rest of the molecule is basically not involved in the vibration. Other modes involve movement of several atoms in the molecule and lead to absorption bands characteristic of the molecule itself. These bands are usually located between 1600 and 500 cm^{-1} (this range is therefore often referred to as the fingerprint region) and allow for differentiation between molecules that contain similar functional groups. For biological cells, as investigated in this thesis, the most interesting wavenumber region lies between approximately 1900 and 800 cm^{-1} (sometimes referred to as the bio-fingerprint region, see also chapter 2.2 Mid-IR spectroscopy of microorganisms, pages 40 ff.).

As a type of absorption spectroscopy, IR spectra can be evaluated quantitatively as the absorption follows Beer's law (sometimes also Beer-Lambert law). Beer's law relates the absorbance A of a sample consisting of only one molecular species with the molar decadic absorption coefficient ε ($\text{m}^2\text{ mol}^{-1}$), the concentration c (mol m^{-3}) and the length d (m) of light interaction with the sample (Equation (5)). Experimentally, the absorbance is determined by measuring the intensity of light $I_0(\tilde{\nu})$ that reaches the detector without the

sample in place, i.e. the background or reference channel^{vii}, and the intensity of light $I(\tilde{\nu})$ that reaches the detector when the sample is in place, i.e. the sample (channel); these intensity spectra are also referred to as single beam spectra. For low concentrations and assuming no interaction between molecular species Beer's law is additive; for a mixture of n molecules, it can be calculated as the sum of the respective absorbance of each molecular species (Equation (6)).

$$A(\tilde{\nu}) = \varepsilon(\tilde{\nu}) \cdot c \cdot d = -\log \frac{I(\tilde{\nu})}{I_0(\tilde{\nu})} \quad (5)$$

$$A_n(\tilde{\nu}) = \sum_{i=1}^n \varepsilon_i(\tilde{\nu}) \cdot c_i \cdot d \quad (6)$$

For small molecules in the gas phase at low densities IR absorption bands consist of many narrow lines. They stem from a large number of transitions between the rotational-vibrational energy levels. In the condensed phase, these bands are broadened due to intermolecular interactions. For liquid samples it is therefore sufficient to record spectra with a resolution of 4 or 8 cm⁻¹. On the other hand due to the broadening of the bands it is harder to differentiate between different molecules in mixture, as these bands tend to overlap. For these data, univariate analysis of spectra, i.e. using absorption values at a single wavenumber, is usually not sufficient. Multivariate approaches like principal component analysis (PCA), which can be used to identify spectral regions with the greatest variation within a set of spectra, or partial least squares regression (PLS-R), which allows for quantification of analytes of interest, have to be employed. An introduction to the chemometric methods used in the course of this thesis can be found in Chapter 1.4 (page 16 ff.).

1.3.1 Infrared spectroscopic measurement principles for condensed phase samples

Mid-IR spectra of condensed phase samples can be acquired in transmission, transflexion (double transmission), or reflection mode, respectively, or by attenuated total reflection (ATR) spectroscopy. The following paragraphs concentrate on transmission and ATR measurements (Figure 2), as these were the major focus of this thesis. A short overview of

^{vii} The reference channel (reference single beam spectrum) takes into account the transmission characteristics of the spectrometer (or measurement set-up) itself.

the respective measurement principle is given and typical realizations of experimental set-ups are presented.

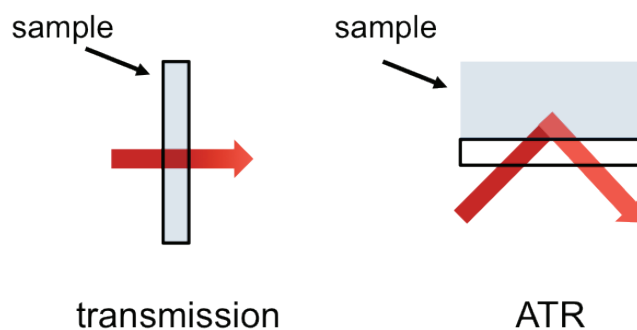


Figure 2: The two main measurement principles used for mid-IR spectroscopy of condensed phase samples.

In transmission mode, the intensity of the light after it has interacted with the sample is compared to the intensity of the incident beam (Figure 2, left). Solid (powdered) samples can be ground up and mixed with potassium bromide (KBr), a material that has no absorption lines within the mid-IR range; this mix is subsequently pressed into a disk shape and measured in transmission. For liquid samples, e.g. analytes of interest in solution, flow-through cells comprising of two slides with low IR absorption, e.g. calcium fluoride (CaF_2) or zinc selenide (ZnSe)^{viii}, held at a fixed distance using a spacer (usually Teflon) (Figure 3) are used. To take the reflection and absorption of the windows into account, the intensity of the IR-beam passing through the cell filled with the pure solvent is used as background $I_0(\tilde{\nu})$. When dealing with aqueous samples, the high absorption cross-section of water has to be taken into account. Comparison of normalized single beam spectra^{ix} of air and of H_2O in a $12\ \mu\text{m}$ thick flow through cell (Figure 4) shows that this (short) interaction path length is enough for total absorption around $1645\ \text{cm}^{-1}$ (O-H-O bending vibration) and between 3000 and $3600\ \text{cm}^{-1}$ (symmetric and asymmetric O-H stretch). The two minima around $2350\ \text{cm}^{-1}$ visible in the single beam spectrum of water are due to the ambient CO_2 and the numerous small, fine bands between approximately 1350 and $2000\ \text{cm}^{-1}$ in the single beam spectrum of air are caused by the vibrational rotational energy levels of water vapor, i.e. the

^{viii} KBr is freely soluble in water and therefore generally unsuitable for measurement of liquids.

^{ix} Due to the low IR absorption of air, the aperture of the spectrometer had to be closed to $2\ \text{mm}$ so as to not saturate the MCT detector, while it needs to be completely open ($6\ \text{mm}$) for transmission through the $12\ \mu\text{m}$ flow cell filled with water. Therefore, the absolute intensity values are not comparable, but a qualitative assessment of the transmission characteristics is possible.

ambient humidity. The decrease in intensity below 1000 cm^{-1} is due to absorption of the CaF_2 windows. When dealing with biological samples, clogging and fouling of such short path length-flow-through cells can become a problem (proteins tend to stick to the windows).

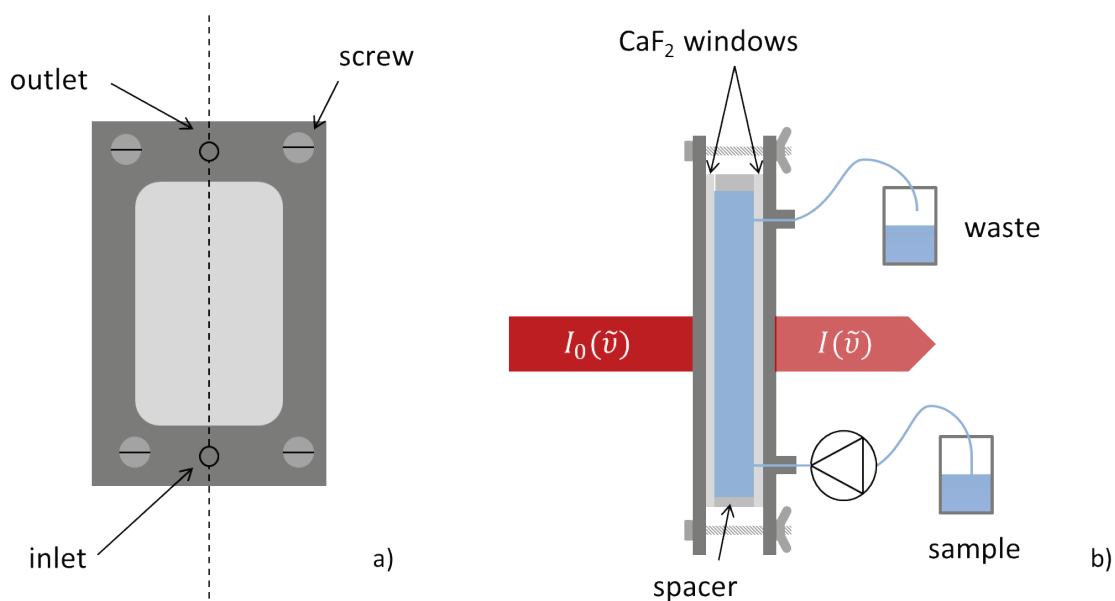


Figure 3: Flow-through cells as used for IR spectroscopy of liquid samples: Top view (a) and cross section (b). The flow-through cell can either be filled using a syringe or sample delivery can be automated with a pump (e.g. peristaltic pump).

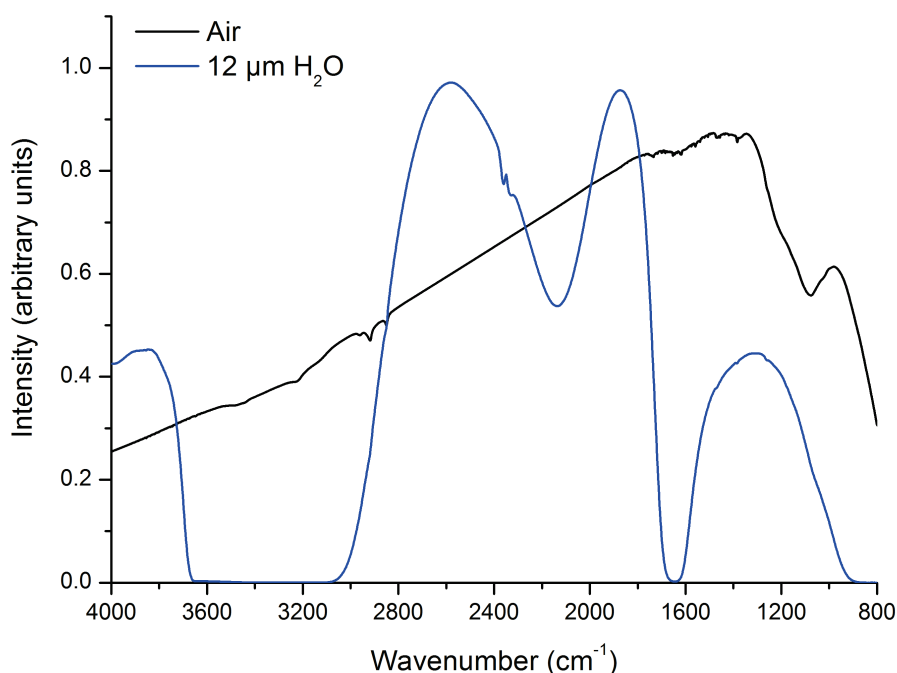


Figure 4: Single beam spectra (i.e. $I(\tilde{\nu})$) of the empty sample compartment (i.e. air, black line) recorded with an aperture of 2 mm and of a 12 μm flow cell filled with H_2O (blue line) recorded with an aperture of 6 mm.

An alternative approach is drop-drying, i.e. placing a drop of defined volume (micropipette) onto an IR-transparent slide and letting the aqueous phase evaporate. The solid residue can then be measured in transmission with a focused IR-beam (Figure 5); typically an IR microscope is used. The advantages of this approach are extended spectral coverage and in general improved signal-to-noise. This method is the standard approach for the acquisition of mid-IR spectra of cells. For high-throughput analysis and increased reliability using this method, Bruker Optics offers a dedicated accessory for their spectrometers: the HTS-XT (high-throughput screening extension). Here, the samples are deposited into 96- or 384-well micro(titer)plates with IR transparent bottoms and, after a drying step, they are automatically measured. These techniques, however, are limited to at-line and off-line measurements, flow cells furthermore allow for on-line measurements. In-line measurements are not possible using either method.

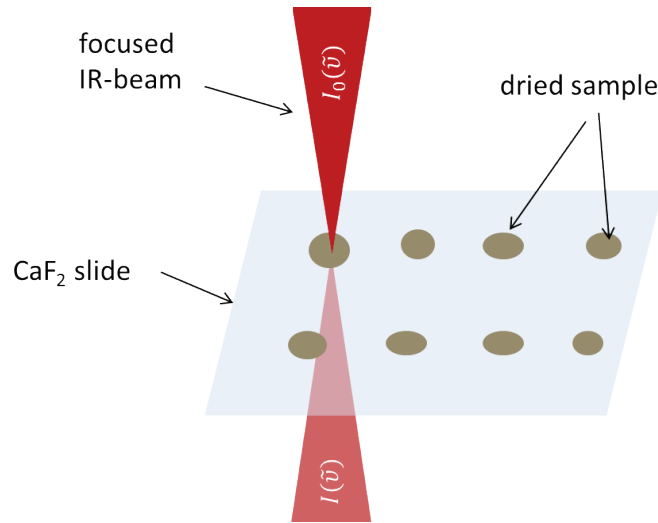


Figure 5: Schematic of transmission measurements of dried liquid samples.

The method of choice for aqueous samples is ATR spectroscopy⁵. ATR spectroscopy is based on the fact that for incident angles ϑ_i greater than a critical incidence angle ϑ_c , light is totally reflected at the interface between a medium with high refractive index n_1 and low refractive index n_2 (Figure 6a). The critical angle ϑ_c can be derived from Snell's law (Equation (7)^x) by setting the angle of the transmitted beam ϑ_t to 90° (thus $\sin \vartheta_t = 1$) and solving for ϑ_c (Equation (8)). The higher n_1 is compared to n_2 , the smaller ϑ_c becomes, and total reflection can be achieved over a wider range of incidence angles.

$$n_1 \sin \vartheta_i = n_2 \sin \vartheta_t \quad (7)$$

$$\vartheta_c = \sin^{-1} \frac{n_2}{n_1} \quad (8)$$

The z-component of the electric field E of the totally reflected wave penetrates into the medium with lower refractive index and is referred to the evanescent field of the wave. The evanescent field decays exponentially and typically penetrates into the medium of lower refractive index in the order of magnitude of a wavelength. For practical purposes the penetration depth d_p of the exponentially decaying wave is defined as the length (i.e. depth) after which its initial amplitude E_0 has decayed to E_0/e ,^{xi} i.e. to approximately 36% of its

^x Note that the refractive indices, and thus ϑ_c , is dependent on the wavelength λ of the light (according to the dispersion relation of the respective material).

^{xi} Theoretically, an exponentially decaying wave does not become zero until infinity. Practically, only contributions from interactions with analytes close to the interface have a significant impact on the absorption pattern.

initial value (Figure 6b). d_p is directly proportional to the wavelength λ of the incident light and depends on the refractive indices of the ATR element and the sample, n_1 and n_2 , respectively, and the angle of incidence ϑ_i :

$$d_p = \frac{\lambda}{2\pi n_1 \sqrt{\sin^2 \vartheta_i - \left(\frac{n_2}{n_1}\right)^2}} \quad (9)$$

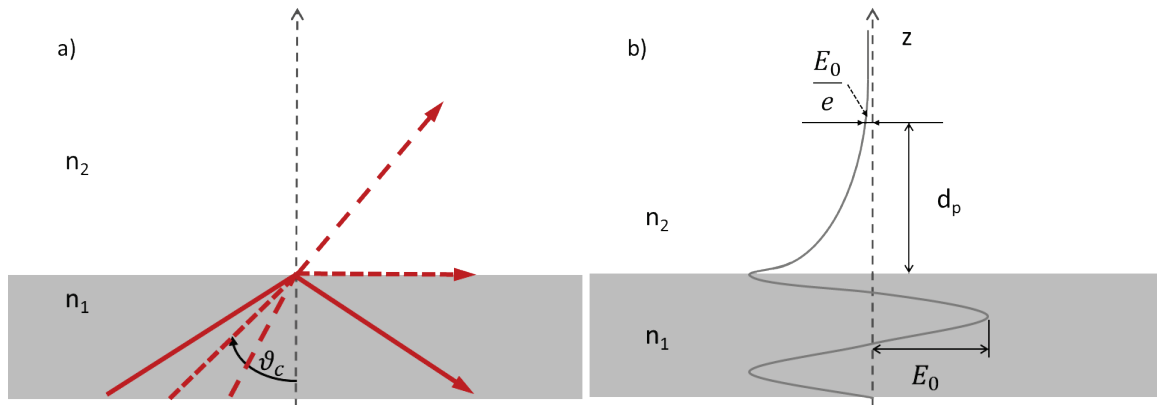


Figure 6: a) Light is refracted at the interface of a medium with a higher refractive index n_1 and a medium with a lower refractive index n_2 (dashed line, Snell's law). When a critical angle ϑ_c is exceeded, the incident light is totally reflected at the interface (solid line). b) The penetration depth d_p of the evanescent wave, the z -component of the electric field of the totally reflected wave.

Typical materials used as ATR element for mid-IR spectroscopy are germanium (Ge), ZnSe and diamond⁶; in this work, diamond ATR elements were used because of their chemical and mechanical robustness. For total reflection at the interface of diamond ($n_1 = 2.41$) and water ($n_2 = 1.34$) the angle of incidence has to be larger than 35° at 1000 cm^{-1} . For a typical incidence angle $\vartheta_i = 45^\circ$, the penetration depth d_p of the evanescent field into the water ranges between $3.77 \text{ }\mu\text{m}$ for a wavelength λ of $25 \text{ }\mu\text{m}$ (i.e. $\tilde{\nu} = 400 \text{ cm}^{-1}$) and $0.377 \text{ }\mu\text{m}$ for $\lambda = 2.5 \text{ }\mu\text{m}$ (i.e. $\tilde{\nu} = 4000 \text{ cm}^{-1}$)^{xii}.

Multiple internal reflections are used to enhance the interaction of the sample with the IR beam lowering the concentration required to obtain an absorption signal (see Beer's law, page 9). The cumulative path length thus obtained is usually determined empirically by

^{xii} Note that is d_p directly proportional to the wavelength λ of the incident light but inversely proportional to its wavenumber $\tilde{\nu}$: it rapidly declines from $3.77 \text{ }\mu\text{m}$ at 400 cm^{-1} to $1.51 \text{ }\mu\text{m}$ at 1000 cm^{-1} and then decreases more slowly as the wavenumbers increase ($0.99 \text{ }\mu\text{m}$ at 1500 cm^{-1} , $0.75 \text{ }\mu\text{m}$ at 2000 cm^{-1} ,...); the results lie on a rectangular hyperbola.

comparison of absorbance values with transmission measurements. To ensure sufficient interaction with the IR beam, pressure is usually applied to press solid samples against the ATR element's surface. In this case, diamond is the material of choice for the ATR element due to its high mechanical stability. The major advantage of ATR measurements for aqueous samples is that there are (almost) no restrictions as to how "thick" the sample can be, thus clogging is not an issue. Furthermore, the method allows for the construction of probes that can be submerged in liquids and used for in-line reaction monitoring etc. On the other hand, even thin depositions on the ATR surface can lead to serious interferences, as it is a surface-sensitive technique.

1.3.2 In-line ATR probes – conduit vs. fiber optic coupling

In-line probes are commercially available from various companies. They can be realized using optical conduits or optical fibers for transmitting the light between the spectrometer and the ATR probe head.

Optical conduit probes use light guides, or hollow conduits, which are based on external reflection of light on metallic or dielectric surfaces and are usually realized as hollow waveguides. Maximum transmittance is reached by using a material with high reflectivity, grazing light incidence (close to 90°), a highly collimated beam and the minimal number of reflections possible⁷. As the conduits are rigid and straight, probes are realized by connecting them by knuckles equipped with adjustable mirrors to make connection to the measurement vessel possible. The transmission characteristics of the conduit are highly dependent on its alignment; for measurements the probe is connected to the vessel and the mirrors are adjusted such that maximum light throughput is obtained. The conduit should not be moved during the experiment, as changes in the throughput will be reflected in the IR spectra (as positive or negative absorption values not stemming from the sample).

Fiber optic probes, like the one used for in-line monitoring of bioprocesses in this thesis, are based on transmission of light by total internal reflection. The principle is widely used for guiding light in the visible range for data transmission using glass (i.e. silica-based) fibers (telecommunications). Brief, comprehensive, introductions to infrared fiber optical materials and fiber optic probes can be found in the Handbook of Vibrational Spectroscopy^{8,9}. For a detailed discussion of infrared fiber optics the interested reader is referred to Sanghera and Aggarwal¹⁰. The short introduction given in the following paragraphs is guided by the Handbook of Vibrational Spectroscopy. A major advantage of

optical fibers over light conduits is that they are flexible up to a certain degree and thus make connection between the interferometer and the measurement vessel easier. Material properties govern the available transmission, i.e. measurement, ranges. The multiphonon edge determines the upper wavelength limit, while electronic absorptions (band gap edge) restrict transmission at the lower wavelength limit. Other factors influencing the transmission properties are scattering losses within the material, impurities, and material defects. The acceptance angle of the fiber, i.e. its numerical aperture (NA), depends on the critical angle for internal total reflection. This is determined by the ratio of refractive indices of the core material (within which the light is totally reflected and thus guided) and the medium surrounding it (either an appropriately chosen cladding layer or a coating, see Snell's law page 13). A larger difference between the refractive indices (i.e. the higher the ratio) leads to a smaller the critical angle for total internal reflection and therefore a higher flexibility in coupling in and out of the optical fiber. Furthermore, transmission is less sensitive to the bending radius of the fiber, as a wider range of angles of incidence lead to total internal reflection. On the other hand, losses due to reflections at the core ends are higher for fibers with high refractive indices. Care should therefore be taken when coupling the light in and out of the optical fiber.

Typical materials used for IR transparent optical fibers are calcogenide and polycrystalline silver halogenide (AgX), most commonly chloride and bromide. In this thesis, AgX fiber optic probes were used due to the available transmission range (from 625 to 2500 cm^{-1}).

1.4 Multivariate data analysis

Data analysis is of key importance when dealing with multivariate data sets such as mid-IR spectra. Usually, spectral data are highly co-linear, i.e. the absorbance value at a specific wavenumber correlates with the absorbances at other wavenumbers. Therefore, special statistical methods have to be used. The following paragraphs give a brief introduction to the chemometrics^{xiii} used in the present thesis. These were used to extract chemical information from the measured spectra (PCA) and to build linear^{xiv} regression models for analytes of interest (using a PLS-R and a multivariate curve resolution-alternating least

^{xiii} Nicely defined by S. Wold in 1994 as: "How to get chemically relevant information out of measured chemical data, how to represent and display this information, and how to get such information into data."¹⁴¹

^{xiv} Linear modelling is suitable as IR spectroscopy obeys Beer's law (Equation (5)), i.e. the absorbance is linearly dependent on analyte concentration.

squares (MCR-ALS) approach). They are guided by the tutorial by Geladi & Kowalski¹¹ and the book “Fundamentals of Statistics” by Hans Lohninger¹².

The goal of multivariate linear regression is to find the regression vector \mathbf{B} that best links the dependent variables \mathbf{Y} (concentrations) to the independent variables \mathbf{X} (absorption spectra) such that $\mathbf{Y} = \mathbf{XB} + \mathbf{E}$ (where \mathbf{E} is the residual or error matrix). In the case of mid-IR spectroscopy, the matrix \mathbf{X} are the mid-IR spectra of the respective samples arranged in rows, i.e. each row of the matrix is a single spectrum, while each column contains the absorption values of all samples at a distinct wavenumber. The dependent variable vector \mathbf{Y} contains the analyte concentration in each sample (Figure 7). Once the regression is established the regression vector \mathbf{B} can be used to determine unknown dependent variables (concentrations) \mathbf{Y} by multiplication with the data matrix \mathbf{X} .

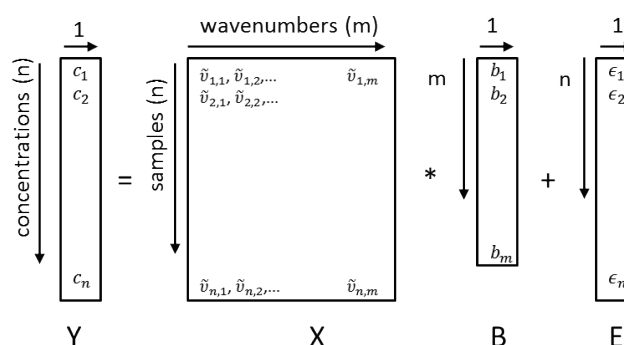


Figure 7: Schematic representation of multivariate linear regression model on the example of spectral data and concentrations.

1.4.1 Principal Component Analysis (PCA)

A frequently used chemometric method for exploratory data analysis is PCA. For a detailed introduction and discussion of PCA, the interested reader is referred to Jolliffe's comprehensive book “Principal Components Analysis”¹³. In brief, PCA reduces data dimensionality by calculating the directions of largest variation in the data set and constructing a new orthogonal coordinate system using these new, uncorrelated, variables. Highly multidimensional data, like mid-IR spectra, are thus reduced to a set of principal components (PCs), which includes as much of the variation of the initial data as possible. This is done by only choosing the first few PCs that contain the majority of variation of the original data. Ideally, PCA thus filters out noise and leaves only meaningful changes. Formally, the data matrix \mathbf{X} is decomposed into two orthogonal matrices \mathbf{V} , the loadings

matrix, and \mathbf{U} , the scores matrix (plus an error matrix \mathbf{E} containing the residuals not covered by the decomposition) (Figure 8):

$$\mathbf{X} = \mathbf{UV}^T + \mathbf{E} \quad (10)$$

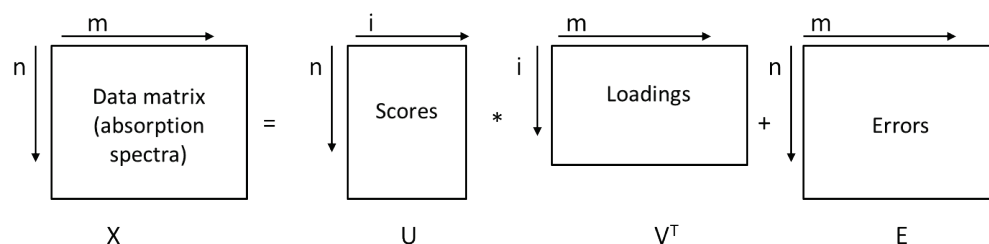


Figure 8: Schematic representation of PCA. The data matrix \mathbf{X} is decomposed into a scores matrix (\mathbf{U}) and a loadings matrix (\mathbf{V}). Unexplained variance is captured by the error matrix (\mathbf{E}).

The scores matrix \mathbf{U} is the original data in the new coordinate system and the loadings matrix \mathbf{V} contains the weights of the original data when the PCs are calculated. The loadings \mathbf{V} of each principal component can be plotted against the initial wavenumber scale of the data \mathbf{X} : high loadings-values \mathbf{V} indicate wavenumber regions that show large variance in the original data and can be correlated with known spectra of analytes of interest. Thus, insight into chemical changes of the chemical system under investigation can be gained. One method to find the orthogonal coordinate system is by solving the eigenvalue problem for the co-variance matrix, $\mathbf{X}^T\mathbf{X}$ (i.e. the mean of each variable is subtracted before multiplication), or the correlation matrix, $\tilde{\mathbf{X}}^T\tilde{\mathbf{X}}$ (i.e. the mean of each variable is subtracted, then divided by standard deviation) of the \mathbf{X} -data^{xv}. The eigenvectors thus determined are the PCs and the corresponding eigenvalues are a measure for the variance explained by the respective PC. An extension of PCA is PCR (principal components regression), where the scores of the PCs are used to build a regression model for a dependent variable \mathbf{Y} .

Within this thesis, PCA was used to identify the major changes in spectra of *S. cerevisiae* acquired in-line using an ultrasound enhanced ATR probe during nitrogen-limited fermentation. The loadings of PC1 corresponded to spectral features of trehalose and glycogen, the storage carbohydrates, which *S. cerevisiae* accumulate during N-limited growth. The complete study was published in **Publication III** (see page 70 for a summary and page 109 for the full paper).

^{xv} Co-variance is a measure for the heterogeneity (or homogeneity) of the data. A co-variance of zero means that data are orthogonal, i.e. not linearly dependent on each other.

1.4.2 Partial Least Squares Regression (PLS-R)

When dealing with FT-IR spectra of multicomponent systems usually multi-variate regression methods have to be used to extract quantitative information on a target analyte. Wold et al.¹⁴ give a good introduction into the mathematics behind PLS-R and give a “recipe” on “how to develop and interpret a PLS-R model” (Chapter 7). PLS-R is a suitable method to correlate FT-IR spectra, i.e. numerous, strongly correlated (co-linear) and often noisy \mathbf{X} -data, with dependent data \mathbf{Y} (i.e. concentration values). The independent \mathbf{X} -data are projected onto a set of “latent variables” which are good predictors of \mathbf{Y} . The reference data \mathbf{Y} have to be known prior to the model building process. They can either be predefined by measuring standards of known concentration, i.e. synthetic standards, or determined by a reference method. For PLS-R the data \mathbf{X} is decomposed into a score matrix \mathbf{T} , a loadings matrix \mathbf{P} , and an error matrix \mathbf{E} (outer relation; Equation (11)). A similar outer relation can be calculated for the dependent (reference) data \mathbf{Y} (Equation (12)). Now a regression model is iteratively calculated using the scores matrices of the \mathbf{X} and \mathbf{Y} data, \mathbf{T} and \mathbf{U} , the inner relation (Equation (13)), under the condition to minimize the error matrix \mathbf{F} . A schematic representation of the algorithm is illustrated in Figure 9.

$$\mathbf{X} = \mathbf{T}\mathbf{P}^T + \mathbf{E} \quad (11)$$

$$\mathbf{Y} = \mathbf{U}\mathbf{Q}^T + \mathbf{F} \quad (12)$$

$$\mathbf{U} = \mathbf{B}\mathbf{T} \quad (13)$$

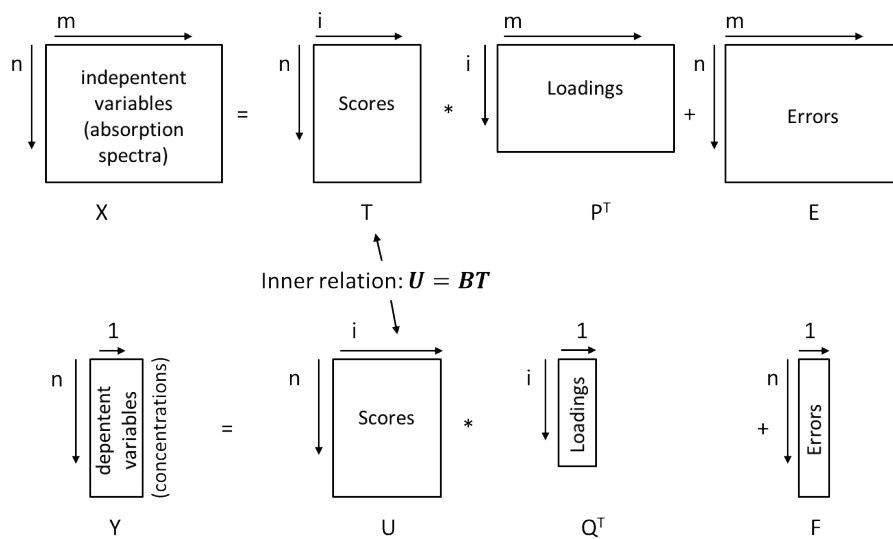


Figure 9: Schematic representation a PLS-R model. Figure adapted from Lohninger¹².

The result is a number of PLS factors or “latent variables” that best describe the variation of the dependent variables. Theoretically, the number of factors can be as large as the rank of \mathbf{X}^{xvi} . Some of the smaller components, however, will only describe the noise in the data. Therefore, the choice of optimum number of components is an important step in model development. Since the algorithm does not provide a stop-criterion, the optimum number has to be determined by the user. This can be done by internal or external validation of the model and evaluation of the root-mean-square error (RMSE). The RMSE is calculated as

$$RMSE = \sqrt{\frac{\sum_{i=1}^n (y_i - \hat{y}_i)^2}{n}} \quad (14)$$

where y_i are the measured \mathbf{Y} -values, \hat{y}_i the ones predicted^{xvii} from the model and n the number of samples (i.e. number of spectra). When performing internal validation, it is referred to as the RMSECV (root mean square error of cross-validation), while one speaks of the RMESP (root mean square error of prediction) when using external validation. For internal, or cross-validation the \mathbf{X} -data is divided into smaller subsets and one of the subsets, the test-set, is used to test the predictive quality of the model built using the other subsets. Depending on the size and the nature of the data set, different algorithms to choose the subsets can be used. Leave-one-out cross-validation is the most straight-forward way: one sample after the other is left out; it is, however, prone to overly optimistic results, especially when replicate samples are present in the data-set, and can take a long time to calculate for large datasets. A more reliable and versatile validation method is to split the data into random subsets. Each subset is subsequently used as a test-set and the average RMSECV is calculated. Another parameter that has to be chosen by the operator is the size of the subsets (or number of data splits as used in the PLS-toolbox). Ideally the size is chosen in consideration of the size of the data set: a good choice is a subset comprising about ten to twenty percent of the samples. Performing multiple iterations of the selection process increases the reliability of the result, but can quickly lead to long computation times. The model of choice is the one that uses the least factors and has the lowest (or close to the lowest) RMSE. This prevents over-fitting, i.e. when the model describes the data used

^{xvi} The rank of a matrix is defined as the number of linearly independent rows (or columns).

^{xvii} In the context of mathematical modelling the term “predicted” is commonly used instead of “calculated” or “estimated” – this is not meant in a temporal sense, i.e. the prediction of future values/events, but in the sense that the dependent variable is calculated/determined using a model rather than directly measured.

for prediction so well, that it performs poorly when it is applied to unknown data (even if it only slightly deviates from the initial data set).

PLS-R is a frequently employed multivariate regression method in bioprocess monitoring. An overview of work published employing FT-IR spectroscopy and PLS-R for bioprocess monitoring can be found in chapter 2.1.

In the present thesis, PLS-R was used for the quantitative determination of intracellular carbohydrates in *S. cerevisiae* by transmission FT-IR spectroscopy of dried samples (**Publication II**, summary page 68, full paper page 97 ff.). Furthermore, it was used in combination with in-line ATR spectroscopy during *Penicillium chrysogenum* (*P. chrysogenum*) fermentation to monitor the concentration of precursor (phenoxyacetic acid) and product (penicillin V) in the medium (**Publication IV**, summary page 71, full paper page 119 ff.) and for the comparison of performance of two process spectrometers equipped with a fiber optic and an optical conduit ATR probe, respectively (**Publication V**, summary page 72, full text page 129 ff.).

1.4.3 Multivariate Curve Resolution – Alternating Least Squares (MCR-ALS)

The idea behind multivariate curve resolution (MCR) is similar to that of PCA: The measured data X is decomposed (resolved) into a linear combination of pure (unfolded) component spectra S and their respective concentrations C (bilinear decomposition) plus an error matrix E containing the residuals not fitted by the model (Equation (15) and Figure 10). Two reviews by de Juan and Tauler^{15,16} cover a range of multivariate resolution approaches and their application to different chemical multicomponent systems.

$$X = CS^T + E \quad (15)$$

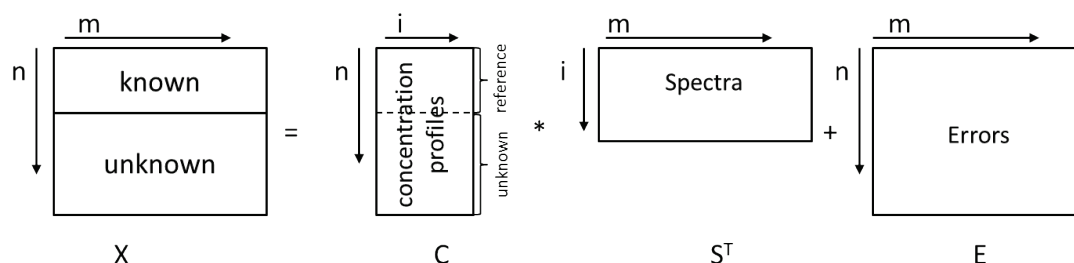


Figure 10: Schematic representation of MCR-ALS including known reference spectra. Adapted from Antunes et al.¹⁷, where further details on the implementation of the correlation constraint between known and unknown concentrations can be found.

The most popular MCR method was introduced by Tauler in 1995¹⁸ and uses an alternating least squares (ALS) approach. Decomposition of \mathbf{X} is achieved by iterative least-squares minimization of (the Euclidian norm of) \mathbf{E} , under suitable constraining conditions during the ALS procedure. These constraints can have a physical, chemical or mathematical meaning and have to be chosen by the user^{xviii}. Examples for constraints are non-negativity of the concentration profiles or closure of the system, i.e. mass balance conservation in chemical reactions. An advantage over PLS-R is that the calculated pure component spectra \mathbf{S} can be compared to measured pure component spectra. Thus the model quality can be directly evaluated. In order to obtain a meaningful model, initialization with system parameters as close to the final results as possible is necessary. An important parameter which has major impact on the resulting model is the number of components i the model is developed for. It can be estimated with prior knowledge of the system or mathematically e.g. by PCA. MCR-ALS can be performed without any further knowledge of the system, however, a good estimation of starting concentrations and/or calibration samples are advantageous. Initial estimates for \mathbf{C} and \mathbf{S} can be obtained using evolving factor analysis (EFA) or SIMPLISIMA (simple to use interactive self-modeling mixture analysis). Furthermore, when reference spectra, i.e. spectra of known concentration, are available a correlation constraint can be implemented. It forces the concentrations found for these reference samples at each ALS iteration to the previously determined ones (Figure 10). Details on the implementation of the constraint can be found in Antunes et al.¹⁷.

Kessler and Kessler¹⁹ applied MCR-ALS to assess the kinetics of biotechnological processes, one of them employing ATR FT-IR spectroscopy to investigate the carbohydrate composition of hemp samples over drying time. Grassi et al.²⁰ used at-line ATR FT-IR spectroscopy and MCR-ALS to monitor the carbohydrate and ethanol content during a beer fermentation process (*S. cerevisiae*). MCR-ALS was able to extract component spectra that corresponded well with the measured spectra of maltose, fructose, sucrose, dextrans, maltotriose and ethanol, respectively. Correlation-constrained MCR-ALS was successfully employed for the quantitative analysis of pharmaceutical and agricultural samples by HPLC-UV/Vis and NIR spectroscopy, respectively²¹, and of blood serum samples and powdered juices in the presence of interferences by fluorescence and UV/Vis spectroscopy, respectively²².

^{xviii} Note: PCA, on the other hand, decomposes the experimental data such that the model explains the maximum variance under the mathematical constraint that the new coordinate system is orthogonal.

In the present thesis, MCR-ALS was used in combination with in-line ATR FT-IR spectroscopy to determine precursor (phenoxyacetic acid) and product (penicillin V) during *P. chrysogenum* fermentations (**Publication IV**, summary page 71, full paper page 119).

1.5 Acoustic particle manipulation - acoustophoresis

The following introduction to acoustic particle manipulation and acoustofluidics is guided by Bruus' publications the Lab-on-a-Chip series "Acoustofluidics"²³ and Gröschl's review in *Acoustica Acta*²⁴.

Particles suspended in a medium are subject to acoustic radiation forces when irradiated by acoustic waves, i.e. longitudinal pressure waves. These forces act on particles that are small relative to the acoustic wavelength, but large enough to experience a pressure difference at either side. Forces exerted by standing wave fields are stronger than those exerted by travelling wave fields and both scale with particle size (up to a limit). For particle manipulation, acoustic resonators and thus standing wave fields are usually exploited; therefore, the following description is limited to these.

Ultrasonic resonators are built up by placing a reflector opposite an ultrasound transducer, i.e. the ultrasound emitter, and the subsequent superposition of incident and reflected wave (Figure 11a). The system is in resonance when the distance between transducer and reflector is equivalent to a multiple of half wavelengths of the acoustic wave. Piezoelectric materials are widely used for the generation of vibrations in the MHz-regime. These materials transform an applied electrical voltage into mechanical stress, strain and displacement (i.e. the inverse piezoelectric effect). For a detailed discussion of the piezoelectric effect and the excitation of acoustic fields for ultrasonic particle manipulation, the interested reader is referred to Dual and Möller (2012)²⁵, here only a brief summary will be given. For particle manipulation, piezoelectric ceramics, e.g. lead zirconate titanate (PZT), are typically used, as they efficiently transform the electrical voltage into mechanical energy, i.e. have a high piezoelectric constant. The piezoceramic element is contacted via opposing electrodes and acts, together with a protective carrier layer^{xix} onto which it is mounted, as the ultrasound transducer (Figure 11b). The electrodes are usually realized in

^{xix} The carrier layer acts as an electrical insulator between the piezoceramic element and the liquid. Its material properties and thickness are chosen such that an efficient transport of the acoustic energy into the liquid is possible.

a wrap-around configuration so that both the electric leads can be connected on the same surface. For round piezoceramic disks, a bull's eye configuration is often employed where the bottom electrode extends onto the top surface of the disk and is separated from the top electrode by an insulation band (Figure 11c).

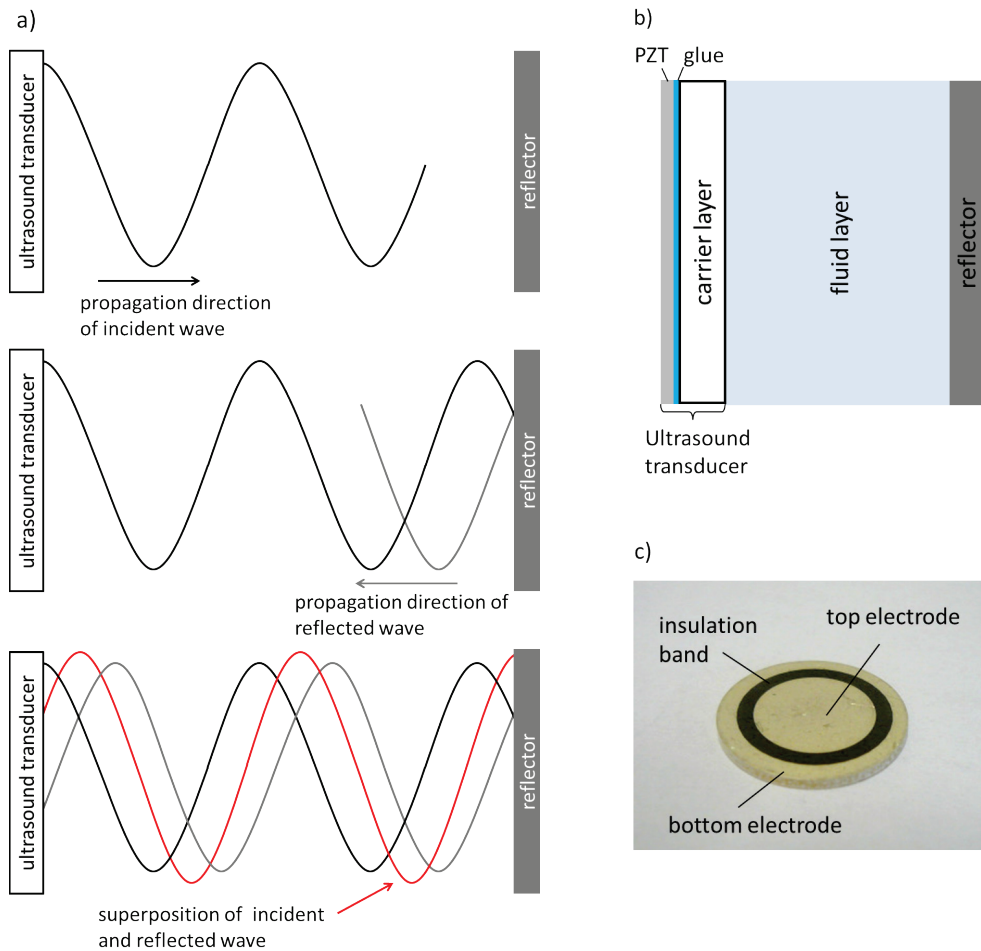


Figure 11: A standing wave is generated in an ultrasonic resonator by superposition of the incident and reflected wave. The sinusoidal line represents the amplitude of the pressure change (note that acoustic waves are longitudinal waves). The resulting standing wave's envelope, i.e. the minima and maxima, are fixed in space (a). The structure of an ultrasonic resonator: the PZT glued to a carrier layer makes up the ultrasound transducer (b). Photograph of a PZT disk with a bull's eye electrode that allows for connection of both electric leads at the surface (c).

The forces acting on the particles can be divided into primary and secondary forces: the primary radiation forces are caused by direct interaction of the acoustic pressure wave and a single particle. It can be divided into two components relative to the direction of sound propagation. The primary axial radiation force, i.e. acting in direction of sound propagation, pushes particles into certain areas of the acoustic standing wave field and leads to a

periodic pattern of particles agglomerating in planes perpendicular to direction of sound propagation (parallel to the ultrasound transducer, to the acoustic wave fronts). The primary transverse radiation force leads to the concentration of particles in certain areas within these planes. It is caused by the inhomogeneous distribution of acoustic amplitude over the surface of the transducer (e.g. the amplitude is zero at the edges due to continuity reasons for finite sized transducers). The secondary radiation force, or Bjerkens force, is based on particle-particle interactions, i.e. the interaction of particles with the wave field scattered from other particles. It leads to a fine structure within the particle agglomerates.

King²⁶ derived the acoustic radiation force for incompressible spheres in 1934. Yosioka and Kawasima²⁷ extended the theory to compressible spheres in plane acoustic wave fields in 1955. Gorko'v²⁸ summarized and extended their work to include the viscosity of the host fluid/medium. The force that has the major contribution to acoustic particle manipulation is the *primary axial radiation force*. For a plane standing wave field with wavelength λ propagating in z-direction the primary axial radiation force F_z^{rad} acting on a spherical particle with radius a and $\lambda \gg a$ is given by Equation (16).

$$F_z^{rad} = 4\pi \cdot \phi(\tilde{\kappa}, \tilde{\rho}) \cdot ka^3 \cdot E_{ac} \cdot \sin(2kz) \quad (16)$$

$$\phi(\tilde{\kappa}, \tilde{\rho}) = \frac{1}{3} \left(\frac{5\tilde{\rho} - 2}{2\tilde{\rho} + 1} - \tilde{\kappa} \right) \quad (17)$$

The magnitude of the force depends on the acoustic energy density $E_{ac} = \frac{p_a^2}{4\rho_0 c_0^2}$ transmitted into in the medium, where ρ_0 and c_0 are the density and speed of sound in the medium, respectively, and p_a is the acoustic pressure amplitude. Furthermore, the force scales with the acoustic contrast factor $\phi(\tilde{\kappa}, \tilde{\rho})$ (Equation (17)) which in turn depends on the ratio of mass densities, $\tilde{\rho} = \frac{\rho_p}{\rho_0}$, and compressibilities, $\tilde{\kappa} = \frac{\kappa_p}{\kappa_0}$, between particle (subscript p) and medium (subscript 0), respectively. The compressibility is connected to the speed of sound and the mass density by $\kappa = \frac{1}{\rho \cdot c^2}$. Note that the sign of $\phi(\tilde{\kappa}, \tilde{\rho})$ can be positive or negative: For dense particles ($\rho_p > \rho_0$), e.g. cells, it is positive and the force drives the particles into the pressure nodal planes of the standing wave field. Particles for with $\rho_p < \rho_0$, e.g. oil droplets suspended in water, on the other hand are driven to the pressure anti-nodal planes. This was successfully used by Grenvall et al. for the separation of lipids from cells in milk using a microfluidic set-up. The lipids and cells could be further analyzed separately, furthermore, clogging of the channel due to lipid deposition on the walls was prevented^{29,30}.

Even if the particle and the medium have the same density, the acoustic contrast factor can be non-zero as it also depends on the ratio of compressibilities (and thus speeds-of-sound) of particle and medium. Acoustic particle manipulation can therefore also be used to separate or concentrate suspended particles that have the same mass density as the medium, which cannot be achieved by centrifugation (i.e. gravimetrically) or in a microgravity environment^{31,32}.

The periodicity of the force is double that of the acoustic wave, leading to planes where $F_z^{rad} = 0$ – pressure nodal planes – every half wavelength of the acoustic wave (given by the term $\sin(2kz)$, with the wavenumber $k = \frac{2\pi}{\lambda} = \frac{\omega}{c} = \frac{2\pi f}{c}$).

A typical frequency f used for acoustic particle manipulation of micrometer-sized particles is 2 MHz, the speed of sound in water c_0 is approximately 1500 ms^{-1} , and therefore, the wavelength λ of the acoustic wave is $750 \text{ }\mu\text{m}$. If a standing wave field is built up, the pressure nodal planes are thus approximately $375 \text{ }\mu\text{m}$ apart. For this frequency, the lower threshold of particle sizes (i.e. diameter) that can be manipulated is approximately one micrometer³³.

1.5.1 Potential bioeffects of ultrasound

In a biotechnological environment ultrasound is mainly associated with ultrasonic cell lysis, while it is regarded as a safe, non-invasive, diagnostic tool in medicine^{xx}. The major differences between the ultrasonic cell lysis and medical ultrasound are the employed frequency ranges, a few tens of kHz compared to a few MHz, and the transmitted energy. In the Acoustofluidics Series in Lab-on-Chip Wiklund³⁴ reviews several reports on cell viability in microfluidic ultrasonic resonators, nicely summarizing the “physical mechanisms of ultrasound causing a bioeffect”: Temperature increase, cavitation, the radiation forces themselves, and acoustic streaming.

Absorption of the acoustic wave in the liquid causes a temperature increase^{xxi}. The higher the frequency of the acoustic wave, the stronger is the absorption, i.e. the damping. Heating due to absorption (and due to electromechanical losses of the transducer) can be

^{xx} It is regarded so safe, as a matter of fact, that even unborn babies are exposed to ultrasound during ultrasonography on a regular basis for diagnostic purposes – FDA however discourages excessive exposure to ultrasound for non-medical reasons¹⁴².

^{xxi} When the acoustic wave is absorbed by a material, the mechanical energy is converted to heat (conservation of energy).

minimized by actively controlling the temperature of the resonator chamber. In the present work, heating is of minor concern, as bioreactors are temperature controlled and heavily stirred.

The following short introduction to acoustic cavitation, which can cause severe damage in cells, is based on Leighton's review³⁵ of ultrasound and its effects. Cavitation is the formation of gas or vapor filled cavities ("air bubbles"), as can be observed in ultrasonic baths used for cleaning or degassing. These (cavitation) bubbles can either oscillate, continuously growing and shrinking with the changes of the acoustic pressure, or implode violently after growing over just one or two pressure cycles. The first effect, *stable* cavitation, causes highly localized streaming which can lead to shear stress on cells in proximity of the cavitation bubble. Bubbles collapsing during *inertial* cavitation, the latter effect, lead to extremely localized high pressures, high temperatures ($> 1000^{\circ}\text{C}$), and the generation of free radicals. Phenomena like sonoluminescence and chemoluminescence can be consequences of inertial cavitation. These harsh conditions clearly are not beneficial for cells and lead to cell rupture and cell death. Inertial cavitation is a threshold phenomenon, i.e. it depends on the amplitude and frequency of the sound field and the bubble size. It is less likely to occur at low amplitudes and at higher frequencies. Moreover, at a given ultrasound frequency only a certain range of bubble radii can undergo inertial cavitation, and this range narrows with higher frequency. For bubbles smaller than the threshold radius, surface tension prevents the rapid growth necessary for inertial cavitation. Bubbles with radii larger than the upper threshold will not grow enough in a short time and thus the necessary pressure difference between the liquid and the cavity, i.e. the inside of the bubble, is not large enough to generate the necessary high kinetic energy (for a detailed discussion see Refs 71 and 72). In this work, low amplitudes, i.e. low driving voltages, and relatively high frequencies (around 2.4 MHz) were used for acoustic particle manipulation, thus minimizing the probability of inertial cavitation^{xxii}.

Stable cavitation, on the other hand, is less of a problem when the cells are subject a standing wave field: As mentioned before, the direction of the primary axial acoustic radiation force depends on the sign of the acoustic contrast factor $\phi(\tilde{\kappa}, \tilde{\rho})$. Particles with a higher mass density than the suspending medium (cells) are driven in to the pressure nodal planes, while those with a lower mass density (air/gas bubbles) are generally driven to the

^{xxii} In a preliminary project no indication for the presence of free radicals was found using the starch test for free iodine when irradiating an iodide solution in a similar set-up at comparable settings.

pressure anti-nodes. Therefore, the cells are actually protected from the shear stress induced by stable cavitation by the standing wave field.

The effect of the radiation forces on cells is the alignment in the pressure nodal plane. This alignment has been shown to have an effect in vivo when standing wave fields were built up in blood vessels of chick embryos, leading to a reversible arrest of red blood cells, which in turn could induce thrombosis³⁶. For cell suspensions, no adverse effects are expected from being subjected to standing wave fields. As mentioned before, the cells are driven into the pressure nodal planes, therefore they only experience very little to no pressure differences. They will however be “shaken”, as the pressure nodal planes coincide with the velocity anti-nodal planes, i.e. the planes where the velocity of the suspending medium is highest.

This was confirmed by Böhm et al.³⁷ when they subjected plant cells (*Petunia hybrida*) to as standing and a propagating wave field, respectively, employing the same frequency (2.15 MHz) and energy density, i.e. acoustic energy transmitted into the medium per unit volume: after 20 minutes of exposure to the standing wave field, cell viability^{xxiii} remained at 95%, which was also found for the un-sonicated control group, cell viability decreased to approximately 30% after 20 minutes of exposure to the propagating wave. This is in accordance with a study Radel et al.³⁸ who found that the viability of *S. cerevisiae*^{xxiv} irradiated with a 2 MHz standing wave field for up to 120 minutes did not increase compared to un-sonicated controls. When the cells were dynamically driven through the standing wave field due to a change of acoustic contrast factor induced by addition of ethanol, however, viability decreased significantly.

Studies of mammalian cells held in 3D agglomerates in microfluidic cell traps revealed no adverse effects of the ultrasound irradiation. Bazou et al. found no changes in the in vitro surface receptor interactions of neural cells³⁹ or of the gene expression or the pluripotency of the embryonal stem cells⁴⁰. Hulström et al. investigated the viability and proliferation of COS-7 cells after ultrasonic trapping up to 75 minutes and found no changes compared to un-sonicated control groups⁴¹.

It can be concluded that cells are generally not harmed during acoustic particle manipulation, as long as they remain in the pressure nodal planes of the standing wave field. This is exploited in state-of-the-art perfusion filters for mammalian cell cultures,

^{xxiii} As tested by uptake and cleavage of fluorescein diacetate (FDA).

^{xxiv} As tested by methylene blue staining.

where the ultrasonic standing wave field it is used to hold cells back against a continuous flow of medium without detrimental effects^{42–44}.

1.6 Microorganisms studied

Fermentations of two microorganisms were investigated by in-line mid-IR spectroscopy for this thesis. The yeast *S. cerevisiae* served as a model system for the acquisition of mid-IR spectra of cell in-line during fermentation by ultrasound enhanced ATR FT-IR spectroscopy (**Publications I, II and III**). Two types of multivariate calibrations (PLS-R and MCR-ALS) were compared for monitoring precursor and product in *P. chrysogenum* fermentations (**Publication IV**). This type of fermentation was furthermore used for investigating the performance of a fiber optic and a conduit in-line ATR probe (**Publication V**).

1.6.1 *Saccharomyces cerevisiae*

S. cerevisiae are eukaryotic cells that belong to the kingdom of fungi. The small, single-celled organism is one of most used yeasts and is commonly referred to as baker's yeast. The spherical cells are 5 to 10 μm in diameter, have a rigid cell wall and grow by division, which is referred to as budding. *S. cerevisiae* require the "basic building blocks of life", carbon, nitrogen, hydrogen, and oxygen, and additionally phosphorus, vitamins and trace elements. If the C-source, e.g. glucose, is the growth-limiting nutrient under aerobic conditions, *S. cerevisiae* grow producing biomass and CO_2 . When the external glucose concentration is high, they undergo the Crabtree effect: they produce ethanol and CO_2 rather than biomass. This is also the case during anaerobic growth, i.e. when not enough oxygen is available. *S. cerevisiae* are one of the best studied microorganisms and often serve as model cells for eukaryotic cells. They were chosen for this work for several reasons: First of all, due to their spherical shape the equations derived for acoustic radiation forces can be applied and simulations can be performed. Secondly, numerous reports exist on their successful manipulation by acoustic radiation forces⁴⁵ and it has been shown that exposure to ultrasonic standing waves does not harm them³⁸ or impair their ability to replicate⁴⁶ (see also chapter 2.3 page 44). Furthermore, their metabolism is well known and reliable protocols exist on how to induce specific metabolic responses. One such response is the accumulation of storage carbohydrates (also referred to as reserve carbohydrates in the literature) when *S. cerevisiae* are subject to different kinds of stress, e.g. nutrient

limitations, temperature, etc., during growth⁴⁷. The following paragraph gives a short introduction to this mechanism and the carbohydrates involved.

1.6.1.1 Storage carbohydrates

Carbohydrates make up about 40% of the weight of a *S. cerevisiae* cell. They can be classified by their location within the cell: mannan (Figure 12e), a polysaccharide of mannose (Figure 12c), and (beta-)glucan, polysaccharides of glucose, are located in the cell wall. The storage carbohydrates trehalose (Figure 12b), and glycogen (an alpha-glucan, Figure 12d), a disaccharide and a polysaccharide of glucose (Figure 12a), respectively, are intracellular carbohydrates. When *S. cerevisiae* undergo physiological stress, glucose is stored intracellularly in the form of these storage carbohydrates. For a detailed description of the metabolic pathways that lead to the production of trehalose and glycogen, the interested reader is referred to Francois and Parrou (2001)⁴⁷.

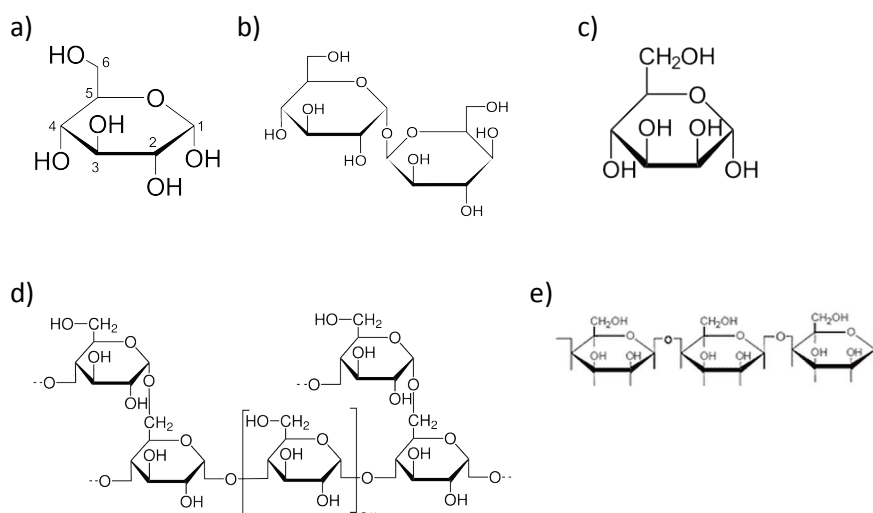


Figure 12: Molecular structure of glucose (a), trehalose (b), mannose (c), glycogen (d), and mannan (e).

1.6.2 *Penicillium chrysogenum*

P. chrysogenum, formerly also *Penicillium notatum*, an ubiquitous filamentous fungi, is one of the major microorganisms used for industrial antibiotic production and a commonly found mold in food spoilage. Its antibiotic effect was (accidentally) discovered by Alexander Fleming in 1928 who observed that bacteria (staphylococci) cultured on agar plates were

dead or dying where that agar plate was contaminated with mold^{xxv}. He cultured the isolated mold and named the substance it released penicillin⁴⁸.

A *P. chrysogenum* hypha is a tubular structure which typically has a diameter of approximately 2 to 5 μm (Figure 13a). Growth occurs only at its tip, i.e. in length (no radial growth), furthermore, the hypha can branch. *P. chrysogenum* cultured submerged (i.e. in a liquid medium) form pellets with up to a few hundred micrometers diameter, made up mainly of entangled branched hyphae.

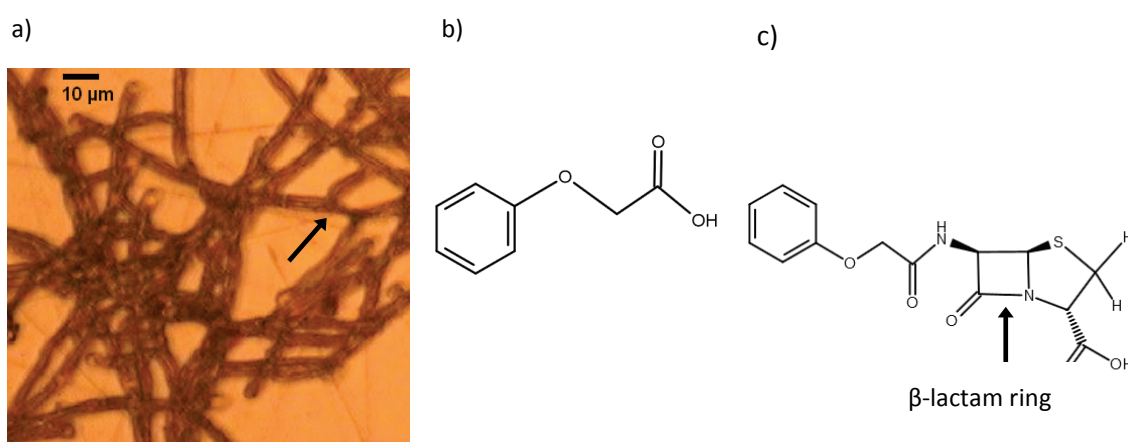


Figure 13: a) Micrograph of *P. chrysogenum* hyphae deposited on a ZnSe slide. The arrow indicates one of the branching locations of a tubular hypha. b) The molecular structure of phenoxyacetic acid, the precursor used for penicillin V production. c) The molecular structure of penicillin V.

Penicillin is a class of β -lactam antibiotics; by adding appropriate precursors to the culture medium of *P. chrysogenum*, these are incorporated into the penicillin molecule as sidechains which alter the chemical and physical properties of the respective penicillin molecule. One such example is the addition of phenoxyacetic acid (Figure 13b): the product is phenoxymethylpenicillin or penicillin V (Figure 13c) which was the first acid-resistant antibiotic and could therefore be administered orally.

^{xxv} As Houbraken et al.¹⁴³ confirmed, the fungal contamination of Fleming's cultures was wrongly identified as *P. notatum*, by which name *P. chrysogenum* was known at the time, but it was actually *P. rubens*, another penicillin producing strain.

2 STATE OF THE ART

2.1 Mid-IR spectroscopy for bioprocess monitoring

Bioprocesses are usually monitored by different sensors to access their physical, chemical and biological variables. Biechele et al.⁴⁹ gave a comprehensive overview over the different available techniques and their respective advantages and disadvantages in their recent review. These sensor systems are used for process control, process development, and, in accordance with the PAT initiative introduced by the FDA in the last decade, gaining process understanding. The bioprocess should no longer be treated as a “black box” with quality control happening prior to start and at the end of the process. Instead, quality should be “built in” by process analysis, increased process knowledge (process understanding) and process modeling.

Both, NIR and mid-IR spectroscopy are commonly used in bioprocess analysis and characterization. NIR spectroscopy offers the advantage that water has lower absorptivity in that range, thus transmission and transflexion set-ups can be realized. These are less sensitive to biofouling than ATR probe surfaces, where, due to the limited depth of penetration (as mentioned before, typically 1 to 2 μm in aqueous solutions), even thin layers lead to spectral interferences and to a strong decrease in desired signal (i.e. the signal of the analyte). Interpretation of NIR spectra, on the other hand, is more difficult than that of mid-IR spectra, due to the nature of the vibrational energy levels probed (combination and overtones) leading to very broad and strongly overlapping features. Absorptivities in the mid-IR are typically higher than in the NIR, therefore absorptions are stronger. This is counter-acted by the fact that the emission maximum of thermal light sources (globars) is shifted towards shorter wavelengths (and thus more energy is available in the NIR), furthermore, detectors are more sensitive in the NIR range. This thesis focuses on the use of mid-IR spectroscopy for bioprocesses monitoring, therefore, the

following literature study is limited to its application for monitoring of substrate and products in the fermentation brothⁱ.

Mid-IR spectroscopy has been employed as at-line, off-line, on-line, and in-line PAT for monitoring of bioprocesses. Roychoudhury et al. published a review showing the potential of mid-IR spectroscopy for real-time bioprocess monitoring in 2006⁵⁰. The review by Landgrebe et al.⁵¹ gives a good overview of the different measurement set-ups employed for real-time fermentation monitoring by (ATR) FT-IR spectroscopy: flow through cells in bypass, optical-conduit probes and (then still experimental) fiber optic probes. In a more recent review Lourenco et al.⁵² summarize the application of different kinds of optical spectroscopy techniques in combination with chemometrics for bioprocess monitoring, focusing on fiber optic approaches.

The first approaches for using FT-IR spectroscopy for bioprocess monitoring were done off-line or at-line. A list of publications on this approach can be found in Table 1. Fayolle et al.⁵³ were the first ones to monitor the concentration of different analytes in the medium of a *Lactobacillus bulgaricus* (*L. bulgaricus*) fermentation with a transmission flow through cell and PLS-R at-line; a similar approach was later employed by Franco et al.⁵⁴ for Kombucha fermentations, extending the analysis to artificial neural networks (ANN) for calibration. In early studies often the native/whole fermentation broth was often used and a calibration for dried biomass or cell optical density was attempted^{55–57}. More recent reports concentrated on filtrated broth and the determination of media components and extra-cellular products^{58–61}. Winder et al. could quantify the concentration of the extracellular product acetate by PLS-R with spectra of washed, dried *E. coli*⁶². Table 2 summarizes the reports of on-line monitoring of bioprocesses. This approach has been developed at the group of Bernhard Lendl in 2001⁶³ (i.e. bioprocess monitoring has a long history in our group). It was employed for monitoring media components in *Escherichia coli* (*E. coli*)^{64–66}, *S. cerevisiae*^{67–69} and *Pichia pastoris* (*P. pastoris*)⁷⁰ fermentations. Furthermore Schenk et al.⁶⁵ used an on-line ATR flow-through cell to monitor the pH of an *E. coli* fermentation by measuring the ratio of protonated and deprotonated acids like phosphoric acid.

ⁱ The application of mid-IR spectroscopy for investigation and monitoring of intracellular products and cellular composition is reviewed in the following chapter (page 29).

Table 1: At-line/off-line analysis of media components and product, including calibration ranges.

Publication	Fermentation	Method	Analytes (g L ⁻¹) ^a
P Fayolle et al. 1997 ⁵³	<i>L. bulgaricus</i>	flow cell (38 µm), whole broth / PLS	lactose (3-70), galactose (0-30), lactic acid (0-30), DCW ^b (0.008-10)
S Sivakesva et al. 2001a ⁵⁶	<i>L. casei</i>	ATR, whole broth / PLS, PCR	glucose (0-80), lactic acid (n.g. ^c), cell OD (n.g.)
S Sivakesva et al. 2001b ⁵⁵	<i>S. cerevisiae</i>	ATR, whole broth / PLS, PCR	glucose (30-70), ethanol (n.g.), cell OD (n.g.)
A Hashimoto et al. 2005 ⁷¹	<i>Oryza sativa</i> , <i>Nicotiana tabacum</i>	ATR / univariate linear regression	ethanol, glucose, fructose, sucrose
VG Franco et al. 2006 ⁵⁴	Kombucha	Flow cell (25 µm), filtrate / PLS, ANN	glucuronic acid (0.7-9.63), gluconic acid (0.04-1.16), glucose (0.62-10.51)
P Roychoudhury et al. 2006 ⁵⁷	<i>Streptomyces clavuligerus</i>	ATR, filtrate & whole broth / PLS	ammonium (0-0.4 ^d), glucose (2-17 ^d), methyl oleate (5-19 ^d), biomass (5-20 ^d)
P Roychoudhury et al. 2007 ⁵⁸	<i>S. clavuligerus</i>	ATR, filtrate / PLS	glycerol (3-16 ^d), clavulanic acid (0.01-0.16 ^d)
F Leitermann et al. 2008 ⁵⁹	<i>Pseudomonas aeruginosa</i>	ATR, cell free / PLS	rhamnolipid 1 (0-8 ^d), rhamnolipid 3 (0-24 ^d), total rhamnolipids (0-32 ^d)
Winder et al. 2011 ⁶²	<i>E. coli</i>	HTS-XT / PCA, PLS, CVA	extracellular acetate quantification from cell spectra
F Capito et al. 2013 ⁶¹	Mammalian culture (CHO)	ATR filtrate / PLS, PCA	HCP ^e (6.8-180)
F Capito et al. 2015 ⁶⁰	Mammalian culture (CHO)	transmission, dried samples	HCP (0.7-3.0), mAb ^f titer (1-28)

^a The concentration ranges given refer to the respective lowest and highest concentration of the analyte either in standard solutions or determined using reference methods, i.e. they refer to the calibration range.

^b dry cell weight

^c n.g. = not given

^d value estimated from graph

^e Host Cell Protein

^f monoclonal Antibody

Table 2: On-line monitoring of bioprocesses by FT-IR mid-IR spectroscopy.

Publication	Fermentation	Method	Analytes (gL ⁻¹) ^a
M Kansiz et al 2001 ⁶³	<i>Clostridium beijerinckii</i>	ATR flow cell coupled by SIA ^b / PLS	acetone (0-5.5) , acetate (0.3-2.7), n-Butanol (0-14.3), butyrate (0-0.6), glucose (0.1-49)
G Jarute et al. 2004 ⁶⁴	<i>E. coli</i>	ATR flow cell coupled by SIA / PLS	glucose (3.8-10.3), intracellular PHB (0.030-0.661)
G Mazarevica et al. 2004 ⁶⁷	<i>S. cerevisiae</i>	ATR flow cell coupled by SIA / PLS	ethanol (0-15), glucose (0-30)
EL Veale et al 2007 ⁶⁸	<i>S. cerevisiae</i>	ATR flow cell coupled by peristaltic pump / PLS, PCA	ethanol (0-30 ^c), glucose (0-75)
J Schenk et al. 2007 ⁷⁰	<i>P. pastoris</i>	ATR flow cell / univariate ^d	methanol (0-15)
J Schenk et al. 2008a ⁶⁵	<i>E. coli</i>	ATR flow cell / MLR ^e (library spectra)	pH, ammonium, glucose, acetate (n.a. ^f)
J Schenk et al 2008b ⁶⁶	<i>E. coli</i>	ATR flow cell (optical conduit)/ CLS ^g (library spectra incl. drift)	ammonium (n.a.), glucose (n.a.), glycerol, acetate (n.a.)
M Dabros et al. 2009 ⁶⁹	<i>S. cerevisiae</i>	ATR flow cell (optical conduit) / PLS	glucose, ethanol, ammonium, glycerol, acetic acid

^a The concentration ranges given refer to the respective lowest and highest concentration of the analyte either in standard solutions or determined using reference methods, i.e. they refer to the calibration range.

^b sequential injection analysis

^c value estimated from graph

^d a two-point linear regression was calculated individually for each fermentation

^e multiple linear regression

^f n.a. = not applicable

^g classical least-squares

A non-exhaustive list of publications on in-line bioprocess monitoring by mid-IR spectroscopy can be found in Table 3. The first application of monitoring in-line was reported by Doak & Phillips⁷² as early as 1999. They employed an optical conduit probe to monitor glucose and acetate during *E. coli* fermentation. Since then, conduit probes have been used for in-line monitoring of media components in bacterial^{73–76}, yeast^{77,78}, and fungal⁷⁹ fermentations and mammalian cell cultures^{80,81}. Fiber optic probes have not been employed as widely for bioprocess monitoring: to the best of the author's knowledge only three reports exist on their use in-line^{82–84}, in the most recent of these reports novel sensor concepts using different types of interferometers, a Fabry-Pérot interferometer and a linear array detector, and a novel type of ATR element were presented⁸⁴. Furthermore, the feasibility of monitoring media components using fiber optic ATR FT-IR probes, has been demonstrated off-line^{85–87}.

Different approaches to building calibration models, mostly PLS-R, were described: either using mid-IR spectra of the fermentation broth and suitable reference analyses, or using mid-IR spectra of synthetic standard solutions, or a combination of the two. Spectra of fermentation broth were either acquired in-line during the fermentation with reference concentrations determined from timed samples drawn from the bioreactor^{72,79}, or off-line, with mid-IR and reference analyses performed on the same sample⁸⁷ for which the inclusion of spectra of broth spiked with a known amount of the desired analyte proved beneficial^{80,81}. Another reported approach was to perform spiking during the fermentation and using these spectra combined with off—line reference analyses^{83,84}. Synthetic models^{74,75,77,86}, i.e. using synthetic standard solutions for calibration, as well as semi-synthetic models^{73,78}, i.e. combining in-line spectra & reference analyses with synthetic standard solutions, were also successfully built. In 2004 Kornmann et al.⁸⁸ showed that updating of PLS-R models in real-time using metabolic balancing for data reconciliation improved the performance for the quantification of fructose, acetate and gluconacetan in a *Gluconacetobacter xylinus* (*G. xylinus*) fermentation. Sagmeister et al.⁷⁶ built a simple univariate calibration for glucose and used the obtained concentration values as input for a soft-sensor for the determination of biomass and specific growth rate in an *E. coli* fermentation.

Table 3: Overview of publications on fermentation monitoring by optical conduit and/or fiber optic ATR probes. Measurements were performed in-line (in situ) unless otherwise stated.

Publication	Fermentation	Method	Analytes (gL ⁻¹) ^a
DL Doak & JA Phillips 1999 ⁷²	<i>E. coli</i>	conduit / PLS (in-line spectra & off-line reference)	glucose (0-25), acetate (0-25)
P Fayolle et al. 2000 ⁸²	<i>Yeast (not specified) and L. bulgaricus</i>	fiber dispersive spectrometer / PLS	glucose (0-90 ^b), fructose (5-90 ^b), lactose (15-80 ^b), galactose (0-25 ^b), ethanol (0-90 ^b), lactic acid (0-26 ^b)
D Pollard et al. 2001 ⁷⁹	<i>G. lozoyensis</i>	conduit / PLS (in-line spectra & off-line reference for calibration)	glucose (0.1-18), fructose (0.1-20, 20.1-60), phosphate (7.5-11) glutamate (0.5-8), proline (0.5-12)
MH Rhiel et al. 2002a ⁸¹	Mammalian cell culture (CHO)	conduit / PLS (off-line unaltered & spiked samples for calibration)	glucose (0-22 mM ^b), lactate (0-60 mM ^b)
M Rhiel et al. 2002b ⁸⁰	Mammalian cell culture	conduit / PLS (off-line unaltered & spiked samples for calibration)	glucose (0-18.8 mM), lactate (1.35-56.4 mM)
HM Heise et al. 2002 ⁸⁵	anaerobic fermentation	off-line fiber	spectral quality would allow for quantitative analysis
H Kornmann et al. 2003 ⁷³	<i>G. xylinus</i>	conduit / PLS (in-line spectra & off-line reference + synthetic standards)	fructose (10-35 ^b), acetate (0-5 ^b), ethanol (0-5 ^b), gluconacetan (0-6 ^b)
H Kornmann et al. 2004a ⁷⁴	<i>G. xylinus</i>	conduit / PLS (synthetic standards)	fructose (0-32), ethanol (0-7), acetate (0-15), gluconacetan (0-10), ammonium (0-15), phosphate (0-8); results used for feed control (ethanol & fructose)
H Kornmann et al. 2004b ⁸⁸	<i>G. xylinus</i>	conduit / PLS (in-line spectra & concentrations determined by metabolic balance to update calibration)	fructose (0-40), acetate (0-10), gluconacetan (0-6)
J Schenk et al. 2007 ⁷⁷	<i>S. cerevisiae</i>	conduit / CLS (library spectra)	glucose, ethanol, ammonium (n.a. ^b)
R. Foley et al. 2012 ⁸⁶	Mammalian cell culture	off-line conduit & fiber (synthetic standards)	glucose, glutamine, ammonia, phosphate, glutamate, lactate, HEPES, bicarbonate (n.g. ^c)
J Dahlbacka et al 2012 ⁷⁸	<i>P. pastoris</i>	conduit / PLS (synthetic standards + semisynthetic in-line spectra for methanol)	glycerol (5-45) , methanol (0.8-8)

Publication (cntd.)	Fermentation (cntd.)	Method (cntd.)	Analytes (gL ⁻¹) ^a (cntd.)
J. Dahlbacka et al. 2013 ⁷⁵	<i>Streptomyces peucetius</i>	conduit / PCA, PCR, PLS (synthetic standards + synthetic multi-constituent spectra)	glucose (0-20) , acetate (0-2)
M Sandor et al. 2013 ⁸³	Mammalian cell culture (CHO)	fiber/ PLS (in-line spectra + spiking & off-line reference)	glucose (0-9), lactate (0-4), total cell concentration (0-1.8E7)
J-M Girard et al. 2013 ⁸⁷	<i>S. obliquus</i> (microalga)	off-line fiber/ univariate & PLS	relative content of lactose, glucose, galactose
P Sagmeister et al. 2013 ⁷⁶	<i>E. coli</i>	conduit / univariate linear calibration (in-line spectra)	glucose (input for growth rate estimation by soft sensor)
A Bogomolov et al. 2015 ⁸⁴	<i>S. cerevisiae</i>	2 diamond ATR probes: Fabry-Pérot interferometer, grating spectrometer & line sensor; in-line polychrystalline fiber loop / PLS (in-line spectra + spiking & off-line reference for calibration)	ethanol (0-150 ^b), glucose(0-300 ^b), fructose (0-150 ^b)

^a The concentration ranges given refer to the respective lowest and highest concentration of the analyte either in standard solutions or determined using reference methods, i.e. they refer to the calibration range.

^b value estimated from graph

^c n.a. = not applicable

^d n.g. = not given

These studies are clear indications of the applicability of in-line mid-IR ATR spectroscopy for bioprocess monitoring, however the use of fiber optic probes was very limited so far. In this thesis, a fiber optic ATR probe was used in-line in a *P. chrysogenum* fermentation for the determination of phenoxyacetic acid (precursor) and penicillin V (product) in the fermentation broth. Semi-synthetic calibration models, i.e. using spectra acquired in-line combined with on-line HPLC reference analysis, were successfully built using two different chemometric methods: PLS-R and MCR-ALS (**Publication IV**). Furthermore, the performance of an optical conduit ATR probe and a fiber optic ATR probe were compared using the same biological system. This is, to the best of the authors' knowledge, the first report on the simultaneous use of two different ATR probes in-line (**Publication V**).

2.2 Mid-IR spectroscopy of microorganisms

The basic building blocks of biomass, proteins, carbohydrates, nucleic acids and lipids, lead to characteristic absorption bands in the mid-IR spectra of microorganisms. The following band assignments are based on References 79 and 80. In the fingerprint region of a typical transmission spectrum of dried *S. cerevisiae* (Figure 14), absorptions from C=O stretching of ester groups in lipids around 1730 cm^{-1} are visible. Absorptions from proteins can be found around 1655 cm^{-1} (amide I band, C=O stretching and to a lesser extent N-H bend and C-N stretch), around 1550 cm^{-1} (amide II band, N-H bend, C-N stretch), and around 1300 cm^{-1} (amide III band, complex combination of different vibrations). Between 1450 and 1200 cm^{-1} numerous C-H and O-H deformation vibrations contribute to the spectrum (from lipids and carbohydrates). DNA, RNA, and phospholipids lead to absorptions around 1240 cm^{-1} (antisymmetric PO_2^- stretching vibrations). C-O stretching originating from carbohydrates dominates the region between 950 and 1200 cm^{-1} , with minor contributions around 1100 cm^{-1} from symmetric PO_2^- stretching (again, DNA, RNA, and phospholipids).

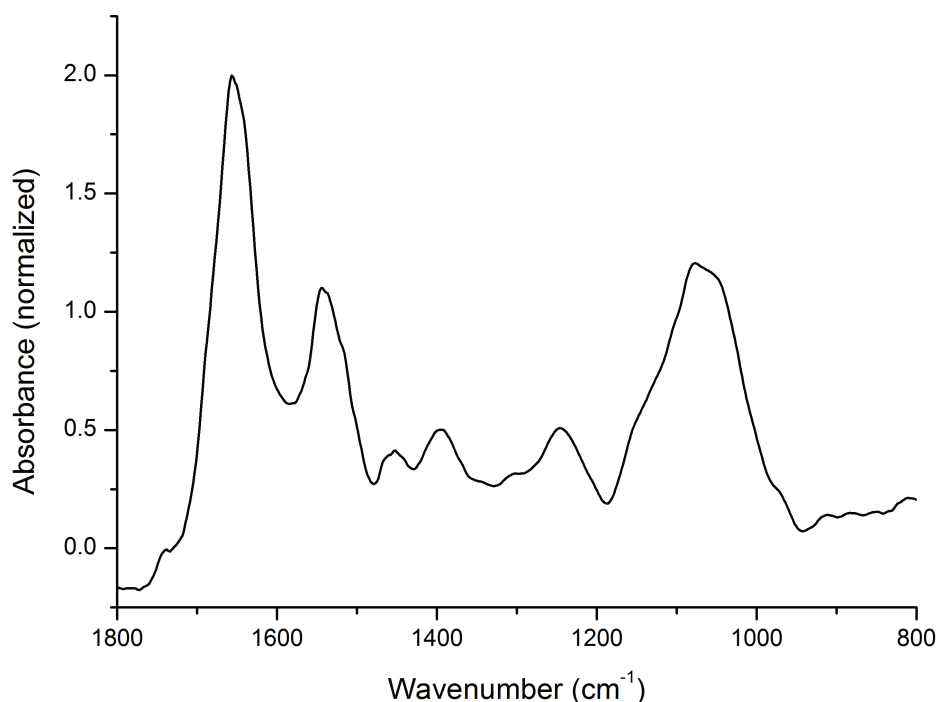


Figure 14: Mid-IR absorption spectrum of dried *S. cerevisiae* acquired in transmission mode. The spectrum is normalized to the Amide I band (~1655 cm⁻¹).

The first report on FT-IR spectroscopy as a means to differentiate and identify pathogenic bacteria was published by Naumann in 1985⁹¹. He developed a reliable method for the acquisition of spectra of cells by depositing drops of cell suspensions onto IR-transparent slides and, after a drying step, measuring them in transmission mode. This led to a joint project of the Robert Koch-Institute in Berlin (Germany) and Bruker Optics (Germany) during which a prototype of a dedicated IR accessory for high throughput screening of dried microbial samples was developed, the HTS-XT⁹⁰. By 2001 as many as 40 publications on “Discrimination, classification, identification of microorganisms using FT-IR spectroscopy and chemometrics” had been published and were comprehensively reviewed by Mariey et al⁹². Mid-IR spectroscopy in combination with different chemometric methods, most frequently PCA and HCA (hierarchical cluster analysis, an unsupervised clustering method), has since become an established method for the identification and differentiation of microorganism. Furthermore, Naumann gave a comprehensive overview of infrared spectroscopy in microbiology in his chapter of the Encyclopedia of Analytical Chemistry⁹³. Santos et al. reviewed the use of FT-IR spectroscopy for the identification and characterization of filamentous fungi and yeast and concluded that due to the fast and easy

sample preparation and the relatively inexpensive equipment it is a method well suitable for use in medical laboratories and hospitals or food and water industries.

Apart from identification and differentiation, mid-IR spectroscopy has been successfully used to investigate the biochemical response of microorganisms to different culture conditions and the accumulation of intracellular productsⁱ, e.g. inclusion bodies. A non-exhaustive list of publications on this can be found in Table 4. In this regard, mid-IR spectroscopy clearly qualifies as a PAT tool, as the spectra can help to elucidate physiological responses to changes of critical process parameters and the kinetics of product formation.

Zeroual et al.⁹⁴ were the first ones to report on differences in spectra of dried bacteria (*Bradyrhizobium japonicum*) in response to different culture conditions. FT-IR spectroscopy has since been used for the investigation of different physiological states of bacteria due to cell cycle stage^{95,96} or as a response to extracellular stressing agents^{97,98}. FT-IR spectroscopic studies on yeast cells and their metabolism cover the autolysis of *S. cerevisiae* in a base wine studying partial hydrolysis of proteins, increase of peptides, free nucleotides, lipids, mannans, and beta-1,3 glucans^{99,100}. Furthermore the metabolomic alterations of *S. cerevisiae* induced by four chemical compounds: ethanol, sodium hypochlorite, sodium chloride and sulfur dioxide¹⁰¹, and the biosurfactant N-alkyltropinium bromide¹⁰², were investigated. Kuligowski et al.¹⁰³ developed a rapid method for the discrimination of entire *P. pastoris* cells grown under different conditions based on the direct acquisition of mid-IR spectra in the bio-fingerprint region (900 – 1800 cm⁻¹) and PLS-DA (partial least squares-discriminant analysis).

The application of FT-IR spectroscopy of whole microorganisms for the analysis of intracellular products was shown for *E. coli* (poly(beta-hydroxybutrate))¹⁰⁴ and recombinant proteins^{105,106}, *Bacillus subtilis* (poly-glutamic acid)¹⁰⁷, *Pseudomonas fluorescens* (alginate)¹⁰⁸, *Rhodotorula* (fatty acid content)¹⁰⁹ and different strains of *Pseudomonas aeruginosa*, *Streptococcus* mutants and *Staphylococcus epidermidis* (total carbohydrate content)¹¹⁰. In most cases quantification was achieved by PLS-regression, except for Refs. 94 and 99, where difference spectra and band area ratios, respectively, were used.

ⁱ The spectral features reflecting different physiological states result from differences in cellular composition, which is of course also the case when a product is accumulated intracellularly. The major difference is that the production of a product is desired and often realized recombinantly, while changes in the physiological state of the microorganisms can be undesired and are simply a response the cells' environment.

Table 4: FT-IR spectroscopic studies on physiological states of microorganism, intracellular products and metabolites.

Publication	Microorganisms	Method	Aim of the study
W Zeroual et al. 1994 ⁹⁴	<i>Bradyrhizobium japonicum</i>	transmission	response to different culture conditions / media
D Helm et al. 1995 ⁹⁵	<i>Bacillus subtilis</i> , <i>Clostridia</i>	transmission	intracellular capsules of poly-glutamic acid, endospore production
KC Schuster et al. 1999 ⁹⁶	<i>C. beijerinckii</i>	transmission / HCA	acetone-butanol-ethanol fermentation, physiological states
M Kansiz et al. 2000 ¹⁰⁴	<i>E. coli</i>	transmission / PLS	quantification of intracellular poly-(beta-hydroxybutyrate)
D Ami et al. 2005 ¹⁰⁵	<i>E. coli</i>	transmission microspectroscopy	kinetics of inclusion bodies (recombinant lipase); difference spectra
D Ami et al. 2006 ⁹⁸	<i>E. coli</i>	microspectroscopy	membrane composition due to cellular stress
S Gross-Selbeck et al. 2007 ¹⁰⁶	<i>E. coli</i>	HTS-XT / PLS-R	quantification of inclusion bodies (protein)
L Marcotte et al. 2007 ¹¹⁰	<i>P. aeruginosa</i> , <i>Streptococcus</i> , <i>S. epidermidis</i>	transmission / band area ratios	quantification of total (poly-)saccharide content
M Burattini et al 2008 ¹¹¹	<i>S. cerevisiae</i>	transmission & ATR microspectroscopy / HCA, PCA	investigation of autolysis
(AP Dean et al. 2008 ¹¹²)	<i>Chlamydomonas reinhardtii</i> (algae)	double-transmission synchrotron microspectroscopy	investigation of carbon allocation in response to growth phase and phosphorus concentration in medium
M Cavagna 2010 ¹⁰⁰	<i>S. cerevisiae</i>	ATR microspectroscopy / PCA	monitoring of autolysis during wine production
L Corte et al. 2010 ¹⁰¹	<i>S. cerevisiae</i>	HTS-XT / PLS	quantitative stress response to ethanol, sodium hypochloride, sodium chloride, sulfur dioxide
RK Saharan et al. 2011 ⁹⁷	<i>Pachysolen tannophilus</i>	KBr tablets	effects of physiological stress induced by ethanol
E Correa et al. 2012 ¹⁰⁸	<i>Pseudomonas fluorescens</i>	HTS-XT / PCA, CVA ^a , PLS	intracellular alginate, cellular composition due to different media
J Kuligowski et al. 2012 ¹⁰³	<i>P. pastoris</i>	transmission microspectroscopy / PLS-DA	differentiation between physiological states induced by N- and P- limitation
J Vongsivut et al. 2013 ¹⁰⁹	strains of <i>Rhodotorula</i> ^b , <i>Thraustochytrium</i> ^c	microspectroscopy / PCA, PLS-DA, SIMCA ^d , HCA, PLS	differentiation and quantification of polyunsaturated fatty acid content
L Corte et al 2014 ¹⁰²	<i>S. cerevisiae</i> , <i>Candida albicans</i>	HTS-XT	stress response to N-alkyltropinium bromide (biosurfactant)

^a canonical variate analysis

^b a marine yeast

^c algae-like fungi

^d Soft independent modelling by class analogy

These reports clearly demonstrate the potential of FT-IR spectroscopy for identification and investigation of different physiological states of microorganisms and the possibility for quantification of intracellular products. In this thesis, the quantification of the storage carbohydrates trehalose and glycogen in *S. cerevisiae* during N-limited growth by FT-IR microspectroscopy was shown off-line (**Publication II**). Employing a novel ultrasound enhanced in-line ATR probe, the spectral changes of the cells could also be observed in-line during fermentation (**Publication III**).

2.3 Acoustic particle manipulation of cells

Acoustic particle manipulation has been used for touch-free, gentle manipulation of biological cells and microorganisms in macro- and microfluidic (sensor) set-ups. A number of articles in the recent Acoustofluidics Series in Lab on a Chip¹¹³ covered different applications for sorting, filtration, separation and concentration of cells: Lenshof et al.¹¹⁴ reviewed microscale continuous flow set-ups, while acoustic trapping of particles and cells in microfluidic systems was covered by Evander and Nilsson¹¹⁵. Wiklund et al.¹¹⁶ report on enhancement of immunoassays and particle sensors by ultrasound, both in microfluidic and macrofluidic set-ups.

Concentration and filtration of cells can be performed in the same set-up: a standing wave is built up inside a flow channel with half-wavelength width, i.e. the pressure nodal plane is located in the center of the channel parallel to the flowⁱ. The cells are concentrated in the pressure nodal plane and the flow is split into different fractions at the end of the channel. One fraction contains the concentrated cell suspension, the other fraction filtered medium. This principle was successfully used for concentration of red blood cells (RBCs) and prostate cancer cells¹¹⁷, the removal of RBCs for the preparation of diagnostic plasma for clinical analysis¹¹⁸, the separation of RBCs and platelets in a high-throughput device¹¹⁹ and for separation of lipids and somatic cells in raw milk for subsequent separate FT-IR analysis³⁰, to name but a few.

Most studies on yeast cells employ larger scale ultrasonic filters for the enrichment or filtration of cells. Several reports on the filtration of *S. cerevisiae* and *E. coli* in different macroscopic resonator set-ups showed that the larger yeast cells (approximately 5 μm diameter) could be efficiently removed, while for the smaller bacteria (approximately 1 μm)

ⁱ The direction of sound propagation is perpendicular to the flow.

the set-up proved less efficient at similar cell concentrations^{120–122}. The large difference in efficiency could successfully be used for separation of the two cell types¹²¹. The dynamics of aggregation of *S. cerevisiae* was studied in a two-wavelength¹²³ and a half-wavelength¹²³ ultrasonic trap, respectively. A microfluidic device for transferring yeast cells from one medium to another (cell washing) was presented in 2004¹²⁴. Radel et al. investigated the viability³⁸ and morphology¹²⁵ of *S. cerevisiae* in standing and propagating wave fields in a multi-wavelength resonator. In a similar set-up the spatial arrangements of *S. cerevisiae* in the ultrasonic standing wave field was studied by immobilizing them in an acrylamide gel in situ¹²⁶ and their proliferation was later studied by immobilization in an agar gel⁴⁶. Radel et al. successfully positioned suspended *S. cerevisiae* in the focus of a confocal Raman microscope and showed that the resulting spectrum was significantly higher than that obtained from the freely suspended cells¹²⁷. Furthermore, the agglomeration of *S. cerevisiae* in a standing wave field was exploited for on-line bioprocesses monitoring by ATR spectroscopy¹²⁸. The set-up described by Jarute et al.⁶⁴ for the on-line determination of intracellular PHB concentration in *E. coli* was slightly modified: by placing an ultrasound transducer opposite the ATR element a resonator was constructed. Spectra of yeast cells could be acquired faster due to the increased settling speed of the cell aggregates as compared to freely suspended cells.

In this thesis, acoustic particle manipulation was combined with in-line ATR probes to enable the acquisition of mid-IR spectra of cells in suspension. With a prototype in-line applicable ultrasound enhanced ATR probe (prototype 1) selective acquisition of *S. cerevisiae* spectra in a stirred suspension could be shown (**Publication I**). With a second prototype (prototype 2), which was designed and built according to ASME (American Society of Mechanical Engineers) Bioprocessing equipment regulations¹²⁹, mid-IR spectra of *S. cerevisiae* could be recorded in-line during fermentation for the first time (to the best of the author's knowledge). Spectral changes due to the intracellular accumulation of trehalose and glycogen could be confirmed by PCA (**Publication III**).

3 ULTRASOUND ENHANCED IN-LINE ATR PROBE

The limited penetration depth of the evanescent wave, approximately 1 to 2 μm , has so far made the in-line acquisition of mid-IR spectra of suspended solid particles, e.g. cells, basically impossible. A reversible agglomeration of the particles within the evanescent field needs to be achieved – while not interfering with the mid-IR spectra or the process, without altering the particles, with high reliability and employing small components to make integration in an in-line probe possible.

The main goal of this thesis was the development of such a method for the acquisition of mid-IR spectra of cells – and other solid particles in suspension – in-line. This was achieved by using acoustic radiation forces exerted by ultrasound in the MHz-regime to deliberately position the cells in the sensitive region of an ATR mid-IR probe or away from it. The principle was first shown by Radel et al.¹³⁰ in a dedicated experimental vessel using an in-line applicable ATR probe fixed opposite an ultrasound transducer for the acquisition of mid-IR spectra of (sub-)micron-sized PTFE particles suspended in tetrahydrofuran. In the following chapter the working principle, design considerations for bioprocess monitoring probes, and two prototype ultrasound enhanced in-line ATR probes are presented.

3.1 Acoustic particle manipulation and ATR spectroscopy

The primary axial radiation force exerted by an ultrasonic (standing) wave can be used to move particles in suspension into the evanescent field of an ATR element, or to keep them away from it. Spectra of particles can thus be acquired even in stirred suspensions. A resonator is built up between an ultrasound transducer and the ATR probe that is placed opposite it and serves as reflector for the ultrasound. A schematic of the principle is shown in Figure 15. The pressure nodal plane of the standing wave is located between either just inside of the surface of the ATR probe (Figure 15 left) when the “pushing frequency”, f_p , is used, and a quarter-wavelength, i.e. $\lambda/4$ of the acoustic wave, away from it (Figure 15 right), when the resonator is driven at the “retracting frequency”, f_r . Since the penetration depth of

the IR beam, and thus the sensitive region of the ATR probe, is limited to 1 to 2 μm , contributions of the cells to spectra acquired during the application of the retracting frequency f_r can be safely excluded.

The combination of the two methods for the targeted acquisition of mid-IR spectra of particles in suspension was first described and patented by Lendl, Radel and Brandstetter^{130–132}. In a previous project Brandstetter¹³² investigated the potential interaction between the ultrasonic and the evanescent field. He concluded that, due to the different nature of the waves and the differences in frequency, the only effect of the ultrasonic field is an increase in temperature of the host fluid (due to damping of the acoustic wave). As the IR-absorption of water depends strongly on temperature, the heating due to the ultrasonic field would lead to changes in the absorbance. Brandstetter showed that this is indeed the case until (thermal) equilibrium is reached. In the present work heating is of no concern, as temperature is well controlled in bioreactors.

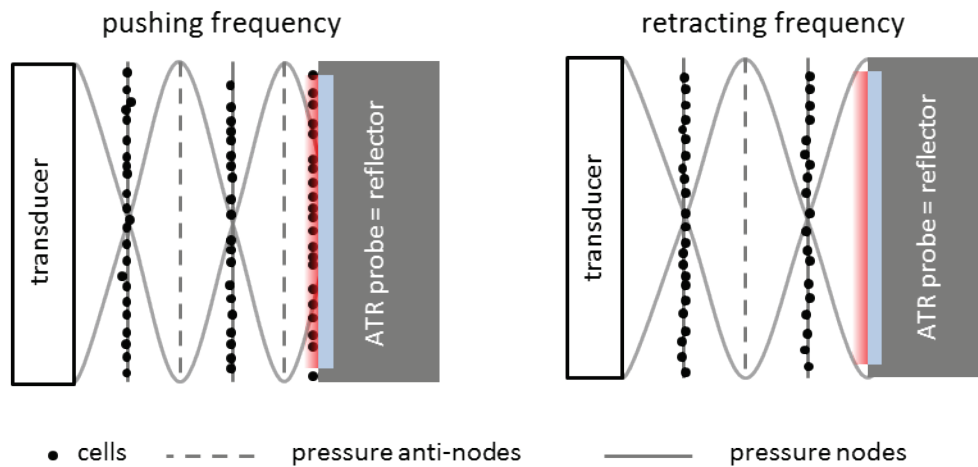


Figure 15: Working principle of the ultrasound enhanced in-line ATR probe: the two modes of operation. The stationary envelope of the pressure amplitude distribution is indicated in light grey. Adapted from Koch et al. (2015) – Publication III. (CC-BY license)

3.2 Design requirements

In order to exploit ultrasonic particle manipulation for in-line mid-IR ATR spectroscopy, a suitable resonator configuration had to be constructed. The basic idea for realizing this was to build an accessory that contained the ultrasound transducer and the wiring for it, into which a commercial ATR probe could be inserted. Basically it consists of a tube with an outer diameter of 25 mm and an inner diameter chosen such that the ATR probe fits tightly.

A with water-tight housing containing the ultrasound transducer is attached to it in such a way that sample can freely flow between the ATR probe (holder) and the ultrasound transducerⁱ. The whole construction has to be compatible with a standard 25-mm-port of a bioreactorⁱⁱ, needs to be autoclavable, and comply with ASME rules for constructions of bioprocessing equipment (ASME BPE [Bioprocessing Equipment])¹²⁹.

3.2.1 Resonator construction

Planar, parallel surfaces of transducer and reflector are important, as they ensure that an acoustic standing wave can be built up and as little acoustic energy as possible is lost. A detailed analysis of the effect of an inclined reflector wall on the resonance quality factor Q (a description of the sound attenuation of a material or system at a given acoustic wavenumberⁱⁱⁱ; the higher the resonance quality factor, the more acoustic energy is stored within the acoustic standing wave and thus the higher the primary axial radiation force F_z^{rad}) is given by Gröschl¹³³: for 32 mm resonator length, an inclination of the reflector of only 1 mrad leads to a 10 to 20% decrease of the quality factor.

Therefore, the ultrasound transducer and the reflector, i.e. ATR probe, need to be held as plane-parallel to each other as possible. As the whole device is inserted into a bioreactor, it has to be robust against vibrations introduced by stirring (i.e. the motor). Furthermore, an electrical connection of the piezoelectric transducer with a signal generator has to be incorporated. The thinnest off-the-shelf coaxial cable available at the time of design was 1.37 mm in diameter, thus a channel of at least 2 mm diameter had to be implemented.

The ultrasound transducer housing is limited to an outer diameter of 25 mm, has to be water-tight, and hold the transducer safely in place. Furthermore, during the assembly of the probe, soldering of the signal transmission cable to the PZT's bull's eye electrode has to be possible. Macor®, a class ceramic developed by Corning Inc. (USA), was identified as a suitable carrier layer for the ultrasound transducer. It has similar acoustic properties (mass density and speed of sound) as borosilicate glass, which has been successfully used as carrier in previous studies^{133,134}, but has the advantage of being machinable.

ⁱ Similar to in-line NIR transmission probes.

ⁱⁱ 25-mm ports are commonly found in industrial bioreactors and in bioreactors used for process development. Another commonly used diameter is 12 mm, due to the diameter of typical ATR probes, construction of an ultrasound accessory that could incorporate such a probe was not feasible.

ⁱⁱⁱ $Q = \frac{k}{2\alpha}$, where k is the wavenumber of the acoustic wave and α is the attenuation coefficient.

3.2.2 ATR probe

In a previous study two different ATR probe tip configurations were tested for applicability: one that has a truncated conic ATR element protruding from it and one that has a plane surface into which the ATR element is integrated. It was possible to acquire spectra of suspended particles (PTFE and *S. cerevisiae*, respectively) with both probes, however, as the sensitive region of the truncated cone-shape ATR are on its lateral surface, an additional ultrasound reflector element had to be designed and attached to the ATR probe to successfully agglomerate particles in this region^{130,132}. Using the flat-tipped probe, this additional reflector could be avoided. Therefore, only flat-tipped ATR probes were used in the present work.

As mentioned before, the outer diameter of the ultrasound accessory needs to fit into a 25-mm-port, thus the diameter of the ATR probe should not exceed approximately 15 mm, to ensure that the remaining wall thickness can house the cable for signal transmission to the ultrasound transducer and at least one O-ring for sealing against the port.

3.2.3 Bioprocessing equipment requirements

Bioprocessing equipment needs to comply with certain rules concerning the design and employed materials. A rule that had to be taken into consideration is the “3D rule” to prevent dead legs, i.e. notches, blind holes or piping segments that are exposed to the process, but do not experience the normal flow. In a bioreactor dead legs can lead to issues with sterility, as the required temperatures for autoclaving cannot be guaranteed in the dead leg and cells could settle there. The 3D rule states that the depth of a sealed piping segment, blind hole or notch should not be more than three times its diameter. This way the turbulent flow maintained inside the bioreactor by stirring keeps up a constant flow in the blind hole.

O-rings are the preferred type of sealing and were therefore used in the developed probe designs wherever possible. The employed materials have to be corrosion resistant, bio-compatible and have comparable thermal expansion coefficients. Examples for FDA-approved materials are fluoroelastomers^{iv} or perfluoroelastomers^v for seals and a number of stainless steels with defined surface finish. Furthermore, machinability of the employed

^{iv} Commonly known by the brand name Viton® (DuPont).

^v Commonly known by the brand name Kalrez® (DuPont).

materials and the availability of tools have to be taken into consideration. A problem encountered concerning these was the maximum drillable length of a (straight) 2 mm hole in stainless steel.

3.3 Prototype 1

The first in-line applicable prototype was designed in cooperation with Stefan Radel, Markus Brandstetter and Volker Bauer. A detailed (German) description can be found in Bauer's project report¹³⁵, the engineering drawings are attached as Appendix A.

Prototype 1 was built in-house (machine shop of the Institute for Applied Physics, TU Vienna). The availability of machines and the desired accuracy narrowed the choice of possible materials; in the end brass was chosen. Brass is not an FDA-compliant material for bioprocessing equipment, but this compromise was made to ensure timely, cost-efficient production. The sealings were cut from Viton® sheets and the PZT was glued to the Macor carrier using Araldite AV 171® (Huntsman Advanced Materials, USA), a one-component epoxy resin, and the bonding was subsequently heat cured. The ultrasound accessory was assembled and combined with a custom made fiber optic ATR probe with 6 mm diameter (IFS, Germany). The ultrasound enhanced ATR mid-IR probe (Figure 16) was then coupled to a Bruker Matrix FT-IR spectrometer using an off-axis mirror and a fiber detector-coupling to an external liquid N₂-cooled MCT (mercury cadmium telluride) detector (Figure 17). This set-up was used for a systematic off-line characterization of ultrasound enhanced ATR mid-IR spectroscopy of *S. cerevisiae* suspensions (**Publication I**). A frequency power synthesizer (FPS2540 limited to 2.5 W output, PSI Systems, Austria) was connected to the PZT for ultrasonic signal generation. Furthermore, the probe was coupled to a bioreactor and several cycles of autoclaving were performed to test the tightness and the robustness of the set-up.

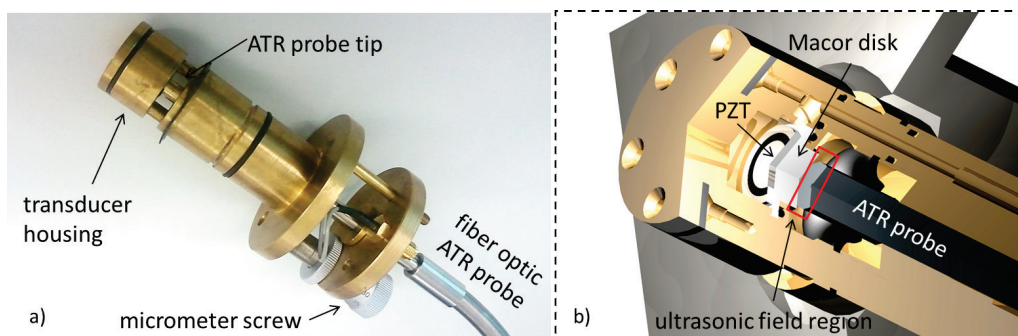


Figure 16: Photograph (a) and rendering of the tip (b) of prototype 1.

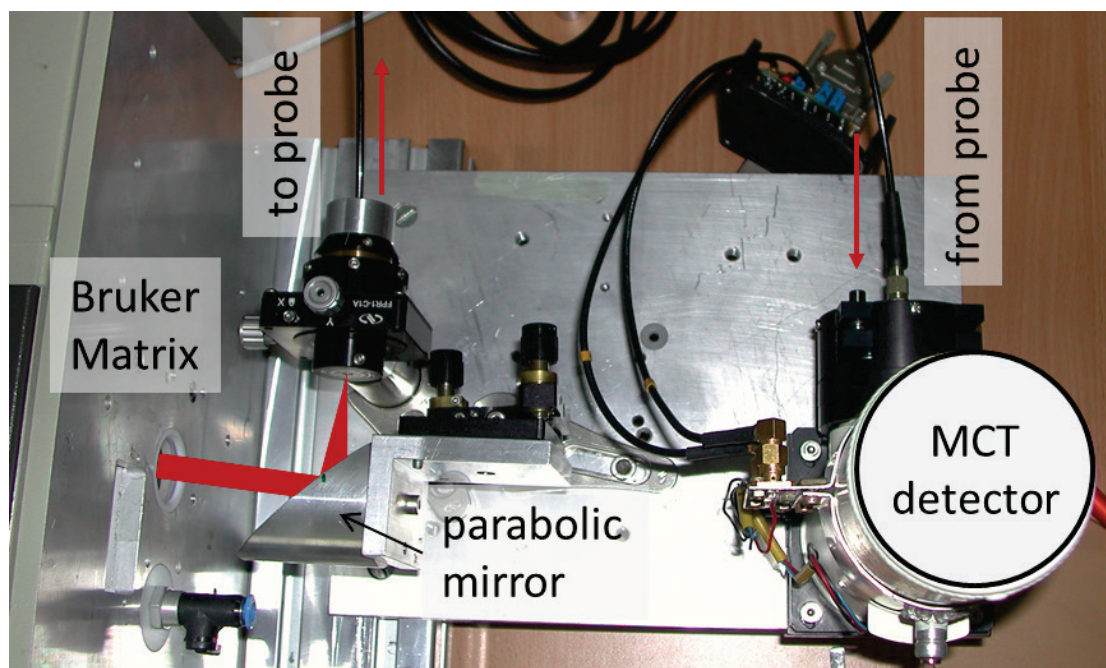


Figure 17: The optical set-up used for prototype 1. A Bruker Matrix spectrometer equipped with an external liquid N₂-cooled MCT detector was used. A parabolic mirror was used for coupling of the IR beam with the optical fiber.

An exploded-view drawing of prototype 1 is shown in Figure 18; the numbers used for the different parts hereafter refer to the numbering in Figure 18. Basically, the construction consisted of the probe holder (6) into which the ATR probe (1) was inserted and a transducer housing (14) held opposite the end of the probe holder by three connector rods (10 & 11). One of the connector rods (11) had a through hole for the cable for signal transmission to the PZT (17). The transducer housing (14) had a through hole at the side facing the ATR probe (1) where the Macor carrier (16) could be inserted. An O-ring (15) was used to seal the carrier (16) and the housing (14) off. The top of the transducer housing (14) was closed by a lid (19) and a flat seal (18). The lid (19) was designed such that it pressed the Macor carrier (16) against the O-ring (15) and ensured tightness. A 10-mm PZT disk (17) was chosen, as the connector rods (10 & 11) considerably limited the available space. A detailed rendering of this part of the construction is shown in Figure 16.

The construction allowed for fine-adjustment of the ultrasound resonator length, i.e. the distance between the ultrasound transducer and the ATR probe tip by means of a micrometer screw (2). By turning this screw, the ATR probe (1), which was fixed to the small disk (3) by a clamping sleeve (4), could be moved relative to the probe holder (6). A flexible membrane seal (9) was used to seal off the ATR probe and the probe holder. The

tube (6) was fixed to a mounting disk (7) that was screwed to the bioreactor's Ingold port using a ring clamp and thus a robust connection with the bioreactor could be established.

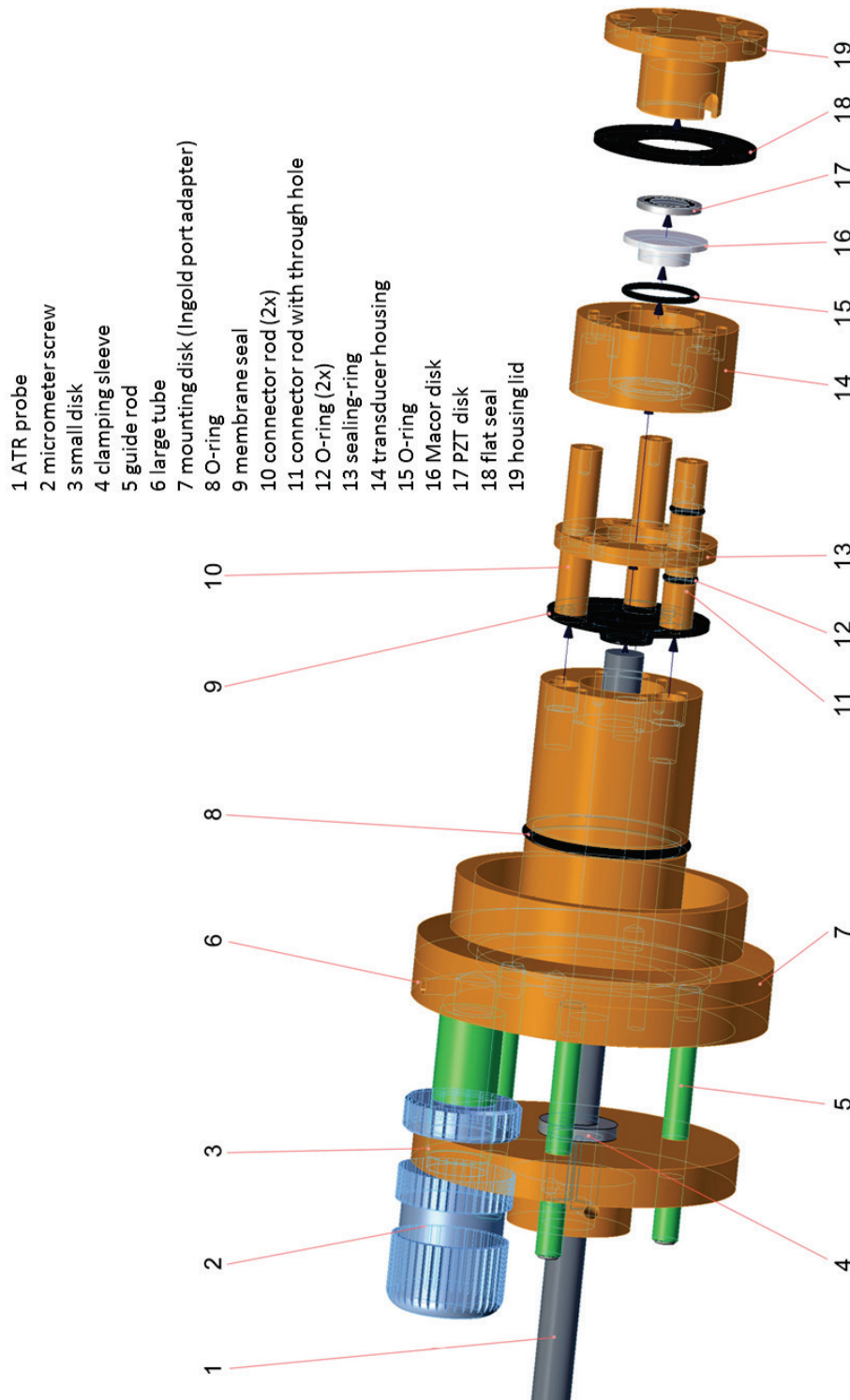


Figure 18: Exploded-view rendering of prototype 1 (adapted with permission from Ref. ¹³⁵).

3.4 Prototype 2

Prototype 2 was designed with knowledge gathered from experiments with prototype 1. Stefan Radel, Pietro Palmesi and the author of this thesis conceived the design and Pietro Palmesi made the engineering drawings (Appendix B) in the course of his Bachelor thesis¹³⁶. This prototype was intended for use in-line, therefore, an FDA-approved stainless steel (1.4571/DIN X6CrNiMoTi17-12-2) was chosen. Furthermore, the membrane seal used in prototype 1 was replaced by an O-ring for increased robustness. A new, more robust spectroscopic set-up was available: a ReactIR 15 spectrometer, a compact, sealed process FT-IR spectrometer equipped with a liquid N₂-cooled MCT detector, and a fiber optic DS (diamond) DiComp AgX (silver halide) probe (both Mettler Toledo, USA) of 1.5 m length. The probe and the spectrometer could be coupled via a plug and play connector and were fit for use in a production environment.

The ATR probe had a diameter of 9.5 mm, therefore a redesign of the ultrasound accessory was necessary (Figure 19, the numbers used for the different parts hereafter refer to the numbering there). Rods could no longer be used to connect the probe holder (5) and the transducer housing (9), as the remaining wall thickness of the probe holder was not sufficient to attach them: while the probe holder of prototype 1 had a wall thickness of 9.5 mm, the potential wall thickness was reduced to 7.75 mm by the larger ATR probe diameter when using the same concentric design. This would also have resulted in difficulties with the hole for electrical connection of the ultrasound transducer: the grooves for the outer O-ring (6) and for the inner O-ring (7), both with a width of 1.5 mm, needed to be 1.36 mm and 1.35 mm deep, respectively. However, with the chosen material, the remaining wall thickness (5 mm) would not allow for drilling a 2.5 mm hole at a length of approximately 64 mm without the risk of breaking the wall. Therefore, an acentric approach was chosen, which left enough space on one side of the probe holder (5). The probe holder (5) incorporated a transducer housing holder (5a) equipped with two positioning rods for increased stability of the transducer housing (9) and a through hole for the coax cable. The transducer housing was screwed to the transducer housing holder (5a) and the interface sealed by a flat gasket (8). In a schematic cross-section of prototype 2 (Figure 20a) the acentric design can be seen.

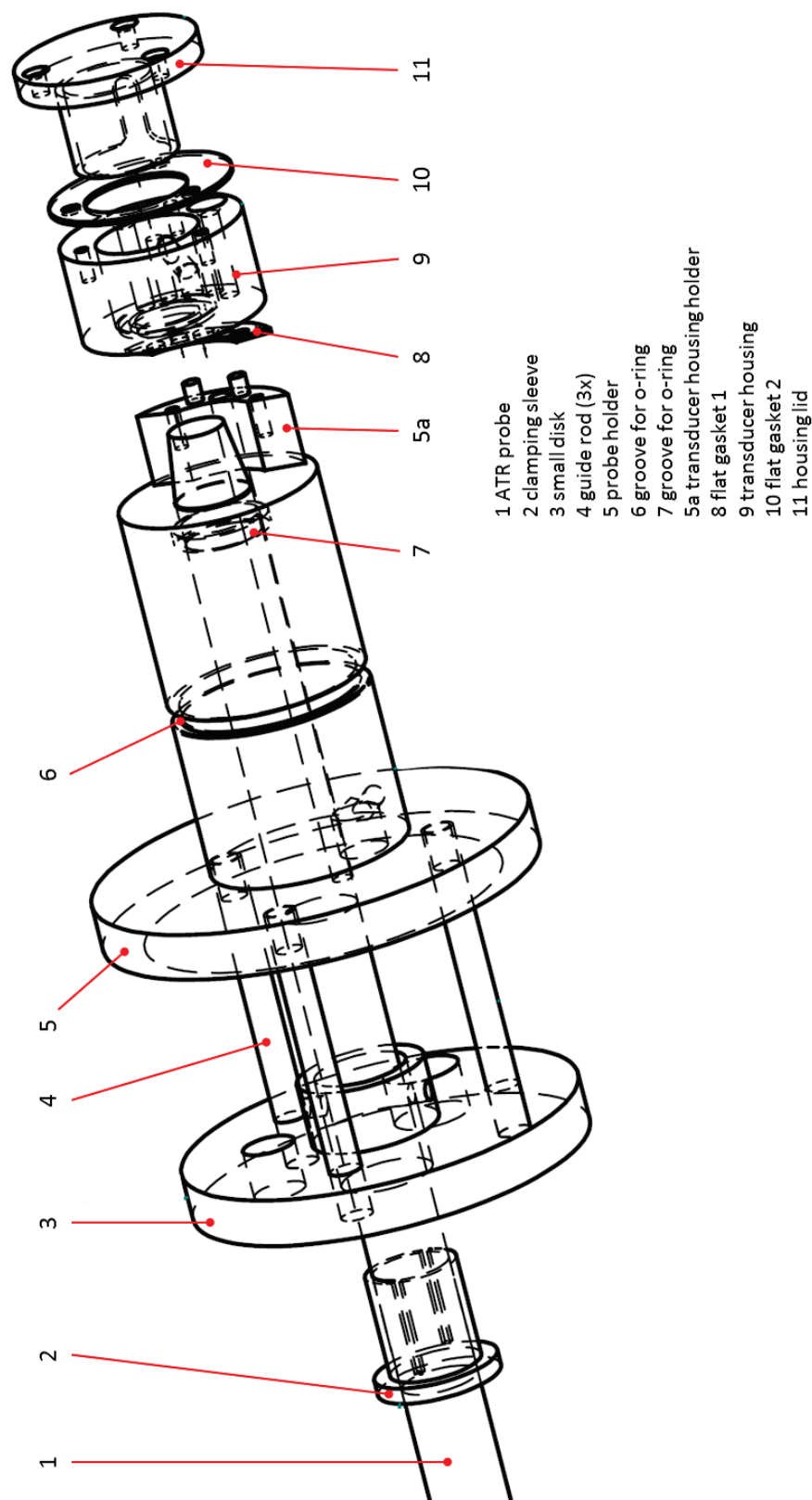


Figure 19: Drawing of prototype 2.

Prototype 2 was built by a machine shop specialized in producing prototypes (APEX technical solutions GmbH, Austria) and subsequently assembled (Figure 20b and Figure 21a). During assembly, a construction fault was discovered: the groove for the inner O-ring (7) was too close to the probe holder surface and, due to the conic shape of the ATR probe tip, tightness could not be guaranteed. As machining a second groove set further back would have led to issues with the 3D rule at the location of the initial groove, the transducer housing holder (5a) was extended. The extension was designed with Lego® pieces in mind: it was held in place by the positioning rods on the transducer housing holder and, in turn, incorporated positioning rods for the transducer housing (for details see Appendix C).

The same modified (limited to 2.5 W max power output) frequency power synthesizer (FPS 2540, PSI Systems, Austria) connected to the PZT as for experiments with prototype 1 was used for ultrasound signal generation and amplification. For automated frequency and power control a custom LabVIEW® script and GUI (graphical user interface) (National Instruments, USA) were developed¹³⁷. Connection of the FPS 2540 with a measurement computer realized via a PCI I/O card (Peripheral Component Interconnect Input/Output; National Instruments type 6025E). The script allowed for automated switching between two user-defined frequencies at user-defined time intervals.

Prototype 2 was coupled to a bioreactor (Figure 21b) and the first mid-IR spectra of *S. cerevisiae* inside a bioreactor (i.e. in situ) were successfully recorded. Changes in the carbohydrate content of the cells due to nitrogen-limitation, i.e. their physiological response to nutrient stress, could be observed from spectra recorded in-line (**Publication III**).

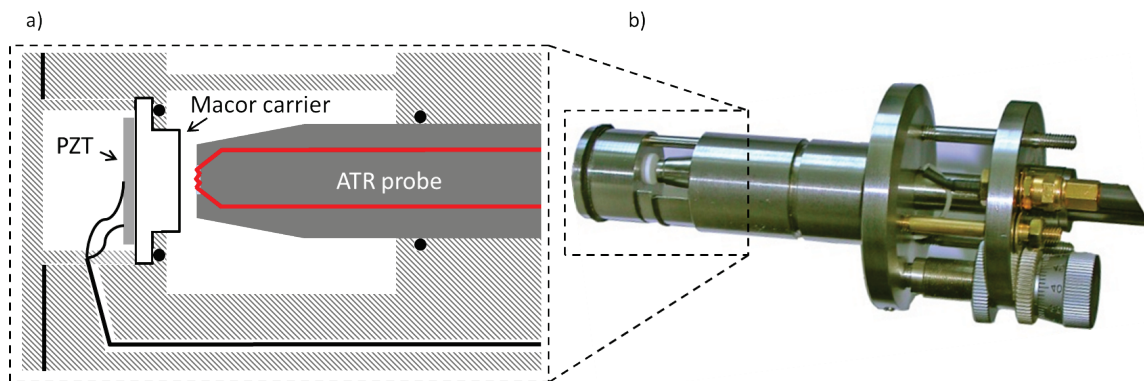


Figure 20: Schematic cross-section of prototype 2 (a): the acentric positioning of the ATR probe relative to the probe housing is clearly visible. Photograph (b) of prototype 2. Both: adapted from Koch et al. 2015 – Publication III

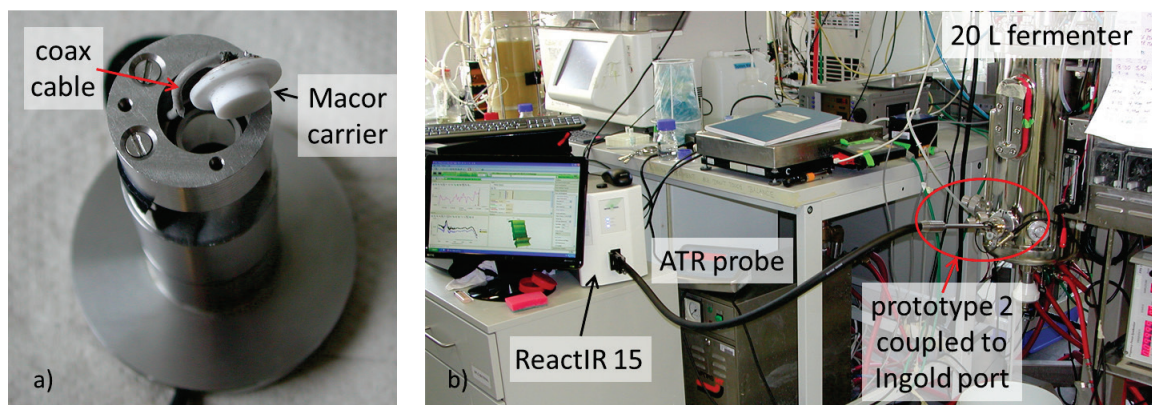


Figure 21: Photograph of prototype 2 during assembly (a): the PZT (not visible) bonded to the Macor carrier is already soldered to the coax cable. Prototype 2 was used for in-line measurements in a bioreactor.

4 PERFORMANCE

In this chapter the employed spectroscopic systems are presented and their performances are compared. Single beam spectra, i.e. the intensity the reaches the detector at each wavenumber when no sample is present in the beam path (i.e. the sample is air), are presented to give insight into the accessible wavenumber ranges and the general transmission characteristics of the respective set-up. For the set-ups that were used for measurement of aqueous samples, i.e. three in-line ATR probes and an ATR element that was coupled to a laboratory spectrometer for the acquisition of reference spectra, the single beam spectra of water as sample are given as well. All spectra were recorded with a spectral resolution of 4 cm^{-1} . The intensity values cannot be compared directly between the set-ups, as they depend on the detector employed and the electronics used for signal acquisition (e.g. the gain factor). They are usually given in arbitrary units without dimensions. The general shape and wavenumber regions in which very little light reaches the detector, i.e. where the intensity becomes very low or reaches zero, can however be compared. Additionally, the spectra of suspended *S. cerevisiae* sedimented onto ATR surface and pushed against it by the acoustic radiation force are compared for the probes used in the two prototypes. An overview over the spectroscopic systems, the accessible wavenumber regions and their use within the publications that make up this thesis is given in Table 5.

Table 5: Spectroscopic measurement set-ups used in this thesis, the respective accessible wavenumber regions.

Measurement set-up	Wavenumber range (cm^{-1})		Publication
	in air	in H_2O	
Bruker Matrix spectrometer & prototype ATR probe	1800 – 600	1400 - 700	I
Bruker Hyperion 3000 coupled to Tensor 37	4000 – 700	n.a.	II
Bruker Tensor 37 equipped with Platinum ATR	3600 – 2400 & 1900 - 800	3100 – 2400 & 1900 - 800	III
Mettler Toledo ReactIR 15 & fiber optic DiComp probe	1800 – 850	1800 – 1750 & 1550 - 900	III, IV, V
Mettler Toledo ReactIR 45 & optical conduit DS4 probe	3600 – 2600 & 1900 - 800	3000 – 2600 & 1800 - 900	V

4.1 Bruker Hyperion 3000 coupled to Tensor 37

The Hyperion 3000, a FT-IR microscope, was used for acquisition of off-line spectra of microorganisms. Drops of washed *S. cerevisiae* suspensions were deposited on ZnSe and CaF₂ slides and the liquid phase was allowed to evaporate. Transmission spectra of the dried cells were obtained with a 15x Cassegrain objective and a liquid N₂-cooled single-point MCT detector. A Bruker Tensor 37 coupled to the microscope served as interferometer. The proprietary software OPUS (versions 6.5 and 7.0, Bruker Optics, Germany) was used for instrument control and data recording. The microscope was equipped with an automated x-y-z-stage. Due to the broad transmission ranges of ZnSe, the complete mid-IR spectrum is accessible with this set-up (Figure 22).

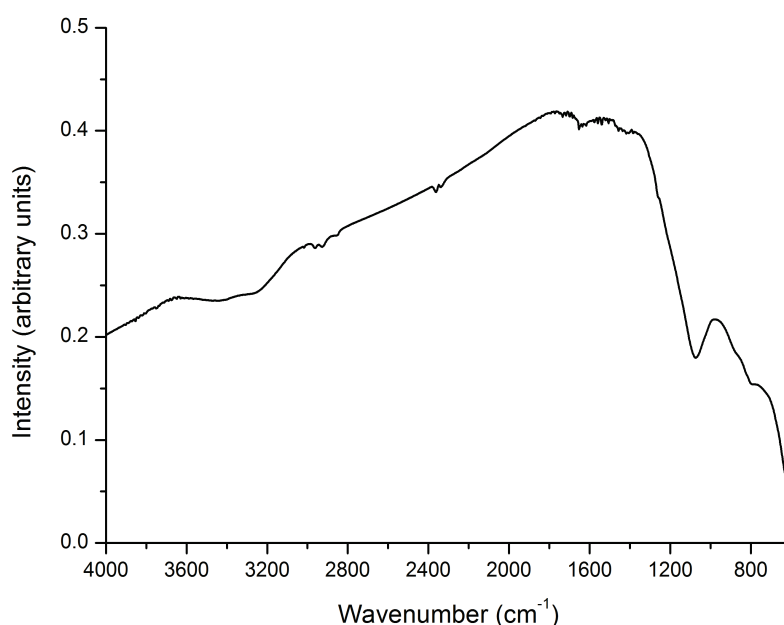


Figure 22: Single beam spectrum recorded with the Bruker Hyperion 3000 microscope coupled to the Tensor 37 spectrometer with a ZnSe slide, as used for transmission measurements of dried cell samples, in the beam path.

4.2 Bruker Tensor 37 equipped with Platinum ATR

A Bruker Tensor 37 spectrometer equipped with a DTGS (deuterated tryglycine sulfate) detector and a Bruker Platinum ATR, a single bounce diamond ATR element, was used for the acquisition of reference spectra carbohydrates in solution and in crystalline form. The short interaction path length with water is reflected by the relatively small intensity

reduction between 1800 and 900 cm^{-1} (Figure 23) compared to air. The wavenumber region between 1900 and 2400 cm^{-1} is not accessible for measurements due to the absorption of the diamond ATR element. Even though the set-up was constantly purged with dry air, intense water vapor bands are visible (1400 – 1800 cm^{-1}).

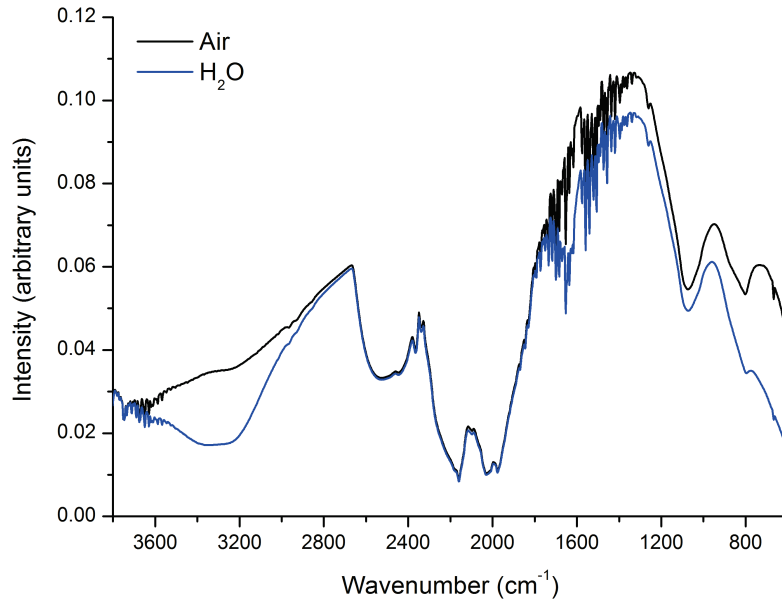


Figure 23: Single beam spectra recorded with the Bruker Tensor 37 spectrometer equipped with Platinum ATR in air (black line) and with a drop of water deposited on the ATR surface (blue line).

4.3 Prototype 1: Bruker Matrix & prototype ATR probe

For optimum exploitation of acoustic particle manipulation a custom-built, flat-topped ATR probe was acquired from Infrared Fiber Sensors (IFS, Germany). It was coupled to a Bruker Matrix spectrometer with an off-axis mirror; a photo of the optical set-up can be seen in Figure 17 (page 52). Opus 6.5 was used for instrument control and data recording. From the single beam spectra of the set-up with either air or water as sample two things are evident: the higher wavenumber region (above 1800 cm^{-1}) is not accessible and water significantly lowers the transmission in the lower wavenumber region (Figure 24a). The high-wavenumber cut-off is due to the transmission characteristics of the AgX fiber and the diamond ATR element, respectively. A possible explanation for the strong decrease of transmission is that the angle of incidence ϑ_i is close to the critical angle for total reflection

ϑ_c for total reflection at the interface of the diamond ATR element and water. This leads to a higher penetration depth into the sample and therefore higher absorption.

This spectroscopy set-up was used in prototype 1 for the acquisition of spectra of *S. cerevisiae* in suspension. In order to assess the maximum achievable absorbance from yeast cells, a drop of a suspension was placed on the horizontal ATR surface (i.e. the probe was held vertically) and the cells were allowed to sediment. Mid-IR spectraⁱ were continuously recorded until the absorbance did not change any more (Figure 24b, black line). This was compared to spectrum obtained by pushing the cells against the ATR element by the acoustic radiation force, i.e. during the application of the pushing frequency f_p , when the probe was immersed in a yeast suspension (Figure 24b, red line). Lower absorbance values were found for ultrasound-enhanced spectra, indicating that fewer cells were in the sensitive region of the ATR element than for the sediment. There are several possible explanations for this: for one, the probe was held at an angle of 135° during ultrasound enhanced spectrum acquisition, i.e. the acoustic radiation force was working against gravity (at a 45° angle). When the cells start to form larger agglomerates under the influence of the radiation force, at some point the gravitational force becomes larger than the radiation force (as used in acoustic cell filters^{42,134}). Secondly, only cells present in the small volume between the ATR surface and the first pressure antinode (compare Figure 15 right, page 48) will be pushed against the surface and thus contribute to the spectrum, while basically all cells present in the suspension above the ATR element's surface could contribute to the spectrum of the sediment. Furthermore, investigations of the spatial arrangement of yeast cells in the pressure nodal planes of a standing wave field^{46,126} indicated that the cells were not densely packed and were not in direct contact with each other (i.e. not touching). The "thickness" of the agglomerates, i.e. the number of cells held within a pressure nodal plane in direction of sound propagation, was found to vary along the pressure nodal plane from single cells to five or ten cells; an effect of the primary transverse radiation force. When the cells sediment, one would assume a relatively close packing with the cells touching each other.

ⁱ Water was used as a background.

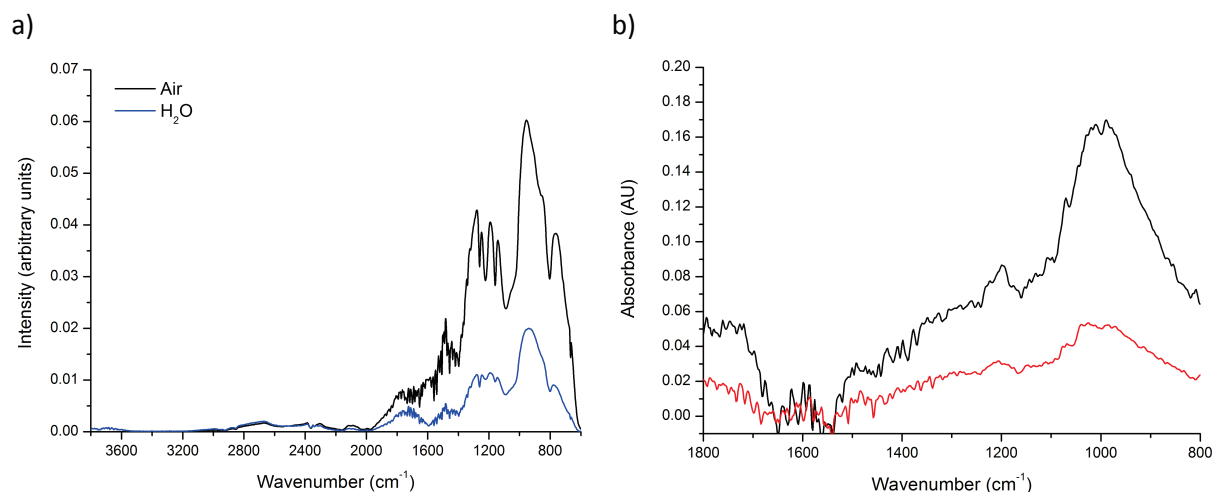


Figure 24: a) Single beam spectra recorded with a Bruker Matrix spectrometer coupled to the fiber optic probe used in prototype 1 in air (black line) and with the probe submerged in water (blue line). b) Spectra of *S. cerevisiae* suspended in water: after sedimentation onto the horizontal ATR element's surface (black line) and by pushing the cells against the ATR by the acoustic radiation force (red line).

4.4 Prototype 2: Mettler Toledo ReactIR 15 & fiber optic DS DiComp probe

The ReactIR 15, a compact, sealed, process spectrometer equipped with a liquid N₂-cooled MCT detector, was connected to a DS DiComp 1.5 m AgX probe (both Mettler Toledo Autochem, Switzerland/USA). Spectrometer control and data recording was handled by the dedicated software iC IR 4.2. This spectrometer and probe were specifically chosen for in-line bioprocess monitoring as they could be combined with the ultrasound accessory. The upper limit of the accessible wavenumber range is again governed by the IR transmission of the silver halide fiber and the diamond ATR element. Multiple internal reflections lead to a discernable decrease in transmission when water is used as sample (compare Platinum ATR, which is a single bounce ATR element), but it is still satisfactory (Figure 25a).

The set-up was used in prototype 2 for the acquisition of spectra of *S. cerevisiae* in situ during fermentation. Using the same experimental protocol as for prototype 1, the maximum attainable absorbance from yeast cells was assessed and compared to the absorbance found when cells were pushed against the ATR element's surface (Figure 25b). Similar to prototype 1, lower absorbance values were found when the cells were pushed against the ATR element's surface. Spectral features, however, were better resolved with this probe compared to prototype 1.

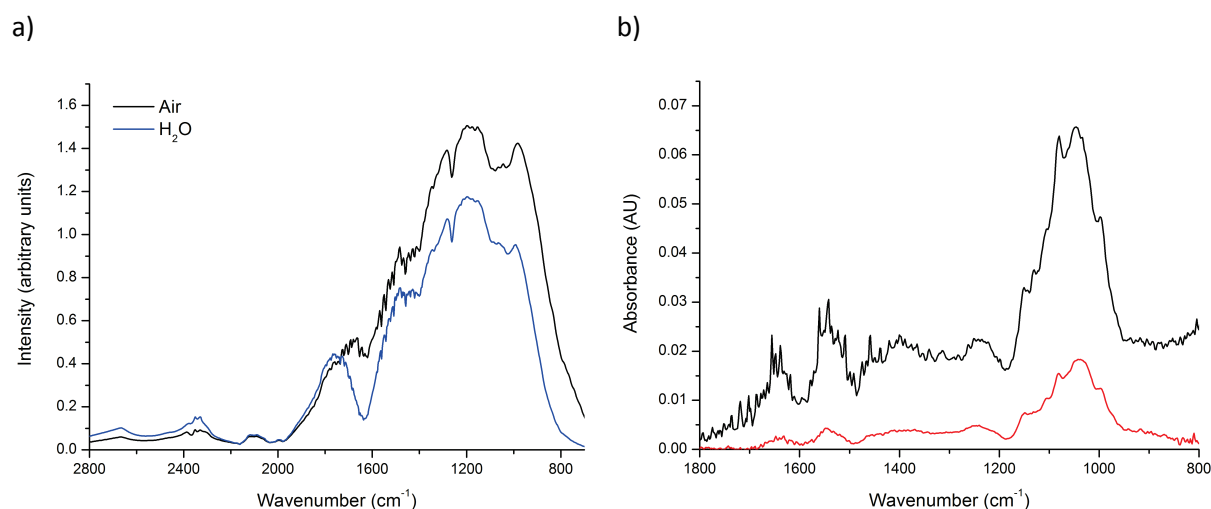


Figure 25: a) Single beam spectra recorded with the Mettler Toledo ReactIR 15 spectrometer equipped with DS DiComp AgX probe (prototype 2) in air (black line) and with a drop of water deposited on the ATR surface (blue line). b) Spectra of *S. cerevisiae* suspended in water: after sedimentation onto the horizontal ATR element surface (black line) and by pushing the cells against the ATR by the acoustic radiation force (red line).

4.5 Mettler Toledo ReactIR 45 & optical conduit K4 probe

In addition to the above mentioned ReactIR15 equipped with the fiber optic probe, a more sophisticated process spectrometer could be tested during this thesis: the ReactIR 45 equipped with a liquid N₂-cooled MCT detector. Here, an optical conduit probe with a diamond ATR sentinel probe head for coupling to a 25-mm Ingold standard port was used. The conduit probe was equipped with four mirrored knuckles to facilitate connection to the fermenter. One of the mirrors of the conduit is adjustable by three screws to optimize light transmission in different conduit positions. Spectrometer and optical conduit were purged with dried air. Water as sample leads to a reduced transmission compared to air (Figure 26); the decrease is slightly lower than observed for the fiber optic ATR probe connected to the ReactIR 15.

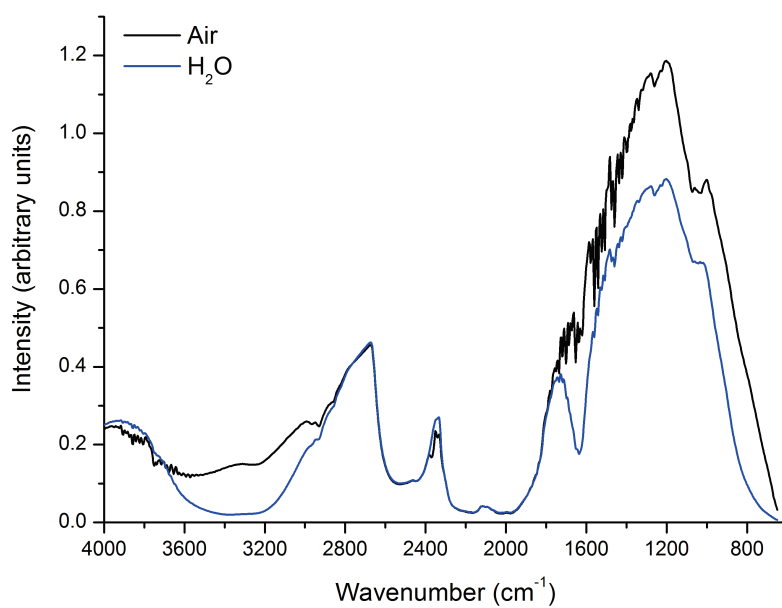


Figure 26: Single beam spectra recorded with the ReactIR 45 equipped with an optical conduit ATR probe with either air (black line) or water (blue line) as sample.

5 INTRODUCTION TO PUBLICATIONS

In this chapter, summaries of the experiments conducted for and the findings of papers published and drafted for this cumulative thesis are given. They are adaptations of the respective abstracts of publications and re-used with permission (CC-BY). Table 6 lists the author's contribution to the individual publications.

Table 6: Author's contribution to the publications for this cumulative thesis

	Publication				
	I	II	III	IV	V
Design of experiment	xxx	xx	xxx	xxx	xxx
Data acquisition	xxx	x	xxx	xxx	xxx
Data analysis	xxx	xxx	xxx	xx	xxx
Interpretation	xxx	xxx	xxx	xx	xxx
Draft/revision of manuscript	xxx	xx	xxx	xxx	xxx

Level of involvement xxx... strong, xx... medium, x... little

Publication I

Ultrasonic Manipulation of Yeast Cells in Suspension for Absorption Spectroscopy with an Immersible Mid-Infrared Fiberoptic Probe

Cosima Koch, Markus Brandstetter, Bernhard Lendl, Stefan Radel, *Ultrasound in Medicine and Biology* 39(6) (2013), 1094-1101. DOI: 10.1016/j.ultrasmedbio.2013.01.003

This paper shows applicability of ultrasound-enhanced ATR spectroscopy of suspensions presented by Lendl et al.¹³¹ to *S. cerevisiae*. First an experimental set-up as described in Radel et al.¹³⁰ and subsequently prototype 1 of the ultrasound enhanced ATR mid-IR in-line probes was used. The experimental set-up consisted of a brass chamber with openings on

opposing walls, one of which held the ATR probe, the other the ultrasound transducer. The two other walls were made of glass to allow for visual inspection and the angle between acoustic radiation force and gravity was 90° (the ATR probe was held horizontally). Prototype 1 was immersed into a beaker at an angle of about 45° (facing downwards), therefore the angle between the acoustic radiation force and the gravitational force was approximately 135° . For the two set-ups different pushing frequencies were found that enabled the acquisition of cell spectra: 1.863 MHz and 1.990 MHz, respectively. A comparison of the maximum absorbance values reached when letting a *S. cerevisiae* suspension settle onto the vertically positioned ATR probes (i.e. the ATR element was horizontal) with values reached when the same suspension was used to acquire cell spectra in the experimental set-up and with prototype 1 showed that approximately 50% and 30% of the respective maximum absorbance could be reached. This was attributed to the fact that the acoustic radiation force worked partially against the gravitational force acting on the cells in prototype 1.

Furthermore, the repeatability of pushing cells against the and away from the ATR element and the influence of cell concentration on the obtained signal were investigated for prototype 1. It was found that the maximum mid-IR absorption of *S. cerevisiae*-specific bands during application of a sequence of switching between pushing and retracting frequency correlated with cell concentration. These bands also increased faster, i.e. reached the maximum attainable value faster, for higher cell concentrations when the pushing frequency was applied.

The results of these experiments led to the development of prototype 2 (**Publication III**).

Publication II

Determination of carbohydrates present in Saccharomyces cerevisiae using mid-infrared spectroscopy and partial least squares regression

Maria Reyes Plata, Cosima Koch, Patrick Wechselberger, Christoph Herwig, Bernhard Lendl, Analytical and Bioanalytical Chemistry 405(25) (2013), 8241-50. DOI: 10.1007/s00216-013-7239-9

This paper shows the feasibility of quantitative determination of carbohydrates in dried *S. cerevisiae* cells by transmission FT-IR microspectroscopy and PLS-R. In order to build the

regression models, reliable reference methods for trehalose, glucose, glycogen and mannan quantification had to be identified and optimized.

High performance liquid chromatography (HPLC) coupled with a refractive index (RI) detector was identified as a suitable method for monosaccharide and disaccharide quantification. A Recex RCM-Monosaccharide Ca^{2+} column was used to obtain complete separation of glucose, mannose and trehalose peaks. Yeast cells in suspensions were ruptured by bead-milling in order to access the intracellular carbohydrates; samples were subsequently split into three aliquots: one for determination of total carbohydrates using the phenol-sulphuric method, one for determination of mannan as mannose by HPLC-RI after hydrolysis by HCl, and one for determination of glucose, trehalose and glycogen. This last aliquot was centrifuged and the glucose and trehalose content in the supernatant was determined by HPLC-RI. Glycogen, which is insoluble in water, was extracted from the pellet by enzymatic hydrolysis (amyloglucosidase enzyme) to glucose and subsequently determined by HPLC-RI. Linear concentration range, accuracy, precision, limit-of-detection and limit-of-quantification were examined to check the reliability of the chromatographic method for each analyte.

With these reference analyses in place, the change in carbohydrate content of *S. cerevisiae* during nitrogen-limited fed-batch fermentation was studied. FT-IR spectra of washed, dried cells were acquired with a FT-IR microscope and PLS-R models for glycogen, trehalose, and mannose were successfully built. Determination of intracellular carbohydrates by FT-IR microspectroscopy could be performed within 30 minutes of sampling, while the reference analyses took between one hour and 26 hours (glycogen determination).

The suitability of FT-IR spectroscopy for quantitative determination of intracellular metabolites accumulated due to nutrient stress, i.e. trehalose and glycogen, could be shown. These results led to the experiments presented in **Publication III**: could these changes also be observed in-line using the ultrasound enhanced ATR probe?

Publication III

Ultrasound-Enhanced Attenuated Total Reflection Mid-infrared Spectroscopy In-Line Probe: Acquisition of Cell Spectra in a Bioreactor

Cosima Koch, Markus Brandstetter, Patrick Wechselberger, Bettina Lorantfy, Maria Reyes Plata, Stefan Radel, Christoph Herwig, Bernhard. Lendl, *Analytical Chemistry* 87(4) (2015), 2314-2320. DOI: 10.1021/ac504126v

This article presents a novel method for selective acquisition of FT-IR spectra of microorganisms in-line during fermentation on the example of *S. cerevisiae*. Prototype 2 of the ultrasound enhanced in-line ATR probes was presented and tested in-line during fed-batch fermentations of *S. cerevisiae*. The aim was to monitor changes of cellular composition due to nutrient limitation as observed in **Publication II**. Control over the position of the cells was achieved by tuning the ultrasound frequency: a frequency of 2.41 MHz was used for acquisition of spectra of the cells (f_p) and 1.87 MHz for retracting the cells from the ATR element and, therefore, allowing for acquisition of spectra of the medium. Investigation of different stirring speeds (600 – 1200 rpm) showed that an acceptable signal-to-noise could be maintained at 800 rpm. The results show that the proposed design is fit-for-purpose. A lack of nitrogen-source in the feed medium induced the accumulation of storage carbohydrates (trehalose and glycogen) inside the cells. Changes in biochemical composition were visible in the spectra of the cells recorded in-line during application of f_p . The method described in **Publication II** was used for acquisition of reference FT-IR spectra of samples drawn from the bioreactor. The changes observed in the off-line spectra corresponded to those found in **Publication II**, i.e. an increase in trehalose and glycogen was observed. Comparison with single analyte ATR spectra of trehalose, glycogen, glucose and mannan, i.e. the major carbohydrates present in *S. cerevisiae*, and principal components analysis revealed that the changes observed in the in-line cell spectra correlated well with the bands specific for trehalose and glycogen.

The applicability and capability of ultrasound enhanced in-line ATR mid-IR spectroscopy as real-time PAT method for in situ monitoring of biochemistry of cells during fermentation could be shown.

Publication IV

Multi-analyte quantification in bioprocesses by Fourier-transform-infrared spectroscopy by partial least squares regression and multivariate curve resolution

Cosima Koch, Andreas E. Posch, Héctor C. Goicoechea, Christoph Herwig, Bernhard Lendl, *Analytica Chimica Acta* 807 (2014), 103 – 110. DOI: 10.1016/j.aca.2013.10.042

This paper presents the quantification of penicillin V and phenoxyacetic acid, its precursor, in-line during *P. chrysogenum* fermentations by FT-IR spectroscopy and PLS-R and MCR-ALS.

First, the applicability of a mid-IR ATR fiber optic probe was assessed off-line by measuring standards of the analytes of interest and investigating matrix effects of the fermentation broth. Wavenumber regions specific for the analytes where other components of the fermentation broth did not interfere were identified. Subsequently, measurements were performed in-line during four fed-batch fermentations with on-line HPLC for the determination of penicillin V and phenoxyacetic acid as reference analysis. Semi-synthetic, i.e. using spectra of synthetic standards and in-line spectra acquired during fermentation, PLS and MCR-ALS models were built taking the previously identified wavenumber regions into account. Different preprocessing steps were tested; for both analytes and regression methods mean-centered first-derivate (Savitzky-Golay) spectra gave the best results (identified by the lowest RMSECV and RMSEP, respectively). MCR-ALS was performed using the following constraints: non-negativity for analyte concentrations (physical constraint), correspondence among species in the experiments (mass balance) and correlation of the concentrations of analytes in calibration samples with previously determined reference concentrations.

Validation was performed by comparison of single analyte spectra with the selectivity ratio of the PLS models and the extracted spectral traces of the MCR-ALS models, respectively. The achieved RMSECV and RMSEP, respectively, were comparable: for the PLS regressions RMSECV of 0.22 g L⁻¹ for penicillin V and 0.32 g L⁻¹ for phenoxyacetic acid and for MCR-ALS the RMSEP were 0.23 g L⁻¹ for penicillin V and 0.15 g L⁻¹ for phenoxyacetic acid. MCR-ALS required smaller wavenumber regions than PLS for the achieved prediction/cross-validation errors. The major difference between PLS and MCR-ALS is that PLS does not require any process knowledge apart from reference concentration values, while a priori

knowledge can and should be implemented by choosing the appropriate constraints for MCR-ALS.

A general work-flow for building and assessing chemometric regression models for the quantification of multiple analytes in bioprocesses by FT-IR spectroscopy was derived. The choice

Publication V

Comparison of fiber optic and conduit attenuated total reflection (ATR) Fourier transform infrared (FT-IR) setup for in-line fermentation monitoring

Cosima Koch, Andreas E. Posch, Christoph Herwig, Bernhard Lendl, Applied Spectroscopy (major) revisions under way

In this paper, the performances of a fiber optic and an optical conduit in-line ATR mid-IR probe, respectively, for in situ monitoring of *P chrysogenum* fermentations were compared. The fiber optic probe was connected to a sealed, portable, FT-IR process spectrometer (ReactIR 15) via a plug-and-play interface. The optical conduit, on the other hand, was connected to a FT-IR process spectrometer (ReactIR 45) via a knuckled probe with mirrors that had to be adjusted prior to each fermentation and both, optical conduit and spectrometer were purged with dry air. Penicillin V and phenoxyacetic acid concentrations were determined by on-line HPLC and the obtained concentrations were used as reference to build PLS-R models. The same wavenumber regions were used and the same pre-processing was applied to data acquired with both spectrometers to enable comparison of the RMSECV. RMSECV were found to be 0.2 g L^{-1} (phenoxyacetic acid) and 0.19 g L^{-1} (penicillin V) for the fiber optic setup and 0.17 g L^{-1} (both phenoxyacetic acid and penicillin V) for the conduit setup. Higher noise-levels and spectrum-to-spectrum variations of the fiber optic setup lead to higher noise of estimated (i.e. unknown) phenoxyacetic acid and penicillin V concentrations than was found for the conduit setup. It seems that a trade-off has to be made between ease of handling (fiber optic setup) and measurement accuracy (optical conduit setup) when choosing one of these systems for bioprocess monitoring.

6 CONCLUSIONS AND OUTLOOK

Several contributions to advancing mid-IR bioprocess monitoring could be made in the course of the thesis. The herein developed technologies allowed for further insight into bioprocesses in terms of qualitative and quantitative changes occurring in the spectra of microorganisms and fermentation broth, respectively.

An in-depth analysis of mid-IR spectra of dried whole cells acquired off-line allowed for monitoring changes of the chemical composition of *S. cerevisiae* induced by feeding with nitrogen-deficient medium. Qualitative changes in the spectral region of carbohydrates were observed. For quantitative analysis of the spectral data by PLS-R, reliable reference methods, i.e. wet-chemical methods and HPLC-RI, had to be established. The advantages of determination by FT-IR spectroscopy over the reference methods were reduced sample handling and faster analysis (results could be obtained within 30 minutes from sampling compared to between one hour and 26 hours for reference analyses). Even though off-line mid-IR microspectroscopy of microorganisms does not qualify as a PAT tool in the strict sense (off-line instead of in-line, timely results), it is a valuable tool for increasing bioprocess understanding and quality assurance: changes of the chemical composition of cells, i.e. their physiological response to process conditions or variability in raw materials, could be used to identify deviations from desired product quality even before they occur. This opens the path for future “feed-forward” process and quality control.

In a next step, a method for in-line acquisition of cell spectra was developed. For the first time, to the best of the author’s knowledge, mid-IR spectra of cells could be recorded in-line during fermentations. This was achieved by the combination of ultrasonic particle manipulation with a mid-IR ATR fiber optic probe. A prototype ultrasound enhanced fiber optic mid-IR ATR probe was designed and constructed in accordance with ASME standards for bioprocessing equipment: a small, robust, process spectrometer and fiber optic probe were combined with an in-house developed and optimized ultrasound accessory. Real-time monitoring of changes of cellular composition was thus possible without the need for removal of a sample from the process environment.

The described method was robust against stirring at speeds usually employed in bioprocessing and aeration did not influence the acquisition of spectra. The quality of the obtained cell spectra, i.e. the signal-to-noise-ratio, however, was significantly lower than that of spectra of dried cells acquired off-line. This was attributed to the absence of water in off-line spectra and the use of a high-end laboratory microspectrometer. The high spectral background of water furthermore leads to a restricted wavenumber region available for analysis. Quantitative analysis was therefore not possible, but qualitative changes were identified by PCA and correlated well with spectral features of the carbohydrates of interest.

The fact that changes in the carbohydrate content of *S. cerevisiae* could be observed qualitatively using the novel ultrasound enhanced in-line fiber optic ATR probe is a step towards chemical analysis of whole cells in-line in real-time. There is clearly room (and need) for improvement of spectral quality. A comparison of state-of-the-art process spectrometers and ATR probes for in-line quantification of solutes in the medium of *P. chrysogenum* fermentations showed that the signal-to-noise level and overall stability was higher for a high-end process spectrometer equipped with an optical conduit ATR probe than for a compact, robust, process spectrometer equipped with a fiber optic ATR probe. This was attributed to two factors: the high absorption of the AgX fiber compared to the optical conduit, which leads to a reduction in transmitted intensity and a limited wavenumber range, and the less sophisticated spectrometerⁱ. The large diameter of the available optical conduit ATR probe, however, made the integration of an ultrasound accessory for this probe impossible.

One possibility to minimize the effects of the optical fiber is the miniaturization of the spectroscopic set-up. A monolithic approach could be realized using a broadly tunable QCL (quantum cascade laser) as mid-IR source and a planar optical waveguide as sensor element integrated into the probe shaft. The high spectral power density of QCLs allows for increased interaction lengths with aqueous samples (in transmission up to 165 μm in the carbohydrate range¹³⁸ and 38 μm in the amide I region¹³⁹, which coincides with the strong absorption of water due to the H-O-H bending vibration, were realized) which could be realized using surface-sensitive planar wave guides¹⁴⁰. The omission of the AgX fiber would allow for design a compact, rugged set-up and a better signal-to-noise level. Furthermore,

ⁱ Unfortunately, the two spectrometers and probes used different coupling mechanisms, which made switching and thus a direct comparison of the spectrometers impossible.

the ultrasound accessory, which was currently fitted around existing probes, could be integrated in the probe, making fabrication easier (e.g. the long through hole for the signal transmission cable would not be necessary anymore as it could be integrated in the probe itself).

The presented method for acquisition of spectra of suspended cells is not limited to *S. cerevisiae*, but can be employed for a multitude of smallⁱⁱ particles within certain physical restrictions. The primary axial acoustic radiation force can be used to position particles relative to the ATR probe given a non-zero acoustic contrast factor of particles and suspending medium and particle sizes larger than approximately one micrometer for a 2 MHz acoustic wave. For a non-zero acoustic contrast factor, the particles and the suspending medium need to have different mass densities and/or speeds of sound (or compressibility); the higher the acoustic contrast factor the stronger the force.

The lower particle size cut-off makes manipulation of bacterial cells difficult, this can however be circumvented by increasing the acoustic frequency. Ultrasonic particle manipulation has been successfully employed for positioning, filtering, and trapping of a variety of mammalian cell lines, making the application of ultrasound enhanced ATR spectroscopy for acquisition of cell spectra feasible. It has to be noted, that due to the limited penetration depth of the evanescent field, only the surface of the relatively large mammalian cells (10-50 μm diameter) is accessible for analysis. The application has to be tested for each system, as bioprocesses present a complex, variable environment for acoustic particle manipulation (stirring, acoustic contrast factor not constant over time as cell and media composition change over time).

Given the multitude of reports on successful manipulation of particles by acoustic radiation forces, ultrasound enhanced ATR spectroscopy can be viewed as a generic method for acquisition of mid-IR spectra of particulate matter in suspension. Possible fields of application are not limited to bioprocesses, but the method could also be employed to study e.g. polymerization and crystallization processes. Furthermore, ultrasound particle manipulation could be combined with other in-line analysis methods, e.g. in-line Raman spectroscopy or in situ microscopy probes, making selective measurement of particles or suspending medium possible.

ⁱⁱ Small relative to the wavelength of the employed acoustic wave.

The quantification of extracellular precursor and product in *P. chrysogenum* fermentations is, to the best of the author's knowledge, the first report on successfully employing MCR-ALS on data acquired during fermentation taking into account the correspondence of chemical species. This implementation of a first principle, i.e. the stoichiometric balance, for calibration of spectroscopic data is a step towards science-based analysis of bioprocesses.

The developed technologies and presented applications of mid-IR spectroscopy show its great potential in bioprocess monitoring and deepening of bioprocess understanding. This will hopefully help to promote the implementation of mid-IR spectroscopy as a standard PAT tool.

7 BIBLIOGRAPHY

1. U.S.D. of H. and H.S. FDA. Guidance for Industry PAT — A Framework for Innovative Pharmaceutical Development, Manufacturing, and Quality Assurance. 2004. 16.
2. A. Kandelbauer, M. Rahe, W. Kessler, Rudolf. "Industrial Perspectives." In: J. Popp, V. V. Tuchin, A. Chiou, S. Heinemann, editors. Handbook of Biophotonics. Vol.3: Photonics in Pharmaceuticals, Bioanalysis and Environmental Research. First Edit. Wiley-VCH Verlag GmbH & Co KGaA, Germany, 2012. Pp. 1–70.
3. M. Pohlscheidt, S. Charaniya, C. Bork, M. Jenzsch, T.L. Noetzel, A. Luebbert. "Process and fermentation monitoring." In: M.C. Flickinger, editor. Encyclopedia of Industrial Biotechnology. First Edit. John Wiley & Sons, Inc, 2013. Pp. 1469–1492. 10.1002/9780470054581.eib606.pub2.
4. P.R. Griffiths. "Introduction to Vibrational Spectroscopy." In: J. Chalmers, P.R. Griffiths, editors. Handbook of Vibrational Spectroscopy Vol. 1. John Wiley & Sons, Inc, 2002. Pp. 1 – 11.
5. P.R. Griffiths, J.A. de Haseth. "Attenuated Total Reflection." Fourier Transform Infrared Spectrometry Second Edition. 2007. Pp. 321–348.
6. J. Fitzpatrick, J.A. Reffner. "Macro and Micro Internal Reflection Accessories." In: J. Chalmers, P.R. Griffiths, editors. Handbook of Vibrational Spectroscopy Vol. 2. 2nd editi. Wiley & Sons Ltd, 2002. Pp. 1–14.
7. W.M. Doyle. "Hollow Optical Conduits for Vibrational Spectroscopy." Handbook of Vibrational Spectroscopy Vol. 2. 2nd Editio. Wiley & Sons Ltd, 2006. Pp. 1–7.
8. I.R. Lewis, S.S. Rosenblum. "General Introduction to Fiber Optics." In: J. Chalmers, P.R. Griffiths, editors. Handbook of Vibrational Spectroscopy Vol. 2. John Wiley & Sons, Inc, 2002. Pp. 1–8. DOI: 10.1002/0470027320.
9. B. Lendl, B. Mizaikoff. "Optical Fibers for Mid-infrared Spectrometry." In: J. Chalmers, P.R. Griffiths, editors. Handbook of Vibrational Spectroscopy. John Wiley & Sons, Inc, 2002. Pp. 1–10. 10.1002/0470027320.
10. J. Sanghera, I.D. Aggarwal. Infrared Fiber Optics. CRC Press, 1998.
11. P. Geladi, B.R. Kowalski. "Partial least-squares regression: a tutorial." Anal. Chim. Acta. 1986. 185: 1–17.
12. H. Lohninger. "Fundamentals of Statistics." electronic book. 2012. http://www.statistics4u.info/fundstat_eng/.
13. I.T. Jolliffe. Principal Component Analysis, Second Edition. 2002.
14. S. Wold, M. Sjöström, L. Eriksson. "PLS-regression : a basic tool of chemometrics." Chemom. Intell. Lab. Syst. 2001. 58: 109–130.
15. a. de Juan, R. Tauler. "Chemometrics applied to unravel multicomponent processes

- and mixtures." *Anal. Chim. Acta.* 2003. 500(1-2): 195–210. 10.1016/S0003-2670(03)00724-4.
16. A. de Juan, R. Tauler. "Multivariate Curve Resolution (MCR) from 2000: Progress in Concepts and Applications." *Crit. Rev. Anal. Chem.* 2006. 36(3-4): 163–176. 10.1080/10408340600970005.
 17. M.C. Antunes, J.E.J. Simão, A.C. Duarte, R. Tauler. "Multivariate curve resolution of overlapping voltammetric peaks: quantitative analysis of binary and quaternary metal mixtures." *Analyst.* 2002. 127(6): 809–817. 10.1039/b200243b.
 18. R. Tauler. "Multivariate curve resolution applied to second order data." *Chemom. Intell. Lab. Syst.* 1995. 30(1): 133–146.
 19. W. Kessler, R.W. Kessler. "Multivariate curve resolution: A method of evaluating the kinetics of biotechnological reactions." *Anal. Bioanal. Chem.* 2006. 384(5): 1087–1095. 10.1007/s00216-005-0077-7.
 20. S. Grassi, J.M. Amigo, C.B. Lyndgaard, R. Foschino, E. Casiraghi. "Assessment of the sugars and ethanol development in beer fermentation with FT-IR and multivariate curve resolution models." *Food Res. Int.* Elsevier Ltd, 2014. 62: 602–608. 10.1016/j.foodres.2014.03.058.
 21. T. Azzouz, R. Tauler. "Application of multivariate curve resolution alternating least squares (MCR-ALS) to the quantitative analysis of pharmaceutical and agricultural samples." *Talanta.* 2008. 74(5): 1201–10. 10.1016/j.talanta.2007.08.024.
 22. H.C. Goicoechea, A.C. Olivieri, R. Tauler. "Application of the correlation constrained multivariate curve resolution alternating least-squares method for analyte quantitation in the presence of unexpected interferences using first-order instrumental data." *Analyst.* 2010. 135(3): 636–42. 10.1039/b922547a.
 23. H. Bruus. "Acoustofluidics 7: The acoustic radiation force on small particles." *Lab Chip.* 2012. 12(6): 1014–21. 10.1039/c2lc21068a.
 24. M. Gröschl. "Ultrasonic Separation of Suspended Particles-Part I: Fundamentals." *Acta Acust. united with Acust.* 1998. 84(October 1997): 432–447.
 25. J. Dual, D. Möller. "Acoustofluidics 4: Piezoelectricity and application in the excitation of acoustic fields for ultrasonic particle manipulation." *Lab Chip.* 2012. 12(3): 506–14. 10.1039/c1lc20913b.
 26. L. V. King. "On the Acoustic Radiation Pressure on Spheres." *Proc. R. Soc. Lond. A. Math. Phys. Sci.* The Royal Society, 1934. 147(861): 212 – 240.
 27. K. Yosioka, Y. Kawasima. "Acoustic radiation pressure on a compressible sphere." *Acustica.* 1955. 5: 167–173. 10.1017/S0022112094001096.
 28. Gorkov. "On the Forces Acting on a Small Particle in an Acoustical Field in an Ideal Fluid." *Sov. Phys. - Dokl.* 1962. 6: 773–775.
 29. C. Grenvall, P. Augustsson, J.R. Folkenberg, T. Laurell. "Harmonic microchip acoustophoresis: A route to online raw milk sample precondition in protein and lipid content quality control." *Anal. Chem.* 2009. 81(15): 6195–6200. 10.1021/ac900723q.
 30. C. Grenvall, J.R. Folkenberg, P. Augustsson, T. Laurell. "Label-free somatic cell cytometry in raw milk using acoustophoresis." *Cytom. Part A.* 2012. 81 A(12): 1076–1083. 10.1002/cyto.a.22214.
 31. J.J. Hawkes, J.J. Cefai, D. a Barrow, W.T. Coakley, L.G. Briarty. "Ultrasonic manipulation of particles in microgravity." *J. Phys. D. Appl. Phys.* 1999. 31(14): 1673–1680.

- 10.1088/0022-3727/31/14/010.
32. H. Böhm, L.G. Briarty, K.C. Lowe, J.B. Power, E. Benes, M.R. Davey. "Quantification of a novel h-shaped ultrasonic resonator for separation of biomaterials under terrestrial gravity and microgravity conditions." *Biotechnol. Bioeng.* 2003. 82(1): 74–85. 10.1002/bit.10546.
 33. R. Barnkob, P. Augustsson, T. Laurell, H. Bruus. An automated full-chip micro-PIV setup for measuring microchannel acoustophoresis: Simultaneous determination of forces from acoustic radiation and acoustic streaming. *Proc. MicroTAS 2010.* 2010. Pp. 1247–1249.
 34. M. Wiklund. "Acoustofluidics 12: Biocompatibility and cell viability in microfluidic acoustic resonators." *Lab Chip.* 2012. 12(11): 2018–28. 10.1039/c2lc40201g.
 35. T.G. Leighton. "What is ultrasound?" *Prog. Biophys. Mol. Biol.* 2007. 93(1-3): 3–83. 10.1016/j.pbiomolbio.2006.07.026.
 36. M. Dyson, J.B. Pond, B. Woodward, J. Broadbent. "The production of blood cell stasis and endothelial damage in the blood vessels of chick embryos treated with ultrasound in a stationary wave field." *Ultrasound Med. Biol.* 1974. 1(2): 133–148. 10.1016/0301-5629(74)90003-9.
 37. H. Böhm, P. Anthony, M.R. Davey, L.G. Briarty, J.B. Power, K.C. Lowe, et al. "Viability of plant cell suspensions exposed to homogeneous ultrasonic fields of different energy density and wave type." *Ultrasonics.* 2000. 38(1): 629–632. 10.1016/S0041-624X(99)00166-3.
 38. S. Radel, A.J. McLoughlin, L. Gherardini, O. Doblhoff-Dier, E. Benes. "Viability of yeast cells in well controlled propagating and standing ultrasonic plane waves." *Ultrasonics.* 2000. 38(1-8): 633–637.
 39. D. Bazou, L.A. Kuznetsova, W.T. Coakley. "Physical environment of 2-D animal cell aggregates formed in a short pathlength ultrasound standing wave trap." *Ultrasound Med. Biol.* 2005. 31(3): 423–430. 10.1016/j.ultrasmedbio.2004.12.007.
 40. D. Bazou, R. Kearney, F. Mansergh, C. Bourdon, J. Farrar, M. Wride. "Gene Expression Analysis of Mouse Embryonic Stem Cells Following Levitation in an Ultrasound Standing Wave Trap." *Ultrasound Med. Biol.* 2011. 37(2): 321–330. 10.1016/j.ultrasmedbio.2010.10.019.
 41. J. Hultström, O. Manneberg, K. Dopf, H.M. Hertz, H. Brismar, M. Wiklund. "Proliferation and viability of adherent cells manipulated by standing-wave ultrasound in a microfluidic chip." *Ultrasound Med. Biol.* 2007. 33(1): 145–151. 10.1016/j.ultrasmedbio.2006.07.024.
 42. F. Trampler, S.A. Sonderhoff, P.W.S. Pui, D.G. Kilburn, J.M. Piret. "Acoustic Cell Filter for High Density Perfusion Culture of Hybridoma Cells." *Nat. Biotechnol.* 1994. 12: 281–284.
 43. V.M. Gorenflo, L. Smith, B. Dedinsky, B. Persson, J.M. Piret. "Scale-up and optimization of an acoustic filter for 200 L/day perfusion of a CHO cell culture." *Biotechnol. Bioeng.* 2002. 80(4): 438–44. 10.1002/bit.10386.
 44. V.M. Gorenflo, J.B. Ritter, D.S. Aeschliman, H. Drouin, B.D. Bowen, J.M. Piret. "Characterization and optimization of acoustic filter performance by experimental design methodology." *Biotechnol. Bioeng.* 2005. 90(6): 746–53. 10.1002/bit.20476.
 45. M.J. Ruedas-Rama, A. Domínguez-Vidal, S. Radel, B. Lendl. "Ultrasonic trapping of microparticles in suspension and reaction monitoring using Raman

- microspectroscopy." *Anal. Chem.* 2007. 79(20): 7853–7. 10.1021/ac071121l.
46. L. Gherardini, C.M. Cousins, J.J. Hawkes, J. Spengler, S. Radel, H. Lawler, et al. "A new immobilisation method to arrange particles in a gel matrix by ultrasound standing waves." *Ultrasound Med. Biol.* 2005. 31(2): 261–272. 10.1016/j.ultrasmedbio.2004.10.010.
 47. J. Francois, J.L. Parrou. "Reserve carbohydrates metabolism in the yeast *Saccharomyces cerevisiae*." *FEMS Microbiol. Rev.* 2001. 25: 125–145.
 48. American Chemical Society. The discovery and development of penicillin. 1999. 11.
 49. P. Biechele, C. Busse, D. Solle, T. Scheper, K. Reardon. "Sensor systems for bioprocess monitoring." *Eng. Life Sci.* 2015. n/a–n/a. 10.1002/elsc.201500014.
 50. P. Roychoudhury, L.M. Harvey, B. McNeil. "The potential of mid infrared spectroscopy (MIRS) for real time bioprocess monitoring." *Anal. Chim. Acta.* 2006. 571(2): 159–66. 10.1016/j.aca.2006.04.086.
 51. D. Landgrebe, C. Haake, T. Höpfner, S. Beutel, B. Hitzmann, T. Scheper, et al. "On-line infrared spectroscopy for bioprocess monitoring." *Appl. Microbiol. Biotechnol.* 2010. 88(1): 11–22. 10.1007/s00253-010-2743-8.
 52. N.D. Lourenço, J. a Lopes, C.F. Almeida, M.C. Sarraguça, H.M. Pinheiro. "Bioreactor monitoring with spectroscopy and chemometrics: a review." *Anal. Bioanal. Chem.* 2012. 404(4): 1211–37. 10.1007/s00216-012-6073-9.
 53. P. Fayolle, D. Picque, G. Corrieu. "Monitoring of fermentation processes producing lactic acid bacteria by mid-infrared spectroscopy." *Vib. Spectrosc.* 1997. 14: 247–252.
 54. V.G. Franco, J.C. Perín, V.E. Mantovani, H.C. Goicoechea. "Monitoring substrate and products in a bioprocess with FTIR spectroscopy coupled to artificial neural networks enhanced with a genetic-algorithm-based method for wavelength selection." *Talanta.* 2006. 68(3): 1005–12. 10.1016/j.talanta.2005.07.003.
 55. S. Sivakesava, J. Irudayaraj, a Demirci. "Monitoring a bioprocess for ethanol production using FT-MIR and FT-Raman spectroscopy." *J. Ind. Microbiol. Biotechnol.* 2001. 26: 185–190. 10.1038/sj.jim.7000124.
 56. S. Sivakesava, J. Irudayaraj, D. Ali. "Simultaneous determination of multiple components in lactic acid fermentation using FT-MIR, NIR, and FT-Raman spectroscopic techniques." *Process Biochem.* 2001. 37(4): 371–378. 10.1016/S0032-9592(01)00223-0.
 57. P. Roychoudhury, L.M. Harvey, B. McNeil. "At-line monitoring of ammonium, glucose, methyl oleate and biomass in a complex antibiotic fermentation process using attenuated total reflectance-mid-infrared (ATR-MIR) spectroscopy." *Anal. Chim. Acta.* 2006. 561(1-2): 218–224. 10.1016/j.aca.2006.01.037.
 58. P. Roychoudhury, B. McNeil, L.M. Harvey. "Simultaneous determination of glycerol and clavulanic acid in an antibiotic bioprocess using attenuated total reflectance mid infrared spectroscopy." *Anal. Chim. Acta.* 2007. 585(2): 246–52. 10.1016/j.aca.2006.12.051.
 59. F. Leiternann, C. Syltatk, R. Hausmann. "Fast quantitative determination of microbial rhamnolipids from cultivation broths by ATR-FTIR Spectroscopy." *J. Biol. Eng.* 2008. 2(1): 13. 10.1186/1754-1611-2-13.
 60. F. Capito, R. Skudas, H. Kolmar, C. Hunzinger. "At-line mid infrared spectroscopy for monitoring downstream processing unit operations." *Process Biochem.* Elsevier Ltd,

2015. 50(6): 997–1005. 10.1016/j.procbio.2015.03.005.
61. F. Capito, R. Skudas, H. Kolmar, B. Stanislawski. "Host cell protein quantification by Fourier transform mid infrared spectroscopy (FT-MIR)." *Biotechnol. Bioeng.* 2013. 110(1): 252–9. 10.1002/bit.24611.
62. C.L. Winder, R. Cornmell, S. Schuler, R.M. Jarvis, G.M. Stephens, R. Goodacre. "Metabolic fingerprinting as a tool to monitor whole-cell biotransformations." *Anal. Bioanal. Chem.* 2011. 399(1): 387–401. 10.1007/s00216-010-4342-z.
63. M. Kansiz, J.R. Gapes, D. McNaughton, B. Lendl, K.C. Schuster. "Mid-infrared spectroscopy coupled to sequential injection analysis for the on-line monitoring of the acetone–butanol fermentation process." *Anal. Chim. Acta.* 2001. 438(1-2): 175–186. 10.1016/S0003-2670(01)00919-9.
64. G. Jarute, A. Kainz, G. Schroll, J.R. Baena, B. Lendl. "On-line determination of the intracellular poly(beta-hydroxybutyric acid) content in transformed *Escherichia coli* and glucose during PHB production using stopped-flow attenuated total reflection FT-IR spectrometry." *Anal. Chem.* 2004. 76(21): 6353–8. 10.1021/ac049803l.
65. J. Schenk, I.W. Marison, U. von Stockar. "pH prediction and control in bioprocesses using mid-infrared spectroscopy." *Biotechnol. Bioeng.* 2008. 100(1): 82–93. 10.1002/bit.21719.
66. J. Schenk, C. Viscasillas, I.W. Marison, U. von Stockar. "On-line monitoring of nine different batch cultures of *E. coli* by mid-infrared spectroscopy, using a single spectra library for calibration." *J. Biotechnol.* 2008. 134: 93–102. 10.1016/j.jbiotec.2007.12.014.
67. G. Mazarevica, J. Diewok, J.R. Baena, E. Rosenberg, B. Lendl. "On-line fermentation monitoring by mid-infrared spectroscopy." *Appl. Spectrosc.* 2004. 58(7): 804–10. 10.1366/0003702041389229.
68. E.L. Veale, J. Irudayaraj, A. Demirci. "An on-line approach to monitor ethanol fermentation using FTIR spectroscopy." *Biotechnol. Prog.* 2007. 23(2): 494–500. 10.1021/bp060306v.
69. M. Dabros, M.I. Amrhein, D. Bonvin, I.W. Marison, U. von Stockar. "Data Reconciliation of Concentration Estimates from Mid-Infrared and Dielectric Spectral Measurements for Improved On-Line Monitoring of Bioprocesses." *Biotechnol. Prog.* 2009. 25(2): 578–588. 10.1021/bp.143.
70. J. Schenk, I.W. Marison, U. von Stockar. "A simple method to monitor and control methanol feeding of *Pichia pastoris* fermentations using mid-IR spectroscopy." *J. Biotechnol.* 2007. 128(2): 344–53. 10.1016/j.jbiotec.2006.09.015.
71. A. Hashimoto, A. Yamanaka, M. Kanou, K. Nakanishi, T. Kameoka. "Simple and rapid determination of metabolite content in plant cell culture medium using an FT-IR/ATR method." *Bioprocess Biosyst. Eng.* 2005. 27(2): 115–123. 10.1007/s00449-004-0388-7.
72. D.L. Doak, J.A. Phillips. "In Situ Monitoring of an *Escherichia coli* Fermentation Using a Diamond Composition ATR Probe and Mid-infrared Spectroscopy." *Biotechnol. Prog.* 1999. 15: 529–539.
73. H. Kornmann, M. Rhiel, C. Cannizzaro, I. Marison, U. von Stockar. "Methodology for real-time, multianalyte monitoring of fermentations using an in-situ mid-infrared sensor." *Biotechnol. Bioeng.* 2003. 82(6): 702–9. 10.1002/bit.10618.
74. H. Kornmann, S. Valentinotti, P. Duboc, I. Marison, U. von Stockar. "Monitoring and

- control of *Gluconacetobacter xylinus* fed-batch cultures using in situ mid-IR spectroscopy." *J. Biotechnol.* 2004. 113(1-3): 231–45. 10.1016/j.jbiotec.2004.03.029.
75. J. Dahlbacka, K. Kiviharju, T. Eerikäinen, K. Fagervik. "Monitoring of *Streptomyces peucetius* cultivations using FTIR/ATR spectroscopy and quantitative models based on library type data." *Biotechnol. Lett.* 2013. 35(3): 337–43. 10.1007/s10529-012-1093-2.
76. P. Sagmeister, T. Langemann, P. Wechselberger, A. Meitz, C. Herwig. "A dynamic method for the investigation of induced state metabolic capacities as a function of temperature." *Microb. Cell Fact. Microbial Cell Factories*, 2013. 12(1): 94. 10.1186/1475-2859-12-94.
77. J. Schenk, I.W. Marison, U. von Stockar. "Simplified Fourier-transform mid-infrared spectroscopy calibration based on a spectra library for the on-line monitoring of bioprocesses." *Anal. Chim. Acta.* 2007. 591: 132–140. 10.1016/j.aca.2007.03.056.
78. J. Dahlbacka, J. Weegar, N. von Weymarn, K. Fagervik. "On-line measurement of the substrate concentrations in *Pichia pastoris* fermentations using FT-IR/ATR." *Biotechnol. Lett.* 2012. 34(6): 1009–17. 10.1007/s10529-012-0868-9.
79. D. Pollard, R. Buccino, N. Connors, T. Kirschner, R. Olewinski, K. Saini, et al. "Real-time analyte monitoring of a fungal fermentation, at pilot scale, using in situ mid-infrared spectroscopy." *Bioprocess Biosyst. Eng.* 2001. 24(1): 13–24. 10.1007/s004490100226.
80. M. Rhiel, P. Ducommun, I. Bolzonella, I. Marison, U. Von Stockar. "Real-Time In Situ Monitoring of Freely Suspended and Immobilized Cell Cultures Based on Mid-Infrared Spectroscopic Measurements." *Biotechnol. Bioeng.* 2002. 77: 174–185. 10.1002/bit.10134.
81. M.H. Rhiel, M.I. Amrhein, I.W. Marison, U. von Stockar. "The influence of correlated calibration samples on the prediction performance of multivariate models based on mid-infrared spectra of animal cell cultures." *Anal. Chem.* 2002. 74(20): 5227–36.
82. P. Fayolle, D. Picque, G. Corrieu. "On-line monitoring of fermentation processes by a new remote dispersive middle-infrared spectrometer." *Food Control.* 2000. 11(4): 291–296. 10.1016/S0956-7135(99)00105-X.
83. M. Sandor, F. Rüdinger, R. Bienert, C. Grimm, D. Solle, T. Scheper. "Comparative study of non-invasive monitoring via infrared spectroscopy for mammalian cell cultivations." *J. Biotechnol. Elsevier B.V.*, 2013. 168(4): 636–45. 10.1016/j.jbiotec.2013.08.002.
84. A. Bogomolov, M. Heßling, U. Wenzel, S. Princz, T. Hellmuth, M.J.B. Bernal, et al. "Development and testing of mid-infrared sensors for in-line process monitoring in biotechnology." *Sensors Actuators B Chem. Elsevier B.V.*, 2015. 10.1016/j.snb.2015.07.118.
85. H. Heise, L. Küpper, L. Butvina. "Bio-analytical applications of mid-infrared spectroscopy using silver halide fiber-optic probes." *Spectrochim. Acta Part B At. Spectrosc. Elsevier*, 2002. 57(10): 1649–1663.
86. R. Foley, S. Hennessy, I.W. Marison. "Potential of Mid-Infrared Spectroscopy for On-Line Monitoring of Mammalian Cell Culture Medium Components." *Appl. Spectrosc.* 2012. 66(1): 33–39. 10.1366/11-06395.
87. J.-M. Girard, J.-S. Deschênes, R. Tremblay, J. Gagnon. "FT-IR/ATR univariate and multivariate calibration models for in situ monitoring of sugars in complex

- microalgal culture media." *Bioresour. Technol.* Elsevier Ltd, 2013. 144: 664–8. 10.1016/j.biortech.2013.06.094.
88. H. Kornmann, S. Valentinotti, I. Marison, U. von Stockar. "Real-time update of calibration model for better monitoring of batch processes using spectroscopy." *Biotechnol. Bioeng.* 2004. 87(5): 593–601. 10.1002/bit.20153.
89. G. Socrates. *Infrared and Raman Characteristic Group Frequencies*. 3rd editio. Wiley & Sons Ltd, 2001.
90. D. Naumann, D. Helm, H. Labischinski. "Microbiological characterizations by FT-IR spectroscopy." *Nature*. 1991. 351: 81–82.
91. D. Naumann. The Ultra Rapid Differentiation And Identification Of Pathogenic Bacteria Using FT-IR Techniques. In: D.G. Cameron, J.G. Grasselli, editors. *Proc. SPIE 0553, Fourier and Computerized Infrared Spectroscopy*. 1985. P. 268. 10.1117/12.970803.
92. L. Mariey, J.P.P. Signolle, C. Amiel, J. Travert. "Discrimination , classification , identification of microorganisms using FTIR spectroscopy and chemometrics." *Vib. Spectrosc.* 2001. 26(2): 151–159. 10.1016/S0924-2031(01)00113-8.
93. D. Naumann. "Infrared Spectroscopy in Microbiology." In: R.A. Meyers, editor. *Encyclopedia of Analytical Chemistry*. Wiley and Sons, 2000. Pp. 102–131. 10.1002/9780470027318.a0117.
94. W. Zeroual, C. Choisy, S.M. Doglia, H. Bobichon, J. Angiboust, M. Manfait. "Monitoring of bacterial growth and structural analysis as probed by FT-IR spectroscopy." *Biochim. Biophys. actata*. 1994. 1222: 171–178.
95. D. Helm, D. Naumann. "Identification of some bacterial cell components by FT-IR spectroscopy." *FEMS Microbiol. Lett.* 1995. 126: 75–80.
96. K. Schuster, F. Mertens, J. Gapes. "FTIR spectroscopy applied to bacterial cells as a novel method for monitoring complex biotechnological processes." *Vib. Spectrosc.* 1999. 19(2): 467–477. 10.1016/S0924-2031(98)00058-7.
97. R.K. Saharan, S.C. Sharma. "FTIR spectroscopy and biochemical investigation of ethanol stressed yeast *Pachysolen tannophilus*." *Vib. Spectrosc.* Elsevier B.V., 2011. 55(1): 85–89. 10.1016/j.vibspec.2010.08.003.
98. D. Ami, A. Natalello, P. Gatti-lafranconi, T. Schultz, M. Lotti, A. De Marco, et al. "FT-IR spectroscopy for the study of bacterial membrane stress induced by recombinant protein production." *Microb. Cell Fact.* 2006. 2: 1–2. 10.1186/1475-2859-5-S1-P2.
99. E. Burattini, M. Cavagna. "A FTIR microspectroscopy study of autolysis in cells of the wine yeast *Saccharomyces cerevisiae*." *Vib. Spectrosc.* 2008. 47(2): 139–147. 10.1016/j.vibspec.2008.04.007.
100. M. Cavagna, R. Dell'Anna, F. Monti, F. Rossi, S. Torriani. "Use of ATR-FTIR microspectroscopy to monitor autolysis of *Saccharomyces cerevisiae* cells in a base wine." *J. Agric. Food Chem.* 2010. 58(1): 39–45. 10.1021/jf902369s.
101. L. Corte, P. Rellini, L. Roscini, F. Fatichenti, G. Cardinali. "Development of a novel, FTIR (Fourier transform infrared spectroscopy) based, yeast bioassay for toxicity testing and stress response study." *Anal. Chim. Acta.* 2010. 659(1-2): 258–65. 10.1016/j.aca.2009.11.035.
102. L. Corte, M. Tiecco, L. Roscini, R. Germani, G. Cardinali. "FTIR analysis of the metabolomic stress response induced by N-alkyltropinium bromide surfactants in the yeasts *Saccharomyces cerevisiae* and *Candida albicans*." *Colloids Surf. B.*

- Biointerfaces. Elsevier B.V., 2014. 116: 761–71. 10.1016/j.colsurfb.2014.01.054.
103. J. Kuligowski, G. Quintás, C. Herwig, B. Lendl. "A rapid method for the differentiation of yeast cells grown under carbon and nitrogen-limited conditions by means of partial least squares discriminant analysis employing infrared micro-spectroscopic data of entire yeast cells." *Talanta*. Elsevier, 2012. 99: 566–73. 10.1016/j.talanta.2012.06.036.
 104. M. Kansiz, H. Billman-Jacobe, D. McNaughton. "Quantitative Determination of the Biodegradable Polymer Poly (β -hydroxybutyrate) in a Recombinant Escherichia coli Strain by Use of Mid-Infrared Spectroscopy and Multivariate Statistics Quantitative Determination of the Biodegradable Polymer Poly (" . " *Appl. Environ. Microbiol.* 2000. 66(8): 3415–3420. 10.1128/AEM.66.8.3415-3420.2000.Updated.
 105. D. Ami, A. Natalello, P. Gatti-Lafrancini, M. Lotti, S.M. Doglia. "Kinetics of inclusion body formation studied in intact cells by FT-IR spectroscopy." *FEBS Lett.* 2005. 579(16): 3433–6. 10.1016/j.febslet.2005.04.085.
 106. S. Gross-Selbeck, G. Margreiter, C. Obinger, K. Bayer. "Fast quantification of recombinant protein inclusion bodies within intact cells by FT-IR spectroscopy." *Biotechnol. Prog.* 2007. 23(3): 762–6. 10.1021/bp070022q.
 107. D. Naumann, S. Keller, D. Helm, C. Schultz, B. Schrader. "FT-IR and FT-Raman spectroscopy are powerful analytical tools for the non-invasive characterization of intact microbial cells." *J. Mol. Struct.* 1995. 347: 399–406.
 108. E. Correa, H. Sletta, D.I. Ellis, S. Hoel, H. Ertesvåg, T.E. Ellingsen, et al. "Rapid reagentless quantification of alginate biosynthesis in *Pseudomonas fluorescens* bacteria mutants using FT-IR spectroscopy coupled to multivariate partial least squares regression." *Anal. Bioanal. Chem.* 2012. 403(9): 2591–9. 10.1007/s00216-012-6068-6.
 109. J. Vongsvivut, P. Heraud, A. Gupta, M. Puri, D. McNaughton, C.J. Barrow. "FTIR microspectroscopy for rapid screening and monitoring of polyunsaturated fatty acid production in commercially valuable marine yeasts and protists." *Analyst.* 2013. 138(20): 6016–31. 10.1039/c3an00485f.
 110. L. Marcotte, G. Kegelaer, C. Sandt, J. Barbeau, M. Lafleur. "An alternative infrared spectroscopy assay for the quantification of polysaccharides in bacterial samples." *Anal. Biochem.* 2007. 361(1): 7–14. 10.1016/j.ab.2006.11.009.
 111. E. Burattini, M. Cavagna, R. Dell'Anna, F. Malvezzi Campeggi, F. Monti, F. Rossi, et al. "A FTIR microspectroscopy study of autolysis in cells of the wine yeast *Saccharomyces cerevisiae*." *Vib. Spectrosc.* 2008. 47(2): 139–147. 10.1016/j.vibspec.2008.04.007.
 112. A.P. Dean, J.M. Nicholson, D.C. Sigee. "Impact of phosphorus quota and growth phase on carbon allocation in *Chlamydomonas reinhardtii* : an FTIR microspectroscopy study Impact of phosphorus quota and growth phase on carbon allocation in *Chlamydomonas reinhardtii* : an FTIR microspectroscopy study." *Eur. J. Phycol.* 2008. 43(4): 345–354. 10.1080/09670260801979287.
 113. H. Bruus, J. Dual, J.J. Hawkes, M. Hill, T. Laurell, J. Nilsson, et al. "Forthcoming Lab on a Chip tutorial series on acoustofluidics: acoustofluidics-exploiting ultrasonic standing wave forces and acoustic streaming in microfluidic systems for cell and particle manipulation." *Lab Chip.* 2011. 11(21): 3579–80. 10.1039/c1lc90058g.
 114. A. Lenshof, C. Magnusson, T. Laurell. "Acoustofluidics 8: applications of

- acoustophoresis in continuous flow microsystems." *Lab Chip*. 2012. 12(7): 1210–23. 10.1039/c2lc21256k.
115. M. Evander, J. Nilsson. "Acoustofluidics 20: Applications in acoustic trapping." *Lab Chip*. 2012. 12(22): 4667–76. 10.1039/c2lc40999b.
116. M. Wiklund, S. Radel, J.J. Hawkes. "Acoustofluidics 21: ultrasound-enhanced immunoassays and particle sensors." *Lab Chip*. 2012. 10.1039/c2lc41073g.
117. M. Nordin, T. Laurell. "Two-hundredfold volume concentration of dilute cell and particle suspensions using chip integrated multistage acoustophoresis." *Lab Chip*. 2012. 12(22): 4610–6. 10.1039/c2lc40629b.
118. A. Lenshof, A. Ahmad-Tajudin, K. Järås, A.M. Swärd-Nilsson, L. Åberg, G. Marko-Varga, et al. "Acoustic whole blood plasmapheresis chip for prostate specific antigen microarray diagnostics." *Anal. Chem.* 2009. 81(15): 6030–6037. 10.1021/ac9013572.
119. C.L. Ebbesen, J.D. Adams, R. Barnkob, H.T. Soh, H. Bruus. "Temperature-Controlled High-Throughput (1 L / H) Acoustophoretic Particle Separation in Microchannels." *Design*. 2010. (October): 728–730.
120. M.S. Limaye, J.J. Hawkes, W.T. Coakley. "Ultrasonic standing wave removal of microorganisms suspension in small batch systems." *J. Microbiol. Methods*. 1996. 27(96): 211–220.
121. J.J. Hawkes, M.S. Limaye, W.T. Coakley. Filtration of bacteria and yeast by ultrasound-enhanced sedimentation. *Journal of applied microbiology*. 1997. 39–47.
122. M.S. Limaye, W.T. Coakley. "Clarification of small volume microbial suspensions in an ultrasonic standing wave." *J. Appl. Microbiol.* 1998. 84(6): 1035–42.
123. J.F. Spengler, W.T. Coakley. "Ultrasonic Trap To Monitor Morphology and Stability of Developing Microparticle Aggregates." *Langmuir*. 2003. 19(9): 3635–3642. 10.1021/la026798c.
124. J.J. Hawkes, R.W. Barber, D.R. Emerson, W.T. Coakley. "Continuous cell washing and mixing driven by an ultrasound standing wave within a microfluidic channel." *Lab Chip*. 2004. 4(5): 446–52. 10.1039/b408045a.
125. S. Radel, L. Gherardini, A.J. McLoughlin, O. Doblhoff-Dier, E. Benes. Breakdown of immobilisation/separation and morphology changes of yeast suspended in water-rich ethanol mixtures exposed to ultrasonic plane standing waves. *Bioseparation*. 2000. 369–377.
126. L. Gherardini, S. Radel, S. Sielemann, O. Doblhoff-Dier, M. Gröschl, E. Benes, et al. "A study of the spatial organisation of microbial cells in a gel matrix subjected to treatment with ultrasound standing waves." *Bioseparation*. 2002. 10(4): 153–162. 10.1023/A:1016311410219.
127. S. Radel, J. Schnöller, A. Dominguez, B. Lendl, M. Gröschl, E. Benes. "Raman spectroscopy of particles in suspension concentrated by an ultrasonic standing wave." *e i Elektrotechnik und Informationstechnik*. 2008. 125(3): 82–85. 10.1007/s00502-008-0515-2.
128. S. Radel, J. Schnöller, M. Gröschl, E. Benes, B. Lendl. "On Chemical and Ultrasonic Strategies to Improve a Portable FT-IR ATR Process Analyzer for Online Fermentation Monitoring." *IEEE Sens. J.* 2010. 10(10): 1615–1622.
129. ASME BPE - 2014: Bioprocessing Equipment. ASME, 2014. 324.
130. S. Radel, M. Brandstetter, B. Lendl. "Observation of particles manipulated by

- ultrasound in close proximity to a cone-shaped infrared spectroscopy probe." *Ultrasonics*. 2010. 50(2): 240–246.
131. B. Lendl, S. Radel, M. Brandstetter. Device for FTIR Absorption Spectroscopy. PCT/AT2010/000006. Austria, Europe, US, Issued 2010.
 132. M. Brandstetter. Ultrasonically enhanced in-line Attenuated Total Reflection (ATR) infrared absorption spectroscopy of suspensions. Vienna University of Technology, 2009.
 133. M. Gröschl. "Ultrasonic Separation of Suspended Particles-Part II: Design and Operation of Separation Devices." *Acta Acust. united with Acust.* 1998. 84(October 1997): 632–642.
 134. S. Radel. Ultrasonically Enhanced Settling : The effects of ultrasonic plane wave fields on suspensions of the yeast *Saccharomyces cerevisiae*. Vienna University of Technology, 2002.
 135. V. Bauer. Entwicklung einer Messeinrichtung zur ultraschallgestützten IR-Spektroskopie. TU Vienna, Vienna, Austria, 2009.
 136. P. Palmesi. Entwicklung einer Infrarotsonde zur Verwendung in Bioreaktoren. TU Vienna, 2011.
 137. L. Strobl. Labview program for the Frequency Synthesizer PFS2540 to control the Ultrasonic enhanced IR sensor. TU Wien, 2011.
 138. M. Brandstetter. Quantitative Chemical Analysis of Aqueous Solutions using Broadly Tunable Mid – Infrared Quantum Cascade Lasers. TU Wien, 2014.
 139. M.R. Alcaráz, A. Schwaighofer, C. Kristament, G. Ramer, M. Brandstetter, H. Goicoechea, et al. "External-Cavity Quantum Cascade Laser Spectroscopy for Mid-IR Transmission Measurements of Proteins in Aqueous Solution." *Anal. Chem.* 2015. 87(13): 6980–6987. 10.1021/acs.analchem.5b01738.
 140. G. Ramer, J. Kasberger, M. Brandstetter, A. Saeed, B. Jakoby, B. Lendl. "A broadband grating-coupled silicon nitride waveguide for the mid-IR: characterization and sensitive measurements using an external cavity quantum cascade laser." *Appl. Phys. B*. 2013. 116(2): 325–332. 10.1007/s00340-013-5695-8.
 141. S. Wold. "Chemometrics; what do we mean with it, and what do we want from it?" *Chemom. Intell. Lab. Syst.* 1995. 30(1): 109–115. 10.1016/0169-7439(95)00042-9.
 142. U.S.D. of H. and H.S. FDA. Avoid Fetal "Keepsake" Images, Heartbeat Monitors. FDA Consumer Health Information. U.S. Food and Drug Administration, 2015. 2.
 143. J. Houbraken, J.C. Frisvad, R.A. Samson'. "Fleming's penicillin producing strain is not *Penicillium chrysogenum* but *P. rubens*." *IMA Fungus*. 2011. 2(1): 87–95. 10.5598/ima fungus.2011.02.01.12.

8 SCIENTIFIC PUBLICATIONS

Publication I

Cosima Koch, Markus Brandstetter, Bernhard Lendl, Stefan Radel, *Ultrasound in Medicine and Biology* 39(6) (2013), 1094-1101. (c) 2013 World Federation for Ultrasound in Medicine & Biology under a Creative Commons Attribution (CC-BY) License.

DOI: 10.1016/j.ultrasmedbio.2013.01.003

● *Original Contribution***ULTRASONIC MANIPULATION OF YEAST CELLS IN SUSPENSION
FOR ABSORPTION SPECTROSCOPY WITH AN IMMERSIBLE MID-INFRARED
FIBEROPTIC PROBE**COSIMA KOCH, MARKUS BRANDSTETTER, BERNHARD LENDL, and STEFAN RADEL
Institute of Chemical Technologies and Analytics, Vienna University of Technology, Vienna, Austria

(Received 26 September 2012; revised 8 January 2013; in final form 10 January 2013)

Abstract—Recent advances in combining ultrasonic particle manipulation with attenuated total reflection infrared spectroscopy of yeast suspensions are presented. Infrared spectroscopy provides highly specific molecular information about the sample. It has not been applicable to in-line monitoring of cells during fermentation, however, because positioning cells in the micron-thin measurement region of the attenuated total reflection probe was not possible. Ultrasonic radiation forces exerted on suspended particles by an ultrasonic standing wave can result in the buildup of agglomerates in the nodal planes, hence enabling the manipulation of suspended cells on the microscopic scale. When a chamber setup and a prototype in-line applicable probe were used, successful control over the position of the yeast cells relative to the attenuated total reflection sensor surface could be proven. Both rate of increase and maximum mid-infrared absorption of yeast-specific bands during application of a pushing frequency (chamber setup: 1.863 MHz, in-line probe: 1.990 MHz) were found to correlate with yeast cell concentration. (E-mail: stefan.radel@tuwien.ac.at) © 2013 World Federation for Ultrasound in Medicine & Biology.

Key Words: Ultrasonic particle manipulation, Fourier transform infrared spectroscopy, Acoustic radiation force, Ultrasonic standing wave, Attenuated total reflection, *Saccharomyces cerevisiae*.

INTRODUCTION

When an ultrasonic standing wave (USW) is applied to a suspension, radiation forces are exerted on the suspended particles. The origin of these forces are the spatial gradients of the sound wave's acoustic pressure (King 1934). Depending on the mass density and speed of sound of the particles and the host liquid, respectively, the particles are driven into regions of vanishing displacement or pressure. Therefore, the nodes within a standing wave are regions where particle aggregation (or thinning) can be observed; solid particles typically travel into the pressure nodes of the sound field. Acoustic radiation forces have previously been used for reliable sample concentration in sensor applications (Coakley 1997; Hill et al. 2004), including medical environments (Barnes et al. 1998). Furthermore, Saito et al. (2002) showed that locomotive particles could be manipulated/positioned by a combination of perpendicularly aligned ultrasonic standing wave fields. The ability of an USW to deposit particles on

a surface has been investigated with functionalized surfaces (Hawkes et al. 2004) and by optical means (Glynne-Jones et al. 2009).

Mid-infrared (mid-IR) Fourier transform infrared (FT-IR) spectroscopy is a well-developed method in chemical analysis. In combination with attenuated total reflection (ATR) sensing elements, (mid-IR) spectroscopy appears to be a very promising method for process monitoring, particularly useful in (bio)process applications. The ATR technique exploits the occurrence of total reflection of light at the interface of two media with different refractive indices and, thus, only has a detection range of some microns, that is, within the evanescent field. New devices and concepts for advanced chemical analysis based on this technique have been developed over the years (Harrick 1967). For measurements in suspension, additional measures are necessary to bring a sufficient amount of suspended particles into the evanescent field region. Recently, the mid-IR spectroscopic assessment of biological cell sediment onto a horizontal ATR element was reported (Jarute et al. 2004; Schnöller and Lendl 2004). Sedimentation, however, is not an option for in-line measurements, for example, in bioreactors.

Address correspondence to: Stefan Radel, Institute of Chemical Technologies and Analytics, Vienna University of Technology, Getreidemarkt 9/164 AC, 1060 Vienna, Austria. E-mail: stefan.radel@tuwien.ac.at

The recording of an FT-IR absorbance spectrum of a given sample consists of two successive measurements. In each measurement the intensity recorded at the detector for different wavenumbers $\tilde{\nu}$ (reciprocal λ , expressed in cm^{-1}) is recorded. First, the background spectrum I_0 (cm^{-1}) is obtained where all components but the sample of interest are present in the optical path of the spectrometer. In the experiments described in this work, this corresponds to the mounted ATR unit with the active part of the ATR element covered with solvent. Subsequently, the sample, here particles contained in the solvent, is placed on the ATR element, and the spectrum I (cm^{-1}) is recorded. Calculation of the absorbance spectrum following the Beer–Lambert law

$$A(\tilde{\nu}) = -\log \frac{I(\tilde{\nu})}{I_0(\tilde{\nu})}$$

yields the specific absorption spectrum of the sample (particles) only, as all other contributions to the achieved light throughput by optical components and solvent cancel out and only the contribution of the particles remains.

An IR absorption spectrum can be acquired in minutes to seconds and delivers specific molecular information about the sample in the optical pathway (Chalmers and Griffiths 2002). In industrial environments it has become state of the art to connect the ATR sensor to the spectrometer with flexible mid-IR conducting fibers. With this technology, the ATR sensor can be immersed in a reactor, thus enabling in-line assessment of the production process.

We set out to exploit the particle manipulation abilities of an USW in ATR spectroscopy. USWs had already been applied with a horizontal ATR unit, attached to a standard FT-IR spectrometer, to improve long-term stability during online bioprocess monitoring (Radel *et al.* 2010a). In an online configuration, a process stream is continuously taken from the bioreactor and directed to the FT-IR spectrometer. Also, we reported the first successful application of an USW to direct particles of various laboratory suspensions into the evanescent field of an ATR (Lendl *et al.* 2010).

In continuing these successful attempts to combine an USW and an ATR FT-IR fiberoptic probe, we present our results obtained with prototype setups approaching the research goal of an in-line device, that is, a device in which the ATR sensor is immersed in the bioreactor. With in-line spectroscopy applications in biotechnology in mind, we describe the application on suspensions of *Saccharomyces cerevisiae*, baker's yeast in this work. The choice of yeast as a biological model was guided by availability and simplicity in handling (Hawkes *et al.* 1997). However, in the context of ultrasonic radiation forces, the spherical shape of the yeast cell is advantageous with respect to the applicability of theoretical

results, where spherical particles are usually investigated (Doinikov 1997; Gröschl 1998a; King 1934).

Generally, exposure to an USW does not harm the cells; yeast have been shown to be viable after sonication (Radel *et al.* 2000b). Moreover, it has been shown that yeast are able to reproduce after ultrasonic arrangement in a cluster (Gherardini *et al.* 2005). Only when the cells left the pressure nodes of the USW significant alterations in viability were observed (Radel *et al.* 2000a). Spengler *et al.* (2000) investigated the effects of primary axial and transverse acoustic radiation forces on yeast in a one-wavelength resonator. They observed a distinct, reproducible pattern of yeast cell clump formation, indicating that the transverse acoustic radiation force (resulting from the energy density distribution over the transducer surface) can have a strong effect on cell distribution. As yeasts are of industrial relevance, reports on the use of ultrasound in respective bioprocesses exist (Chisti 2003; Palme *et al.* 2010).

To combine the optical and ultrasonic techniques it was necessary to implement an USW in proximity of the ATR probe tip. One way to accomplish this was to use the ATR probe as the reflector of an ultrasonic resonator. Therefore, the USW was built up between an ultrasonic transducer and an ATR fiber probe. As a consequence, suspended cells agglomerated in the pressure nodal planes, parallel to the surface of the ATR probe (Radel *et al.* 2010b). As the position of the nodal planes depends on the driving signal, it was expected that the precise location of these cell aggregates relative to the evanescent field could be controlled by the ultrasonic frequency. Figure 1 shows this effect on the example of polystyrene beads in tetrahydrofuran (THF). One can clearly see the particles, which agglomerated in planes. The same behavior was expected for yeast cells in water; however, because of the turbid appearance of yeast suspensions, photographic proof was not feasible.

METHODS

Experimental setups

Two different setups were investigated: a brass/glass chamber containing the suspension with the ultrasonic field oriented horizontally and an USW equipped in-line probe immersed in a vessel that could be inclined at any angle relative to gravitational forces.

In both cases the ATR probe was connected to the spectrometer by flexible silver halide fibers, and both probes contained an ATR unit at the top. Diamond was used as the ATR element because of its optical properties (refractive index) and inertness. The optical setups provided a bandwidth from 600 to 1960 cm^{-1} , a range including the “fingerprint region” most important for the analysis of

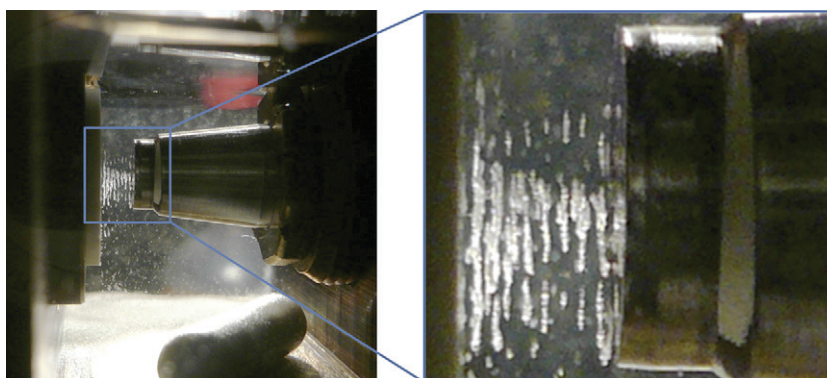


Fig. 1. An ultrasonic standing wave is built up between the transducer and the attenuated total reflection (ATR) probe acting as reflector. The enlargement on the right-hand side shows the half-wavelength structure of the particle agglomerates (polystyrene beads were used here for demonstration purposes). By changing the frequency, the location of the pressure nodal planes is altered, and therefore, the evanescent field of the ATR is either populated with particles or depopulated. Taken from: Brandstetter M. Ultrasonically enhanced in-line attenuated total reflection (ATR) infrared absorption spectroscopy of suspensions. Master Thesis, Vienna University of Technology, 2009.

organic molecules. Spectra were recorded by the accumulation of 32 scans at a spectral resolution of 4 cm^{-1} .

For both devices, frequency values for retracting the cells from the ATR (retracting frequency, f_1) and pushing them onto the ATR (pushing frequency, f_2) were assessed in advance. Successful control over the position of the yeast cells relative to the ATR sensor surface was demonstrated when significant increases and decreases in the measured absorption bands specific to yeast occurred.

Chamber setup. The chamber ($70 \times 40 \times 40\text{ mm}^3$) consisted of a brass bottom and two brass walls opposite each other. The other two walls were made of glass to allow for visual observation of particle manipulation. The ATR probe was mounted adjustably in an opening in one of the brass walls exactly facing the ultrasonic transducer in the opposite wall (Fig. 2).

A brass fitting with a $M20 \times 1$ fine-pitch outside thread and a 12-mm inner drilling enclosed the ATR probe and maintained proper fixation within the feed-through of the chamber. Hence, by rotation of the brass fitting, the distance between the ATR's front face and the transducer surface could be adjusted; a gap width of 1.6 mm was used for the experiments described here.

The sound source, a piezoelectric sandwich transducer, consisted of a 16-mm-diameter, 1-mm-thick PZT (lead–zirconate–titanate) element equipped with a wrap-around electrode (PZT 181, PI Ceramics, Lederhose, Germany) glued to a carrier. The resonance frequency of this element was approximately 2 MHz. This carrier was made of Macor (Corning, Corning, NY, USA), a glass ceramic that approximately meets the acoustic properties needed for the matching layer and is electrically insulating as necessary. Unlike glass, however, it is machinable and, therefore, more suitable than the glass carriers used before in similar applications (Gröschl 1998b).

The IR spectra in the chamber setup were acquired with a React IR 45 m FT-IR spectrometer and a 9.5-mm DiComp process analysis probe (both from Mettler Toledo, Giessen, Germany).

In-line probe. A prototype in-line probe for use inside a bioreactor was manufactured in house. The probe was designed in accordance with U.S. Food and Drug Administration regulations, and only biocompatible materials (brass, Macor, Viton [DuPont Dow, Wilmington, DE, USA]) were used. The sound source, a 10-mm-diameter, 1-mm-thick PZT transducer (resonance frequency = approximately 2 MHz) equipped with a wraparound electrode (PZT 181, PI Ceramics) glued to a Macor carrier, was held exactly opposite the ATR probe by three rods, one of which acted

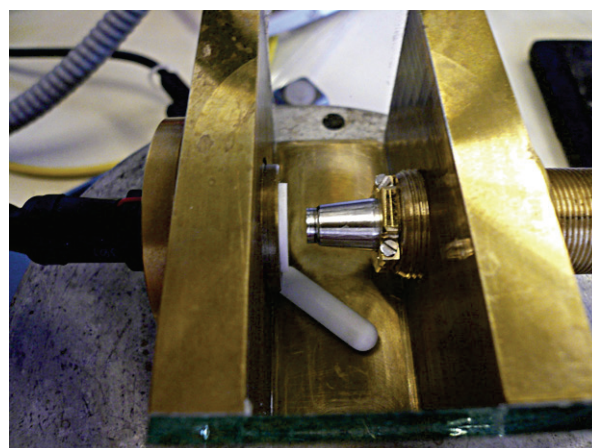


Fig. 2. Experimental chamber setup made of brass; on the left hand side the Macor part of the ultrasonic transducer is visible. Facing it, the ATR probe is mounted onto the right wall of the chamber. By turning the fitting, the distance between the probe and the transducer can be adjusted. The white object at the bottom of the chamber is the magnetic stirrer.

as a guide for the cable connecting the transducer to the frequency power synthesizer. The distance between the ATR probe and the transducer could be adjusted with a micrometer screw gauge moving the ATR probe along its axis (Fig. 3).

For the experiments described here, the in-line probe was immersed in a beaker equipped with a magnetic stirrer holding the cell suspensions. The angle of the ultrasonic field with respect to gravitational forces could be chosen arbitrarily; here it was set to 135° , with the ATR sensor surface pointing downward.

For the in-line probe, a Matrix MFT-IR spectrometer (Bruker Optics, Ettlingen, Germany) and a 6-mm ATR probe (custom-built, FS, Aachen, Germany) were used.

Experimental procedure

The equipment (probe, chamber setup, *etc.*) was carefully cleaned with the appropriate solvent (water, ethanol) and dried with paper towels prior to each experiment. A fresh suspension of baker's yeast (dried active yeast, Allinson, Maidenhead, UK) in water was prepared, and the cell concentration was adjusted to approximately 5×10^7 cells/mL for the proof-of-principle experiments. To investigate the concentration dependency of the measurement system, a series of concentrations (14, 17, 20, 24, 29, 35 and 42 g/L dry weight) were measured with the in-line setup. Depending on the setup used, the chamber or the beaker was filled with the cell suspension and stirred at 300–500 rpm with a magnetic stirrer placed on the bottom.

Subsequently, a frequency power synthesizer (FPS2540, Psi, Hinterbrühl, Austria) was switched on. This device was connected to the PZT delivering the driving signal with approximately 1 W true electrical power input; the operating frequency was adjusted in the range 1.8–2 MHz.

As a preliminary proof-of-principle experiment, the appropriate ultrasonic frequencies at which the yeast cells were pushed to and retracted from the ATR respectively

were determined. This was done by observation of the FTIR spectra recorded when different ultrasonic frequencies were applied to a yeast suspension. From the change in absorption bands specific for yeast cells, appropriate pushing and retracting frequencies were identified. The location of the nodal planes is influenced by the acoustic wavelength, which, in turn, is a function of the speed of sound and is therefore influenced, for example, by the ambient temperature. Thereafter, when the respective experiments were performed, the ultrasonic field was applied for a series of cycles at the retracting frequency (hereafter f_1) and the pushing frequency (hereafter f_2), respectively. During these sequences, IR spectra were recorded continuously every 10 s for experiments with the chamber setup and every 16 s when the in-line probe was used (the acquisition time is dependent on the optical resolution and differed for the two spectrometers). The change between the frequencies of the ultrasonic field was performed as quickly as possible by turning a knob; typically this was accomplished in less time than it took to acquire one IR spectrum.

Switching off the ultrasonic field concluded the sequence; in the chamber setup a purging step was performed when the IR spectra suggested that some material was attached to the ATR. This was accomplished by driving the transducer at a frequency of about 170 kHz at 1 W true electrical power input.

RESULTS

Measurement of reference spectra of yeast

Reference spectra were acquired by letting yeast cells sediment on the tip of the vertically aligned ATR fiber probe. Figure 4 shows the resulting absorption spectra. The bands just below 1650 cm^{-1} and around 1550 cm^{-1} are called amide I and amide II, respectively, and reflect the presence of proteins in the evanescent field of the ATR. The high absorption around 1047 cm^{-1} is caused by the C–O stretching and C–O–H deformation oscillations of the carbohydrates contained in the yeast cells.

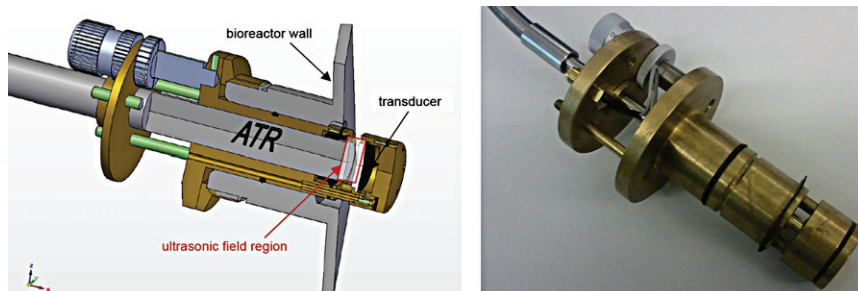


Fig. 3. (Left) Workshop drawing of the in-line probe connected to the bioreactor. The position of the ATR probe could be adjusted with the micrometer screw gauge along the axis, thus changing the resonator length between ATR probe and transducer. (Right) Photograph of the in-line probe.

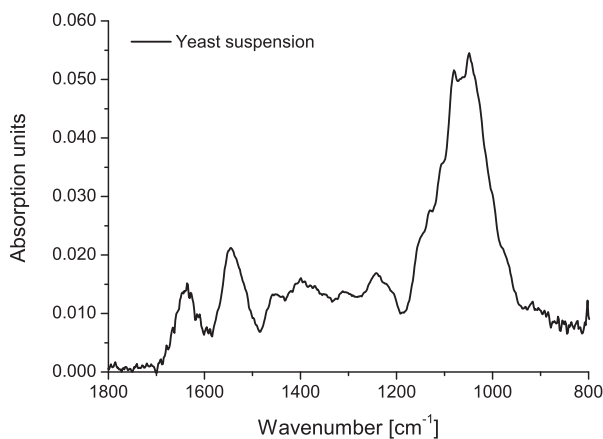


Fig. 4. Absorption spectrum of yeast cell sediment on top of the ATR fiber probe tip.

Measurements in chamber setup

Prior to the construction and application of an in-line probe, the brass chamber described before was used to prove that the concept of ultrasound-enhanced ATR spectroscopy of suspensions presented in Radel et al. (2010b) is applicable to yeast cells.

Figure 5 shows absorption spectra recorded during the experiments in the chamber setup. Spectra of yeast cells could be recorded when the pushing frequency ($f_2 = 1.863$ MHz) was applied at the time indicated by the black marker arrow in Figure 6.

The gray line in Figure 5 depicts the situation when cells are retracted from the evanescent field of the ATR by the USW at $f_1 = 1.878$ MHz (indicated by dark gray marker arrow in Fig. 6). A significant decrease in absorption by carbohydrates and amide II was detected. However, the amide I band was not lowered to the same

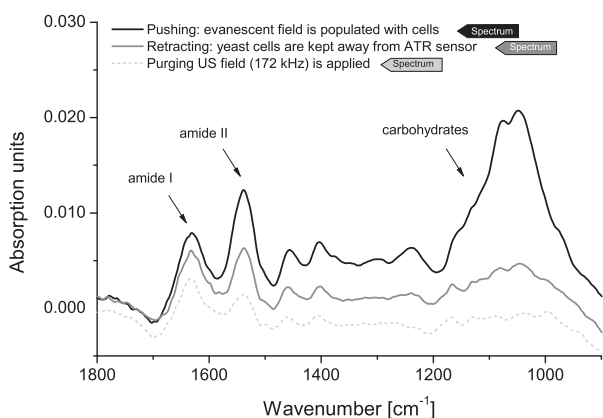


Fig. 5. Absorption spectra obtained when the evanescent field was populated with yeast cells (pushing frequency, black line) and when it was depopulated (retracting frequency, gray line) by the acoustic radiation forces. The dashed line represents the measurement obtained after application of a purge field at 170 kHz at the end of the experiment. The marker arrows in the legend refer to Figure 6.

extent. Application of the purge field at 170 kHz somewhat cleaned up the evanescent field region, as suggested by the further decrease in absorption (dashed line).

Figure 6 shows development of the absorption band at 1047 cm^{-1} (carbohydrate) during the sequences of pushing frequency and retracting frequency. Successful population and depopulation of the evanescent field at the surface of the ATR probe are strongly suggested by the steep increase in absorption at the switch to the pushing value f_2 . The increase was persistent while the transducer was driven at this frequency; however, the rate of increase decayed. As soon as retracting frequency f_1 was applied, absorption decreased abruptly. Again an ongoing decline was observed; however, it was less pronounced compared with the increase.

Over the course of the experiment, the maximum absorption reached during one cycle increased. Also, the absorption detected in retraction mode at f_1 increased over time, suggesting the occurrence of biofouling on the ATR surface. However, after a short application of the purging frequency (170 kHz) at the end of the experiment, the signal dropped to or even below the initial level, suggesting that the ATR sensor surface was free of cellular material.

Table 1 gives the maximum absorption reached when applying the pushing frequency f_2 and when letting the cells sediment on the ATR element (the same yeast suspension was used). In this setup, absorption using acoustic radiation forces reached about 50% of the maximum absorption when the cells sedimented onto the ATR.

Measurements with in-line probe

After the successful experiments with the chamber setup, the in-line probe was constructed, assembled and

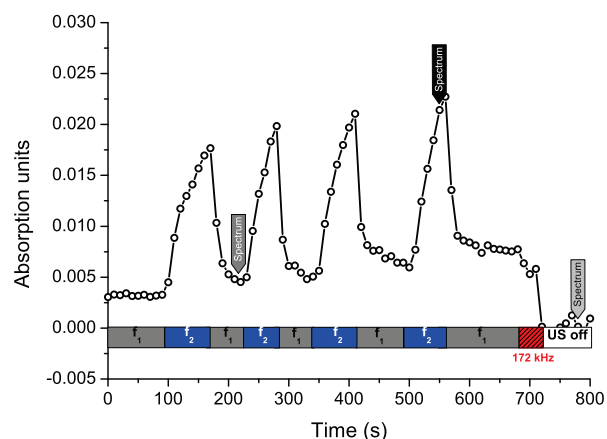


Fig. 6. Change in the carbohydrate absorption band at 1047 cm^{-1} during repeated applications of the pushing and retracting frequencies in the chamber setup. The absorption reflects the amount of yeast cells in the evanescent field of the ATR probe.

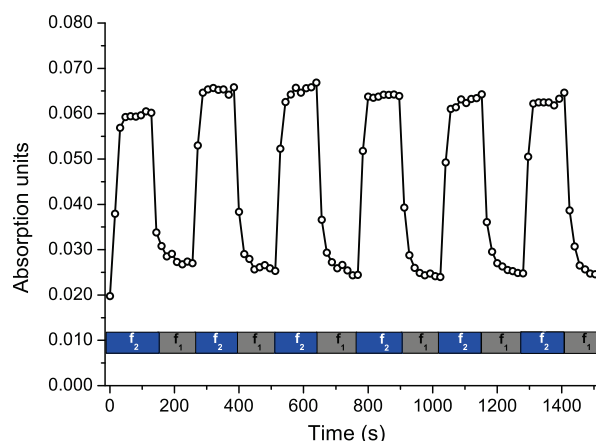
Table 1. Maximum absorption found when applying the pushing frequency and when letting the cells sediment onto the ATR element of the respective setup.

Setup	Maximum absorption (mAU)	
	Ultrasound	Sedimentation
Chamber	23	54
In-line probe	46	164

tested. For the in-line probe setup the yeast cells were pushed into the evanescent field of the ATR probe at $f_2 = 1.990$ MHz and retracted at $f_1 = 1.956$ MHz. The repeated switching of the USW between pushing and retracting frequency again resulted in distinct increases and decreases in absorption. The absorption measured after the ultrasonic field had been switched off was significantly reduced, indicating that most of the cells had left the evanescent field. The respective maximum absorption values for the same yeast suspension when the cells were allowed to sediment on the ATR element and when measured in-line are given in Table 1. In the presence of ultrasound, the maximum absorption observed was about 30% of the value seen when cells were allowed to sediment on the probe.

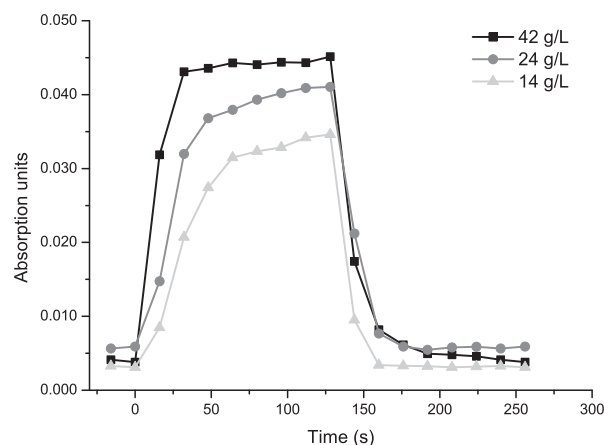
The change in the carbohydrate absorption band over time is shown in Figure 7. Pushing frequency f_2 was applied during the recording of eight absorption spectra, where each absorption measurement is represented by a data point in Figure 7; then a switch to retracting frequency f_1 was made and again eight spectra were recorded. This was repeated five times. Absorbance increased rapidly when the switch was made from retracting frequency f_1 (gray bar in Fig. 7) to pushing frequency f_2 (blue bar in Fig. 7). After the switch back to f_1 , the signal dropped instantaneously, indicating that the cells were removed from the evanescent field very quickly. The maximum absorption values were seen to increase slightly with successive cycles. When the ultrasonic field was switched off at the end of the experiment, the signal dropped to zero quickly, which was assumed to be caused by gravity; application of the purging frequency was not necessary, in contrast to the chamber setup (Fig. 6).

Differences in the rate of increase are suggested by the data illustrated in both Figure 6 and Figure 7. An influence of cell concentration was suspected. The measurements shown in Figure 8 were conducted to evaluate the influence of this parameter. Maximum absorption was found to increase with yeast cell concentration, as can be seen in Figure 8. There, the average absorption values recorded for yeast concentrations of 14, 24 and 42 g/L are shown as an example. Moreover, during a pushing cycle, a change in the rate of absorption increase with yeast cell concentration is noticeable.


 Fig. 7. Repeated applications of the pushing (f_2) and the retracting (f_1) frequencies recorded with the in-line probe. Population/depoulation of the ATR is indicated by the temporal development of an absorption band (carbohydrates) of the yeast cells.

Values close to maximum absorption are reached faster for 42 g/L than for 14 g/L.

To analyze this change in increase rate further, the absorption values measured at each concentration were normalized to the respective absolute maximum found and the single pushes were averaged. In other words, the respective spectra acquired during application of the pushing frequency f_2 were averaged for each time point of the push: the absorptions acquired immediately after applying f_2 ($\Delta t = 16$ s) were averaged, the absorptions found at $\Delta t = 32$ s after the switch to f_2 were averaged (*i.e.*, the second spectrum acquired after switching to f_2 for each push), and so on. The first push was omitted because the increase differed from those for the


 Fig. 8. Change in absorption of the carbohydrate band with yeast cell concentration when the pushing frequency is applied (recorded with the in-line probe). Each data point was calculated as the average absorption measured at the time elapsed (Δt) after sonication at pushing frequency; that is, $t = 0$ s corresponds to the last spectrum before application of the pushing frequency, $\Delta t = 16$ s is the average of the first spectrum after pushing frequency was switched on, and so on.

consecutive six pushes for all concentrations. In Figure 9 these data are shown for yeast cell concentrations of 14, 17, 24, 35 and 42 g/L (from top to bottom). The different increase rates are well visible; maximum absorption is reached later at low concentrations (14–24 g/L) than at high concentrations (29–42 g/L). Furthermore, the variations between single pushes are reflected by the standard deviations; low concentrations showed higher push-to-push variations than high concentrations. The standard deviation (*i.e.*, push-to-push variation) for 14 g/L is higher than that for 17 g/L; the same holds true for 35 and 42 g/L.

The average normalized absorption values measured at $\Delta t = 16$ s (first spectrum after application of f_2 for pushes 2 to 7) differ significantly from each other for all concentrations (two-sided t-test, $\alpha = 0.05$), except for the two highest concentrations; the mean absorption

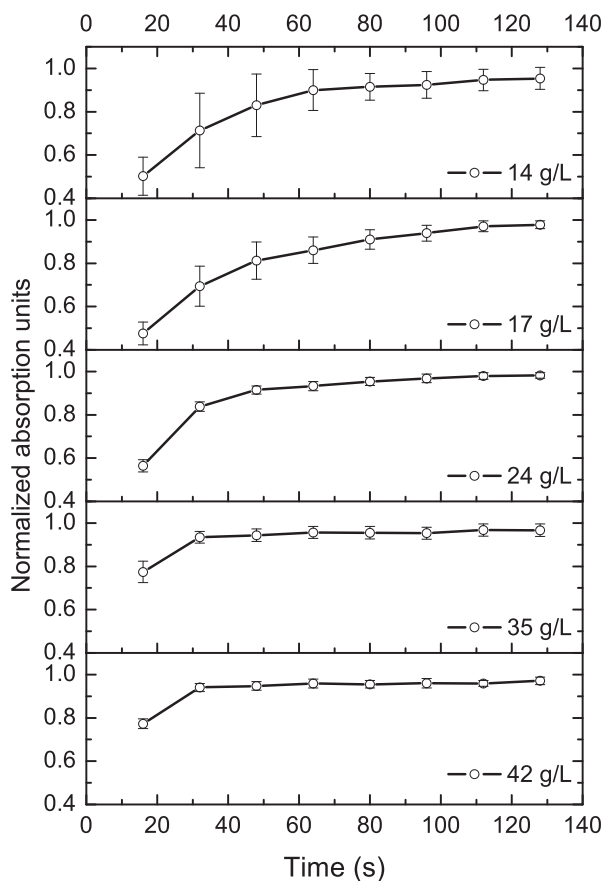


Fig. 9. Absorptions normalized to the absolute maximum found for each concentration and averaged over the applications of pushing frequency (averaged over all spectra acquired at $\Delta t = 16$ s after application of pushing frequency, at $\Delta t = 32$ s, *etc.*) recorded with the in-line probe. Note the change in the rate of increase in relative absorption with changing concentration and the differences in standard deviation with cell concentration stemming from push-to-push variations which are greater for smaller concentrations.

found for 35 g/L does not differ significantly from that found for 42 g/L. After $\Delta t = 80$ s (fifth spectrum after switching to f_2) no significant difference was found between mean normalized absorptions for all concentrations, indicating that values close to the absolute maximum had been reached by then for all pushes.

DISCUSSION

For both setups, substantial increases in the observed carbohydrate absorption bands were detected immediately after application of the respective pushing frequency. Cells located in the small volume between the ATR probe and the closest pressure nodal plane were obviously pushed toward the probe tip into the evanescent field region. Subsequently, additional cells were driven into this area because of the agitation of the suspension, leading to an increase in the signal up to a threshold. Moreover, the radiation forces might have increased the cell concentration at the location of sensitivity of the ATR.

With the pushing frequency applied, the rate of increase in absorption was observed for both experimental setups. In the chamber setup, the slopes appeared to be steeper. This could indicate an influence of the angle between the gravitational forces and the axial ultrasonic radiation force. This angle was different for the two setups, with a higher net pushing force for the chamber setup (90° between ultrasonic radiation force and gravitational force) than for the in-line probe (135° between the respective forces).

The absorption achieved when cells were actively pushed into the evanescent field by the USW was compared with the absorption reached by simple sedimentation of yeast cells on the ATR. It revealed that approximately 50% of the achievable absorption of the sediment was reached in the chamber setup and roughly 30% in the in-line probe, respectively. The reason for this difference might again be that the ultrasonic field was horizontal in the chamber setup, whereas the radiation forces had to push the cells 135° upward against gravity in the case of the in-line probe.

The increase in the peak value of absorption over several cycles of switching between retracting and pushing frequency is larger for the in-line probe than for the chamber setup. This could be attributed in part to the duration of the application of the retracting frequency at the beginning of the experiment. This period lasted about 180 s in the chamber setup, but only about 130 s for the in-line probe. During this time cells were possibly “pre”-agglomerating in the pressure nodal planes outside the evanescent field.

Measurements of different yeast cell concentrations with the in-line probe showed that high concentrations led to very fast increases in absorption toward the

maximum value observed; for low cell concentrations, this increase was found to be slower and more variable throughout consecutive applications of pushing frequency f_2 . This is most likely dependent on the number of cells available to contribute to mid-IR absorption, which is of course concentration dependent.

CONCLUSIONS

In this first step toward an inline ATR FT-IR spectroscopy probe for fermentation monitoring, we could successfully record spectra of yeast cells in stirred suspensions by applying ultrasonic radiation forces for particle manipulation. Yeast cells could in this way actively be forced into and out of the evanescent field region of an ATR probe. Hence, this ultrasound-enhanced fiber-optic probe enabled measurement of cells and supernatant separately. Furthermore, it was observed that the rate of increase in yeast-specific absorption bands during application of an USW at the pushing frequency depended on the cell concentration in the suspension. At all concentrations investigated, 90% of the maximum absorption measured was reached within 32 s. This would allow measurement intervals that are sufficiently short for quasi-real-time in-line fermentation monitoring.

Acknowledgments—The authors thank Volker Bauer and Herbert Schmidt for their efforts in construction and assembly of the in-line probe and Mettler Toledo (AutoChem, Dr. Kleimann) for provision of the ATR fiberoptic probe and the Fourier transform infrared spectrometer. We gratefully acknowledge the support of the Austrian Science Fund (FWF) within the Translational Research Project scheme, No. L416-N17. Cosima Koch gratefully acknowledges the support of the Applied Bioscience Technology (ABTec) Graduate School of Vienna University of Technology and of the FWF within the stand-alone project scheme, No. P24154.

REFERENCES

- Barnes RA, Jenkins P, Coakley WT. Preliminary clinical evaluation of meningococcal disease and bacterial meningitis by ultrasonic enhancement. *Arch Dis Child* 1998;78:58–60.
- Chalmers J, Griffiths P. *Handbook of vibrational spectroscopy*. New York: Wiley; 2002.
- Chisti Y. Sonobioreactors: Using ultrasound for enhanced microbial productivity. *Trends Biotechnol* 2003;21:89–93.
- Coakley T. Ultrasonic separations in analytical biotechnology. *Trends Biotechnology* 1997;15:506–511.
- Doinikov A. Acoustic radiation force on a spherical particle in a viscous heat-conducting fluid: III. Force on a liquid drop. *J Acoust Soc Am* 1997;101:731–739.
- Gherardini L, Cousins CM, Hawkes JJ, Spengler J, Radel S, Lawler H, Devic-Kuhar B, Gröschl M, Coakley WT, McLoughlin AJ. A new immobilisation method to arrange particles in a gel matrix by ultrasound standing waves. *Ultrasound Med Biol* 2005;31:261–272.
- Glynn-Jones P, Boltryk RJ, Hill M, Zhang F, Dong L, Wilkinson J, Melvin T, Harris N, Brown T. Flexible acoustic particle manipulation device with integrated optical waveguide for enhanced microbead assays. *Anal Sci* 2009;25:285–291.
- Gröschl M. Ultrasonic separation of suspended particles: Part I: Fundamentals. *Acustica* 1998a;84:432–447.
- Gröschl M. Ultrasonic separation of suspended particles: Part II. Design and operation of separation devices. *Acustica* 1998b;84:632–642.
- Harrick N. *Internal reflection spectroscopy*. New York: Interscience; 1967.
- Hawkes JJ, Limaye MS, Coakley WT. Filtration of bacteria and yeast by ultrasound-enhanced sedimentation. *J Appl Microbiol* 1997;82:39–47.
- Hawkes JJ, Long MJ, Coakley WT, McDonnell MB. Ultrasonic deposition of cells on a surface. *Biosensors Bioelectronics* 2004;19:1021–1028.
- Hill M, Hawkes JJ, Harris N, McDonnell M. Resonant ultrasonic particle manipulators and their applications in sensor systems. In: *Proceedings, 3rd IEEE Conference on Sensors*. IEEE, 2004:794–797.
- Jarute G, Kainz A, Schroll G, Baena J, Lendl B. On-line determination of the intracellular poly(beta-hydroxybutyric acid) content in transformed *Escherichia coli* and glucose during PHB production using stopped-flow attenuated total reflection FT-IR spectrometry. *Anal Chem* 2004;76:6353–6358.
- King LV. On the acoustic radiation pressure on spheres. *Proc R Soc A* 1934;147:212–240.
- Lendl B, Radel S, Brandstetter M. Device for FTIR absorption spectroscopy. WO Patent 2010. G01N 21/55.
- Palme O, Comanescu G, Stoinea I, Radel S, Benes E, Develter D, Wray V, Lang S. Sphorolipids from *Candida bombicola*: Cell separation by ultrasonic particle manipulation. *Eur J Lipid Sci Technol* 2010;112:663–673.
- Radel S, Gherardini L, McLoughlin A, Doblhoff-Dier O, Benes E. Breakdown of immobilisation/separation and morphology changes of yeast suspended in water-rich ethanol mixtures exposed to ultrasonic plane standing waves. *Bioseparation* 2000a;9:369–377.
- Radel S, McLoughlin A, Gherardini L, Doblhoff-Dier O, Benes E. Viability of yeast cells in well controlled propagating and standing ultrasonic plane waves. *Ultrasonics* 2000b;38:633–637.
- Radel S, Schnöller J, Gröschl M, Benes E, Lendl B. On chemical and ultrasonic strategies to improve a portable FT-IR ATR process analyzer for online fermentation monitoring. *IEEE Sensors J* 2010a;10:1615–1622.
- Radel S, Brandstetter M, Lendl B. Observation of particles manipulated by ultrasound in close proximity to a cone-shaped infrared spectroscopy probe. *Ultrasonics* 2010b;50:240–246.
- Saito M, Kitamura N, Terauchi M. Ultrasonic manipulation of locomotive microorganisms and evaluation of their activity. *J Appl Phys* 2002;92:7581.
- Schnöller J, Lendl B. A portable FTIR-ATR process analyzer-online fermentation control. In: *Proceedings, 3rd IEEE Conference on Sensors*. IEEE, 2004;2:742–745.
- Spengler J, Jekel M, Christensen K, Adrian R, Hawkes J, Coakley W. Observation of yeast cell movement and aggregation in a small-scale MHz-ultrasonic standing wave field. *Bioseparation* 2000;9:329–341.

Publication II

Maria Reyes Plata, Cosima Koch, Patrick Wechselberger, Christoph Herwig, Bernhard Lendl, *Analytical and Bioanalytical Chemistry* 405(25) (2013) 8241-50. (c) The author(s) 2013 under a Creative Commons Attribution (CC-BY) License.

DOI: 10.1007/s00216-013-7239-9

Determination of carbohydrates present in *Saccharomyces cerevisiae* using mid-infrared spectroscopy and partial least squares regression

Maria R. Plata · Cosima Koch · Patrick Wechselberger ·
Christoph Herwig · Bernhard Lendl

Received: 26 May 2013 / Revised: 24 June 2013 / Accepted: 9 July 2013
© The Author(s) 2013. This article is published with open access at Springerlink.com

Abstract A fast and simple method to control variations in carbohydrate composition of *Saccharomyces cerevisiae*, baker's yeast, during fermentation was developed using mid-infrared (mid-IR) spectroscopy. The method allows for precise and accurate determinations with minimal or no sample preparation and reagent consumption based on mid-IR spectra and partial least squares (PLS) regression. The PLS models were developed employing the results from reference analysis of the yeast cells. The reference analyses quantify the amount of trehalose, glucose, glycogen, and mannan in *S. cerevisiae*. The selection and optimization of pretreatment steps of samples such as the disruption of the yeast cells and the hydrolysis of mannan and glycogen to obtain monosaccharides were carried out. Trehalose, glucose, and mannose were determined using high-performance liquid chromatography coupled with a refractive index detector and total carbohydrates were measured using the phenol–sulfuric method. Linear concentration range, accuracy, precision, LOD and LOQ were examined to check the reliability of the chromatographic method for each analyte.

Keywords FT-IR spectroscopy · Partial least squares regression · *Saccharomyces cerevisiae* · Carbohydrates · HPLC-RI · Reference analysis

Electronic supplementary material The online version of this article (doi:10.1007/s00216-013-7239-9) contains supplementary material, which is available to authorized users.

M. R. Plata · C. Koch · B. Lendl (✉)
Institute of Chemical Technologies and Analytics,
Vienna University of Technology,
Getreidemarkt 9/164-UPA, 1060 Vienna, Austria
e-mail: bernhard.lendl@tuwien.ac.at

P. Wechselberger · C. Herwig
Institute of Chemical Engineering,
Vienna University of Technology,
Gumpendorferstraße 1a/166-4, 1060 Vienna, Austria

Introduction

The commercial exploitation of different microorganisms to convert chemical substrates to products of higher values is very important for several industries such as agricultural, pharmaceutical, and food industry. Yeast is the most widely used microorganism in industry and is especially important to brewing, wine production, distilling, and baking [1, 2]. The analysis of cells is of great scientific interest in the field of quality control of industrial processes. The variations in carbohydrate content of yeast suggest that these compounds play important roles during the yeast cycle [3, 4] and the control and quantification of these compounds is important because their concentrations are related to the metabolism of the yeast cells. The most common methods for studying the carbohydrate composition (mannan, trehalose, glucose, glycogen, etc.) are based on enzymatic and chromatography techniques (e.g., gas chromatography or high-performance liquid chromatography (HPLC)) [5–8]. In these techniques, tedious pretreatment steps of the cells are necessary to carry out carbohydrate determinations.

Fourier transform infrared (FT-IR) spectroscopy in the mid-IR range (400–4,000 cm^{-1}) can be applied as a useful tool for the analysis of entire yeast cells providing a fast, effective, reagent-free, and simple method [9, 10]. Since Beer's law is obeyed, the observed absorptions are proportional to analyte concentrations. In complex samples, linear regression between absorption band areas and analyte concentrations determined by a reference method are not enough to provide robust calibration; here, multivariate methods, like partial least squares (PLS) regression, have to be employed. Wold et al. [11] give a comprehensive introduction to PLS regression models, also discussing the validity and the predictive power of the PLS models. In the case of biological cells, a multitude of components contribute to the recorded mid-IR

spectra, which leads to strong overlapping of the absorption bands. PLS regression, however, can extract information on contributing components from the recorded spectra. In the last decades, several applications using FT-IR spectroscopy and multivariate chemometric tools have been published to monitor yeast metabolism taking advantage of the high sensitivity to small changes in the composition of cells [12–15]. FT-IR spectroscopy is a powerful tool for the time resolved and noninvasive measurement of multi-substrate/product interactions in complex metabolic networks such as the oscillating glycolysis in yeast extract identifying glycolytic intermediates [12]; the autolysis of *Saccharomyces cerevisiae* cells in a base wine studying partial hydrolysis of proteins; increase of peptides, free nucleotides, lipids, mannans, and beta-1,3 glucans [13, 14]; and the metabolic alterations of yeast cells induced by four chemical compounds: ethanol, sodium hypochlorite, sodium chloride, and sulfur dioxide taking into account five different spectral regions (fatty acids from 3,000 to 2,800 cm^{-1} , amides from 1,800 to 1,500 cm^{-1} , mixed region from 1,500 to 1,200 cm^{-1} , carbohydrates from 1,200 to 900 cm^{-1} , and typing region from 900 to 700 cm^{-1}) [15]. Kuligowski et al. [10] developed a rapid method for the discrimination of entire *Pichia pastoris* cells grown under different conditions based on the direct acquisition of mid-IR spectra in the fingerprint region (900–1,800 cm^{-1}) and partial least squares discriminate analysis.

The main objective of this study was to investigate the applicability of FT-IR spectroscopy as a rapid, precise, and accurate method not requiring sample preparation, for the determination and quantification of carbohydrate composition of *S. cerevisiae*. As a prerequisite, robust reference analysis methods for carbohydrates are needed. Only when reliable reference methods are available, a robust calibration for the different carbohydrates with respect to the recorded FT-IR spectra of the cells can be established. *S. cerevisiae* was selected because it is the most studied yeast due to the easy cultivation and short generation time and serves as a model of a eukaryotic cell. The main carbohydrates of yeast such as mannan, a cell wall polysaccharide composed of mannose units, and the intracellular carbohydrates, trehalose, a disaccharide of glucose, and glycogen, a polysaccharide of glucose, were studied. For reference analysis, the optimization of the cell disruption and hydrolysis processes and the validation of quantification methods are essential to avoid alterations in the final compositional results. The phenol–sulfuric method, a well-known method to determine the total carbohydrates, was used and a separation technique, liquid chromatography with refractive index detector, was used to determine individual carbohydrates, trehalose, glucose, glycogen, and mannan. The developed method uses a single sample with low sample volume requirement, generating reliable and precise results without interferences. These robust reference data are the basis for building PLS regression models for the individual

carbohydrates. Robust models, indicated by low cross-validation errors (root mean square errors of cross validation (RMSECV), to be more precise), show the suitability of FT-IR spectroscopy for simple and reagent-free determination of carbohydrates in yeast cells.

Materials and methods

Chemicals and reagents

All reagents were of analytical grade. For stock standard solutions, D-(+)-glucose monohydrate supplied by Fluka (Steinheim, Germany), trehalose and D-(+)-mannose obtained from Merck (Darmstadt, Germany), and glycogen desiccate type II from Oyster and mannan from *S. cerevisiae* purchased from Sigma (Saint Louis, USA) were used.

For the total carbohydrate method, phenol and sulfuric acid 95–98 % were supplied by Sigma-Aldrich (Saint Louis, USA). For glycogen hydrolysis, amyloglucosidase from *Aspergillus niger* were obtained from Fluka (Steinheim, Germany), and for mannan hydrolysis, hydrochloric acid 37 % and sodium hydroxide ≥ 98 % were purchased from Sigma-Aldrich (Saint Louis, USA).

All of the solutions were prepared in high purity deionized Milli-Q water (Millipore, Molshem, France).

Apparatus and materials

For acquisition of FT-IR spectra of dried yeast samples, a Bruker Optics Hyperion 3000 FT-IR microscope connected to a Bruker Optics Tensor 37 spectrometer (both Ettlingen, Germany) was used. It was equipped with a liquid nitrogen-cooled single point mercury–cadmium–telluride detector and a 15-fold Cassegrain objective. The dedicated software OPUS 7 (Bruker Optics) was used for recording spectra and instrument control. A Genesys 20 Visible spectrophotometer (Thermo Scientific, Waltham, USA) was used for all the photometric measurements, a heating oven (Binder, Tuttlingen, Germany) for biomass dry weight determination, and a heating plate (Ika Labortechnik, Staufen, Germany) and a Vortex (Yellow Line TTS2, Wilmington, USA) for shaking the samples. An Eppendorf Mini Spin centrifuge for microcentrifuge tubes and an Eppendorf 5810R centrifuge (Hamburg, Germany) for centrifuge tubes were used. The pH measurements were carried out using the portable WTW pH meter 3400i (Weilheim, Germany). Fermentations were carried out in a 15-L autoclavable, fully automated and controlled-stirred bioreactor (Infors, Switzerland) coupled to the integrated process control and management system Lucullus (SecureCell AG, Schlieren, Switzerland).

Microorganism and culture conditions

In order to optimize the experimental conditions for carbohydrate measurements, commercial pressed baker's yeast (*S. cerevisiae*, "Mautner Markhof"—Austria Hefe AG, Austria) were used. The yeast was stored at 8 °C and was taken out just before running the experiment to avoid contamination. The yeast cells were suspended in deionized water following centrifugation at $6,575\times g$ for 10 min. The supernatant was decanted and, subsequently, the cells were resuspended in deionized water and vortexed to ensure good mixing. The washing procedure was repeated four times. After that, different amounts of cells were resuspended in 4 mL of water and used as standards.

For yeast fermentation, yeast peptone glucose (YEPG) medium was prepared as preculture medium (40 g L⁻¹ glucose, 5 g L⁻¹ peptone, and 5 g L⁻¹ yeast extract). The YEPG medium was autoclaved at 121 °C for 20 min. One milliliter of frozen stock of *S. cerevisiae* (strain, CBS 8340) was added to 200 mL of YEPG medium under sterile conditions and subsequently incubated for 24 h at 30 °C and 220 rpm in shake flasks.

Six liters of batch medium was prepared using 20 g L⁻¹ glucose, 5 g L⁻¹ ammonium sulfate, 3 g L⁻¹ potassium hydrogen phosphate, and 0.5 g L⁻¹ magnesium sulfate heptahydrate. Additionally, 2.67 mL L⁻¹ of sterile vitamin and trace element solutions, respectively, as well as 0.1 mL L⁻¹ of sterile antifoam were added after autoclavation (121 °C, 20 min). For the subsequent fed-batch fermentation, 4 L of feed medium containing 100 g L⁻¹ glucose, 3 g L⁻¹ potassium hydrogen phosphate, 0.5 g L⁻¹ magnesium sulfate heptahydrate, and 2.67 mL L⁻¹ of sterile vitamin and trace element solutions, respectively, as well as 0.1 mL L⁻¹ of sterile antifoam was made. The conditions of the batch fermentation were 6 L min⁻¹ (1 vvm) of airflow, 800 rpm speed of agitation, temperature was set to 30 °C, and the pH automatically adjusted to 4.8 by addition of 2 M NaOH. All reagents for yeast media were supplied by Carl Roth GmbH (Karlsruhe, Germany). The batch process was started by inoculation with 600 mL of preculture (10 % of batch volume). During the fed-batch phase, conditions were the same as for the batch phase except that the airflow was adjusted to remain at 1 vvm, i.e., increased with culture volume.

Sampling and pretreatment

During the fermentations, several samples from the bioreactor were taken. Each sample was split up for duplicate biomass dry weight determination (5 mL in pre-weighted test tubes) and a pellet sample for carbohydrate determinations by FT-IR spectroscopy of whole cells and by HPLC after a disruption process (20 mL). A schematic of sampling and pretreatment steps can be seen in Fig. 1a. All the samples were centrifuged for 10 min at $5,000\times g$ and 4 °C and,

afterwards, the medium (supernatant) was discarded. The yeast cells were resuspended in distilled water and centrifuged again for 10 min to rinse the cells. The washing procedure was repeated two times in order to eliminate potential interferences of the medium. The supernatants were removed carefully. During the whole process, the samples were stored on ice to avoid and stop further reactions. The pellet samples for carbohydrate determination were stored in the freezer (-20 °C).

For determination of biomass dry weight, the yeast cells in the pre-weighted test tubes were dried in a heating oven for 72 h at 105 °C. The cell dry weight was determined gravimetrically.

For carbohydrate measurements, each sample (pellet) was resuspended in 5 mL Milli-Q water and split off to carry out FT-IR measurements (1 mL) and reference analyses (4 mL).

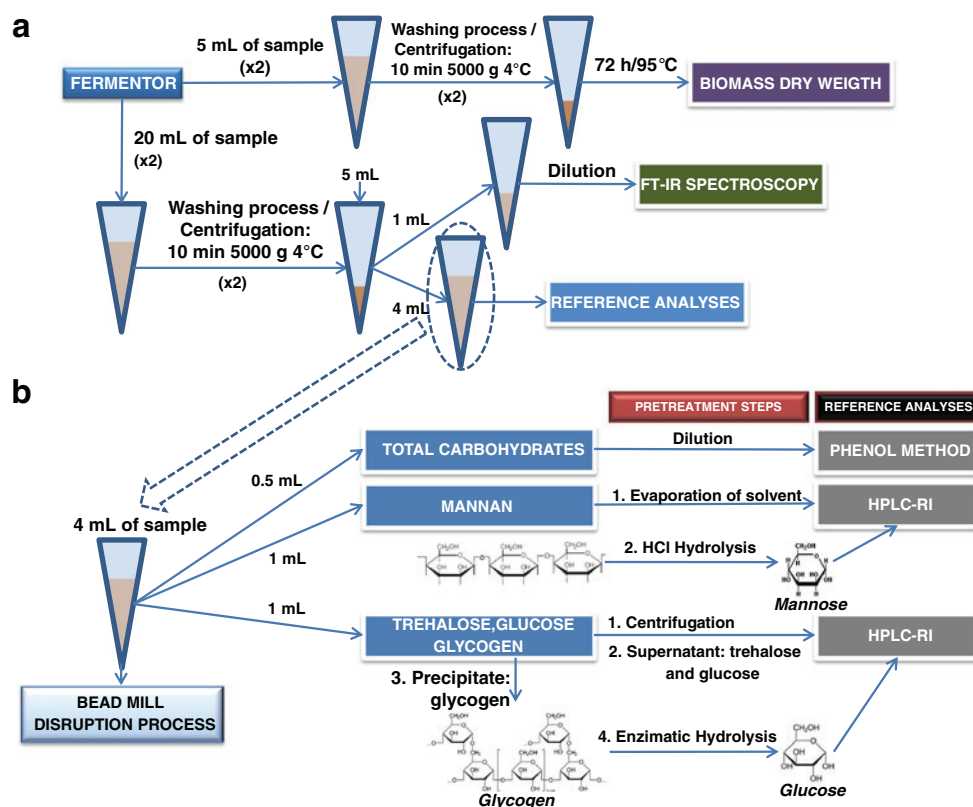
FT-IR spectroscopy of dried yeast samples

One milliliter of the washed and resuspended fermentation sample (pellet) was used for FT-IR spectroscopy. The measurement procedure was guided by Kuligowski et al. [10]. Absorbance spectra were recorded in the spectral range between 4,000 and 600 cm⁻¹ with a spectral resolution of 4 cm⁻¹ as the co-addition of 32 scans in transmission mode. Dilution rates were adjusted between 1:10 and 1:20 depending on the initial biomass concentration of the respective sample. Three spots of 3 µL each were pipetted onto a zinc selenide (ZnSe) slide and the H₂O was allowed to evaporate in the dry air-purged sample compartment of the microscope. Built-in shutters were used to limit the area of acquisition to 100×100 µm. A background spectrum was acquired on a clean part of the ZnSe slide and 40 to 50 spectra of each yeast sample spot were recorded at different positions. Measurement time for each sample spot was around 3 min. A mean spectrum of each sample spot was calculated for further analysis, thus three spectra per sample were available.

Reference analyses

To obtain reference results for FT-IR spectroscopy, the carbohydrates of yeast cells were measured using several pretreatment steps and different methods as can be seen in Fig. 1b. For reference analyses, it was necessary to rupture the cells using 6 g acid-washed glass beads (diameter: 0.45–0.55 mm) from Sigma (St. Louis, USA) as abrasive and 4 mL cell suspension (dry weight from 20 mL fermentation sample) in a glass tube. The cell disruptions were carried out using a bench-top vortex homogenizer at 2,500 rpm 12 times for 1 min each, with 1 min of pauses on ice bath between vortexing.

Fig. 1 Diagram of the sampling and pretreatment steps of real samples (a); experimental process to carry out the reference analyses (b)



After the disruption, the sample was split to measure total carbohydrates (0.5 mL), mannan (1 mL), glucose, trehalose, and glycogen (1 mL). The aliquots were kept on ice at a temperature below 4 °C to avoid the hydrolysis of trehalose to glucose by enzymes released by cell disruption.

For total carbohydrate measurements, the phenol-sulfuric acid method [16] using glucose as standard was used. One milliliter of suspension containing between 20 and 200 µg of carbohydrates was mixed with 1 mL of 5 % (w/v) phenol solution. Subsequently, 5 mL of sulfuric acid was added and carefully mixed using a vortex. The absorbance at 488 nm after incubation for 10 min at room temperature and 20 min at 30 °C is proportional to the initial carbohydrate concentration of the sample. A calibration curve using a series of standards of glucose between 0 and 200 mg L⁻¹ was constructed. Several dilutions were carried out in function of the concentration of yeast to obtain suitable absorbance values. For yeast cell concentrations from 0 to 5 g L⁻¹, dilution factor (DF) was 10, from 5 to 25 g L⁻¹ DF was 50, for 25–50 g L⁻¹ DF was 125, for 50–100 g L⁻¹ DF was 250, and for 100–150 g L⁻¹ DF was 375.

The measurement of the individual carbohydrates was achieved using an ion exchange chromatographic method. An Ultimate 3000 Dionex HPLC equipment (Thermo Scientific, USA) coupled with a refractive index detector (Shodex® RI-101, Shoko Scientific, Japan) was used. The Chromeleon

Chromatography Management Software from Dionex was used for chromatogram acquisition and data analysis. The column used to achieve the complete separation of carbohydrates was the Recex RCM-Monosaccharide Ca²⁺ column with a size of 300 × 7.8 mm (Phenomenex, Germany). In order to protect the analytical column, a Security Guard Cartridge (Carbo Ca²⁺, 4 × 3 mm, Phenomenex) was used. The stationary phase of both, the guard and the analytical column, was an anion exchange resin with Ca²⁺ counter ions, with a particle size of 8 µm and 8 % cross-linkage. The experimental conditions summarized in Table 1 have been published by Mazaverica et al. [17] and Kuligowski et al. [18]. This separation method is, however, only applicable to disaccharides

Table 1 HPLC conditions to separate carbohydrates with HPLC and RI detection

Experimental conditions	
Mobile phase	Milli-Q Water
Chromatographic mode	Isocratic
Flow rate	0.6 mL
Temperature	80 °C
Injection	20 µL
Detector temperature	35 °C

and monosaccharides. Therefore, it was necessary to carry out pretreatments of the sample to obtain mannose and glucose from the mannan and glycogen, respectively. In the case of mannan, a hydrolysis process was utilized. One milliliter of suspension sample after the disruption process was dried at 95 °C during 24 h and then resuspended in 3 mL of 2 M HCl and heated in sealed glass tubes at 100 °C for 7 h [6]. The tubes were cooled on ice and the hydrosylate was neutralized with 2 M NaOH. Several standards using mannan from *S. cerevisiae* (333–2,570 mg L⁻¹) were prepared to relate the mannan concentration with the real samples. No interferences were found because the only polysaccharide containing mannose was mannan. Finally, the last aliquot, 1 mL of disrupted cell suspension, was used to determine trehalose, glucose, and glycogen. Glycogen is insoluble in water; therefore, the suspension was centrifuged at 6,575×g for 10 min at 4 °C to separate the supernatant, containing trehalose and glucose, and precipitate, containing glycogen (Fig. 1b). The supernatant was directly determined using the chromatographic separation. The precipitate, however, needed a pretreatment step to hydrolyze the glycogen to glucose for chromatographic measurements. Since trehalose and glucose were removed first, the enzyme could only digest glycogen, therefore avoiding interferences and the overestimation of the glycogen content. The glycogen was hydrolyzed using the amyloglucosidase enzyme. One milliliter of solution containing 1 mg mL⁻¹ of amyloglucosidase was added to the disrupted cells and incubated for 2 h at 60 °C. Several standards using glycogen from *Oyster* (240–3,000 mg L⁻¹) were prepared to relate the glycogen concentration with real samples.

Partial least squares regression

The PLS toolbox 6.2.1 (Eigenvector Research, Wenatchee, WA, USA) and Matlab 7.10.0 (Mathworks, Natick, MA, USA) were used for data treatment and building PLS regression models, correlating the FT-IR spectra with mannose, trehalose, and glycogen concentrations found with the reference methods described above. To compensate for differences in sample thickness, spectra were normalized (min–max) to the amide I band (1,740–1,575 cm⁻¹) since the protein content of

the cells remained nearly constant over the course of the fermentation (determined using the bicinchoninic acid assay, data not shown). Appropriate spectral regions for calibration were chosen with consideration of pure analyte spectra. For all three analytes, the wavenumbers chosen were in the carbohydrate region of C–O and C–O–C stretching (900–1,200 cm⁻¹) [19]. To test the PLS regression models for their ability to predict new, unseen data, i.e., their ability to predict analyte concentrations from spectra not included in the calibration set, cross-validation was performed using random subsets. For this purpose, the calibration set was divided into a set number of subsets and a PLS regression model excluding one of the subsets was built. The excluded subset was used to validate the PLS model, i.e., the concentrations predicted by the PLS model (y_i) for these data were compared to the values determined by reference analysis (\hat{y}_i). One iteration of the process corresponded to repeating the process until all subsets had been used for validation of models built excluding these. The RMSECV, i.e., the normalized sum square of the residuals, which is calculated as

$$\text{RMSECV} = \sqrt{\frac{\sum_i^n (\hat{y}_i - y_i)^2}{n}}$$

was calculated using these data; it is a measure of the error one can expect when predicting analyte concentrations from unknown spectra using the PLS model, a low RMSECV is therefore desirable. Here, eight data splits and three iterations were used for the calculation of the RMSECV. Different data preprocessing methods were tested and the methods leading to the lowest RMSECV were chosen. For all three analytes, calculation of second derivative (Savitzky–Golay, polynomial order 2, window size 15) and mean centering of data led to the best results.

Table 2 Figures of merit for trehalose and glucose standards and for glucose and mannose after hydrolysis process using a HPLC with RI detection

Analyte	Linear regression equation ^a	Linear range (mg L ⁻¹)	R ²	LOD (mg L ⁻¹)	LOQ (mg L ⁻¹)
Mannose ^b	$y = (0.0016 \pm 0.0000)x + (0.5204 \pm 0.0409)$	333–2,570	0.991	26	87
Trehalose	$y = (0.0036 \pm 0.0000)x - (0.0013 \pm 0.0040)$	50–5,000	0.999	12	39
Glucose	$y = (0.0036 \pm 0.0000)x - (0.0337 \pm 0.0689)$	50–5,000	0.999	12	39
Glycogen ^b	$y = (0.0017 \pm 0.0000)x + (0.2278 \pm 0.0447)$	240–3,000	0.992	25	82

^a Calibration curve obtained with standards. Concentration versus peak area

^b After hydrolysis process

Results and discussion

Reference analyses

Several processes of reference analyses such as the disruption method, mannan hydrolysis, and glycogen hydrolysis were selected and optimized in order to get precise and reliable results. Moreover, the validity of the reference analyses was tested by carrying out repeatability, reproducibility, and linearity studies; results are shown in the section below.

Selection of disruption method

For the purpose of determining the intracellular carbohydrate content of yeast, the cells must be disintegrated by mechanical means or non-mechanical methods (physical, chemical, or enzymatic) [20, 21]. The method of choice needs to be compatible with the measurements of the chemical content of the yeast without interferences. Furthermore, a high percentage of cell disruption, adequate for small-scale applications with a high throughput and of course short times is desirable. The mechanical methods are most efficient for cell disruption at small and large scale [22]. Several methods/protocols based on mechanical methods were tested and optimized: ultrasound, homogenization, boiling, freeze–thawing, and bead milling disruption (details see [Electronic Supplementary Material](#)). The best results were achieved when the bead milling method was applied. This procedure is particularly efficient in the disruption of yeasts which have rigid cell walls constituted by polysaccharides (80–90 %) [21]. Factors governing the performance of the bead mill process including impeller speed, cell density, amount, and size of the glass beads were optimized [21]. Percentages of cell breakage higher than 80 % were achieved using this modified Ricci-Silva et al. method [21]. Disruptions were carried out in glass tubes with a ratio of 1 mL of suspension/1.5 g of glass beads (diameter, 0.45–0.5 mm) for 12 cycles, each using a bench-top vortex at 2,500 rpm with 1 min intervals on ice (see [“Materials and methods”](#)).

Selection and optimization of mannan hydrolysis

Mannan, composed mainly of D-mannose, is a major constituent of the yeast cell wall, accounting for approximately 13 % (w/w) [23]. This polysaccharide possesses a backbone of α -(1–6)-linked D-mannose units which are substituted by side chains containing (1–2) and (1–3)-linked D-mannose units [24]. Two methods to hydrolyze mannan to mannose were tested. First of all, α -mannosidase from *Canavalia ensiformis* (Jack bean) (Sigma-Aldrich) was used; 0.5 mL of 0.45 mg L^{−1} α -mannosidase solution was added to 1.5 mg of mannan in presence of 1.5 mL of 20 mM sodium acetate (pH = 8). The final concentration of mannan was 750 mg L^{−1}. The solution was kept overnight at room temperature. No peak was obtained

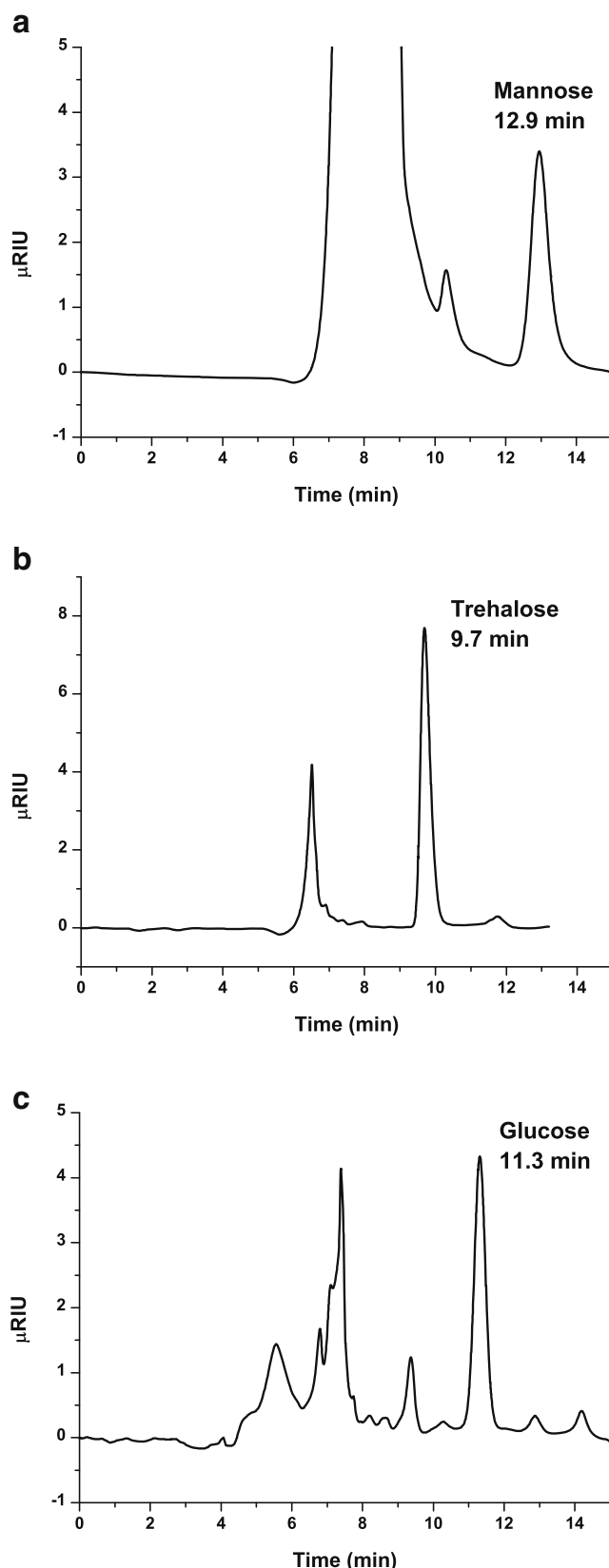


Fig. 2 Chromatograms of mannose using a mannose standard solution (a); trehalose and glucose (b) and glucose from glycogen (c) using a yeast standard sample

when the sample was analyzed by HPLC-refractive index (RI) method. Therefore, HCl hydrolysis was selected to hydrolyze mannan samples based on the method published by Dallies et al. [6]. The dried mannan samples were mixed with 3 mL of 2 M HCl and heated in sealed tubes at 100 °C for 1–10 h. Then, the tubes were cooled on ice and the hydrolysate was neutralized with 2 M NaOH. The effect of the heating time (1 to 10 h) of the glass tubes was studied and 7 h was selected for achieving the best yield of disruption of mannan.

Selection and optimization of glycogen hydrolysis

Glycogen is a branched polymer of α -(1–4) and α -(1–6)-glycoside bonds. The hydrolysis of both types of bonds is achieved using the enzyme amyloglucosidase from *A. niger* which is thus well suited for complete degradation of glycogen [7]. Several publications found that the enzyme degraded 97 % of glycogen [7, 25]. The optimized hydrolysis is based on the Bernfeld method [26]. Parameters such as the concentration of the enzyme, temperature, and exposure time of the hydrolysis process were optimized to obtain the maximum percentage of glucose for the same amount of glycogen (see Electronic Supplementary Material Figure S1). The diluted glycogen standard samples (DF 50) were injected into the chromatographic system after the hydrolysis process. The area of the glucose peak was calculated and used to monitor the hydrolysis reaction and hence the yield of this reaction could easily be evaluated. The optimal conditions are described in section “Materials and methods.”

Analytical features of HPLC-RI

The characteristic parameters of the analytical method obtained under the optimum conditions were evaluated. Mannan and glycogen samples after the hydrolysis process and standard of trehalose and glucose were used. The respective LODs and LOQs were determined and the precision of the method was checked in terms of repeatability and intermediate precision (reproducibility) (details see Electronic Supplementary Material and Table S1). Table 2 shows the

LOD and LOQ values for each analyte. The calibration curve was checked by analyzing standard solutions of each analyte at eight different levels. A linear regression equation with a regression coefficient near to the unit was obtained (Table 2). To check the accuracy of the proposed method, several synthetic mixtures containing the analytes in variable amounts were prepared and analyzed in triplicate using the HPLC-RI method. Quantification was achieved in terms of peak areas and the results were expressed as mean value and recoveries were calculated. In all cases, recoveries were very close to 100 % and relative deviations were between 0.1 and 6.3 %.

Analysis of baker's yeast standards

In order to demonstrate the applicability of the proposed method, six samples with different concentrations of baker's yeast were prepared as standard samples. First of all, the dry weight was determined to calculate the initial concentration of yeast, and then the concentration of each carbohydrate was determined using the respective methods. A chromatogram of 850 mg⁻¹ mannan standard after the hydrolysis process is shown in Fig. 2a. The experimental signal for 0.6 g L⁻¹ standard of yeast after applying the trehalose and glucose method is shown in Fig. 2b. A peak of trehalose can be observed but the area of the glucose peak is not enough to be quantified. Figure 2c corresponds to a 34.5 g L⁻¹ standard of yeast after applying the glycogen method. The area of the glucose peak can be related to the glycogen concentration of yeast. Finally, the percentages of each carbohydrate were calculated by dividing the concentration of carbohydrate by the concentration of yeast and multiplying by 100. The cell concentration in the samples ranged from 10 to 35 g L⁻¹. Table 3 lists the results for carbohydrate content relative to biomass dry weight (%DW) of the respective samples. They are in nice agreement with each other, indicating that dilution factors were correct and the method is valid for the range of cell concentrations. The %RSD values for all methods were between 2.7 and 7.1 %.

Table 3 Percentages of carbohydrates from baker's yeast samples after disruption process by the developed methods, phenol method for total carbohydrates, and trehalose, glucose, glycogen, and mannose using the HPLC-RI ($n=3$)

Analyte	Sample 1	Sample 2	Sample 3	Sample 4	Sample 5	Sample 6	Average \pm SD
Total carbohydrates	48.1 \pm 0.2	45.6 \pm 0.7	43.2 \pm 0.3	42.3 \pm 0.5	42.6 \pm 0.1	39.9 \pm 0.1	43.6 \pm 2.9
Mannose ^a	8.9 \pm 0.1	9.4 \pm 0.1	8.4 \pm 0.1	8.6 \pm 0.1	9.5 \pm 0.3	9.8 \pm 0.0	9.1 \pm 0.6
Trehalose	8.7 \pm 0.1	9.3 \pm 0.2	9.4 \pm 0.1	9.2 \pm 0.1	9.3 \pm 0.1	9.1 \pm 0.0	9.2 \pm 0.2
Glucose	2.0 \pm 0.2	2.4 \pm 0.2	2.2 \pm 0.1	2.1 \pm 0.1	2.2 \pm 0.1	2.2 \pm 0.1	2.2 \pm 0.1
Glycogen ^a	1.9 \pm 0.1	2.0 \pm 0.1	2.1 \pm 0.0	2.0 \pm 0.0	2.3 \pm 0.1	2.2 \pm 0.0	2.1 \pm 0.1
Sum	21.5 \pm 0.5	23.1 \pm 0.6	22.1 \pm 0.3	21.9 \pm 0.3	23.3 \pm 0.5	23.3 \pm 0.1	22.5 \pm 0.8

^a After hydrolysis process

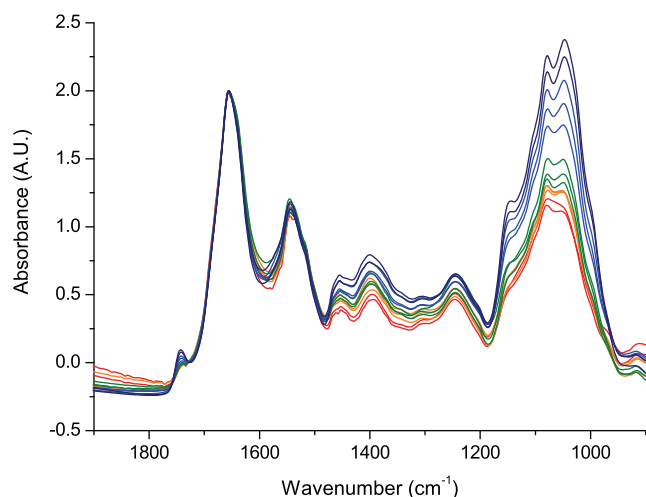


Fig. 3 FT-IR spectra of whole *S. cerevisiae*. Samples were drawn from nitrogen limit fed-batch fermentation 1 at different times over the course of the fermentation

Analysis of yeast samples from fed-batch fermentations

The outlined method has been used to study the carbohydrate content of *S. cerevisiae* in nitrogen-limited fed-batch fermentation. After 24 h of batch cultivation, the conditions changed to a nitrogen-limited fed-batch fermentation. A medium deficient in nitrogen lead to the accumulation of storage carbohydrates such as trehalose and glycogen and structural modifications. The change of the carbohydrate composition could be studied using the proposed method and reference analyses using several samples taken from the fermentor during the fed-batch process. The FT-IR spectrum of each sample was measured in triplicate for both fermentations. In Fig. 3, the average mid-IR absorbance spectra acquired from samples at different time points between 1,900 and 900 cm^{-1} are shown for fed-batch fermentation 1. In the depicted region, the main spectral contributions are derived from proteins (amide I (1,660 cm^{-1}) and amide II (1,540 cm^{-1}) bands), the region from 1,500 to 1,250 cm^{-1} with less intense and strongly overlapping bands which correspond to proteins, lipids, and storage carbohydrates and the region between 1,250 and 900 cm^{-1} for carbohydrates with a minor contribution of phosphate bands from DNA, RNA, and phospholipids. The data were normalized to the amide I band and significant changes over fermentation time can be observed. To get an estimate of the total carbohydrate content of the cells, the

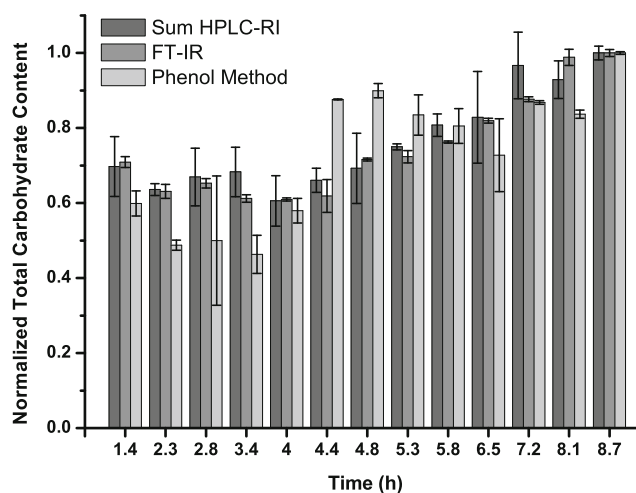


Fig. 4 Variations of normalized total carbohydrate content for real samples from nitrogen limited fed-batch fermentation 1 of *S. cerevisiae* applying reference and FT-IR methods

area under the carbohydrate bands (1,186–936 cm^{-1}) was calculated and normalized by biomass. The carbohydrate content relative to protein content increased with time and spectral features in the carbohydrate region changed, indicating a change in the carbohydrate constitution of the cells. These results were compared to data obtained by the phenol method and the sum of values obtained by HPLC-RI for each carbohydrate (mannan, trehalose, and glycogen). Figure 4 shows the normalized total carbohydrate content in function of time for each method. In accordance with the data obtained from FT-IR spectra, both the phenol method and the sum of carbohydrates determined by HPLC-RI increase over the course of the fermentation. The carbohydrate content found by calculation of the sum of HPLC-RI measurements of the respective analytes and by FT-IR spectroscopy are in good agreement with each other over the course of the fermentation. The total carbohydrate content was practically constant until 4.4 h, and a linear increase was observed for times greater than 4.8 h. The results obtained from the phenol method, however, show a different development: an almost sinusoidal development was observed. When only comparing the values found at the beginning and at the end of the fermentation, the same trend as for the other data was found: an increase of the total carbohydrate content. It should be noted that the standard deviations of experimental data for FT-IR method are lower than those of the two other

Table 4 Parameters and root mean square error of cross-validation of PLS models for trehalose, glycogen, and mannan

Analyte	Calibration range (% dry weight)	Spectral range (cm^{-1})	Latent variables	RMSECV (% dry weight)
Mannan	14.40–22.90	1,184–895	7	1.17
Trehalose	0.55–3.31	1,184–956	5	0.33
Glycogen	0.91–6.10	1,188–925	4	0.56

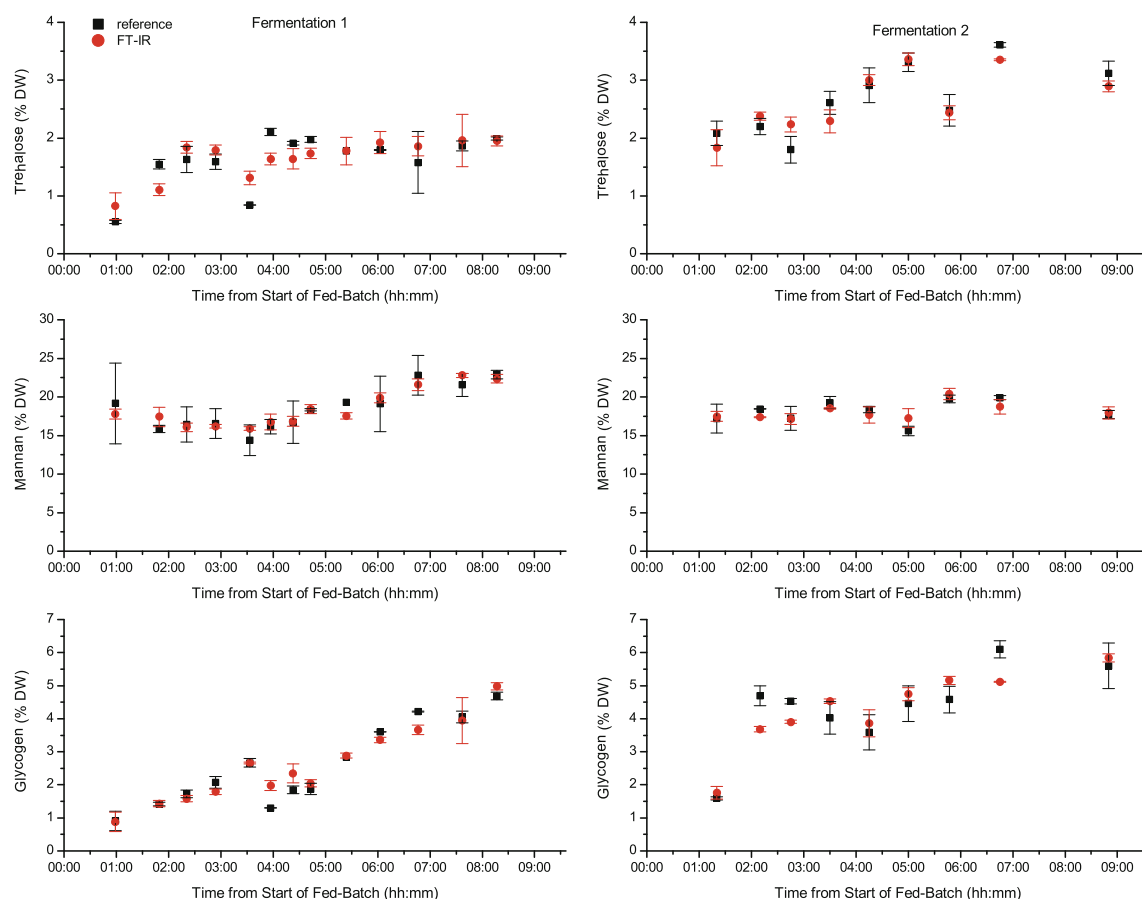


Fig. 5 Relative trehalose, mannan, and glycogen content of the samples drawn from fermentations 1 and 2 at different times determined by reference analysis (black squares) and from FT-IR spectra by cross-validated PLS regression (red circles)

methods. The low reproducibility of values obtained by the HPLC-RI and the phenol method, respectively, are most likely due to differences in cell disruption efficiency and the necessary but error-prone sample handling. Similar results were obtained for fed-batch fermentation 2 (data not shown).

Prediction of concentration values from FT-IR spectra by PLS regression

Parameters and results of the PLS regression models for trehalose, glycogen, and mannan are summarized in Table 4. The number of latent variables used to build the PLS regression models was seven for trehalose and mannan and five for glycogen, and the RMSECV were found to be 0.33 % DW for trehalose, 0.55 % DW for glycogen, and 1.17 % DW for mannan. Considering the concentration ranges used for calibration, these values show that FT-IR spectroscopy is a promising technique for fast, reagent-free measurement of intracellular carbohydrates. The analyte concentrations determined by cross-validated PLS regression and the reference concentrations found for the different samples drawn from the two fermentations are shown in Fig. 5. The black squares indicate the values found by reference analysis and the red circles correspond to the

values predicted from cross-validated PLS regression, i.e., the average concentration predicted from the spectra of each of the three sample spots. The values are in good agreement with each other and the expected changes in carbohydrate content of the yeast cells. Generally, the data found by FT-IR spectroscopy show a smoother trend/development over time than the respective reference data, where in some cases steep slopes, i.e., big differences between consecutive samples, were found. These large increases and decreases in reference values are also the points where FT-IR data and reference data deviate strongly. Each single value obtained by reference analysis is prone to errors due to the necessary sample pretreatments and handling. When calculating a PLS regression model from these data, the erroneous values (which are both positive and negative deviations from the true value) are averaged over the whole calibration set and resulting PLS predictions show a smoother time course.

Conclusions

Most of the published articles to determine the carbohydrate composition of yeast cells describe time-consuming wet

chemical assays requiring handling-intensive pretreatment steps. The proposed FT-IR spectroscopy method of whole *S. cerevisiae* cells presents clear advantages with respect to the other methods such as operational simplicity, lower sample consumption, and no reagent consumption, avoiding the risk of errors as a result of the labor-intensive cell disruption and sample handling. The method determines the content of several polysaccharides such as mannan and glycogen and the disaccharide trehalose by cross-validated PLS regression. Results can be obtained within 30 min from sampling, including the most time-consuming step, i.e., drying of the sample. Using the instrumentation and settings in this study, acquisition of spectra took approximately 3 min per sample spot, showing that significant improvement of measurement time is possible by using other drying methods, e.g., a desiccator. The obtained results show that concentration values are in good agreement with reference values.

Acknowledgments European Social Fund from European Union and Junta de Comunidades de Castilla-La Mancha are gratefully acknowledged for supporting given through a Postdoctoral research contract for Maria R. Plata. Partial financial support of the Austrian Science Fund (FWF) through the stand-alone project scheme (project number, P24154), and the Austrian research funding association (FFG) under the scope of the COMET program within the research network “Process Analytical Chemistry (PAC)” (contract # 825340) is gratefully acknowledged. The authors want to express their gratitude to Bettina Lórantfy for guidance in media design and Daniela Roxana Ghiță for her support with the experimental work.

Open Access This article is distributed under the terms of the Creative Commons Attribution License which permits any use, distribution, and reproduction in any medium, provided the original author(s) and the source are credited.

References

1. Milic TV, Rakin M, Siler-Marinkovic S (2007) Utilization of baker's yeast (*Saccharomyces cerevisiae*) for the production of yeast extract: effects of different enzymatic treatments on solid, protein and carbohydrate recovery. J Serb Chem Soc. doi:10.2298/JSC0705451V
2. Sceni P, Palazolo GG, Vasallo MDC et al (2009) Thermal and surface behavior of yeast protein fractions from *Saccharomyces cerevisiae*. Food Sci Technol-Leb. doi:10.1016/j.lwt.2009.02.010
3. Kath F, Kulicke W-M (1999) Mild enzymatic isolation of mannan and glucan from yeast *Saccharomyces cerevisiae*. Angew Makromol Chem. doi:10.1002/(SICI)1522-9505(19990701)268:1<59::AID-APMC59>3.3.CO;2-6
4. Lillie SH, Pringle JR (1980) Reserve carbohydrate metabolism in *Saccharomyces cerevisiae*: responses to nutrient limitation. J Bacteriol 143:1384–1394
5. Prieto MA, Vázquez JA, Murado MA (2011) Hydrolysis optimization of mannan, curdlan and cell walls from *Endomyces fibuliger* grown in mussel processing wastewaters. Process Biochem. doi:10.1016/j.procbio.2011.04.014
6. Dallies N, François J, Paquet V (1998) A new method for quantitative determination of polysaccharides in the yeast cell wall. Application to the cell wall defective mutants of *Saccharomyces cerevisiae*. Yeast. doi:10.1002/(SICI)1097-0061(1998100)14:14<1297::AID-YEA310>3.0.CO;2-L
7. Schulze U, Larsen ME, Villadsen J (1995) Determination of intracellular trehalose and glycogen in *Saccharomyces cerevisiae*. Anal Biochem 228:143–149
8. Parrou JL, François J (1997) A simplified procedure for a rapid and reliable assay of both glycogen and trehalose in whole yeast cells. Anal Biochem. doi:10.1006/abio.1997.2138
9. Naumann D, Keller S, Helm D et al (1995) FT-IR spectroscopy and FT-Raman spectroscopy are powerful analytical tools for non-invasive characterization of intact microbial cells. J Mol Struct 347:399–405
10. Kuligowski J, Quintás G, Herwig C, Lendl B (2012) A rapid method for the differentiation of yeast cells grown under carbon and nitrogen-limited conditions by means of partial least squares discriminant analysis employing infrared micro-spectroscopic data of entire yeast cells. Talanta. doi:10.1016/j.talanta.2012.06.036
11. Wold S, Sjöström M, Eriksson L (2001) PLS-regression: a basic tool of chemometrics. Chemometr Intell Lab 58:109–130
12. Mair T, Zimányi L, Khoroshyy P et al (2006) Analysis of the oscillatory kinetics of glycolytic intermediates in a yeast extract by FT-IR spectroscopy. Biosystems 83:188–194
13. Burattini E, Cavagna M, Dell'Anna R et al (2008) A FTIR microspectroscopy study of autolysis in cells of the wine yeast *Saccharomyces cerevisiae*. Vib Spectrosc. doi:10.1016/j.vibspec.2008.04.007
14. Cavagna M, Dell'Anna R, Monti F et al (2010) Use of ATR-FTIR microspectroscopy to monitor autolysis of *Saccharomyces cerevisiae* cells in a base wine. J Agr Food Chem. doi:10.1021/jf902369s
15. Corte L, Rellini P, Roscini L et al (2010) Development of a novel, FTIR (Fourier transform infrared spectroscopy) based, yeast bioassay for toxicity testing and stress response study. Anal Chim Acta. doi:10.1016/j.aca.2009.11.035
16. DuBois M, Gilles KA, Hamilton JK et al (1956) Colorimetric method for determination of sugars and related substances. Anal Chem. doi:10.1021/ac60111a017
17. Mazarevica G, Diewok J, Baena JR et al (2004) On-line fermentation monitoring by mid-infrared spectroscopy. Appl Spectrosc. doi:10.1366/0003702041389229
18. Kuligowski J, Quintás G, Lendl B (2010) High performance liquid chromatography with on-line dual quantum cascade laser detection for the determination of carbohydrates, alcohols and organic acids in wine and grape juice. Appl Phys B:Lasers O. doi:10.1007/s00340-010-4013-y
19. Naumann D (2000) In: Meyers RA (ed) Encyclopedia of analytical chemistry. Wiley, New York
20. Geciova J, Bury D, Jelen P (2002) Methods for disruption of microbial cells for potential use in the dairy industry—a review. Int Dairy J 12:541–553
21. Ricci-Silva M, Vitolo M, Abraha J (2000) Protein and glucose 6-phosphate dehydrogenase releasing from baker's yeast cells disrupted by a vertical bead mill. Process Biochem 35:831–835
22. Engler CR (1985) In: Moo-Young M, Cooney CL (eds.) Comprehensive biotechnology. Pergamon, Oxford
23. Förster J, Famili I, Fu P et al (2003) Genome-scale reconstruction of the *Saccharomyces cerevisiae* metabolic network. Genome Res. doi:10.1101/gr.234503
24. Stewart TS, Ballou CE (1968) A comparison of yeast mannans and phosphomannans by acetolysis. Biochemistry 7:1855–1863
25. Becker JU (1978) A method for glycogen determination in whole yeast cells. AnalBiochem 86:56–64
26. Bernfeld P (1955) Amylases, alpha and beta. Methods Enzymol 1:149–158

Publication III

Cosima Koch, Markus Brandstetter, Patrick Wechselberger, Bettina Lorantfy, Maria Reyes Plata, Stefan Radel, Christoph Herwig, Bernhard. Lendl, *Analytical Chemistry* 87(4) (2015) 2314-20. (c) 2015 American Chemical Society under a Creative Commons Attribution (CC-BY) License.

DOI: 10.1021/ac504126v



Ultrasound-Enhanced Attenuated Total Reflection Mid-infrared Spectroscopy In-Line Probe: Acquisition of Cell Spectra in a Bioreactor

Cosima Koch,[†] Markus Brandstetter,^{†,§} Patrick Wechselberger,^{‡,⊥} Bettina Lörantfy,^{‡,||} Maria Reyes Plata,[†] Stefan Radel,[†] Christoph Herwig,^{‡,⊥} and Bernhard Lendl^{*,†}

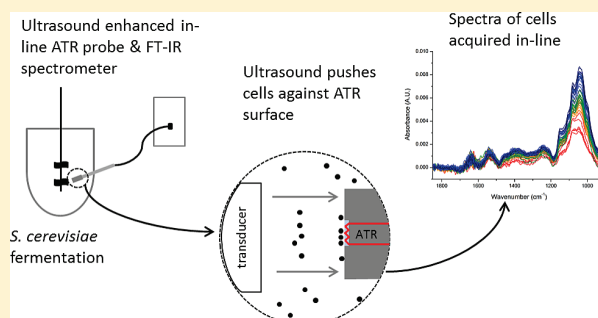
[†]Institute of Chemical Technologies and Analytics, Vienna University of Technology, Getreidemarkt 9/164-UPA, 1060 Vienna, Austria

[‡]Institute of Chemical Engineering, Vienna University of Technology, Gumpendorferstraße 1a, 1060 Vienna, Austria

[⊥]Christian Doppler Laboratory for Mechanistic and Physiological Methods for Improved Bioprocesses, Institute of Chemical Engineering, Vienna University of Technology, Getreidemarkt 9/166, 1060 Vienna, Austria

Supporting Information

ABSTRACT: This article presents a novel method for selective acquisition of Fourier transform infrared (FT-IR) spectra of microorganisms in-line during fermentation, using *Saccharomyces cerevisiae* as an example. The position of the cells relative to the sensitive region of the attenuated total reflection (ATR) FT-IR probe was controlled by combining a commercially available ATR in-line probe with contact-free, gentle particle manipulation by ultrasonic standing waves. A prototype probe was successfully constructed, assembled, and tested in-line during fed-batch fermentations of *S. cerevisiae*. Control over the position of the cells was achieved by tuning the ultrasound frequency: 2.41 MHz was used for acquisition of spectra of the cells (pushing frequency f_p) and 1.87 MHz, for retracting the cells from the ATR element, therefore allowing spectra of the medium to be acquired. Accumulation of storage carbohydrates (trehalose and glycogen) inside the cells was induced by a lack of a nitrogen source in the feed medium. These changes in biochemical composition were visible in the spectra of the cells recorded in-line during the application of f_p and could be verified by reference spectra of dried cell samples recorded off-line with a FT-IR microscope. Comparison of the cell spectra with spectra of trehalose, glycogen, glucose, and mannan, i.e., the major carbohydrates present in *S. cerevisiae*, and principal components analysis revealed that the changes observed in the cell spectra correlated well with the bands specific for trehalose and glycogen. This proves the applicability and capability of ultrasound-enhanced in-line ATR mid-IR spectroscopy as a real-time PAT method for the in situ monitoring of cellular biochemistry during fermentation.



Fourier transform infrared (FT-IR) spectroscopy is an established method for at-line, online, and in-line bioprocess analysis and monitoring, especially in the mid-IR region (400–4000 cm^{-1}). Because water, a strong infrared absorber, is the most abundant solvent and maximum interaction lengths are a few tens of micrometers, attenuated total reflection (ATR) configurations are the most commonly used. The light is totally reflected within an ATR element, resulting in an evanescent field that interacts with the sample, with typical penetration depths of approximately 1 to 2 μm .¹ Multiple reflections lead to enhanced interaction with the sample without having to face the challenges encountered when measuring transmission (clogging, path length changes due to pressure drops, etc.). Multivariate data analysis can be used to extract chemical information from data (i.e., chemometrics); this makes quantification of spectroscopic measurements possible. Lourenço et al.² gave a good general overview of

optical spectroscopy methods in combination with chemometrics used for bioreactor monitoring, including mid-IR spectroscopy, whereas a mini-review by Landgrebe et al.³ summarizes recent applications of near- and mid-IR spectroscopy for bioprocess monitoring. A frequently used chemometric method is principal component analysis (PCA). ATR mid-IR spectroscopy in combination with PCA has been, e.g., successfully used for the classification and identification of chemical differences of edible fats and oils,⁴ Robusta and Arabica coffees,⁵ and injured and intact *Listeria monocytogenes*.⁶

For various bioprocesses, spectra of media components and excreted secondary metabolites have been recorded at-line,^{7–10} online, and in-line. Online bypass systems were successfully

Received: November 5, 2014

Accepted: January 12, 2015

Published: January 12, 2015

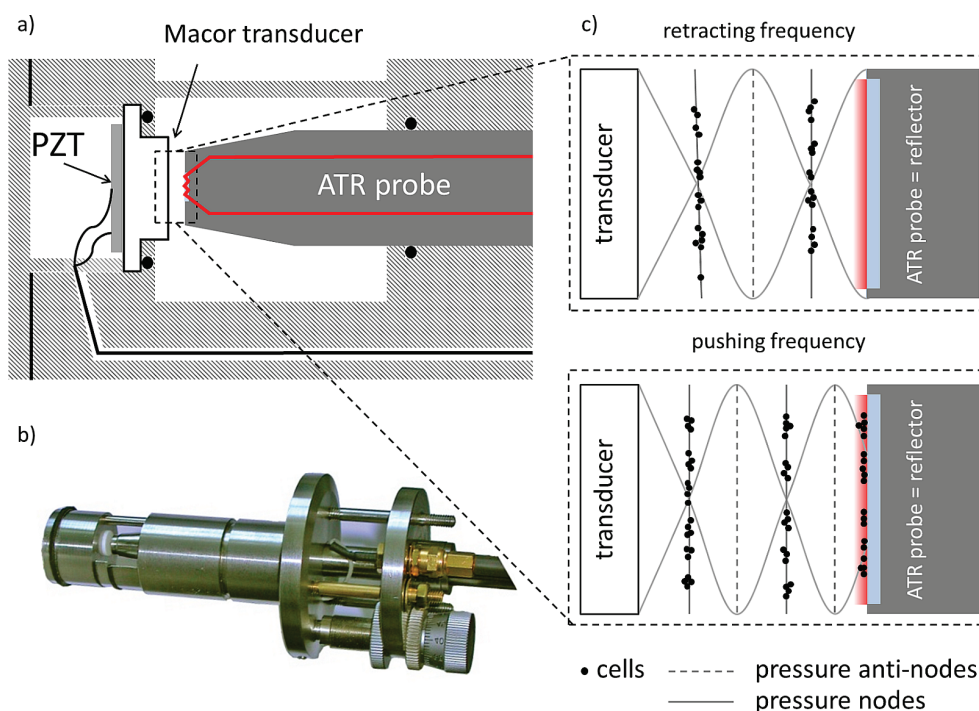


Figure 1. Schematic (a) and photograph (b) of the prototype probe: commercial ATR probe and the custom-built ultrasound accessory. (c) The two operating modes. The cells and the evanescent field are magnified by a factor of 10 in comparison to the other dimensions for visibility.

used to monitor media composition and products^{11–13} and for pH control¹⁴ in different types of bioprocesses. In-line ATR probes are realized using fiber optics (typically, silver halide) or light conduits and are commercially available. Doak and Phillips reported the first use of a conduit probe to monitor *Escherichia coli* fermentation in 1999;¹⁵ since then, numerous reports of in-line, i.e., in situ (the more commonly used term in bioprocess engineering), monitoring of fermentation have been published.^{16–20}

Spectra of microorganisms are acquired at-line or off-line and allow for differentiation between physiological states, reflected by biochemical composition and the quantification of secondary metabolites accumulated inside cells. In most studies, transmission spectra of washed, dried cells were measured, either by FT-IR microspectroscopy^{21,22} or with the dedicated microplate reader accessory HTS-XT for high-throughput analysis (Bruker Optics).^{23–27} Transmission and ATR FT-IR microspectroscopy were successfully used for the analysis and differentiation of physiological states in the yeast *Saccharomyces cerevisiae*.^{28–31} Jarute et al. presented the first online setup for the quantification of poly beta-hydroxybutyric acid (PHB) in *E. coli* using a horizontal ATR in combination with a stopped-flow system.³² When the flow was on, spectra of the medium were acquired; subsequently, the flow was switched off, and the cells sedimented onto the ATR surface and thus spectra of the cells could be acquired. Biofouling was avoided by chemical cleaning of the ATR as necessary.

Ultrasound Particle Manipulation. Ultrasonic standing wave fields, built up between an ultrasound transducer and a reflector, are a contact-free, gentle method for manipulation of small particles in suspension. Particle sizes between one and a few tens of micrometers require ultrasound frequencies between 1 and 10 MHz. The axial acoustic radiation force, i.e., in the direction of sound propagation, acting on the

particles depends on particle volume, the ultrasound frequency, the acoustic energy density, i.e., the power that is transmitted into the medium, and the acoustic contrast factor.^{33–35} The force results in a pattern of planes that are half of a wavelength apart, into which the particles are driven. These planes are either the pressure nodal planes (i.e., the planes of minimum acoustic pressure) or the pressure antinodal planes of the standing wave field, depending on the acoustic contrast factor between the particles and the carrier medium. This, in turn, depends on the ratio of the sound speeds and mass densities between the particles and the medium; dense particles, like cells, are driven into the pressure nodes of the standing wave field. Ultrasound particle manipulation is not harmful to cells^{36,37} and is a state-of-the-art method for perfusion filtering of mammalian cell cultures, where it is used to hold cells against a continuous flow of medium.^{38–40}

Ultrasound particle manipulation was used to increase the robustness of online cell spectra acquisition (*S. cerevisiae*) in a setup similar to that of Jarute et al.,³² by using the radiation force to lift the cells off of the horizontal ATR surface, which acted as ultrasound reflector.⁴¹ Furthermore, the settling speed, and thus the measurement intervals, could be increased by the formation of cell aggregates in the pressure nodal planes, which sedimented faster than single cells once the ultrasound and the flow were switched off. A major drawback of bypass setups are sterility issues. This can be overcome by taking the system in-line.⁴² Radel et al. showed in 2010 that the combination of ultrasound particle manipulation and a fiber optic ATR probe made acquisition of mid-IR spectra of PTFE particles in stirred suspensions possible.⁴³ Here, the ATR element was oriented vertically, and the particles were pushed against it by tuning the ultrasound frequency such that a net acoustic radiation force acted in the direction of the ATR element. In 2013, we showed

that spectra of *S. cerevisiae* could be acquired with a prototype in-line applicable probe.⁴⁴

This article presents a major step forward in this development: an autoclavable, in-line ultrasound-enhanced fiber optic mid-IR ATR probe constructed according to FDA guidelines and its application during *S. cerevisiae* fermentation in-line in a semi-industrial fermenter. Within fed-batch fermentation, the cells were deliberately nitrogen-limited by the design of the media and therefore started to accumulate storage carbohydrates, i.e., trehalose and glycogen, which was investigated. We recently showed the possibility of off-line quantification of these carbohydrates in whole *S. cerevisiae* by FT-IR microspectroscopy.³¹ Here, we investigated the possibility of monitoring these biochemical changes in-line by comparing them to off-line reference spectra and principal component analysis.

■ EXPERIMENTAL SECTION

Ultrasound-Enhanced Fiber Optic ATR FT-IR Probe. Spectrometer and In-Line Probe. FT-IR spectra were acquired in-line with the process spectrometer ReactIR 15 equipped with an attenuated total reflection DS DiComp (diamond) 9.5 mm probe connected via a 1.5 m AgX (silver halide) fiber (all Mettler Toledo, Greifensee, Switzerland). The spectrometer was equipped with a liquid nitrogen cooled mercury–cadmium–telluride (MCT) detector. Spectra were acquired with resolutions of 4 and 8 cm^{-1} , respectively, in the spectral region from 700 to 2800 cm^{-1} as the co-addition of 256 scans. iC IR 4.2 software (Mettler Toledo, Greifensee, Switzerland) was used for acquisition and basic data manipulation such as single-point baseline offset correction (1840 cm^{-1} set to zero). The DS DiComp probe was chosen due to its flat top, which makes it especially suitable as a reflector for the ultrasonic wave.

Ultrasound Technology: Material and Design Considerations. The fiber optic probe was equipped with an in-house-designed ultrasound accessory that allowed for manipulation of particles in suspension (Figure 1a,b). The materials were chosen with consideration of FDA regulations, i.e., standard materials used in biotechnology were applied (body, stainless steel material no. 1.4571/DIN X6CrNiMoTi17-12-2; screws, stainless steel A4 (1.4404) (Bossard, Zug, Switzerland); seals and O-rings, ZruElast and ZruElast FPM 75 shore (both Zrunek, Vienna, Austria)). The ultrasound composite transducer consisted of a 10 mm PZT (lead zirconium titanate, type PIC 181, PI Ceramics, Lederhose, Germany) disc with wrap-around silver electrodes glued to a Macor cylinder with a one-component epoxy resin (Araldite AV 171, Huntsman Advanced Materials, The Woodlands, TX, USA). The assembled ultrasound-enhanced mid-IR ATR probe complies with the 3D rule to avoid turbulent flow stagnation, i.e., indentations were limited to three times their respective widths, and it is autoclavable in situ (121 °C, 20 min). A modified (limited to 2.5 W max power output) frequency power synthesizer (FPS 2540, SinePhase Instruments, Hinterbrühl, Austria) connected to the PZT was used for ultrasound signal generation and amplification; frequency and power were controlled using a custom LabView script and GUI (National Instruments, Austin, TX, USA). The distance between the ultrasound transducer and ATR probe was adjusted to approximately 1.35 mm.

The working principle is shown in the inset in Figure 1c: At retracting frequency f_r , cells are held in the pressure nodal planes away from the evanescent field of the ATR probe,

whereas they are pushed against the ATR surface and thus into the evanescent field when the pushing frequency f_p is applied.

Laboratory FT-IR Spectrometers: Reference Spectra. Reference spectra of glucose, trehalose, and mannan solutions and glycogen mixed with H_2O were acquired with a Tensor 37 FT-IR spectrometer equipped with a DTGS (deuterated triglycine sulfate) detector using a Platinum diamond ATR (all Bruker Optics, Ettlingen, Germany). Instrument control and spectrum acquisition were performed with OPUS 7 software (Bruker Optics). Spectral resolution was set to 2 cm^{-1} , and spectra were recorded as the co-addition of 32 scans.

Sampling, pretreatment of the off-line samples, and acquisition of reference spectra of dried yeast samples drawn during fermentation have been described elsewhere.³¹

***S. cerevisiae* Cultivations.** Fermentation of *S. cerevisiae* (strain CBS8340) was carried out in two different, fully automated and controlled stirred bioreactors: a 10 L glass/steel bioreactor (Chemap, Switzerland) and a 15 L steel bioreactor (Infors, Bottmingen, Switzerland). Both were equipped with 25 mm Ingold ports for coupling with the ultrasound-enhanced mid-IR ATR probe. Media preparation and cultivation conditions are described in detail in the Supporting Information (Experimental, page S2, and Table S1, page S2); the stirring speed was varied (800–1200 rpm), and the pO_2 level was always kept above 80% by adjusting the inflow of air. CO_2 content of the off-gas was measured using an off-gas analyzer (Bluesens, Snirgelskamp, Germany). Biomass was determined off-line by measuring the optical density at 600 nm with a Genesys 20 visible spectrophotometer (Thermo Scientific, Waltham, MA, USA).

After the batch phase on glucose was completed, the bioprocess was carried on as a C-limited fed-batch with an exponential feed strategy. The feed medium was deficient in a nitrogen source. Under C-limited feeding conditions, no excess carbon source was present in the medium. The nitrogen limitation led to the synthesis and accumulation of storage carbohydrates, i.e., trehalose and glycogen, inside the cells.

Experimental Procedure for Ultrasound-Enhanced Mid-IR Spectroscopy. During fermentations, f_p was 2.410 MHz at 1.8–1.9 W true electrical power input (t.e.p.i.), and f_r was 1.870 MHz at 1.6 W t.e.p.i.

Data Analysis. Matlab (Mathworks, Natick, MA, USA) and the PLS toolbox (Eigenvector Research, Wenatchee, WA, USA) were used for data manipulation and PCA. For PCA, the spectra were area normalized in the carbohydrate region (938–1186 cm^{-1}) prior to calculation of the second derivative (Savitzky-Golay, second order, window width 9 or 11 depending on spectral resolution). Single-analyte spectra were normalized and differentiated using the same settings for comparison.

■ RESULTS AND DISCUSSION

In-Line Procedure. Spectra were acquired in-line during fermentation, alternating between pushing and retracting frequency every 10 min. Three FT-IR spectra were acquired at each ultrasound frequency; they were subsequently averaged for further data analysis, resulting in a single, average, spectrum for each frequency application. The background was acquired in batch medium with the probe in its final position in the bioreactor after autoclaving. This was used as the background for the absorbance spectra of the medium, i.e., spectra recorded during the application of the retracting frequency. Absorbance

spectra of the cells were calculated as difference spectra between a spectrum acquired during the application of the pushing frequency and the respective previous media spectrum (Figure 2). This was necessary to compensate for changes in

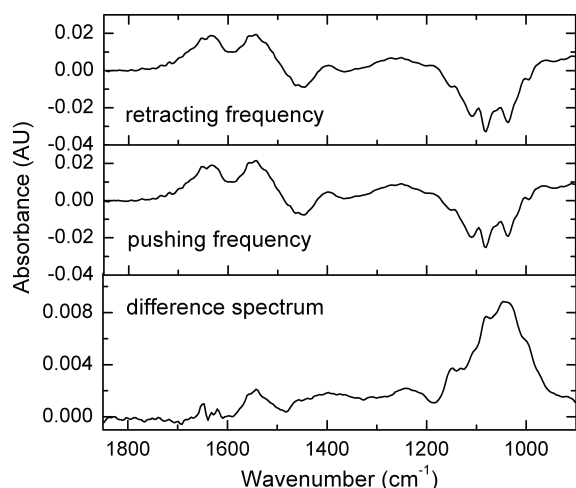


Figure 2. In-line spectra acquired during *S. cerevisiae* fermentation when applying retracting frequency (top) or pushing frequency (middle) and their difference spectrum showing typical spectral features of yeast cells.

the medium composition, as there is always medium in the probed volume and analyte concentrations are higher (and vary stronger over the course of the fermentation) in the medium than in the cells themselves. Samples were drawn from the bioreactor at different times for biomass determination and the acquisition of cell reference spectra.

Optimization of Experimental Conditions. In total, four fermentations were conducted; the influence of the ultrasound frequency for pushing and retracting, stirring speed, and spectral and temporal resolution were investigated, and the optima were subsequently used. The highest yeast-related absorption values in difference spectra were found using a pushing frequency of 2.410 MHz and a power of 1.8–1.9 W t.e.p.i. (f_p). For retracting the particles from the evanescent field of the ATR element, the ultrasound transducer was driven around f_r 1.870 MHz (at 1.6 W t.e.p.i.). Stirring speeds between 600 and 1200 rpm were tested: an increase in stirring speed led to a decrease of absorption values of the recorded spectra due to Stokes drag (data not shown). As a compromise between sufficient stirring and satisfactory signal of the mid-IR spectra of cells, a stirring speed of 800 rpm was identified. Comparison of spectral resolutions of 4 and 8 cm^{-1} showed that the broad absorption bands of *S. cerevisiae* were sufficiently resolved by the latter (data not shown). Temporal resolution was governed by spectrum acquisition time (i.e., 1 min at 8 cm^{-1} resolution and co-addition of 256 scans), sufficient data redundancy (in case of erroneous spectra and to increase the signal-to-noise ratio), and maximum handleable file size. Spectra were acquired every 2 min; thus, as mentioned before, three spectra were available for averaging during alternating application of the ultrasound frequencies for 10 min each. These parameters were determined during the first fermentation and were subsequently used. The spectra recorded during the four fermentations showed similar trends, and an exemplary one will be presented here.

Influence of Growth Conditions on Yeast Cells. In order to study changes on the (bio)chemical composition of the cells, the fermentation was carried out in two parts: a batch phase, with an excess of glucose (C-source) and ammonium (N-source), and subsequently a C-limited fed-batch phase during which no additional N-source was fed and trehalose and glycogen were accumulated inside the cells.

Batch Phase. At the beginning of the batch phase, glucose was present in excess in the medium, leading to the production of ethanol as a main metabolite in addition to biomass (Crabtree effect, overflow metabolism). The cells exhibited characteristic diauxic growth: first, glucose was metabolized to ethanol in parallel with biomass formation (0–12 h) and then, after a short lag phase, the extracellular ethanol was metabolized as a carbon source (12–20 h). This was reflected by the CO_2 off-gas profile and the FT-IR spectra of the medium (Figure 3).

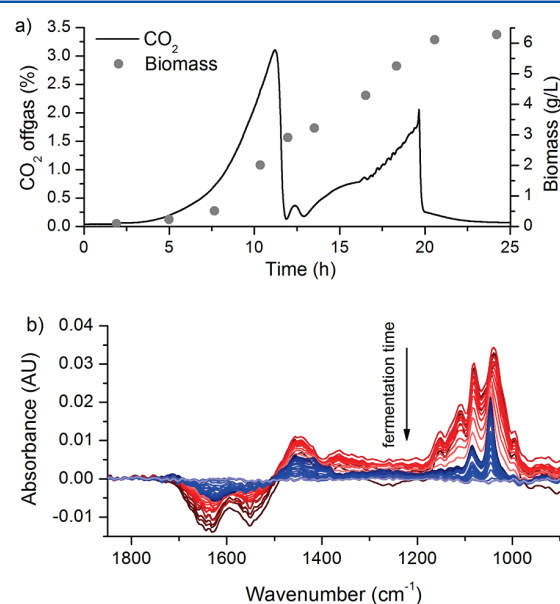


Figure 3. (a) CO_2 off-gas and biomass over the course of the batch phase. (b) ATR FT-IR spectra of the medium (i.e., retracting frequency applied) over the course of the batch phase.

Characteristic spectral features of glucose were predominant at first (Figure 3b, dark red spectra, bands at 1150, 1110, 1080, and 1037 cm^{-1}) followed by a superposition of glucose and ethanol (light red spectra). Once the glucose was depleted, ethanol dominated the FT-IR spectra, with its characteristic bands at 1045 and 1080 cm^{-1} (blue spectra), which gradually decreased until the end of the batch phase (light blue spectrum).

During batch phase, yeast cell composition did not change; only biomass growth occurred, which was reflected by an increase in absorbance over time, whereas spectral features remained similar (see Supporting Information Figure S1).

Fed-Batch Phase. The spectra of dried *S. cerevisiae* fed-batch samples acquired off-line (Figure 4a) show spectral features typical for the constituents of biological cells (from refs 45 and 46): The C=O stretching of ester groups in lipids leads to an absorption around 1730 cm^{-1} . Proteins lead to absorptions around 1655 cm^{-1} (amide I band, mainly from C=O stretching and, to a lesser extent, N–H bend and C–N stretch), around 1550 cm^{-1} (amide II band, N–H bend, and

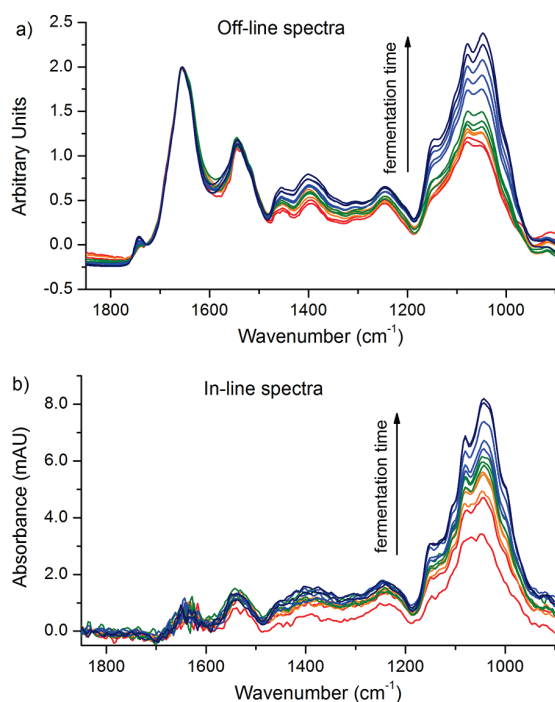


Figure 4. (a) Spectra of dried *S. cerevisiae* acquired off-line using a laboratory FT-IR microscope (normalized to amide I band). (b) Spectra of *S. cerevisiae* acquired in-line using the ultrasound-enhanced mid-IR ATR probe at the times when samples for off-line analysis were drawn.

C–N stretch), and around 1300 cm^{-1} (amide III band, complex combination of different vibrations). In the region between 1450 and 1200 cm^{-1} , numerous C–H and O–H deformation vibrations contribute to the spectrum (lipids, carbohydrates). Antisymmetric PO_2^- stretching vibrations of DNA, RNA, and phospholipids lead to absorptions around 1240 cm^{-1} . The region between 950 and 1200 cm^{-1} (hereafter, carbohydrate region) is dominated by C–O stretching originating from carbohydrates, with contributions around 1100 cm^{-1} from symmetric PO_2^- stretching (again, DNA, RNA, and phospholipids).

The changes in carbohydrate content induced by N-limited growth are reflected by changes in the shape of the spectra acquired off-line (Figure 4a, normalized to the amide I band). The relative carbohydrate content increases with fermentation time, and the shape of the carbohydrate region changes as trehalose and glycogen are formed in the cells. The carbohydrate bands of the difference spectra of the cells acquired in-line at the time points of sampling (Figure 4b, offset baseline corrected) are in good agreement with the off-line spectra (Figure 4a). Differences can be attributed to matrix influence, band shifts due to acquisition in ATR mode, and the lower signal-to-noise ratio for in-line spectra.

A major difference between the off- and in-line measurements was observed in the amide I and amide II regions: here, H_2O absorbs strongly (H–O–H bending at approximately 1640 cm^{-1}) and therefore the intensity reaching the detector is low, leading to a high noise level. The protein bands (amide I and II) are only weakly visible in the in-line spectra, most likely because the H_2O present when the f_r spectrum is acquired is simply replaced by the protein present in *S. cerevisiae* when f_p is applied, leading to approximately the same absorption.

Furthermore, when f_p is applied, H_2O is, for the most part but never completely, replaced by yeast cells (even assuming close packing of equal spheres, approximately 26% of the space would still be occupied by H_2O).

Since changes associated with switching to nitrogen-limited growth are mainly visible in the carbohydrate region of the FT-IR spectra, further analysis was focused on this region. The main carbohydrates of yeast were studied: mannan, a cell wall polysaccharide composed of mannose units, and intracellular carbohydrates trehalose, a disaccharide of glucose, glycogen, a polysaccharide of glucose, and glucose. ATR FT-IR reference spectra of the major carbohydrates (area normalized as described in the Experimental Section) present in yeast cells are shown in Figure 5a. At 994 cm^{-1} , trehalose, one of the

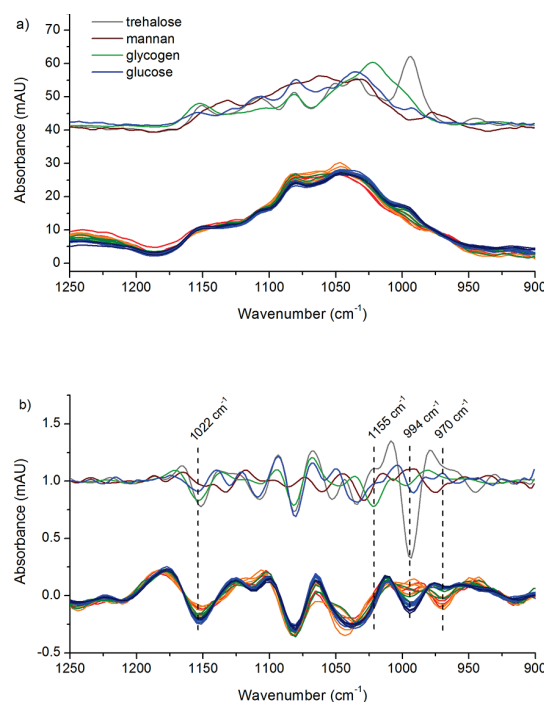


Figure 5. (a) Spectra of major carbohydrates present in yeast cells (off-line ATR, in solution) and spectra of yeast cells acquired in-line over the course of the fermentation. (b) Second-derivative spectra of major carbohydrates present in yeast cells and of yeast cells acquired over the course of the fermentation, respectively. In both graphs, carbohydrate spectra are offset for better visibility.

storage carbohydrates accumulated during N-limited growth, has an intense and specific absorption. In the spectral region between 1025 and 1175 cm^{-1} , trehalose and glucose show bands at similar positions; their relative intensities are, however, different. Glucose absorbs strongest at 1035 cm^{-1} , whereas the relative absorption maximum of trehalose in this region is shifted toward slightly higher wavenumbers and is lower in intensity. At around 1155 cm^{-1} , trehalose and glycogen have a common absorption band. Glycogen absorbs broadly between 970 and 1170 cm^{-1} , with a distinct maximum at 1022 cm^{-1} and smaller maxima at 1080 and 1152 cm^{-1} . Mannan has a broad absorption band between 1000 and 1150 cm^{-1} , with a distinct maximum at 1060 cm^{-1} . The exact positions of absorption maxima are even clearer when looking at second derivatives of the spectra: maxima in the spectra are minima here (Figure 5b, top).

In the yeast, changes in the carbohydrate composition can be observed by spectra acquired in-line as difference spectra over the course of the N-limited fed-batch fermentation (Figure 5a, bottom). The shape of the carbohydrate band changed with fermentation time, most notably between 1050 and 950 cm^{-1} . The blue spectra, which were acquired toward the end of the fermentation, show higher absorption around 990 cm^{-1} , correlating well with the absorption spectra of trehalose. This becomes even clearer when investigating second-derivate spectra: The decrease around 994 cm^{-1} and the increase around 970 cm^{-1} in the spectra acquired toward the end of the fermentation (blue) correlate well with the trehalose second-derivative spectrum (gray). Between 1030 and 1000 cm^{-1} , the slope of the second-derivative yeast spectra steepens with fermentation time. The minimum at $\sim 1150 \text{ cm}^{-1}$, which further decreases with fermentation time, correlates with an increase in both glycogen and trehalose. Since this minimum is less pronounced for trehalose compared to the one at 994 cm^{-1} , it can be concluded that glycogen mainly contributes to this change.

PCA. We have recently shown that quantitative determination of carbohydrates is possible from off-line yeast spectra;³¹ from the in-line difference spectra, only qualitative information on the changes in carbohydrate composition could be observed. Normalization of the spectra proved to be difficult because changes in biomass and in the carbohydrate content occurred simultaneously, and this correlation could not be broken. To evaluate if the trends observed in the in-line difference spectra are statistically detectable and related to carbohydrate features, PCA was performed on the second-derivative spectra.

Individual PCA of the four fermentations resulted in very similar principal component 1 (PC1), which explained between 53 and 73% of the variation in the respective fermentation spectra. A PCA of the combined spectra from all four fermentations again resulted in a PC1 with very similar features; however, only 40% of the variance was explained. This can be attributed to interfermentation variations leading a smaller contribution from changes induced by N-limited growth. To concentrate on the biochemical changes inside the cells, the following discussion is based on the PCA of a single fermentation.

The loading vector of PC1 and the second-derivative spectra of trehalose, glycogen, glucose, and mannan show similar features (Figure 6). Spectral region A (1020–970 cm^{-1}) of PC1 correlates with trehalose: the minimum is around

995 cm^{-1} for both, followed by a maximum at 980 cm^{-1} and a shoulder around 960 cm^{-1} . This region also varies the most between spectra, reflected by the highest values of the first loading vector. The plateau at 1035 cm^{-1} followed by a minimum around 1025 cm^{-1} in PC1 correlates with glycogen, superimposed with trehalose and glucose (thus, the shift of the minimum toward higher wavenumbers). In spectral region B (1050 to 1103 cm^{-1}), trehalose, glycogen, glucose, and PC1 show very similar features, and a clear attribution cannot be made. Around 1155 cm^{-1} (spectral region C), the minimum in PC1 corresponds to a superposition of the minima of both trehalose and glycogen.

CONCLUSIONS AND OUTLOOK

The presented method allows for the selective acquisition of mid-IR spectra of either dissolved analytes (media components) or suspended particles (cells). This is, to the best of our knowledge, the first report on the acquisition of mid-IR spectra of microorganisms (*S. cerevisiae*) inside a semi-industrial bioreactor during fermentation without the necessity of drawing a sample. The cell spectra acquired in-line are in good agreement with spectra of dried cell samples that were recorded off-line. Trends in the changes of the biochemical composition of the cells during N-limited fed-batch fermentation were visible, showing the potential of ultrasound-enhanced ATR mid-IR spectroscopy to be used as a PAT (process analytical technology) probe to detect the cells' physiological response to nutritional limitations. Quantitative analysis proved to be difficult, as the number of cells present in the evanescent field is hard to estimate and the amide I band, which could be used for normalization off-line, was not accessible in-line. Furthermore, the signal-to-noise ratio of the difference spectra still needs to be improved to make quantitative analysis by, e.g., partial least-squares regression possible. More insight into the spatial distribution of the cells in the evanescent field could potentially be gained using the gel method proposed by Gherardini et al.;⁴⁷ with a better understanding of the number of cells held in the evanescent field at a given time under different conditions, the before-mentioned challenges will be addressed in a follow-up project.

The described novel method is generic and suitable for (ideally spherical) cells within a size range of 1 to approximately 40 μm , as is often employed in white and red biotechnology and biorefinery. It delivers real-time information on the chemical composition of cells in situ, thus aiding the optimization of process conditions and media composition. Moreover, physiological responses of cells can be investigated, helping to obtain a basic understanding of cell physiology/metabolism. In industrial fermentation, the method could serve as a quality control tool: here, complex media are often employed, for which exact determination of nutrient concentrations would usually require extensive and laborious chemical analyses or is not possible at all. By measuring the cell's biochemical composition, potential limitations could be detected, and appropriate measures to ensure the desired quality could be taken early in the process.

Apart from bioprocesses, the presented method can, for example, be applied to gain insight into crystallization processes.

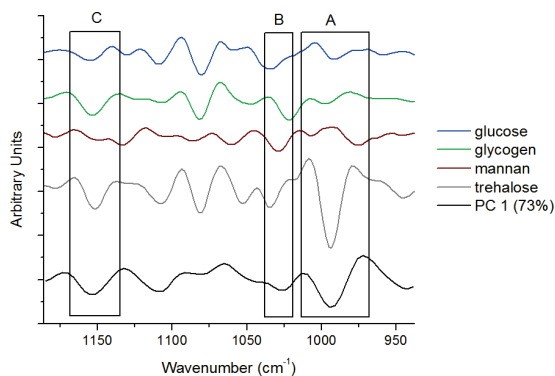


Figure 6. Second-derivative spectra of trehalose, glycogen, glucose, and mannan and PC1 of spectra acquired during N-limited growth.

■ ASSOCIATED CONTENT

■ Supporting Information

Experimental details on media preparation and cultivation conditions. Table S1: Overview of the setup and conditions of the fed-batch fermentations. Figure S1: Spectra of *S. cerevisiae* acquired in-line during batch phase fermentation. This material is available free of charge via the Internet at <http://pubs.acs.org>.

■ AUTHOR INFORMATION

Corresponding Author

*E-mail: bernhard.lendl@tuwien.ac.at.

Present Addresses

§(M.B.) Research Center for Non Destructive Testing GmbH, Altenbergerstraße 69, 4040 Linz, Austria.

|| (B.Lo.) Division of Life Sciences—Industrial Biotechnology, Department of Chemical and Biological Engineering, Chalmers University of Technology, Kemivägen 10, 412 96 Gothenburg, Sweden.

Notes

The authors declare no competing financial interest.

■ ACKNOWLEDGMENTS

The authors express their gratitude to Lukas Strobl for realization of the Labview control of the ultrasound frequency generator and Gerhard Fritsch for assistance in the assembly of the prototype probe and with preliminary experiments. Partial financial support provided by the Austrian Research Promotion Agency (FFG) under the scope of the COMET program within the research network “Process Analytical Chemistry (PAC)” (contract no. 825340) (C.K. and M.B.) and the Austrian Science Fund FWF (project no. P24154-N17) (C.K. and S.R.) is gratefully acknowledged. C.K. gratefully acknowledges partial financial support by the AB-Tec graduate school (TU Wien). European Social Fund from European Union and Junta de Comunidades de Castilla-La Mancha are gratefully acknowledged for supporting given through a Postdoctoral research contract for M.R.P.

■ REFERENCES

- (1) Griffiths, P. R.; de Haseth, J. A. *Fourier Transform Infrared Spectrometry*, 2nd ed.; Wiley-Interscience: Hoboken, NJ, 2007; pp 321–348.
- (2) Lourenço, N. D.; Lopes, J. A.; Almeida, C. F.; Sarragaça, M. C.; Pinheiro, H. M. *Anal. Bioanal. Chem.* **2012**, *404*, 1211–1237.
- (3) Landgrebe, D.; Haake, C.; Höpfner, T.; Beutel, S.; Hitzmann, B.; Scheper, T.; Rhiel, M.; Reardon, K. F. *Appl. Microbiol. Biotechnol.* **2010**, *88*, 11–22.
- (4) Dupuy, N.; Duponchel, L.; Huvenne, J. P.; Sombret, B.; Legrand, P. *Food Chem.* **1996**, *51*, 245–251.
- (5) Briandet, R.; Kemsley, E. K.; Wilson, R. H. *J. Agric. Food Chem.* **1996**, *44*, 170–174.
- (6) Lin, M.; Al-Holy, M.; Al-Qadiri, H.; Kang, D.-H.; Cavinato, A. G.; Huang, Y.; Rasco, B. A. *J. Agric. Food Chem.* **2004**, *52*, 5769–5772.
- (7) Sivakesava, S.; Irudayaraj, J.; Ali, D. *Process Biochem.* **2001**, *37*, 371–378.
- (8) Franco, V. G.; Perin, J. C.; Mantovani, V. E.; Goicoechea, H. C. *Talanta* **2006**, *68*, 1005–1012.
- (9) Roychoudhury, P.; Harvey, L. M.; McNeil, B. *Anal. Chim. Acta* **2006**, *561*, 218–224.
- (10) Roychoudhury, P.; McNeil, B.; Harvey, L. M. *Anal. Chim. Acta* **2007**, *585*, 246–252.
- (11) Kansiz, M.; Gapes, J. R.; McNaughton, D.; Lendl, B.; Schuster, K. C. *Anal. Chim. Acta* **2001**, *438*, 175–186.

- (12) Mazarevica, G.; Diewok, J.; Baena, J. R.; Rosenberg, E.; Lendl, B. *Appl. Spectrosc.* **2004**, *58*, 804–810.
- (13) Schenk, J.; Marison, I. W.; von Stockar, U. *J. Biotechnol.* **2007**, *128*, 344–353.
- (14) Schenk, J.; Marison, I. W.; von Stockar, U. *Biotechnol. Bioeng.* **2008**, *100*, 82–93.
- (15) Doak, D. L.; Phillips, J. A. *Biotechnol. Prog.* **1999**, *15*, 529–539.
- (16) Pollard, D.; Buccino, R.; Connors, N.; Kirschner, T.; Olewinski, R.; Saini, K.; Salmon, P. *Bioprocess Biosyst. Eng.* **2001**, *24*, 13–24.
- (17) Kornmann, H.; Rhiel, M.; Cannizzaro, C.; Marison, I.; von Stockar, U. *Biotechnol. Bioeng.* **2003**, *82*, 702–709.
- (18) Kornmann, H.; Valentiniotti, S.; Duboc, P.; Marison, I.; von Stockar, U. *J. Biotechnol.* **2004**, *113*, 231–245.
- (19) Dahlbacka, J.; Weegar, J.; von Weymarn, N.; Fagervik, K. *Biotechnol. Lett.* **2012**, *34*, 1009–1017.
- (20) Koch, C.; Posch, A. E.; Goicoechea, H. C.; Herwig, C.; Lendl, B. *Anal. Chim. Acta* **2014**, *807*, 103–110.
- (21) Kansiz, M.; Billman-Jacobe, H.; McNaughton, D. *Appl. Environ. Microbiol.* **2000**, *66*, 3415–3420.
- (22) Stehfest, K.; Toepel, J.; Wilhelm, C. *Plant Physiol. Biochem.* **2005**, *43*, 717–726.
- (23) Dean, A. P.; Sigee, D. C.; Estrada, B.; Pittman, J. K. *Bioresour. Technol.* **2010**, *101*, 4499–4507.
- (24) Wagner, H.; Liu, Z.; Langner, U.; Stehfest, K.; Wilhelm, C. *J. Biophotonics* **2010**, *3*, 557–566.
- (25) Winder, C. L.; Cornmell, R.; Schuler, S.; Jarvis, R. M.; Stephens, G. M.; Goodacre, R. *Anal. Bioanal. Chem.* **2011**, *399*, 387–401.
- (26) Scholz, T.; Lopes, V. V.; Calado, C. R. C. *Biotechnol. Bioeng.* **2012**, *109*, 2279–2285.
- (27) Corte, L.; Rellini, P.; Roscini, L.; Fatichenti, F.; Cardinali, G. *Anal. Chim. Acta* **2010**, *659*, 258–265.
- (28) Burattini, E.; Cavagna, M.; Dell’Anna, R.; Malvezzi Campeggi, F.; Monti, F.; Rossi, F.; Torriani, S. *Vib. Spectrosc.* **2008**, *47*, 139–147.
- (29) Cavagna, M.; Dell’Anna, R.; Monti, F.; Rossi, F.; Torriani, S. *J. Agric. Food Chem.* **2010**, *58*, 39–45.
- (30) Kuligowski, J.; Quintás, G.; Herwig, C.; Lendl, B. *Talanta* **2012**, *99*, 566–573.
- (31) Plata, M. R.; Koch, C.; Wechselberger, P.; Herwig, C.; Lendl, B. *Anal. Bioanal. Chem.* **2013**, *405*, 8241–8250.
- (32) Jarute, G.; Kainz, A.; Schroll, G.; Baena, J. R.; Lendl, B. *Anal. Chem.* **2004**, *76*, 6353–6358.
- (33) King, L. V. *Proc. R. Soc. London, Ser. A* **1934**, *147*, 212–240.
- (34) Yosioka, K.; Kawasima, Y. *Acustica* **1955**, *5*, 167–173.
- (35) Gor’kov, L. P. *Phys.-Dokl.* **1962**, *6*, 773–775.
- (36) Radel, S.; McLoughlin, A. J.; Gherardini, L.; Doblhoff-Dier, O.; Benes, E. *Ultrasonics* **2000**, *38*, 633–637.
- (37) Wiklund, M. *Lab Chip* **2012**, *12*, 2018–2028.
- (38) Trampler, F.; Sonderhoff, S. A.; Pui, P. W. S.; Kilburn, D. G.; Piret, J. M. *Nat. Biotechnol.* **1994**, *12*, 281–284.
- (39) Gorenflo, V. M.; Smith, L.; Dedinsky, B.; Persson, B.; Piret, J. M. *Biotechnol. Bioeng.* **2002**, *80*, 438–444.
- (40) Gorenflo, V. M.; Ritter, J. B.; Aeschliman, D. S.; Drouin, H.; Bowen, B. D.; Piret, J. M. *Biotechnol. Bioeng.* **2005**, *90*, 746–753.
- (41) Radel, S.; Schnöller, J.; Gröschl, M.; Benes, E.; Lendl, B. *IEEE Sens. J.* **2010**, *10*, 1615–1622.
- (42) Lendl, B.; Radel, S.; Brandstetter, M. Device for FTIR Absorption Spectroscopy. PCT/AT2010/000006, 2010.
- (43) Radel, S.; Brandstetter, M.; Lendl, B. *Ultrasonics* **2010**, *50*, 240–246.
- (44) Koch, C.; Brandstetter, M.; Lendl, B.; Radel, S. *Ultrasound Med. Biol.* **2013**, *39*, 1094–1101.
- (45) Socrates, G. *Infrared and Raman Characteristic Group Frequencies: Tables and Charts*, 3rd ed.; Wiley & Sons Ltd: New York, 2001.
- (46) Naumann, D.; Helm, D.; Labischinski, H. *Nature* **1991**, *351*, 81–82.
- (47) Gherardini, L.; Radel, S.; Sielemann, S.; Doblhoff-Dier, O.; Gröschl, M.; Benes, E.; McLoughlin, A. *Bioseparation* **2001**, *10*, 153–162.

Publication IV

Cosima Koch, Andreas E. Posch, Héctor C. Goicoechea, Christoph Herwig, Bernhard Lendl

Analytica Chimica Acta 807 (2014), 103 – 110. (c) 2013 The authors under a Creative Commons Attribution (CC-BY) License.

DOI: 10.1016/j.aca.2013.10.042



Contents lists available at ScienceDirect

Analytica Chimica Acta

journal homepage: www.elsevier.com/locate/aca

Multi-analyte quantification in bioprocesses by Fourier-transform-infrared spectroscopy by partial least squares regression and multivariate curve resolution[☆]

Cosima Koch^a, Andreas E. Posch^b, Héctor C. Goicoechea^c,
Christoph Herwig^b, Bernhard Lendl^{a,*}

^a Institute of Chemical Technologies and Analytics, Vienna University of Technology, Getreidemarkt 9/164 AC, 1060 Vienna, Austria

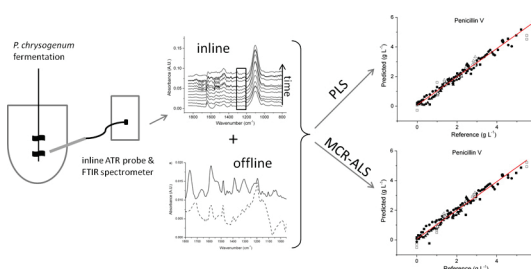
^b Christian Doppler Laboratory for Mechanistic and Physiological Methods for Improved Bioprocesses, Research Area Biochemical Engineering, Institute of Chemical Engineering, Vienna University of Technology, Gumpendorfer Strasse 1a, 1060 Vienna, Austria

^c Laboratorio de Desarrollo Analítico y Quimiometría-LADAQ, Universidad Nacional del Litoral-CONICET, Facultad de Bioquímica y Ciencias Biológicas, Ciudad Universitaria, 3000 Santa Fe, Argentina

HIGHLIGHTS

- Selective quantification using inline fiber optic ATR probe and midIR spectroscopy.
- Comparison of performance and ease of interpretation of PLS and MCR-ALS.
- General workflow for reliable quantification by FTIR spectroscopy in bioprocesses.

GRAPHICAL ABSTRACT



ARTICLE INFO

Article history:

Received 7 August 2013

Received in revised form 14 October 2013

Accepted 23 October 2013

Available online 11 November 2013

Keywords:

Inline bioprocess monitoring

FTIR spectroscopy

P. chrysogenum

Partial least squares regression

Multivariate curve resolution

Chemometrics

ABSTRACT

This paper presents the quantification of Penicillin V and phenoxyacetic acid, a precursor, inline during *Penicillium chrysogenum* fermentations by FTIR spectroscopy and partial least squares (PLS) regression and multivariate curve resolution – alternating least squares (MCR-ALS). First, the applicability of an attenuated total reflection FTIR fiber optic probe was assessed offline by measuring standards of the analytes of interest and investigating matrix effects of the fermentation broth. Then measurements were performed inline during four fed-batch fermentations with online HPLC for the determination of Penicillin V and phenoxyacetic acid as reference analysis. PLS and MCR-ALS models were built using these data and validated by comparison of single analyte spectra with the selectivity ratio of the PLS models and the extracted spectral traces of the MCR-ALS models, respectively. The achieved root mean square errors of cross-validation for the PLS regressions were 0.22 g L⁻¹ for Penicillin V and 0.32 g L⁻¹ for phenoxyacetic acid and the root mean square errors of prediction for MCR-ALS were 0.23 g L⁻¹ for Penicillin V and 0.15 g L⁻¹ for phenoxyacetic acid. A general work-flow for building and assessing chemometric regression models for the quantification of multiple analytes in bioprocesses by FTIR spectroscopy is given.

© 2013 The Authors. Published by Elsevier B.V. All rights reserved.

1. Introduction

The advantage of spectroscopic methods over classical analytical methods employed for bioprocess analysis is the simultaneous determination of multiple target analytes through multivariate data analysis. Data are acquired in situ, without the need for sample preparation and can be provided in real-time making it well

[☆] This is an open-access article distributed under the terms of the Creative Commons Attribution-NonCommercial-No Derivative Works License, which permits non-commercial use, distribution, and reproduction in any medium, provided the original author and source are credited.

* Corresponding author. Tel.: +43 1 58801 15140.

E-mail address: bernhard.lendl@tuwien.ac.at (B. Lendl).

suited for process monitoring. Especially attenuated total reflection (ATR) Fourier-transform-infrared (FT-IR) spectroscopy has become increasingly interesting as a process analytical tool (PAT) for inline and online monitoring of (pharmaceutical) bioprocesses [1–14]. Dissolved substrate components, as well as desired and undesired metabolites can be quantitatively determined using multivariate data analysis methods, i.e. chemometrics, like principal component analysis (PCA), partial least squares (PLS) regression and multivariate curve resolution (MCR) [15], to name a few. Landgrebe et al. [16] give a good overview of bioprocesses and specific analytes monitored by online mid- and near-infrared spectroscopy. Lourenço et al. [17] give a more general review of optical spectroscopy methods employed for bioprocess monitoring, including a brief introduction to chemometric methods. ATR-probes designed for process control/monitoring are commercially available and are fit for measurements in harsh and variable process environments, i.e. are autoclavable and made from biocompatible materials.

In this work we concentrated on Penicillin V (PenV), a commonly used beta-lactam antibiotic [18,19]. It is produced in industrial-scale bioprocesses by *Penicillium chrysogenum*. Bioprocess design and control for filamentous fungi still rely greatly on empirical methods. Here, a science-based approach, as facilitated by online and inline sensors combined with simplified mechanistic models, would be beneficial since it helps increase process economics and decrease development time [20]. Accurate determination of optimal harvest time of the bioprocess is crucial to product quality and productivity. Routine measurements of PenV and phenoxyacetic acid (POX) concentrations are typically performed offline by high performance liquid chromatography (HPLC) analysis.

Guzman et al. [21] showed that prediction of termination times of a biotransformation batch process by monitoring the hydrolysis of Penicillin V to phenoxyacetic acid and 6-aminopenicillanic acid using online ATR FT-IR spectroscopy in a bypass system and PLS regression was superior to standard procedures, like offline HPLC analysis. We aim at quantitative determination of the precursor phenoxyacetic acid and product, Penicillin V in fed-batch fermentations of *P. chrysogenum*. Here we present a method that allows for determination of precursor and product inline as well as real-time determination of the optimal harvest time, making sampling unnecessary and thus minimizing possible errors. We compared two different chemometric methods, PLS and MCR-ALS, for prediction of POX and PenV concentrations from FT-IR spectra.

PLS regression is a calibration method that is suitable for numerous, strongly correlated x-variables [22] as presented by FT-IR spectra. It projects the **X** data onto a set of “latent variables” that are good predictors of **Y** using a least-squares approach. These latent variables are often hard to interpret or relate to spectra of pure components. While for PLS regression a reliable reference method is necessary, MCR-ALS is based on the assumption that the multivariate data matrix (**X** or **D**), e.g. FT-IR spectra taken at different times of a chemical reaction, can be approximated as a linear combination of unfolded (pure) component spectra (**S**) weighed by their respective concentration profiles (**C**) plus the residuals that cannot be explained by the model (**E**). The unfolded spectra **S** can be given a chemical meaning when comparing them to measured pure component spectra, thus allowing for evaluation of model quality. Reference data is not necessary for this type of modeling, however, a good estimation of starting concentrations helps. Furthermore, application of different constraints, such as non-negativity for concentrations, or combination with hard models, e.g. a hard equilibrium model describing the acid-base equilibria of simple molecules for quantitative analysis of pH-modulated mixture samples [23], can improve the MCR-ALS model.

2. Material and methods/experimental

2.1. Fermentation of *P. chrysogenum*

Four fed-batch fermentations of *P. chrysogenum* (strain: BCB1) were carried out similar to a recently described protocol except for POX addition [24]. Since accurate determination of the optimal harvest time was the goal, POX was not added continually, but in a pulsed way, so depletion could be observed more than once during a fermentation run. In order to allow applicability of the FT-IR probe with 25 mm Ingold® design however, fed-batch cultivations were performed in a 15 L autoclavable, fully automated and controlled stirred bioreactor (Infors, Switzerland) instead of the previously described 7.5 L glass reactor system [24]. For all fed-batch cultivations, process duration was in the range of 140–160 h.

2.2. FT-IR spectroscopy

FT-IR spectra were recorded with a 1.5 m DiComp AgX (silver halide) fiber optic probe connected to the portable process spectrometer ReactIR 15 (both Mettler Toledo, Switzerland) equipped with a liquid-nitrogen-cooled mercury-cadmium-telluride (MCT) detector. The probe was equipped with a diamond ATR element and a special adapter was designed and built in-house to couple the probe to a 25 mm Ingold® port available in the bioreactor. The ReactIR 15 is a sealed instrument, thus no purging with dry air was required. Spectra were acquired using the dedicated software IclIR 4.2 (Mettler Toledo, Switzerland), with the resolution set to 8 cm^{-1} in the spectral range of $900\text{--}4000\text{ cm}^{-1}$, as the co-addition of 256 scans. Basic data manipulation, like single point baseline correction, was also performed in IclIR 4.2.

The applicability of ATR FT-IR spectroscopy for determination of POX and PenV in complex media matrices was assessed offline. Single analyte and binary solutions of POX and PenV were prepared in 20 mM phosphate buffer adjusted to pH = 6.5 which is the pH level maintained throughout PenV production in the fermentation (for concentration levels see Supplementary data Table A). Phenoxyacetic acid (99%, Sigma Aldrich, USA) and phenoxymethylpenicillin potassium salt (Penicillin V potassium, kindly provided by Sandoz GmbH, Austria) were weighed in and diluted and mixed to the desired final concentrations. The standard solutions and supernatant samples from previous fermentations were measured offline against a water background by depositing a drop of the solution onto the horizontally aligned ATR surface. Inline, spectra were acquired every 2–5 min against a medium background, resulting in approximately 2000 spectra for each fermentation run.

2.3. Reference analysis

Analysis of penicillin V and phenoxyacetic acid was performed by isocratic HPLC using a ZORBAX C-18 column (Agilent Technologies, USA) and 28% ACN, 6 mM H_3PO_4 , 5 mM KH_2PO_4 as elution buffer (all reagents: Sigma Aldrich, USA). The bioreactor was coupled to the HPLC via a $0.2\text{ }\mu\text{m}$ pore size ceramic probe (iba e.V. Heiligenstadt, Germany). Samples of the medium were drawn from the bioreactor at constant flow and were sampled from a flow-through cell as often as possible during pulsed addition of POX (approx. every 15–20 min) and every 3 h during the decrease of POX. The sampling delay was 1 h 15 min in runs 1 to 3 and 15 min for run 4, respectively (a sampling line with thinner diameter was available in this run). The HPLC method was optimized to ensure good separation of peaks, and an automatic dilution step was introduced to keep analyte concentrations within the calibration range.

Additionally, samples were drawn from the bioreactor every 12 h and HPLC measurements were performed offline. These were

in good agreement with the online measurements (data not shown). The relative standard deviation of the HPLC determination alone is small: 0.9% relative standard deviation (RSD) for 3.4 g L^{-1} POX and 1.3% RSD for 0.8 g L^{-1} PenV. When coupling the HPLC online with the bioreactor, the error is expected to increase for several reasons: Due to inferences from media components, the integration method had to be adjusted. Since a relatively small sample volume is drawn for every point in time (i.e. continuously), time resolution is slightly blurred by sampling from the flow-through cell. Furthermore, because of the long sampling line, degradation of the analytes could occur and matching the HPLC measurement times with the acquisition times of FT-IR spectra becomes difficult. We therefore estimated the total error of the method to be roughly 5%.

2.4. Multivariate calibration

To build multivariate calibration models, the three spectra acquired closest to the times of HPLC measurements (see Section 2.3) were averaged and imported into Matlab®. A total of 196 spectra with reference data were available for regression. To break co-linearity between POX and PenV and to correct for potential errors in HPLC reference measurements, single analyte and binary standards were included in the model to increase robustness as previously reported [9]. Furthermore, POX addition was performed continuously for run 1, as would be done in the industrial process, and in a spiked manner for runs 2 to 4, i.e. POX was added quickly to a predetermined concentration after its depletion.

2.4.1. PLS regression

PLS regression models were built using the PLS toolbox 6.2 (Eigenvector Research, Inc., USA) using the SIMPLS algorithm [25]. Suitable spectral regions for calibration were identified from the pure PenV and POX spectra, taking into account interferences of the fermentation broth (for spectral regions used see Table 1). Preprocessing consisted of calculation of first derivative (Savitzky-Golay (Sav-Gol), order 2, window size 11) of spectral data and mean centering of both, spectral and concentration data. Cross-validation of PLS models was performed using random subsets (10 data splits, 3 iterations).

2.4.2. MCR-ALS calibration

The multivariate calibration algorithm MCR-ALS has been extensively described in the literature [15,26] so, only a brief description of it is given here.

The bilinear decomposition of the augmented matrix **D** is performed according to the expression:

$$\mathbf{D} = \mathbf{C}\mathbf{S}^T + \mathbf{E} \quad (1)$$

in which the rows of **D** contain the spectra measured for different samples (pure and mixture standards and fermentation samples), the columns of **C** contain the relative concentrations of the intervening species, the columns of **S** their related unfolded spectra, and **E** is a matrix of residuals not fitted by the model.

Decomposition of **D** is achieved by iterative least-squares minimization of the Frobenius norm of **E**, under suitable constraining conditions during the ALS procedure. MCR-ALS requires initialization with system parameters as close as possible to the final results. In the present work we employed the SIMPLISMA (simple to use interactive self-modeling mixture analysis) methodology [27] in all cases.

During the iterative recalculations of **C** and **S**^T, a series of constraints are applied to give physical meaning to the obtained solutions, and to limit their possible number for the same data fitting. In this paper, the correspondence among species in the experiments was used as restriction together with a correlation

constraint, in which the concentrations of the analytes in calibration samples at each ALS iteration are forced to be correlated to previously known reference concentration values of the analyte in these samples. More details about the implementation of this constraint in previous works can be found elsewhere [28,29]. This latter constraint has been successfully applied in the determination of several compounds in the presence of unexpected interferences using first-order instrumental data [30].

Correlation constrained MCR-ALS was implemented using a MATLAB code which is available on request from R. Tauler (e-mail: Roma.Tauler@idaea.csis.es).

3. Results and discussion

3.1. Workflow

The following, generally applicable workflow for optimal model building and calibration of inline spectroscopic measurements for multi-analyte quantification was followed:

Feasibility study:

1. Pure analyte spectra were recorded in order to assess general IR absorbance characteristics and identify possible cross-correlations. Generally, the chemical and physical environment of the pure analytes should be comparable to that expected in the process, i.e. similar pH, temperature, etc.
2. Then, matrix effects of the (bio)process medium were investigated by spiking real process samples with the analyte of interest (POX).

Multivariate model building:

3. Given accurate and sensitive reference analytics in place, inline measurements were performed at the process and PLS model building based on synthetic standards and inline measurements was performed.
4. Finally, to verify reasonable model building, model validity for each analyte was ensured by selectivity analysis. At this stage, unless acceptance criteria are met, further orthogonal measurements should be included for calibration in order to break undesired cross-correlations.
5. If selectivity cannot be achieved satisfactory with PLS, or not enough calibration samples are available, MCR-ALS, which calculates spectral traces of modeled factors, should be used to ensure that the target analyte is modeled by one of the factors. We have built MCR-ALS models for the analytes of interest and compare their performance to that of PLS regression.

3.2. Investigation of feasibility

To ensure the applicability of ATR FT-IR spectroscopy as a means for quantification of POX and PenV, spectra of synthetic single and binary solutions were acquired. Fig. 1(a) shows the pure component spectra of solutions of PenV and POX in 20 mM phosphate buffer (pH=6.5). Spectral overlap between the two analytes is, as expected, high, but there are some distinct differences that can help to break the co-linearity around 1775 cm^{-1} and in the range between 1100 and 1400 cm^{-1} . In Fig. 1(b) a spectrum of a typical fermentation sample acquired offline is shown. The spectrum is governed by a large absorption peak around 1100 cm^{-1} which is due to (SO_4^{2-}) introduced from ammoniumsulphate addition and sulphuric acid for pH control. Characteristic spectral features of PenV (bands between 1800 and 1750 cm^{-1} , 1270 and 1340 cm^{-1} and 1200 and 1250 cm^{-1}) and POX (bands between 1200 and 1250 cm^{-1}) are visible; they are however relatively weak. Spiking of samples drawn before the addition of POX had been started, thus without any POX or PenV content, showed that the

Table 1

Model parameters and figures of merit for the POX and PenV PLS models.

Model	Calibration range (g L ⁻¹)	Data included	Wavenumber region (cm ⁻¹)	Preprocessing steps	Latent variables	RMSECV (g L ⁻¹)	r ² CV
POX-PLS	0–3.47	Offline: fermentation, standards; fermentations 1–4	1188–1352 & 1747–1817	Mean centering, first derivative (Sav-Gol, order 2, window 11)	6	0.31	0.90
PenV-PLS	0–5.55	Offline: fermentation, standards, fermentations 1 & 3–4	1184–1501 & 1672–1855	Mean centering, first derivative (Sav-Gol, order 2, window 11)	7	0.22	0.97

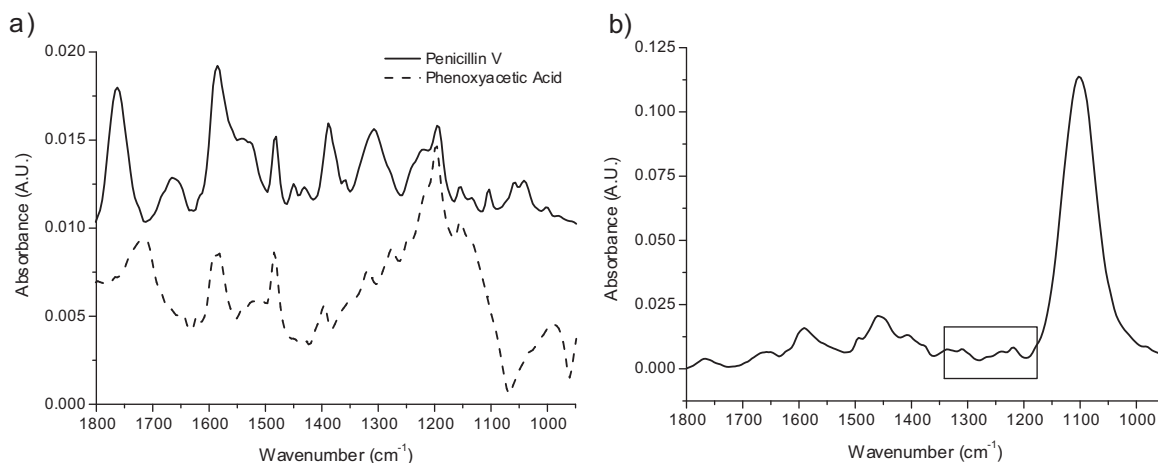


Fig. 1. (a) Reference attenuated total reflection (ATR) spectra of Penicillin V (10 g L⁻¹) and phenoxyacetic acid (3 g L⁻¹) in 20 mM phosphate buffer adjusted to pH = 6.5. Pure phosphate buffer was used as a background. Spectral similarities of the two analytes are obvious, however some differences, especially around 1350 cm⁻¹ and 1750 cm⁻¹, are present. (b) Offline ATR spectrum of a typical fermentation broth sample. Between 1200 and 1350 cm⁻¹ typical features of POX and PenV can be seen (black box), their absorbances are however very low compared to other components, e.g. (SO₄²⁻) which absorbs around 1100 cm⁻¹.

appropriate bands appeared and were proportional to POX concentration (Fig. 2(a)). The difference spectrum of the sample spiked to 1 g L⁻¹ POX final concentration (Spiked 1) and the unspiked sample is highly similar to that of 1 g L⁻¹ POX in 20 mM phosphate buffer (Fig. 2(b)). This strong correlation shows that the spectral features are conserved in the complex fermentation broth matrix and indicate that the determination of POX from fermentation broth spectra is feasible.

The potential of multianalyte determination by mid-IR spectroscopy and chemometric modeling also poses a challenge: cross-correlations with interferents and modeling of general

temporal, rather than concentration changes. Therefore, a validation of the generated chemometric models is very important, especially in complex, variable matrices that are present in bioprocesses.

3.3. PLS regression

The PLS regression models built for POX and PenV were based on prior knowledge of the spectral ranges relevant for the two analytes. The spectral ranges were chosen based on the wavenumber regions where specific bands of POX and PenV were identified and little interference from the fermentation broth was expected.

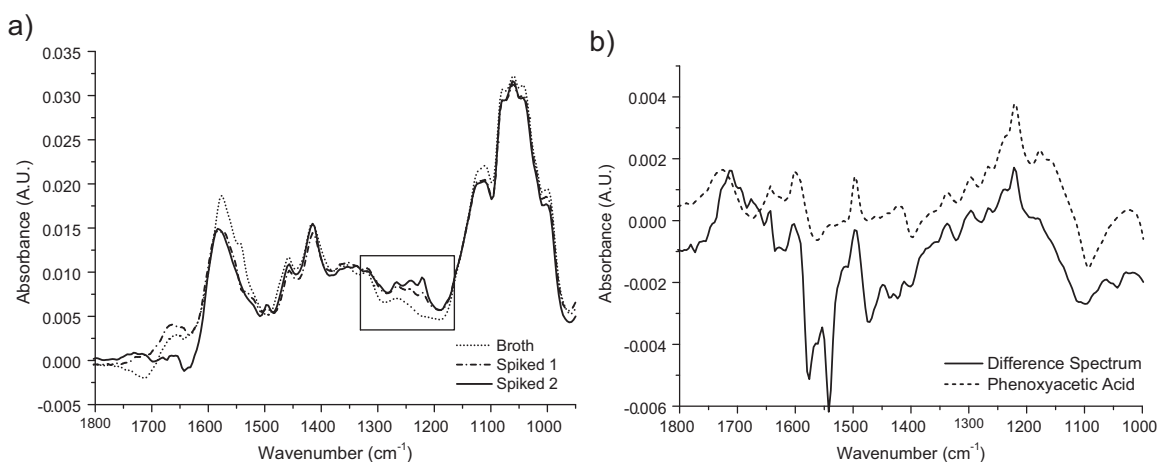


Fig. 2. (a) Spectra of fermentation broth without POX (Broth, dotted line), fermentation broth spiked to a final POX concentration of 1 g L⁻¹ (Spiked 1, dash-dot line) and spiked to a final concentration of POX of 2 g L⁻¹ (Spiked 2, solid line). The spectral range in which POX-specific bands can be seen is indicated by the black box. (b) Difference spectrum of Spiked 1 (1 g L⁻¹ POX) and the Broth spectrum (solid line) and spectrum of 1 g L⁻¹ POX in 20 mM phosphate buffer (dashed line). The correlation between the spectra is very good, especially in the region between 1200 and 1400 cm⁻¹ (spectra are offset for clarity).

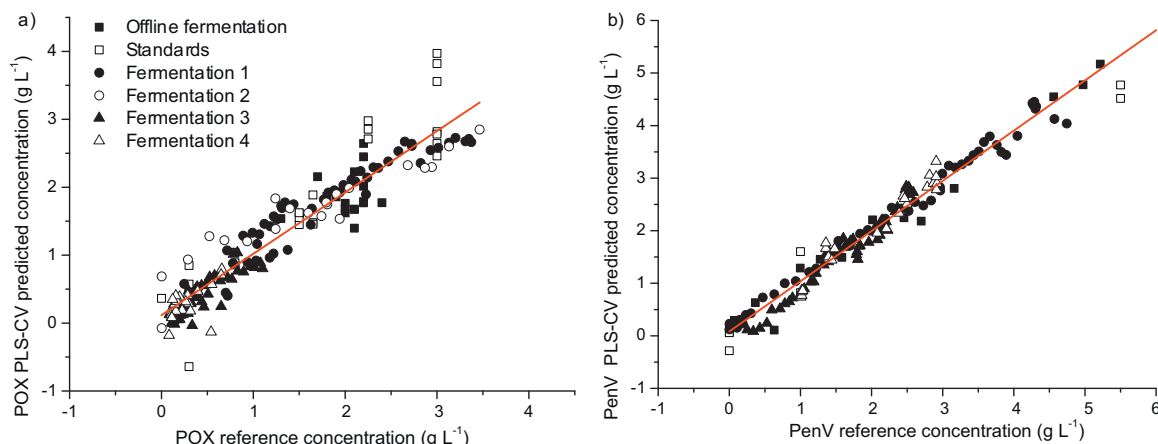


Fig. 3. (a) Calibration curve for POX. (b) Calibration curve for PenV. Reference concentrations determined by HPLC or gravimetrically are plotted vs. the POX concentrations predicted by the cross-validated PLS model. The origin of the data is indicated by different marker symbols.

Different spectral ranges were tested, i.e. PLS models built, and the spectral regions that performed best for each analyte and for which selectivity ratios indicated specificity (see below) were chosen. The relative changes in the observed wavenumber regions over the course of a single fermentation can be seen in Supplementary data Fig. B, a PCA scoreplot of all data used for calibration can be seen in Supplementary data Fig. C. Apart from variations in the spectral range employed for model construction, different preprocessing steps (raw spectra, first and second derivative (Sav-Gol) spectra) were tested. For both analytes, first derivative spectra gave the best

results, since baseline shifts could thus be omitted. The relatively small signal to noise ratio for the analytes of interest made second derivative spectra unsuitable for modeling. The wavenumber regions used for the respective analytes were different. Details about the PLS-models for POX and PenV are given in Table 1. The POX PLS-model was based on all offline spectra and the spectra obtained in fermentation runs 1–4. In fermentation run 2 one HPLC outlier was omitted and two were omitted from fermentation run 3 (comparison with previous and subsequent HPLC results and approximate calculation of POX concentration). For the PenV PLS-model data

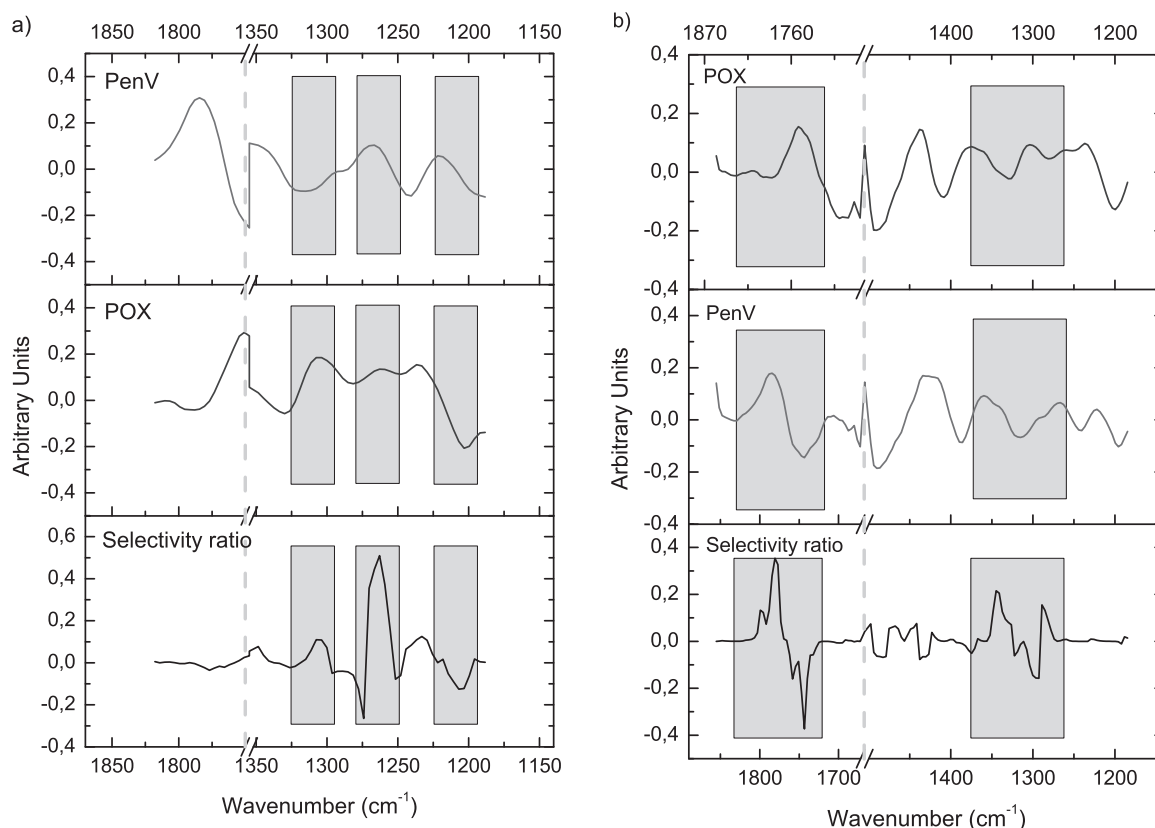


Fig. 4. (a) Selectivity ratio multiplied by the sign of the correlation vector (bottom) for POX-PLS model compared to the first derivative, mean centered spectra of POX and PenV (vector normalized). (b) Selectivity ratio multiplied by the sign of the correlation vector (bottom) for PenV-PLS model compared to the first derivative, mean centered spectra of POX and PenV (vector normalized). A high absolute value of the selectivity ratio points to spectral regions that have a strong influence on the model, while the sign indicates whether the correlation is positive or negative.

Table 2
Parameters and figures of merit for the POX and PenV MCR-ALS models.

Model	Calibration range (g L ⁻¹)	Calibration data	Data predicted	Wavenumber region (cm ⁻¹)	Preprocessing steps	Factors	RMSEP (g L ⁻¹)	r ² prediction
POX-MCR-ALS	0–3.0	Offline: fermentation, standards	Single analyte standards; fermentations 1–4	1281–1352 & 1747–1817	Mean centering, first derivative (Sav-Gol, order 2, window 11)	5	0.16	0.97
PenV-MCR-ALS	0–5.55	Offline: fermentation, standards	Offline: fermentation, standards; fermentations 1 & 3–4	1307–1352 & 1747–1817	Mean centering, first derivative (Sav-Gol, order 2, window 11)	5	0.23	0.95

from fermentation run 2 were omitted, since no PenV was produced during this run. Models including these data performed worse in cross-validation than when the data were predicted using models built omitting the data, i.e. the RMSECV was higher than the RMSEP. We concluded that the introduction of these additional data lead to an introduction of noise to the model increasing the RMS error. The calibration curve of POX concentrations determined by HPLC vs. the values predicted from cross-validation for the POX PLS model is shown in Fig. 3(a). The RMSECV for POX was determined as 0.31 g L⁻¹; the RMSECV normalized to the calibration range is 9% which is slightly worse than the estimated error of reference analysis (5%). Fig. 3(b) shows the calibration curve for PenV; the respective RMSECV was determined as 0.22 g L⁻¹ and the normalized RMSECV (to calibration range) is 4%, which is in the range of the expected error of the reference method.

As a means to check the validity of the developed PLS models, the selectivity ratio, which is the ratio of explained to residual variance for each variable, i.e. wavenumber, was calculated [31]. A high selectivity ratio indicates wavenumber regions that have a strong impact on the prediction, and the type of correlation is inferred from the regression vector (i.e. positive or negative). By comparing spectral regions that have a high selectivity ratio with spectral features of the target analyte and potential interferences, the correctness/validity of the model can be checked. In Fig. 4(a) the preprocessed, i.e. first derivative and mean centered, pure analyte spectra of PenV, the strongest interferent, and POX and the selectivity ratio of the POX-PLS model are shown. Wavenumber regions with a high positive or negative selectivity ratio are highlighted in gray. The highest selectivity ratio is found around 1265 cm⁻¹, which coincides with a maximum for both POX and PenV. Selectivity for POX can be attributed to the positive correlation around 1310 cm⁻¹, where for the POX spectrum a maximum is located, while the PenV spectrum shows a local minimum, and the negative correlation around 1205 cm⁻¹. Here, the first derivative, mean centered POX spectrum has a minimum as well, while the PenV spectrum is close to zero. Fig. 4(b) shows the same plots for the PenV-PLS model. Again, the first derivative, mean centered spectra of PenV and POX are compared to the selectivity ratio multiplied by the sign of the regression vector. Good agreement between the selectivity ratio and the PenV spectrum can be seen in the region between 1725 and 1825 cm⁻¹. For the second region with large selectivity ratios (1250–1380 cm⁻¹), the curve is also very similar to the PenV spectrum. No matches between the POX spectrum and the selectivity ratio of the PenV-PLS model can be observed.

3.4. MCR-ALS models

The MCR-ALS models built for POX and PenV were based on prior knowledge of the spectral ranges relevant for the two analytes derived from single analyte spectra. The wavenumber regions which resulted in the best performance of the MCR-ALS models

for both POX and PenV were smaller than those used in the PLS models (see Table 2). As for the PLS models, mean centered first derivative (Sav-Gol, polynomial order 2, window size 11) spectra gave the best results. For concentration prediction from spectra acquired during the fermentation runs, the concentration information from offline fermentation samples, single analyte standards and binary standards was used for calibration. Calibration curves of MCR-ALS predicted concentrations vs. concentration measured using reference analysis obtained for POX and PenV are shown in Fig. 5. As for the PLS models, good correlations with a high r² value were found. The root-mean-square-error of prediction (RMSEP) for

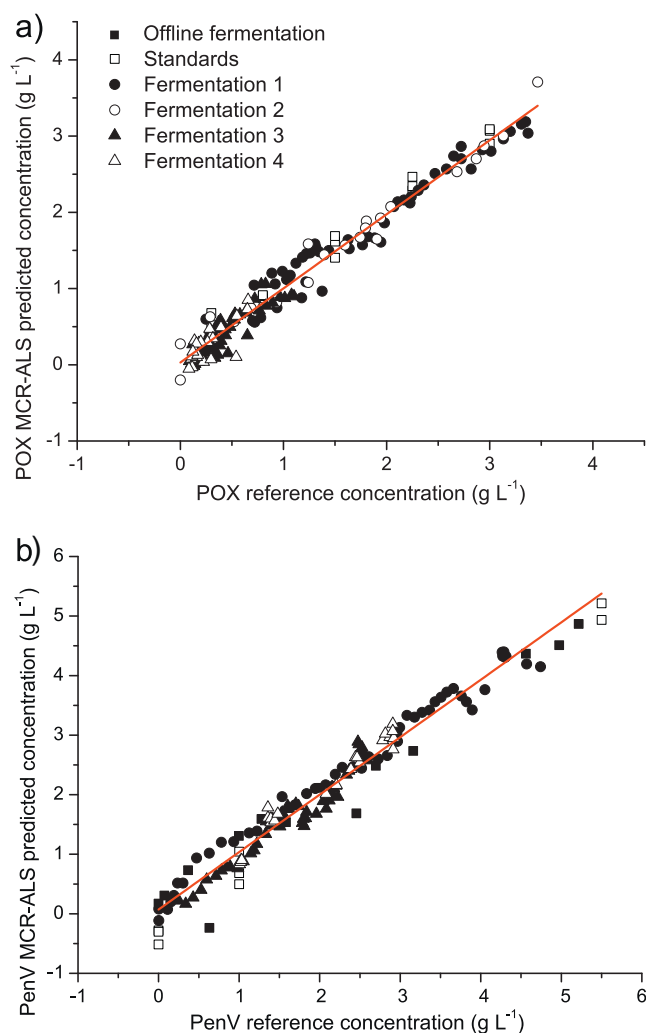


Fig. 5. Calibration curves for the MCR-ALS models for POX (a) and PenV (b). Values predicted using the MCR-ALS models are plotted against values obtained by reference analysis.

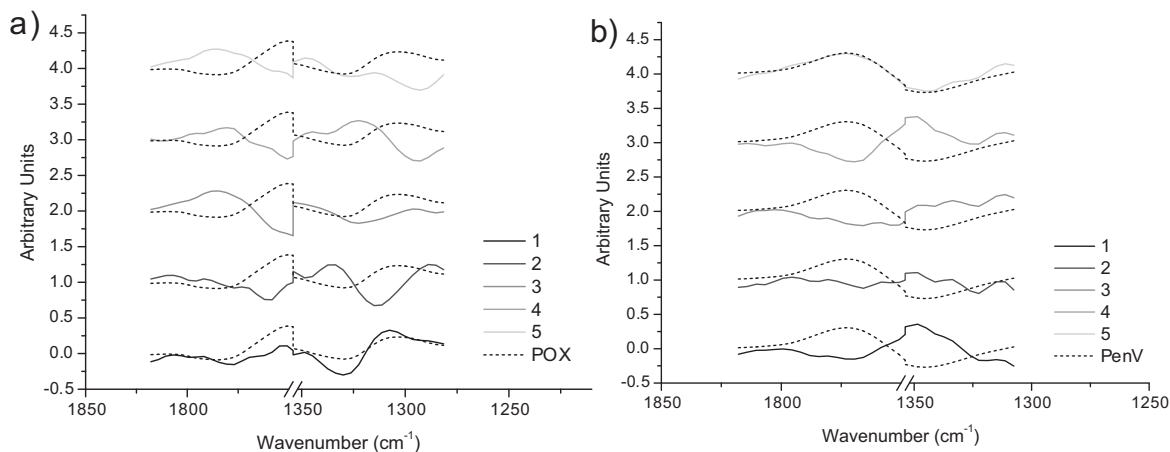


Fig. 6. MCR spectra traces for the MCR-ALS model for POX (a) and for PenV (b). The preprocessed single analyte spectrum of the target analyte (dashed line) for each model is plotted over the calculated spectral traces. For the POX MCR-ALS model, the spectral trace of component 1 (bottom of graph a) is in good agreement with the POX spectrum. The spectral trace of component 5 (top of graph b) of the PenV MCR-ALS model is highly correlated to the PenV spectrum.

POX was determined as 0.16 g L^{-1} (normalized to calibration range: 4.6%), which is significantly lower than the RMSECV of the PLS-POX model and in the range of the estimated reference method error. The higher goodness of fit is also reflected in a higher r^2 of the calibration curve, namely 0.97, for the MCR-ALS model than for the PLS model ($r^2 = 0.90$). For PenV the RMSEP was determined as 0.23 g L^{-1} (normalized to calibration range: 4.1%), making the performance of the MCR-ALS model similar to the PLS model and the estimated reference method error.

Since MCR-ALS is a method that, for a given number of components, calculates concentration profiles and spectral traces that best describe the spectral changes of the data, these spectra can be directly compared to (preprocessed) pure analyte spectra. Fig. 6 shows the spectral traces calculated by MCR-ALS for both the POX (a) and PenV (b) and the respective pure analyte spectra. For both, PenV and POX, good agreement between the respective single analyte spectrum and the spectral trace of one of the components can be seen. Component 1 of the POX MCR-ALS model correlates well with the POX spectrum and component 5 of the PenV MCR-ALS model correlates well with the PenV spectrum.

4. Conclusions

Comparing PLS with MCR-ALS, similar model performances were reached. While, in principle, step 3 may be omitted for MCR-ALS, predictive accuracy proved to be superior when using standard spectra as a means to calibrate the model. Since PLS is the more established method for spectral calibration and does not require as much expertise and not as many input parameters as for MCR-ALS, we recommend it as a starting point. If selectivity analysis is not satisfactory, MCR-ALS modeling should be used, as the spectral traces of the modeled components are calculated directly and can be compared to target analyte spectra. In cases where only a limited number of calibration spectra is available, e.g. due to lack of reliable reference analysis, MCR-ALS should be the method of choice, as the algorithm basically does not require reference concentrations. Furthermore, in some cases the performance of MCR-ALS is better than that of PLS, as is the case for POX in this work.

Applying the suggested workflow, concentrations of PenV and POX were successfully predicted inline. This is a step toward accurate determination of optimal termination time of the bioprocess. To increase the accuracy of predictions, two things have to be considered: the performance of chemometric models is always limited by the accuracy of the reference analysis and by the signal-to-noise

ratio (SNR) of the spectroscopic system in use. With respect to an improved SNR, the elimination of the silver halide fiber in favor of a monolithic sensor design seems to be a promising approach. This could be realized either using External Cavity Quantum Cascade Lasers (EC-QCLs) coupled with waveguides and small pyro-electric detectors, or the use of pulsed mid-IR sources in combination with a multi-reflection ATR-element and line (Bragg) filter detectors. Both approaches use dispersive measurement principles, therefore also eliminating the need for potentially bulky and vibration sensitive interferometers.

Acknowledgements

Partial financial support of the Austrian Science Fund (FWF) through the stand-alone project scheme (project number: P24154), the Austrian research funding association (FFG) under the scope of the COMET program within the research network “Process Analytical Chemistry (PAC)” (contract # 825340) and the Federal Ministry of Economy, Family and Youth in course of the Christian Doppler Laboratory for Mechanistic and Physiological Methods for Improved Bioprocesses is gratefully acknowledged. Cosima Koch and Andreas Posch thankfully acknowledge partial financial support by Sandoz GmbH and Vienna University of Technology (graduate school AB-Tec). We want to thank Simona Capone for her support in the laboratory with the fermentations, Maria Reyes Plata Torres for the preparation of standards and Sandoz GmbH for providing the microorganism.

Appendix A. Supplementary data

Supplementary data associated with this article can be found, in the online version, at <http://dx.doi.org/10.1016/j.aca.2013.10.042>.

References

- [1] D. Pollard, R. Buccino, N. Connors, T. Kirschner, R. Olewinski, K. Saini, P. Salmon, *Bioprocess Biosyst. Eng.* 24 (2001) 13–24.
- [2] J. Dahlbacka, J. Weegar, N. von Weymar, K. Fagervik, *Biotechnol. Lett.* 34 (2012) 1009–1017.
- [3] H. Kornmann, M. Rhiel, C. Cannizzaro, I. Marison, U. von Stockar, *Biotechnol. Bioeng.* 82 (2003) 702–709.
- [4] J. Schenk, I.W. Marison, U. von Stockar, *Biotechnol. Bioeng.* 100 (2008) 82–93.
- [5] M. Kansiz, K.C. Schuster, D. McNaughton, B. Lendl, *Spectrosc. Lett.* 38 (2005) 677–702.
- [6] J. Schenk, I.W. Marison, U. von Stockar, *J. Biotechnol.* 128 (2007) 344–353.
- [7] M. Rhiel, P. Ducommun, I. Bolzonella, I. Marison, U. Von Stockar, *Biotechnol. Bioeng.* 77 (2002) 174–185.

- [8] H. Kornmann, S. Valentinotti, P. Duboc, I. Marison, U. von Stockar, J. Biotechnol. 113 (2004) 231–245.
- [9] G. Mazarevica, J. Diewok, J.R. Baena, E. Rosenberg, B. Lendl, Appl. Spectrosc. 58 (2004) 804–810.
- [10] E.L. Veale, J. Irudayaraj, A. Demirci, Biotechnol. Prog. 23 (2007) 494–500.
- [11] M. Dabros, P. Fe, M.I. Amrhein, D. Bonvin, I.W. Marison, Biotechnol. Prog. 25 (2009) 578–588.
- [12] T. Genkawa, M. Watari, T. Nishii, Y. Ozaki, Appl. Spectrosc. 66 (2012) 773–781.
- [13] G. Jarute, A. Kainz, G. Schroll, J.R. Baena, B. Lendl, Anal. Chem. 76 (2004) 6353–6358.
- [14] M. Kansiz, J.R. Gapes, D. McNaughton, B. Lendl, K.C. Schuster, Anal. Chim. Acta 438 (2001) 175–186.
- [15] R. Tauler, Chemom. Intell. Lab. Syst. 30 (1995) 133–146.
- [16] D. Landgrebe, C. Haake, T. Höpfner, S. Beutel, B. Hitzmann, T. Scheper, M. Rhiel, K.F. Reardon, Appl. Microbiol. Biotechnol. 88 (2010) 11–22.
- [17] N.D. Lourenço, J. a Lopes, C.F. Almeida, M.C. Sarraguça, H.M. Pinheiro, Anal. Bioanal. Chem. 404 (2012) 1211–1237.
- [18] A.L. Demain, Appl. Microbiol. Biotechnol. 52 (1999) 455–463.
- [19] R.P. Elander, Appl. Microbiol. Biotechnol. 61 (2003) 385–392.
- [20] A.E. Posch, C. Herwig, O. Spadiut, Trends Biotechnol. 31 (2013) 37–44.
- [21] M. Guzman, M. DeBang, J. Ruzicka, G.D. Christian, Process Control Qual. 2 (1992) 113–122.
- [22] S. Wold, M. Sjöström, L. Eriksson, Chemom. Intell. Lab. Syst. 58 (2001) 109–130.
- [23] J. Diewok, A. de Juan, M. Maeder, R. Tauler, B. Lendl, Anal. Chem. 75 (2003) 641–647.
- [24] A.E. Posch, C. Koch, M. Helmelt, M. Marchetti-Deschmann, K. Macfeldt, B. Lendl, G. Allmaier, C. Herwig, Fungal Genet. Biol. 51 (2013) 1–11.
- [25] S. de Jong, Chemom. Intell. Lab. Syst. 18 (1993) 251–263.
- [26] J. Saurina, C. Leal, R. Compañó, M. Granados, M.D. Prat, R. Tauler, Anal. Chim. Acta 432 (2001) 241–251.
- [27] W. Windig, J. Guilment, Anal. Chem. 63 (1991) 1425–1432.
- [28] M.C. Antunes, J.E.J. Simão, A.C. Duarte, R. Tauler, Analyst 127 (2002) 809–817.
- [29] T. Azzouz, R. Tauler, Talanta 74 (2008) 1201–1210.
- [30] H.C. Goicoechea, A.C. Olivieri, R. Tauler, Analyst 135 (2010) 636–642.
- [31] O.M. Kvalheim, J. Chemom. 24 (2010) 496–504.

Publication V

Cosima Koch, Andreas E. Posch, Christoph Herwig, Bernhard Lendl, submitted to *Applied Spectroscopy*, (major) revisions under way.

Comparison of fiber optic and conduit attenuated total reflection (ATR) Fourier transform infrared (FT-IR) setup for in-line fermentation monitoring

Cosima Koch¹, Andreas E. Posch², Christoph Herwig^{2,3}, Bernhard Lendl^{1,*}

¹ Institute of Chemical Technologies and Analytics, Vienna University of Technology, Getreidemarkt 9/164 UPA, 1060 Vienna, Austria

² Christian Doppler Laboratory for Mechanistic and Physiological Methods for Improved Bioprocesses, Vienna University of Technology, Gumpendorferstraße 1a, A-1060 Vienna, Austria

³ Research Area Biochemical Engineering, Institute of Chemical Engineering, Vienna University of Technology, Getreidemarkt 9/166, A-1060 Vienna, Austria

*corresponding author: bernhard.lendl@tuwien.ac.at

ABSTRACT

The performance of a fiber optic and an optical conduit in-line attenuated total reflection (ATR) mid-infrared (mid-IR) probe, respectively, during *in situ* monitoring of a *Penicillium chrysogenum* fermentation were compared. The fiber optic probe was connected to a sealed, portable, Fourier transform (FT-IR) process spectrometer via a plug-and-play interface. The optical conduit, on the other hand, was connected to a FT-IR process spectrometer via a knuckled probe with mirrors that had to be adjusted prior to each fermentation, which were purged with dry air. Penicillin V (PenV) and its precursor phenoxyacetic acid (POX) concentrations were determined by on-line HPLC and the obtained concentrations were used as reference to build Partial Least Squares Regression (PLS-R) models. Cross-validated root-mean-square errors of prediction were found to be 0.2 g L⁻¹ (POX) and 0.19 g L⁻¹ (PenV) for the fiber optic setup and 0.17 g L⁻¹ (both POX and PenV) for the conduit setup. Higher noise-levels and spectrum-to-spectrum variations of the fiber optic setup lead to higher noise of estimated (i.e. unknown) POX and PenV concentrations than was found for the conduit setup. It seems that trade-off has to be made between ease of handling (fiber optic setup) and measurement accuracy (optical conduit setup) when choosing one of these systems for bioprocess monitoring.

Introduction

The potential of Fourier-transform infrared (FT-IR) spectroscopy in the mid-IR range (400 – 4000 cm^{-1}) for bioprocess analysis and monitoring^{1,2} has been shown at-line³⁻⁷, on-line⁸⁻¹⁴ and in-line. With the development of in situ attenuated total reflection (ATR) probes, it has become a valuable process analytical tool (PAT) for in-line monitoring and controlling of bioprocesses^{15,16}. Due to the limited interaction length of a few micrometers of the evanescent field and the sample¹⁷, absorption due to water, which is usually the main constituent of fermentation media, is limited. Thus, quantification of soluble analytes is possible, provided reliable reference analysis for multivariate calibration, e.g. Partial Least Squares Regression^{18,19} (PLS-R), multivariate curve resolution – alternating least squares²⁰ (MCR-ALS), is available.

Two ways of connecting the spectrometer and the ATR element are possible: Light guides and optical fibers. Light guides, or hollow conduits, are based on external reflection of light on metallic or dielectric surfaces and are usually realized as hollow waveguides. For maximum transmittance through the light guide, a high reflectivity of the material, grazing incidence (close to 90°), minimal number of reflections and a highly collimated beam are desirable²¹. For in-line ATR probes, the rigid, straight, light conduits are usually coupled by knuckles equipped with adjustable mirrors so that the probe can be connected to the measurement vessel. Once the physical adjustment is completed, light throughput needs to be maximized by adjusting the mirrors. Any change in positioning of the probe leads to changes in the transmission characteristics and thus will deteriorate the quality of the recorded IR spectra. Therefore, once the setup is aligned, vibrations, which might lead to mechanical resonances in the probe and thus change alignment, and/or moving the setup should be avoided. This can be a problem when employing light conduit probes for in-line (in situ) fermentation monitoring, since vibrations from the stirrer might impair the FT-IR measurement. Nevertheless, they have been successfully used for monitoring of different analytes in bioprocesses: The first application of in situ ATR FT-IR spectroscopy with a conduit probe was reported as early as 1999 by Doak & Phillips²², showing possibility to predict glucose and acetate concentrations from spectra acquired in *E.coli* fermentations. Further applications included mammalian cell cultures^{23,24}, bacterial²⁵⁻²⁸ and yeast²⁹⁻³¹ fermentations.

Within optical fibers, light is transmitted by total internal reflection. Transmission ranges depend on material properties: the lower wavelength limit is determined by electronic absorption (band gap edge), while the higher wavelength limit depends on the multiphonon edge (for details see ³²⁻³⁴). Furthermore, transmission depends on losses due light scattering within the material, impurities, and material defects. The Numerical Aperture (NA) or acceptance angle of the fiber, which in turn depends on the critical angle for total internal reflection, i.e. the ratio of refractive indices of core material (within which the light is guided) and the surrounding medium (often an appropriately chosen cladding layer, or the coating). For fibers with high refractive indices, losses due to reflection at core ends, especially at high incidence angles, have to be taken into account. Therefore, care should be taken when coupling the light in and out of the fiber³⁴. A major advantage of optical fibers is their flexibility, it should however be noted that the more the fiber is bent, i.e. the smaller the bending radius, the lower the transmission. This decrease in transmission is due to the fact that the conditions for internal reflection are fulfilled less and less.

Polychrystalline silver halide (AgX) is currently the most commonly used fiber optic material for FT-IR spectroscopy probes. This is because the fingerprint region ($1500 - 900 \text{ cm}^{-1}$) is accessible (transmission ranges from 2500 to 625 cm^{-1})³³. To avoid excessive bending or breaking of the relatively soft and brittle material, commercial probes are usually constructed such that they cannot be bent beyond a certain radius. Very little work on bioprocess monitoring using fiber optic ATR probes has been published: Fayolle et al.³⁵ used a fiber-optic probe to monitor glucose in a bacterial fermentation and we have recently reported the monitoring of precursor and product in a fungal fermentation using PLS-R and MCR-ALS³⁶. We could furthermore show the possibility to not only access information on analytes in solution, but also on the microorganisms themselves with the aid of ultrasonic standing waves³⁷. Foley et al.³⁸ presented a feasibility study for monitoring mammalian cell culture medium components by in-line ATR FT-IR spectroscopy in which they used a fiber-optic and a conduit ATR probe to acquire spectra of single analyte solutions, multilevel mixtures, and spiked culture medium samples off-line. They concluded that the conduit probe was the more accurate one for their experimental setup and that ammonia and glucose could be monitored using both probes.

Here, we want to present a comparison of the performance of a fiber-optic probe connected to a sealed process spectrometer, with a more sophisticated, dry air flushed, process spectrometer, equipped with a conduit probe for in-line bioprocess monitoring. Both setups

were coupled to the same bioreactor and four *P. chrysogenum* fermentations were conducted during which product (phenoxymethylpenicillin or penicillin V, hereafter PenV) and its precursor (phenoxyacetic acid, hereafter POX) were monitored by FT-IR spectroscopy in combination with PLS-R and on-line HPLC. Advantages and potential disadvantages of the respective ATR FT-IR setups will be discussed.

MATERIALS AND METHODS

In-line ATR FT-IR spectrometers

Two setups were used for acquisition of FT-IR spectra in-line: The sealed, portable process spectrometer ReactIR 15 equipped with the in-line fiber optic ATR-probe DS D1comp AgX (silver halide) 9.5 mm (hereafter: RIR15) and the process spectrometer ReactIR 45 connected to K4 conduit probe, a four knuckle, rigid, mirrored conduit, equipped with an in-line diamond ATR sentinel probe head (hereafter: RIR45) (all Mettler Toledo, Switzerland). The mirrors of the conduit are adjustable by three screws to optimize light transmission in different conduit positions; this was done before each fermentation once the probe and spectrometer were in final position. The RIR45 (spectrometer and probe) was constantly purged with dry air at a flow rate of at least 15 liters per hour (purge generator: Parker Balston 75-45, Parker Hannifin USA). Spectra were recorded from 2800 – 800 cm^{-1} (RIR15) and 4000 – 650 cm^{-1} (RIR45) with a resolution of 8 cm^{-1} and each averaged over 256 scans. The dedicated softwares iC IR 4.2 (RIR15) and iC IR 4.02 (RIR45) (both Mettler Toledo), respectively, were used for recording and basic manipulation of data, e.g. single point baseline corrections. Spectra of single analyte standards of POX (99%, Sigma Aldrich, USA) and PenV (pencillin V potassium, kindly provided by Sandoz AG) in 20 mM phosphate buffer (pH 6.5) were recorded with the RIR15.

P. chrysogenum cultivations

Four fed-batch fermentations of *P. chrysogenum* (strain BCB1, kindly provided by Sandoz AG) were carried out in a 15-L autoclavable, fully automated and controlled stirred bioreactor (Infors, Switzerland) coupled to the integrated process control and management system Lucullus (Biospectra AG, Switzerland). Media compositions were as described previously in³⁹, the process was adapted to the larger bioreactor employed in this study and POX addition was performed as described below. Both, the RIR15 and the RIR45 were coupled to the bioreactor through 25 mm Ingold ports (**Figure 1**).

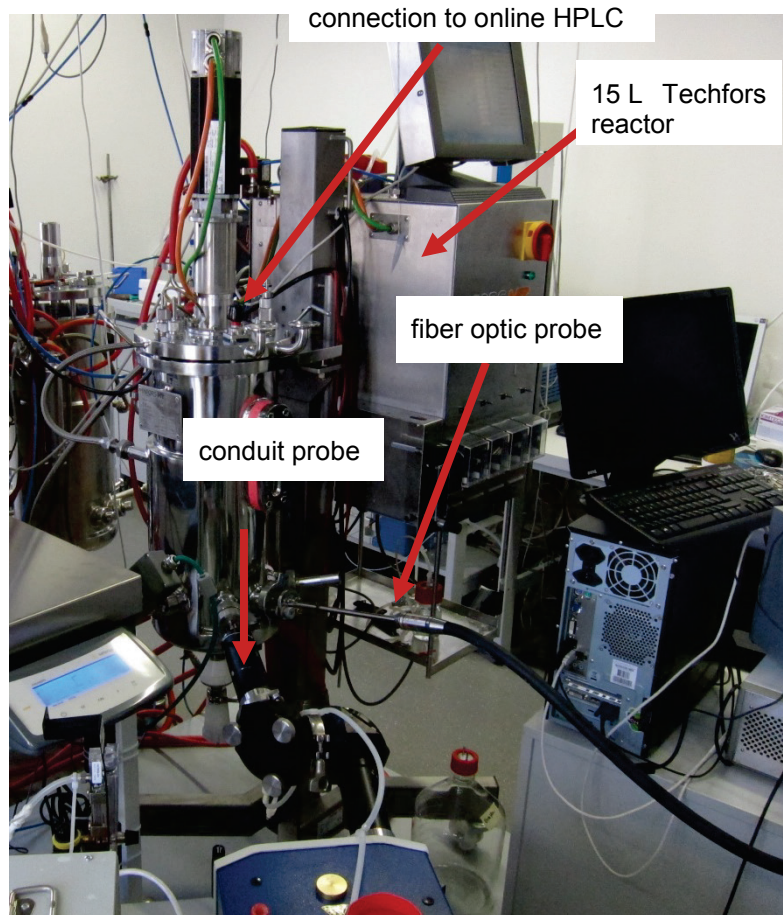


Figure 1: The bioreactor setup.

On-line reference analysis

POX and PenV concentrations were determined by isocratic HPLC using a ZORBAX C-18 column (Agilent Technologies, USA) and 28% acetonitrile, 6 mM H_3PO_4 , 5 mM KH_2PO_4 as elution buffer. On-line coupling of the HPLC to the bioreactor and sampling was realized as described in³⁶. In short it consisted of 2 parts: a ceramic filter (iba e.V. Heiligenstadt, Germany) through which cell-free culture medium was sampled at constant flow with a peristaltic pump and a flow-through cell from which samples were drawn for HPLC analysis.

Characterization of system performance

For comparison of the performances of the two setups of 100% line were recorded with both setups with the probes coupled to the medium-filled bioreactor after autoclavation.

The root-mean-square (RMS) and peak-to-peak (PP) noise of the 100% lines were calculated using OPUS 7.2 (Bruker Optics, Germany) as:

$$RMS\ Noise = \sqrt{\frac{\sum_{i=1}^N (y_i - y_{iFit})^2}{N}} \quad (1)$$

where y_{iFit} is a straight line fitted to the data and y_i the 100% line for each datapoint i in the selected wavenumber region, while the PP noise is the difference of the absolute maximum and absolute minimum absorption value. Here, the RMS and PP noise were calculated between 1200 and 1400 cm^{-1} .

Partial least squares (PLS) regression

For each setup, the three spectra acquired closest to the on-line HPLC sampling times were averaged and used for modelling. Derivatives using the Savitzky-Golay algorithm⁴⁰ were calculated in Matlab (USA) using the `savgol` function (PLS toolbox, Eigenvector Research, USA) and PLS-R models developed and applied in DataLab⁴¹ (Epina Software Labs, Austria). First derivative (2nd order, filter width 11) and mean centering gave the best results and were therefore used in all models. Cross-validation was done by random subsets, either using 15 (approx. 10% of complete sample) or 40 samples as cross-validation group and calculating 20 iterations. The root-mean-square error of prediction (RMSEP), in this case also referred to as the root-mean-square error of cross-validation (RMSECV), was calculated as

$$RMSEP = \sqrt{\frac{\sum_{i=1}^N (y_i - \hat{y}_i)^2}{N}} \quad (2)$$

where y_i are the HPLC reference data and \hat{y}_i the values predicted by PLS for each iteration. The RMSEP was used as a parameter to estimate the quality of the model.

RESULTS AND DISCUSSION

System performance

The single beam spectra of the two setups recorded in-line in fed-batch medium (**Figure 2** left) show the differences in light throughput: The conduit probe transmits light over a broad range of wavenumbers and in combination with the used spectrometer covers between 600 – 4000 cm^{-1} , while the fiber optic probe has an upper limit of about 2500 cm^{-1} . Due to the absorption of the diamond ATR element, both single beam spectra show very low intensities between 1950 and 2200 cm^{-1} . The dip around 1640 cm^{-1} is due to the strong

IR absorption of the ν_2 -vibration (bending) of H_2O . For the RIR45, the intensities in the spectral region where the POX/PenV absorption bands are located are higher than for the RIR15. Performance of the system was investigated by recording 100%-lines, i.e. recording a background and a sample without changing the conditions in the light path (no sample applied, same spectrometer settings, etc.). Thus, the noise of the measurement system due to e.g. physical limitations of detectivity, instabilities of the globar, etc., can be assessed. The 100%-lines (**Figure 2** right) indicate that the noise level of the RIR15 is higher than that of the RIR45. In the spectral region of greatest interest for the quantification of PenV/POX, i.e. 1400 to 1200 cm^{-1} , the RMS and PP noise, respectively, are approximately a factor 2 higher for the RIR15 than the RIR45 (**Table I**).

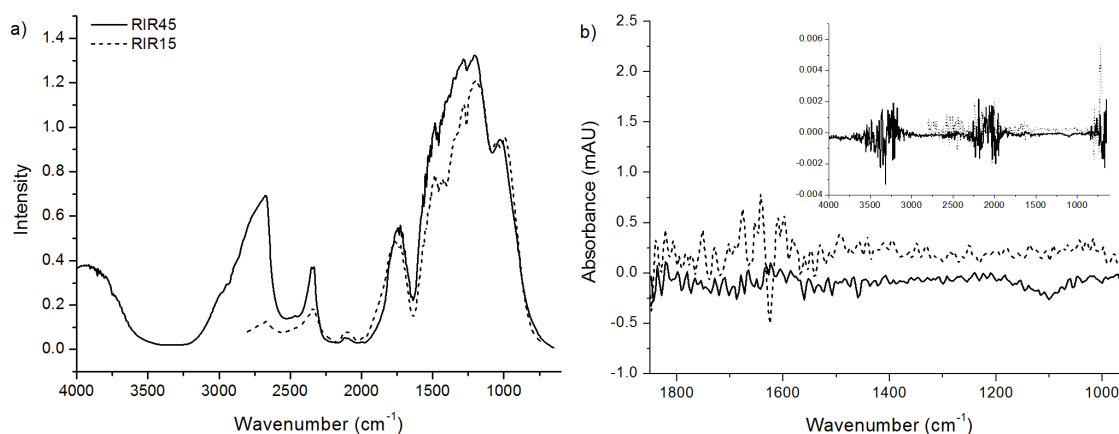


Figure 2: a) Single beam spectra of the two spectrometer systems recorded in fed-batch medium. The wavenumber region that can be accessed with the RIR15 (dashed line) is limited to 800 to 1950 cm^{-1} by transmittance of the AgX fiber. b) The 100% lines of the RIR45 and the RIR15 in the wavenumber region accessible for calibration. The inset shows the 100% percent lines in the respective wavenumber regions covered by each setup.

Table I: The RMS noise and the PP noise calculated between 1200 and 1400 cm^{-1} of the ReactIR 15 and the React IR 45, respectively, found when the probes were in position for measurement in the bioreactor. The 100% lines for calculation were acquired in fed-batch medium.

Setup	RMS Noise (AU)	PP Noise (AU)
RIR15	$5.34 \cdot 10^{-5}$	$23.2 \cdot 10^{-5}$
RIR45	$2.71 \cdot 10^{-5}$	$11.4 \cdot 10^{-5}$

PLS-R models

To gain insight into which wavenumber regions might be of interest for building the PLS-R models, single analyte spectra of POX and PenV were recorded. The absorption bands of POX and PenV (**Figure 3**) are overlapping in large parts of the recorded spectra. Some bands, however, are unique to one of the analytes (e.g. C=O carbonyl band at 1760 cm^{-1} for PenV) and relative intensities are different.

As the on-line HPLC samples were drawn from a flow-through-cell, a clear attribution to a single spectrum could not be made; therefore, average spectra of the three spectra acquired closest to the HPLC sampling time were calculated and used. Another difficulty in assignment of the respective HPLC reference concentrations to the correct spectra was the sampling delay (approx. 90 min) due to the physical distance between the fermenter and the HPLC.

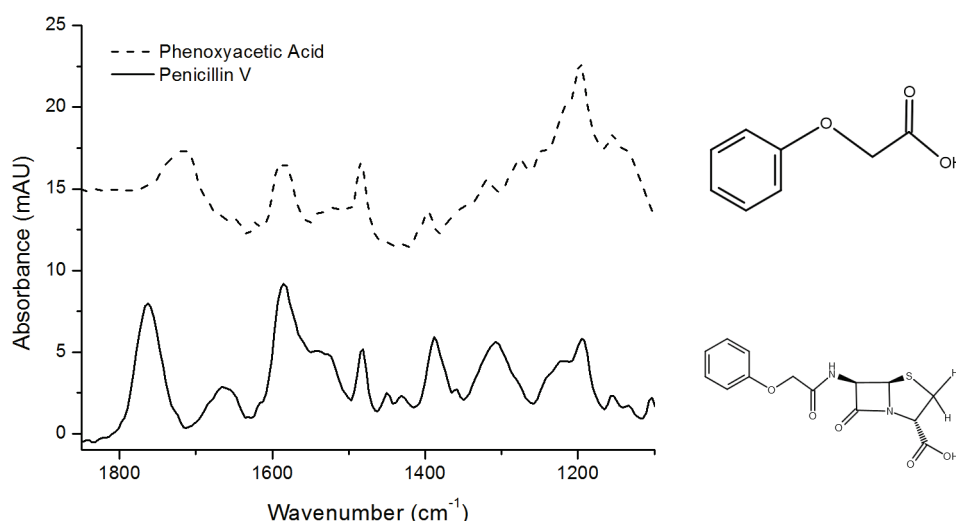


Figure 3: ATR spectra of POX and PenV recorded with the RIR15 (offset 15 mAU for clarity) and their molecular structures.

PLS-R models for POX

PLS-R models of POX were built for both spectrometer setups using results from on-line HPLC measurements as reference values. Two HPLC outliers were identified (unusually high Q-residuals and subsequent plausibility check of value) and thus omitted. The CV-predicted POX concentrations obtained with the RIR15 PLS-model (**Figure 4 a**) deviate more from the HPLC reference values than the ones from RIR45 PLS-model. This is especially true for higher concentration values. In the low concentration range (below approx. 1 g L^{-1}) both models fail to predict accurately. During fermentation B (open circles)

no PenV was produced due to an error in pH control during the early phase of the fed-batch process. In the score plot of PC1 vs. PC2 this deviation from standard conditions is clearly visible for both spectrometers (data not shown). The POX concentrations of fermentation B are more accurately predicted by the RIR45 PLS-model than the RIR15 PLS-model, as is reflected by the RMSEP for this fermentation (0.21 g L⁻¹ for the RIR45 vs. 0.32 g L⁻¹ for the RIR15).

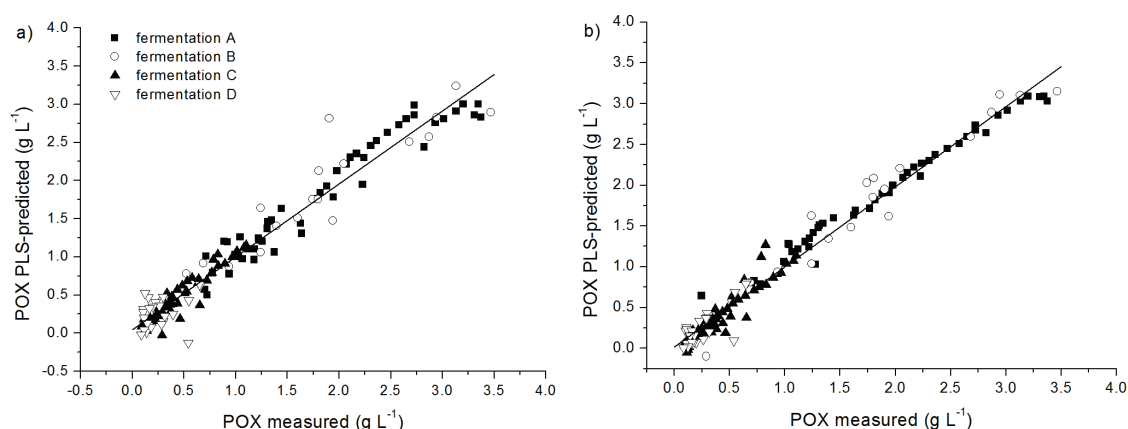


Figure 4: POX concentration measured by on-line HPLC vs. POX concentration predicted by PLS-R from ATR spectra acquired with the RIR15 (a) and RIR45 (b).

Table II: Parameters of POX PLS-R models.

Setup	Wavenumber region (cm ⁻¹)	R ² CV	LV	RMSEP 15 (g L ⁻¹)	RMSEP 40 (g L ⁻¹)
RIR15	1818-1747 & 1423-1188	0.96	6	0.15 +/- 0.01	0.20 +/- 0.01
RIR45	1818-1747 & 1422-1187	0.98	6	0.16 +/- 0.01	0.17 +/- 0.1

PSL-R models for PenV

PLS-R model for PenV were built for both setups from spectra obtained during fermentations A, C, and D. Spectra from fermentation B were omitted, since no PenV production took place due to a fault in the pH regulation early during the fermentation. During fermentation A, water vapor levels inside RIR45 varied over the course of the fermentation due to faults in the pressurized air supply of the purge air generator. To avoid the influence of this (a-normal) variation in the data, the wavenumber region chosen was slightly narrower in the lower wavenumber region than for the POX models (**Table III**),

where these data are not as prominent as spectra from fermentation B were included. The PLS-R models have very similar performances for both spectrometers (**Table III**) and are in the same error range as the POX PLS-R models, even though only 5 latent variables were used (compared to 6 for POX). The lower number of latent variables necessary to model PenV concentrations could be due to the experimental design leading to a wider range of PenV-concentrations.

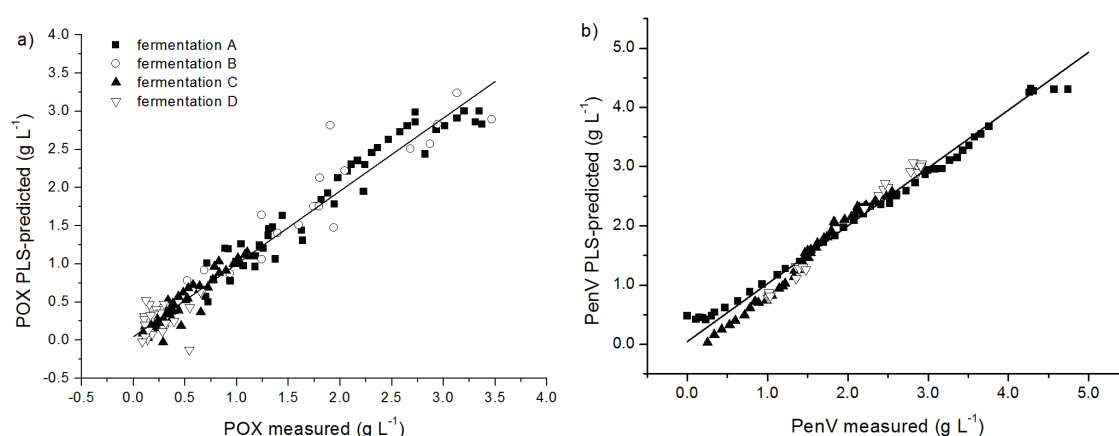


Figure 5: PenV concentration measured by on-line HPLC vs. PenV concentration predicted by PLS-R from ATR spectra acquired with the RIR15 (a) and RIR45 (b).

Table III: Parameters of PenV PLS-R models.

Setup	Wavenumber region (cm ⁻¹)	R ² CV	LV	RMSEP 15 (g L ⁻¹)	RMSEP 40 (g L ⁻¹)
RIR15	1818-1747 & 1352-1185	0.98	5	0.18 +/- 0.01	0.19 +/- 0.01
RIR45	1818-1747 & 1351-1183	0.98	5	0.16 +/- 0.00	0.17 +/- 0.01

Prediction of POX and PenV

The developed PLS-R models were subsequently used to predict POX and PenV from spectra obtained during fermentation C (**Figure 6**). The high spectrum-to-spectrum stability of the RIR45 is reflected by lower variations in the estimated POX and PenV concentrations compared to those obtained from RIR15 spectra. The concentration values measured by HPLC during the application of a POX pulse at $t = 155$ h are a lot higher than the ones estimated by both PLS models and, when compared to the scale signal readings, have to be regarded as outliers. It was hypothesized that the high biomass content at this

point of the fermentation lead to a slower distribution of POX in the vessel and thus the local concentration around the filter probe was higher than the true average concentration.

A shift towards lower estimated concentrations of both POX and PenV for the RIR15 was observed at $t = 135$ h. Visual inspection of the spectra acquired around this process time gave no conclusive explanation on why this shift occurs. For this fermentation, the RIR15 PLS-model for POX slightly overestimates the measured concentration, especially for process times smaller than 135 h, i.e. before the shift had occurred. PenV, on the other hand, is underestimated from this point in the fermentation. The POX concentration estimated with the RIR45 PLS-model is in good agreement with the HPLC reference values for process times smaller than 145 h; after that the difference between the HPLC-determined and the PLS-estimated concentrations gradually increases until it reaches 0.2 g L^{-1} at $t = 152$ h and remains constant after that. The PenV concentration estimated by the RIR45 PLS-model starts to deviate from the HPLC values earlier in process (i.e. at $t = 136$ h) than the estimated POX concentration; it is subsequently overestimated.

Topping up of liquid nitrogen to cool the detectors (times indicated by gray dashed lines in **Figure 6**) generally did not have a great influence on the estimated values, with the exception of RIR15-estimated POX concentrations during the second top up. Here, a temporary decrease in estimated concentration was observed.

The strong cross-correlation of POX and PenV concentrations and of their spectroscopic signatures is obvious for both spectrometers: For the RIR45 PenV is slightly overestimated when POX is very accurately predicted, and starts to be overestimated when POX is underestimated. This is, with certain limitations, also true for the RIR15 models (albeit the other way around; here PenV is underestimated when POX is accurately predicted). When comparing the sums of PLS-estimated and HPLC-measured POX and PenV concentrations for each time point, the RIR45-estimated sums correlate better with the HPLC-measured sums than the RIR15-estimated ones (data not shown).

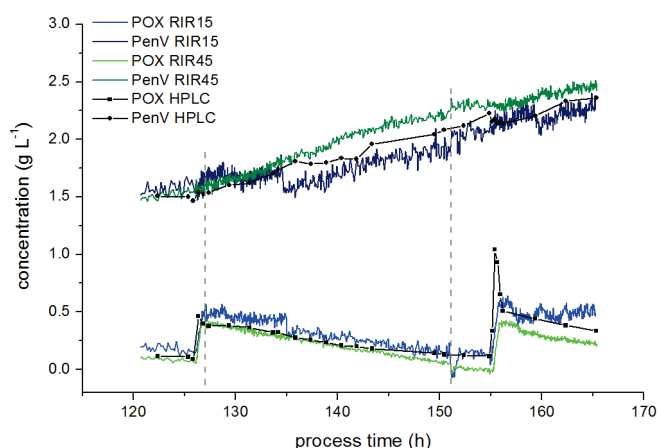


Figure 6: POX (black squares) and PenV (black circles) on-line HPLC measurements obtained during fermentation C and the values estimated by the PLS-R models (RIR15 blue lines, RIR45 green lines). The grey dashed lines indicate the times when the detectors were topped up liquid nitrogen.

CONCLUSIONS

The two setups used in this study, the portable process spectrometer RIR15 equipped with a fiber optic ATR probe and a larger process spectrometer RIR45 equipped with a optical conduit probe, were both successfully used for acquisition of FT-IR spectra in-line during fermentation of *P. chrysogenum*. From these spectra and reference values obtained by online HPLC, PLS-R models for the determination of PenV and its precursor POX were built. The overall performance of the RIR45 was better than that of the RIR15, i.e. lower noise-levels and slightly lower RMSEP were found. As PLS-R is a method that identifies variations in the data that correlate with changes of the given reference data and thus intrinsically filters out random noise, the RMSEP of the RIR15 models, i.e. the ability to accurately estimate unknown concentrations, do not greatly suffer from the higher noise level. Both spectrometers were able to estimate the trends of POX and PenV concentrations during a fermentation within satisfactory limits. The RIR15-estimated concentrations vary more greatly from spectrum to spectrum than the RIR45 ones for both, PenV and POX, here either averaging over more scans (during spectrum acquisition), averaging over a few spectra for concentration estimation or calculation of the moving average of the estimated values could help to decrease the noise.

Overall, both spectrometers and probes were suitable for the estimation of POX and PenV concentrations within approximately $\pm 0.2 \text{ g L}^{-1}$ of HPLC reference during a sample fermentation, with the RIR45 delivering better results. When selecting one of the systems

for bioprocess monitoring, a trade-off has to be made between ease of installation and maintenance (i.e. dry air purging), and measurement accuracy and prize.

ACKNOWLEDGEMENTS

The authors want to thank Simona Capone and Nouredine Ben Abdallah for their support with laboratory work and Hans Lohninger for fruitful discussions about chemometrics. Sandoz AG is thankfully acknowledged for providing partial financial support and the microorganism. Partial financial support from the Austrian Science Fund FWF (project: P24154-N17) is thankfully acknowledged.

References:

1. D. Landgrebe, C. Haake, T. Höpfner, S. Beutel, B. Hitzmann, T. Scheper, et al. "On-line infrared spectroscopy for bioprocess monitoring." *Appl. Microbiol. Biotechnol.* 2010. 88(1): 11–22. 10.1007/s00253-010-2743-8.
2. N.D. Lourenço, J. a Lopes, C.F. Almeida, M.C. Sarraçuça, H.M. Pinheiro. "Bioreactor monitoring with spectroscopy and chemometrics: a review." *Anal. Bioanal. Chem.* 2012. 404(4): 1211–37. 10.1007/s00216-012-6073-9.
3. S. Sivakesava, J. Irudayaraj, D. Ali. "Simultaneous determination of multiple components in lactic acid fermentation using FT-MIR, NIR, and FT-Raman spectroscopic techniques." *Process Biochem.* 2001. 37(4): 371–378. 10.1016/S0032-9592(01)00223-0.
4. V.G. Franco, J.C. Perín, V.E. Mantovani, H.C. Goicoechea. "Monitoring substrate and products in a bioprocess with FTIR spectroscopy coupled to artificial neural networks enhanced with a genetic-algorithm-based method for wavelength selection." *Talanta.* 2006. 68(3): 1005–12. 10.1016/j.talanta.2005.07.003.
5. P. Roychoudhury, L.M. Harvey, B. McNeil. "The potential of mid infrared spectroscopy (MIRS) for real time bioprocess monitoring." *Anal. Chim. Acta.* 2006. 571(2): 159–66. 10.1016/j.aca.2006.04.086.
6. P. Roychoudhury, B. McNeil, L.M. Harvey. "Simultaneous determination of glycerol and clavulanic acid in an antibiotic bioprocess using attenuated total reflectance mid infrared spectroscopy." *Anal. Chim. Acta.* 2007. 585(2): 246–52. 10.1016/j.aca.2006.12.051.
7. P. Roychoudhury, L.M. Harvey, B. McNeil. "At-line monitoring of ammonium, glucose, methyl oleate and biomass in a complex antibiotic fermentation process using attenuated total reflectance-mid-infrared (ATR-MIR) spectroscopy." *Anal. Chim. Acta.* 2006. 561(1-2): 218–224. 10.1016/j.aca.2006.01.037.

8. M. Kansiz, J.R. Gapes, D. McNaughton, B. Lendl, K.C. Schuster. "Mid-infrared spectroscopy coupled to sequential injection analysis for the on-line monitoring of the acetone-butanol fermentation process." *Anal. Chim. Acta*. 2001. 438(1-2): 175–186. 10.1016/S0003-2670(01)00919-9.
9. G. Mazarevica, J. Diewok, J.R. Baena, E. Rosenberg, B. Lendl. "On-line fermentation monitoring by mid-infrared spectroscopy." *Appl. Spectrosc.* 2004. 58(7): 804–10. 10.1366/0003702041389229.
10. J. Schnöller, B. Lendl. A portable FTIR-ATR process analyzer-online fermentation control. *Proceedings of IEEE Sensors*, 2004. IEEE. 2004. 742–745.
11. M. Kansiz, K. Christian Schuster, D. McNaughton, B. Lendl, K.C. Schuster. "Sequential Injection/Mid-Infrared Spectroscopic Analysis of an Acetone-Butanol-Ethanol Fermentation: Analyte Cross-Correlation Effects." *Spectrosc. Lett.* 2005. 38(6): 677–702. 10.1080/00387010500315801.
12. J. Schenk, I.W. Marison, U. von Stockar. "A simple method to monitor and control methanol feeding of *Pichia pastoris* fermentations using mid-IR spectroscopy." *J. Biotechnol.* 2007. 128(2): 344–53. 10.1016/j.jbiotec.2006.09.015.
13. J. Schenk, C. Viscasillas, I.W. Marison, U. von Stockar. "On-line monitoring of nine different batch cultures of *E. coli* by mid-infrared spectroscopy, using a single spectra library for calibration." *J. Biotechnol.* 2008. 134: 93–102. 10.1016/j.jbiotec.2007.12.014.
14. J. Schenk, I.W. Marison, U. von Stockar. "pH prediction and control in bioprocesses using mid-infrared spectroscopy." *Biotechnol. Bioeng.* 2008. 100(1): 82–93. 10.1002/bit.21719.
15. S. Beutel, S. Henkel. "In situ sensor techniques in modern bioprocess monitoring." *Appl. Microbiol. Biotechnol.* 2011. 91(6): 1493–505. 10.1007/s00253-011-3470-5.
16. I. Marison, S. Hennessy, R. Foley, M. Schuler, S. Sivaprakasam, B. Freeland. "The Choice of Suitable Online Analytical Techniques and Data Processing for Monitoring of Bioprocesses." *Advances in Biochemical Engineering/Biotechnology*. 2013. Pp. 249–280. 10.1007/10.
17. P.R. Griffiths, J.A. de Haseth. "Attenuated Total Reflection." *Fourier Transform Infrared Spectrometry Second Edition*. 2007. Pp. 321–348.
18. P. Geladi, B.R. Kowalski. "Partial least-squares regression: a tutorial." *Anal. Chim. Acta*. 1986. 186: 1–17.
19. S. Wold, M. Sjöström, L. Eriksson. "PLS-regression : a basic tool of chemometrics." *Chemom. Intell. Lab. Syst.* 2001. 58: 109–130.

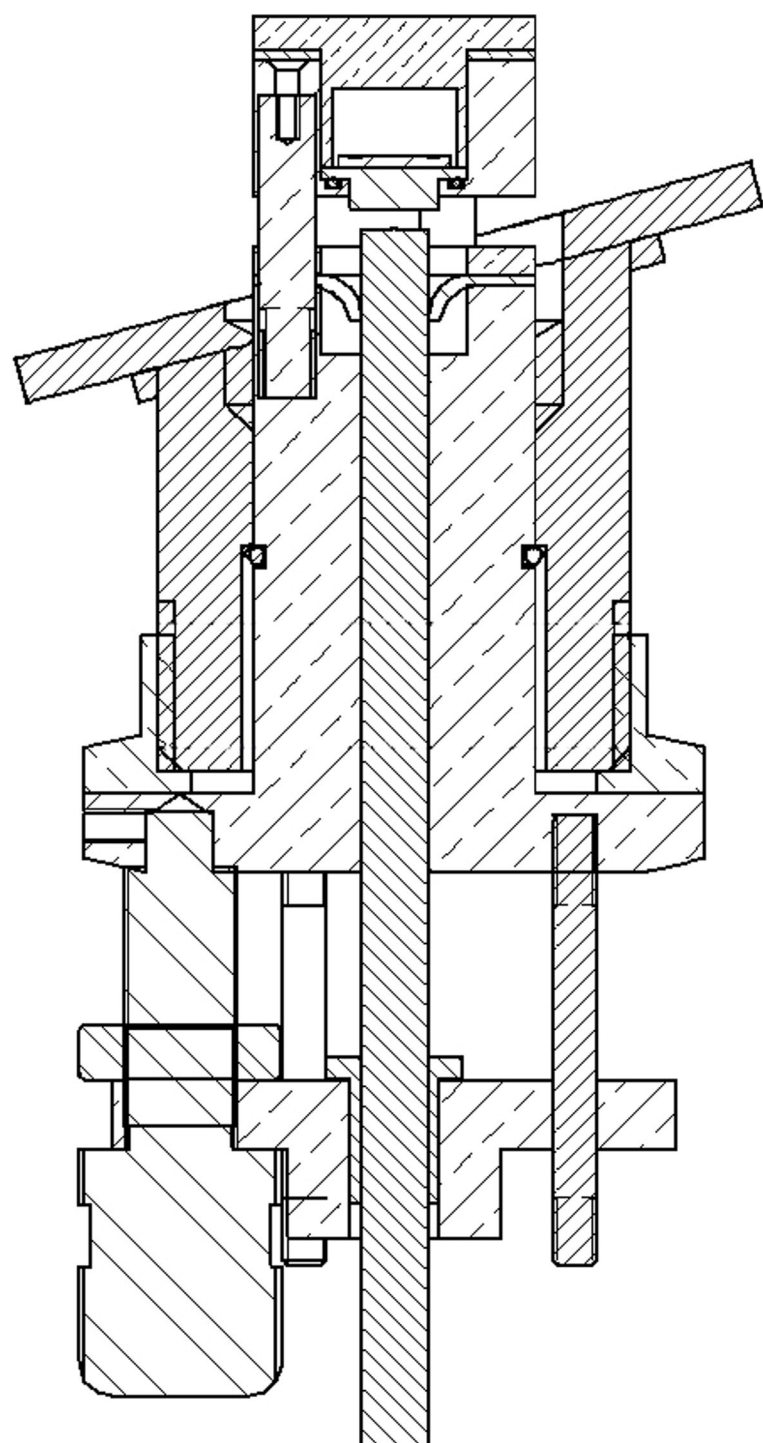
20. R. Tauler. "Multivariate curve resolution applied to second order data." *Chemom. Intell. Lab. Syst.* 1995. 30(1): 133–146.
21. W.M. Doyle. "Hollow Optical Conduits for Vibrational Spectroscopy." *Handbook of Vibrational Spectroscopy Vol. 2.* 2nd Editio. Wiley & Sons Ltd, 2006. Pp. 1–7.
22. D.L. Doak, J.A. Phillips. "In Situ Monitoring of an Escherichia coli Fermentation Using a Diamond Composition ATR Probe and Mid-infrared Spectroscopy." *Biotechnol. Prog.* 1999. 15: 529–539.
23. M.H. Rhiel, M.I. Amrhein, I.W. Marison, U. von Stockar. "The influence of correlated calibration samples on the prediction performance of multivariate models based on mid-infrared spectra of animal cell cultures." *Anal. Chem.* 2002. 74(20): 5227–36.
24. M. Rhiel, P. Ducommun, I. Bolzonella, I. Marison, U. Von Stockar. "Real-Time In Situ Monitoring of Freely Suspended and Immobilized Cell Cultures Based on Mid-Infrared Spectroscopic Measurements." *Biotechnol. Bioeng.* 2002. 77: 174–185. 10.1002/bit.10134.
25. H. Kornmann, S. Valentinotti, P. Duboc, I. Marison, U. von Stockar. "Monitoring and control of Gluconacetobacter xylinus fed-batch cultures using in situ mid-IR spectroscopy." *J. Biotechnol.* 2004. 113(1-3): 231–45. 10.1016/j.jbiotec.2004.03.029.
26. H. Kornmann, M. Rhiel, C. Cannizzaro, I. Marison, U. von Stockar. "Methodology for real-time, multianalyte monitoring of fermentations using an in-situ mid-infrared sensor." *Biotechnol. Bioeng.* 2003. 82(6): 702–9. 10.1002/bit.10618.
27. J. Dahlbacka, K. Kiviharju, T. Eerikäinen, K. Fagervik. "Monitoring of Streptomyces peucetius cultivations using FTIR/ATR spectroscopy and quantitative models based on library type data." *Biotechnol. Lett.* 2013. 35(3): 337–43. 10.1007/s10529-012-1093-2.
28. P. Sagmeister, T. Langemann, P. Wechselberger, A. Meitz, C. Herwig. "A dynamic method for the investigation of induced state metabolic capacities as a function of temperature." *Microb. Cell Fact. Microbial Cell Factories*, 2013. 12(1): 94. 10.1186/1475-2859-12-94.
29. J. Schenk, I.W. Marison, U. von Stockar. "Simplified Fourier-transform mid-infrared spectroscopy calibration based on a spectra library for the on-line monitoring of bioprocesses." *Anal. Chim. Acta.* 2007. 591: 132–140. 10.1016/j.aca.2007.03.056.
30. M. Dabros, M.I. Amrhein, D. Bonvin, I.W. Marison, U. von Stockar. "Data Reconciliation of Concentration Estimates from Mid-Infrared and Dielectric Spectral Measurements for Improved On-Line Monitoring of Bioprocesses." *Biotechnol. Prog.* 2009. 25(2): 578–588. 10.1021/bp.143.

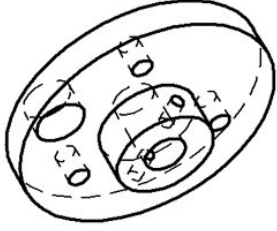
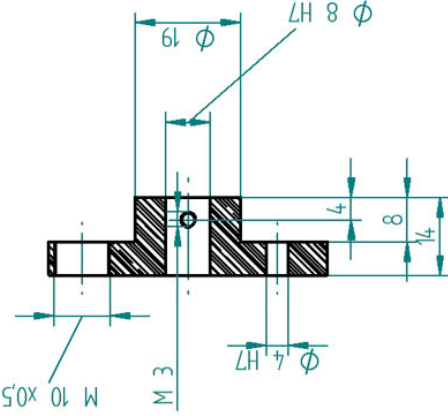
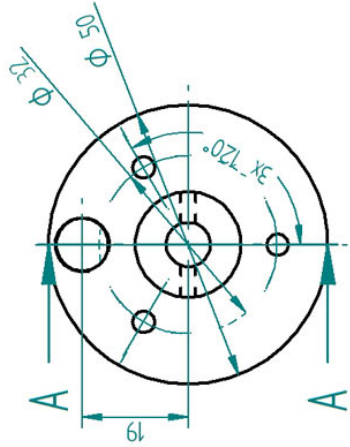
31. J. Dahlbacka, J. Weegar, N. von Weymarn, K. Fagervik. "On-line measurement of the substrate concentrations in *Pichia pastoris* fermentations using FT-IR/ATR." *Biotechnol. Lett.* 2012. 34(6): 1009–17. 10.1007/s10529-012-0868-9.
32. J. Sanghera, I.D. Aggarwal. *Infrared Fiber Optics*. CRC Press, 1998. 368.
33. I.R. Lewis, S.S. Rosenblum. "General Introduction to Fiber Optics." In: J. Chalmers, P.R. Griffiths, editors. *Handbook of Vibrational Spectroscopy*. John Wiley & Sons, Inc, 2002. Pp. 1–8. DOI: 10.1002/0470027320.
34. B. Lendl, B. Mizaikoff. "Optical Fibers for Mid-infrared Spectrometry." In: J. Chalmers, P.R. Griffiths, editors. *Handbook of Vibrational Spectroscopy*. John Wiley & Sons, Inc, 2002. Pp. 1–10. 10.1002/0470027320.
35. P. Fayolle, D. Picque, G. Corrieu. "On-line monitoring of fermentation processes by a new remote dispersive middle-infrared spectrometer." *Food Control*. 2000. 11(4): 291–296. 10.1016/S0956-7135(99)00105-X.
36. C. Koch, A.E. Posch, H.C. Goicoechea, C. Herwig, B. Lendl. "Multi-analyte quantification in bioprocesses by Fourier-transform-infrared spectroscopy by partial least squares regression and multivariate curve resolution." *Anal. Chim. Acta*. Elsevier B.V., 2014. 807: 103–10. 10.1016/j.aca.2013.10.042.
37. C. Koch, M. Brandstetter, P. Wechselberger, B. Lorantfy, M.R. Plata, S. Radel, et al. "Ultrasound Enhanced Attenuated Total Reflection Mid-Infrared Spectroscopy In-line Probe – Acquisition of Cell Spectra in a Bioreactor Ultrasound Enhanced Attenuated Total Reflection Mid-Infrared Spectroscopy In-line Probe – Acquisition of Cell Spectra in." *Anal. C.* 2015. just accep. 10.1021/ac504126v.
38. R. Foley, S. Hennessy, I.W. Marison. "Potential of Mid-Infrared Spectroscopy for On-Line Monitoring of Mammalian Cell Culture Medium Components." *Appl. Spectrosc.* 2012. 66(1): 33–39. 10.1366/11-06395.
39. A.E. Posch, C. Koch, M. Helmelt, M. Marchetti-Deschmann, K. Macfelda, B. Lendl, et al. "Combining light microscopy, dielectric spectroscopy, MALDI intact cell mass spectrometry, FTIR spectromicroscopy and multivariate data mining for morphological and physiological bioprocess characterization of filamentous organisms." *Fungal Genet. Biol.* Elsevier Inc., 2013. 51: 1–11. 10.1016/j.fgb.2012.11.008.
40. A. Savitzky, M.J.E. Golay. "Smoothing and Differentiation of Data by Simplified Least Squares Procedures." *Anal. Chem.* 1964. 36(8): 1627–1639.
41. H. Lohninger. "DataLab." Epina Software Labs. n.d. <http://datalab.epina.at/> [Dec 15 2014].

9 APPENDIX

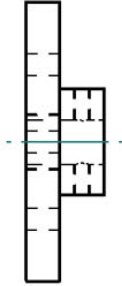
Appendix A

Engineering drawings Prototype 1 – reprinted with permission from Bauer 2009¹³⁵.





Schnitt A-A



1 Stk.

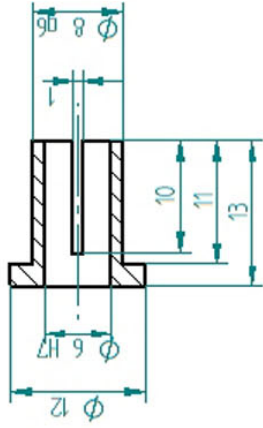
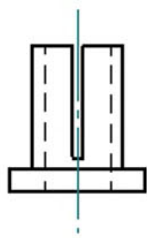
	NAME	DATE	<div>SOLID EDGE</div> <div>UGS - The PLM Company</div> <div>TITLE</div> <div>vordere Scheibe</div> <div>SIZEA4</div> <div>DWG NO</div> <div>REV</div> <div>FILE NAME: Scheibe Vornedft</div> <div>SCALE: 1:1</div> <div>WEIGHT:</div> <div>SHEET 1 OF 1</div>
DRAWN	valker	01/11/09	
CHECKED			
ENG APPR			
MGR APPR			

UNLESS OTHERWISE SPECIFIED

DIMENSIONS ARE IN MILLIMETERS

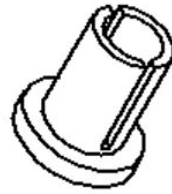
ANGLES ±XX°

2 PL ±XXX 3 PL ±XXXX



Schnitt A-A

1stk.



4

Schnitt A-A

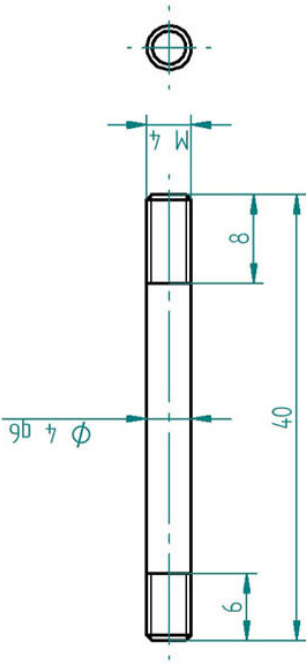
REVISION HISTORY		DATE	APPROVED
REV	DESCRIPTION		

DRAWN	NAME	DATE	SOLID EDGE
CHECKED	volker	01/11/09	UGS - The PLM Company
ENG APPR			TITLE
MGR APPR			geschützte Klemmhülse

UNLESS OTHERWISE SPECIFIED DIMENSIONS ARE IN MILLIMETERS ANGLES ±XX° 2 PL ±XXX 3 PL ±XXXX	SIZE	DWG NO	REV	FILE NAME klemmschale.dft
	A4			SCALE: 2:1 WEIGHT: SHEET 1 OF 1

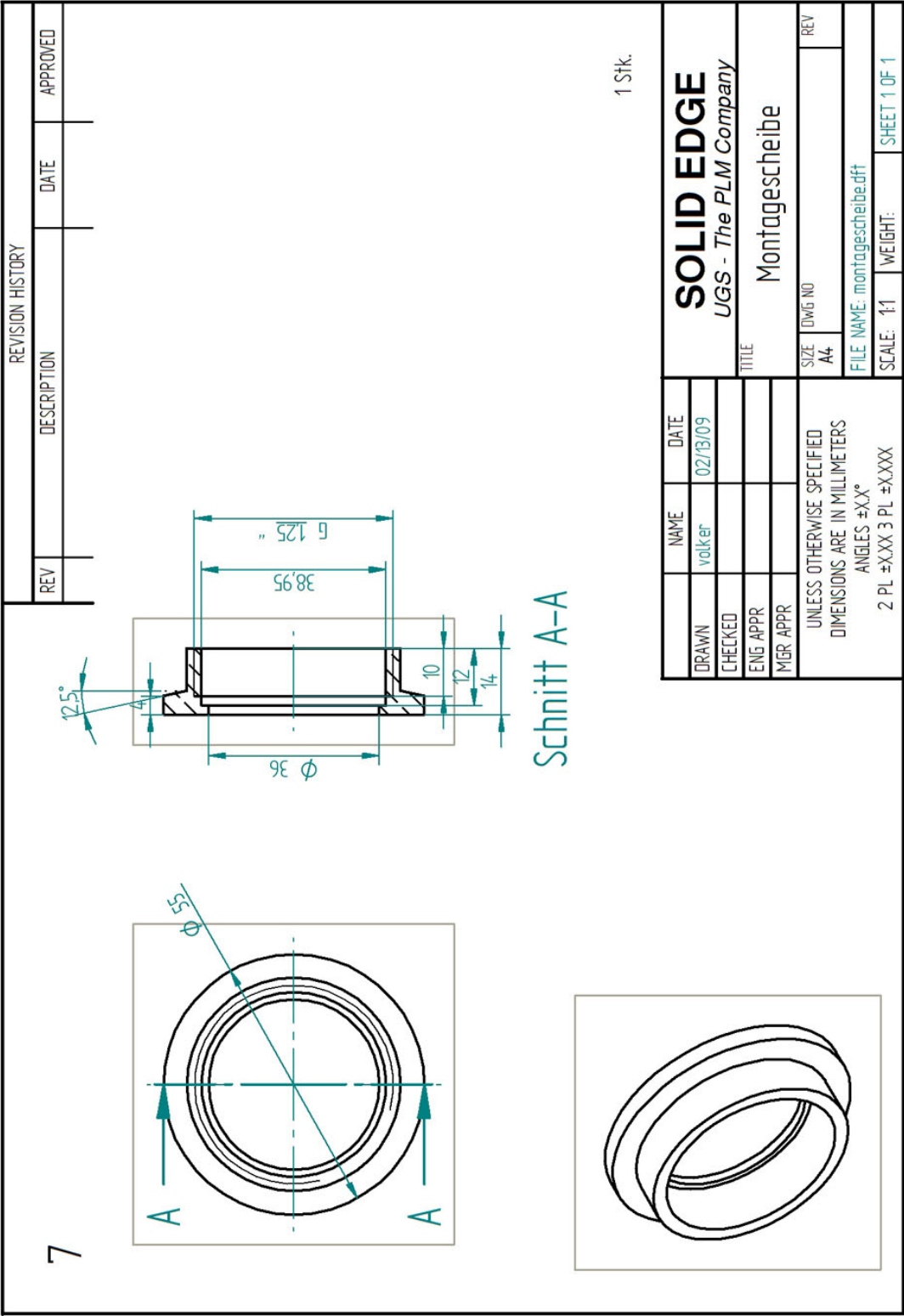
5

REVISION HISTORY			
REV	DESCRIPTION	DATE	APPROVED

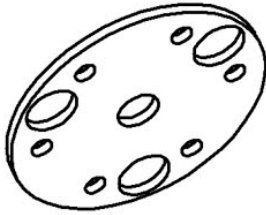
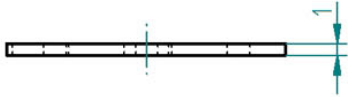
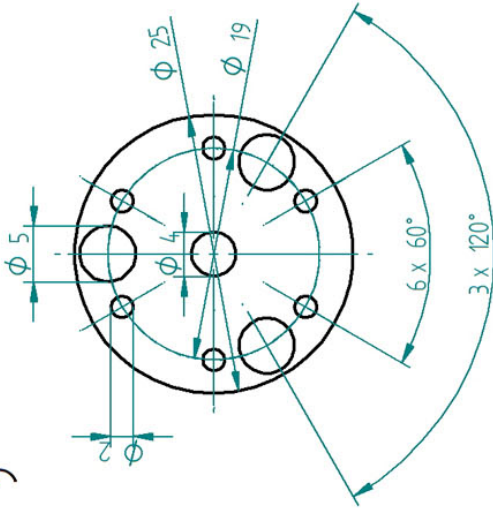


3 Stk.

DRAWN	NAME	DATE	SOLID EDGE <i>UGS - The PLM Company</i>	
	volker bauer	01/11/09		
	CHECKED			
	ENG APPR			
MGR APPR			Führungsstange	
UNLESS OTHERWISE SPECIFIED DIMENSIONS ARE IN MILLIMETERS ANGLES ±XX° 2 PL ±XXX 3 PL ±XXXX			SIZE	REV
			A4	
			FILE NAME: führungsstange.dft	
			SCALE: 2:1	WEIGHT: SHEET 1 OF 1



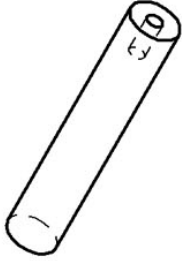
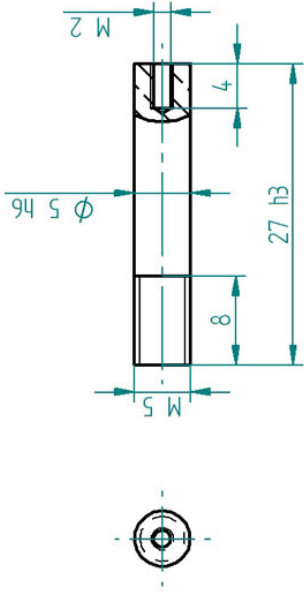
9



Material: FKM75 (Viton)

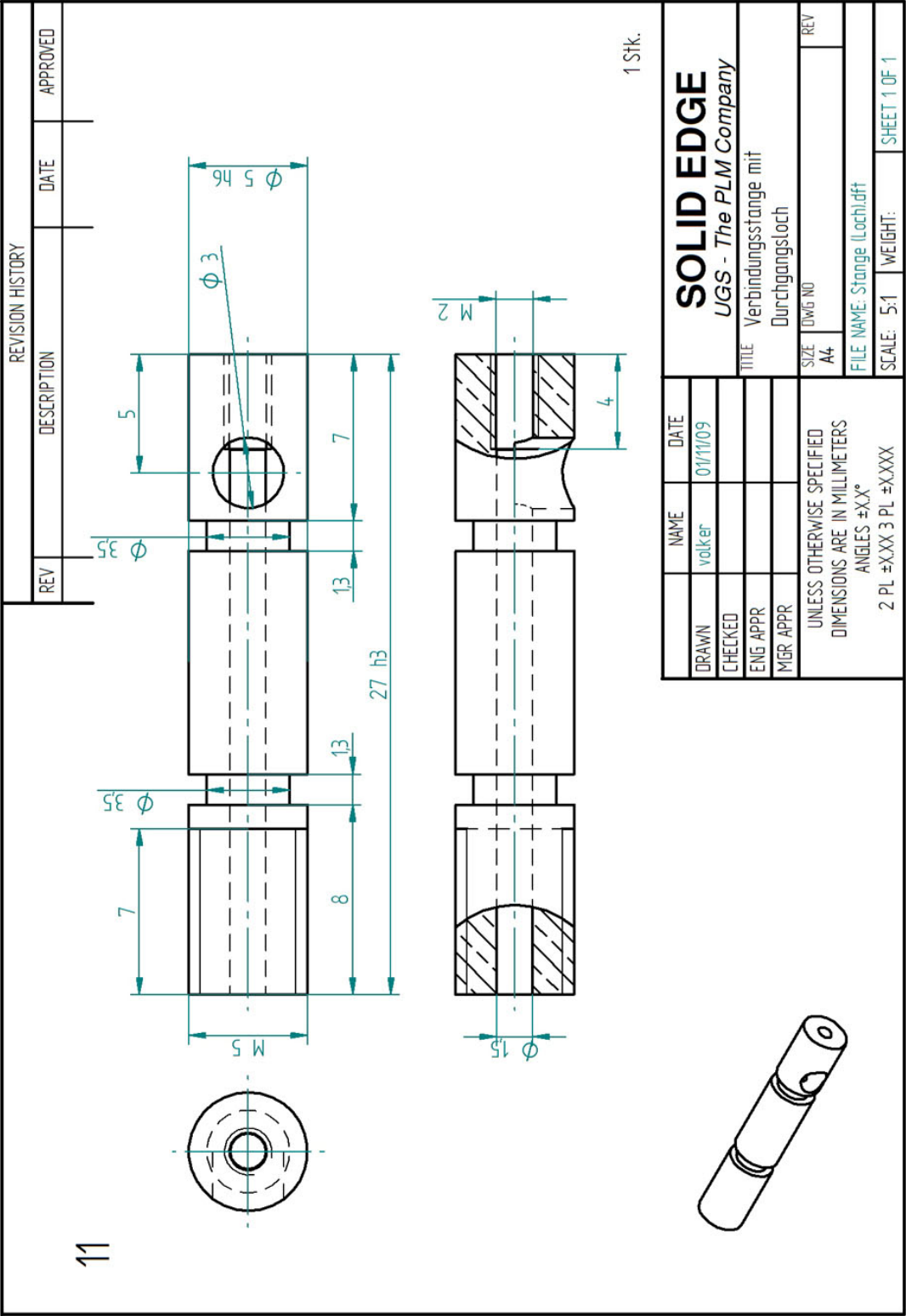
1 Stk.

DRAWN		NAME	DATE
CHECKED		valkerbauer	01/15/09
ENG APPR			
MGR APPR			
UNLESS OTHERWISE SPECIFIED DIMENSIONS ARE IN MILLIMETERS ANGLES ±XX° 2 PL ±XXX 3 PL ±XXXX			
SOLID EDGE		UGS - The PLM Company	
TITLE		Membrandichtung	
SIZE		DWG NO	REV
A4			
FILE NAME: fkm_dichtung_unverformt.dft			
SCALE: 2:1		WEIGHT:	SHEET 1 OF 1



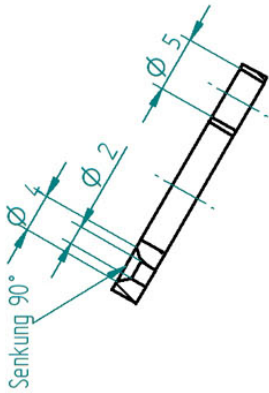
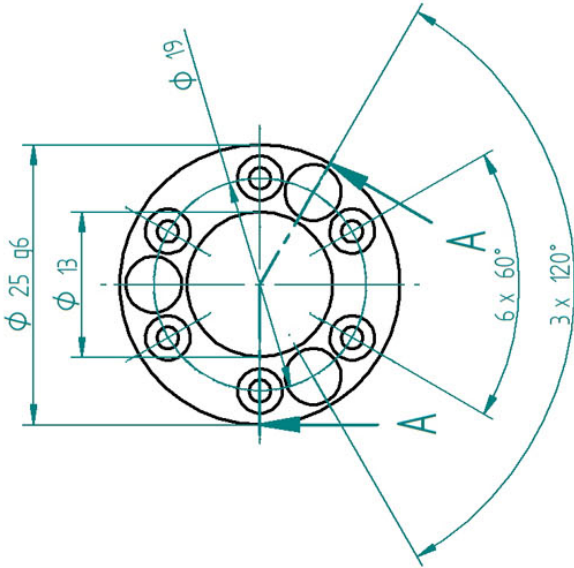
2 Stk.

DRAWN		NAME	DATE
CHECKED		valker	01/11/09
ENG APPR			
MGR APPR			
UNLESS OTHERWISE SPECIFIED DIMENSIONS ARE IN MILLIMETERS ANGLES ±XX° 2 PL ±XXX 3 PL ±XXXX			
TITLE		SIZE	REV
Verbindungsstange		A4	
UGS - The PLM Company		FILE NAME: Stangedft	
SOLID EDGE		SCALE: 2:1	WEIGHT: SHEET 1 OF 1

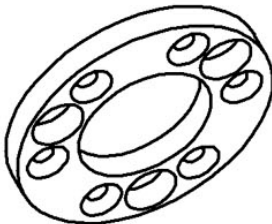


DRAWN	NAME	DATE	SOLID EDGE	
CHECKED	valker	01/11/09	UGS - The PLM Company	
ENG APPR			Verbindungsstange mit	
MGR APPR			Durchgangsloch	
UNLESS OTHERWISE SPECIFIED DIMENSIONS ARE IN MILLIMETERS ANGLES ±XX° 2 PL ±XXX 3 PL ±XXXX			SIZE	REV
			A4	
			FILE NAME: Stange (Loch).dft	
			SCALE: 5:1	SHEET 1 OF 1

13



Schnitt A-A



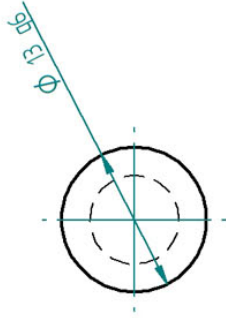
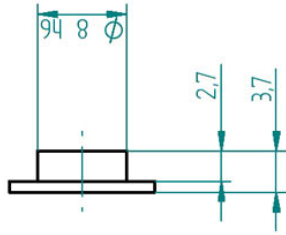
1 Stk.

REVISION HISTORY			
REV	DESCRIPTION	DATE	APPROVED

DRAWN	NAME	DATE
CHECKED	volker	01/11/09
ENG APPR		
MGR APPR		
UNLESS OTHERWISE SPECIFIED DIMENSIONS ARE IN MILLIMETERS ANGLES ±XX°		
2 PL ±XXX 3 PL ±XXXX		

SOLID EDGE UGS - The PLM Company	
TITLE Dichtungsring	
SIZE A4	REV
FILE NAME: dichtungsring_innendf	
SCALE: 2:1	WEIGHT: SHEET 1 OF 1

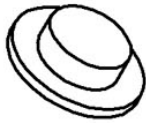
REVISION HISTORY			
REV	DESCRIPTION	DATE	APPROVED

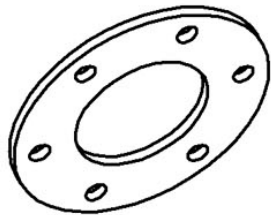
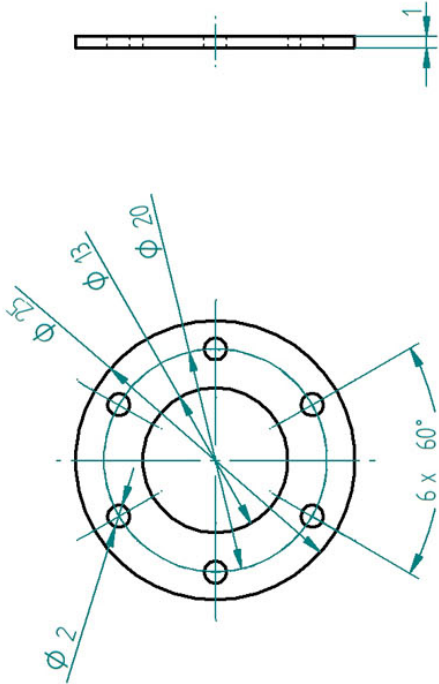


1 Stk.

DRAWN		NAME	DATE
CHECKED		volker	01/11/09
ENG APPR			
MGR APPR			
UNLESS OTHERWISE SPECIFIED DIMENSIONS ARE IN MILLIMETERS ANGLES ±XX° 2 PL ±XXX 3 PL ±XXXX			
TITLE		Macor-Scheibe	
SIZE		DWG NO	REV
A4			
FILE NAME: macor_plattchendf1			
SCALE: 2:1		WEIGHT:	SHEET 1 OF 1

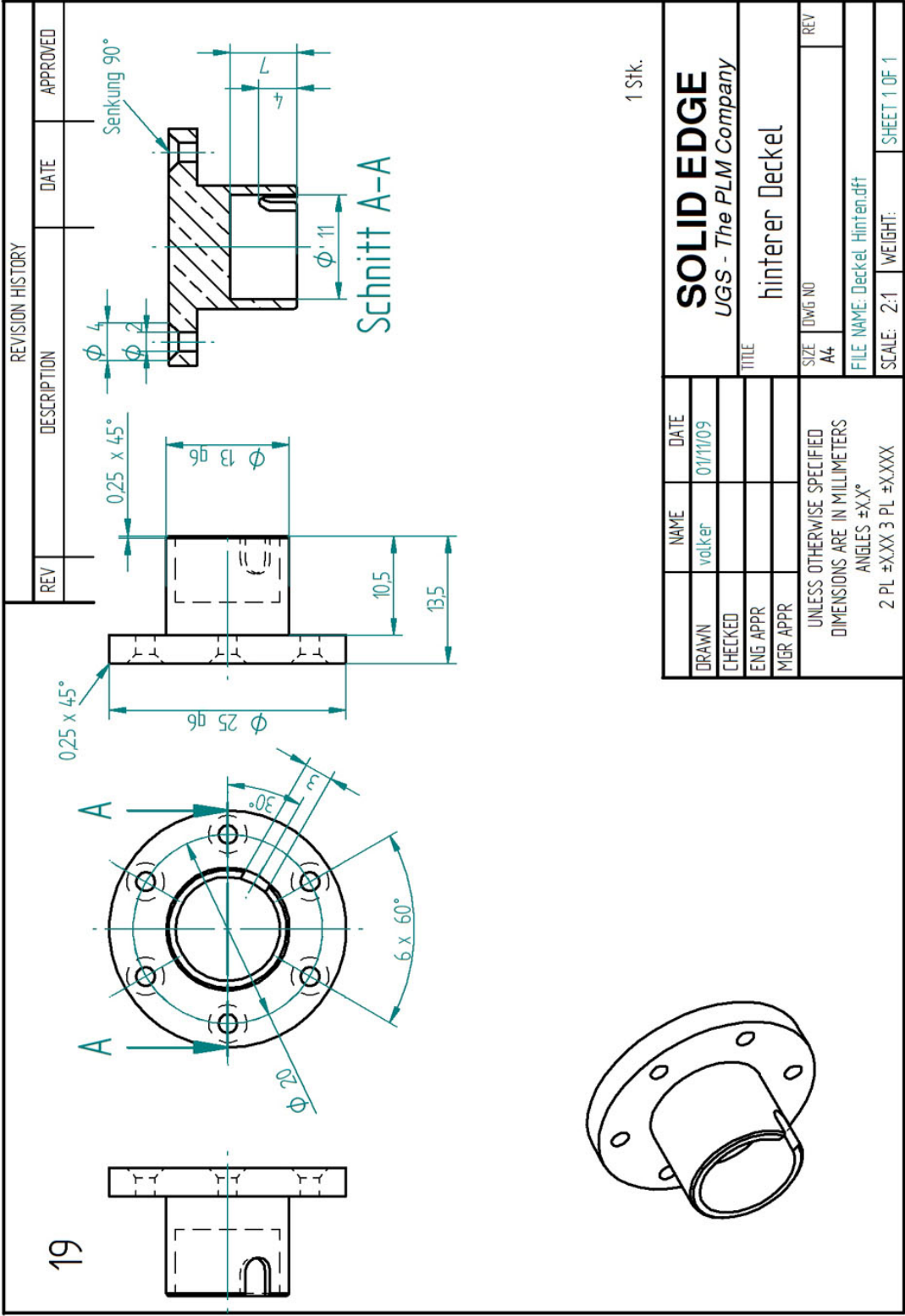
SOLID EDGE
UGS - The PLM Company





Material: FKM75 (Viton) 1 Stk.

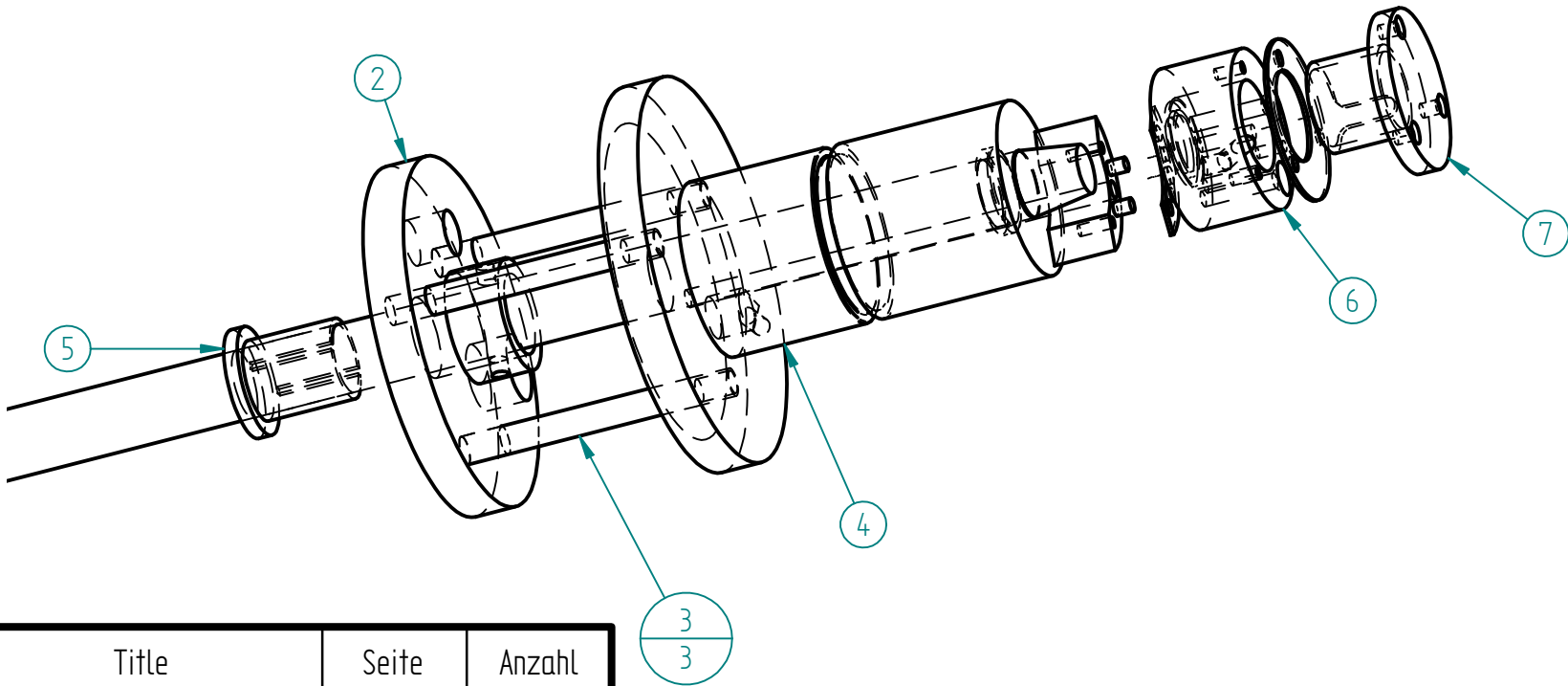
DRAWN		NAME	DATE
CHECKED		volker baue	01/15/09
ENG APPR			
MGR APPR			
UNLESS OTHERWISE SPECIFIED DIMENSIONS ARE IN MILLIMETERS ANGLES ±XX° 2 PL ±XXX 3 PL ±XXXX			
TITLE		SIZE DWG NO	
SOLID EDGE		A4	
UGS - The PLM Company		REV	
Flachdichtung		FILE NAME: fkm dichtung pzt.dft	
SCALE: 2:1		WEIGHT:	
		SHEET 1 OF 1	



Appendix B

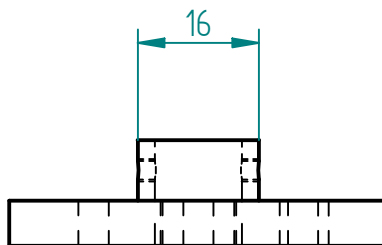
Engineering drawings Prototype 2

REVISION HISTORY			
REV	DESCRIPTION	DATE	APPROVED

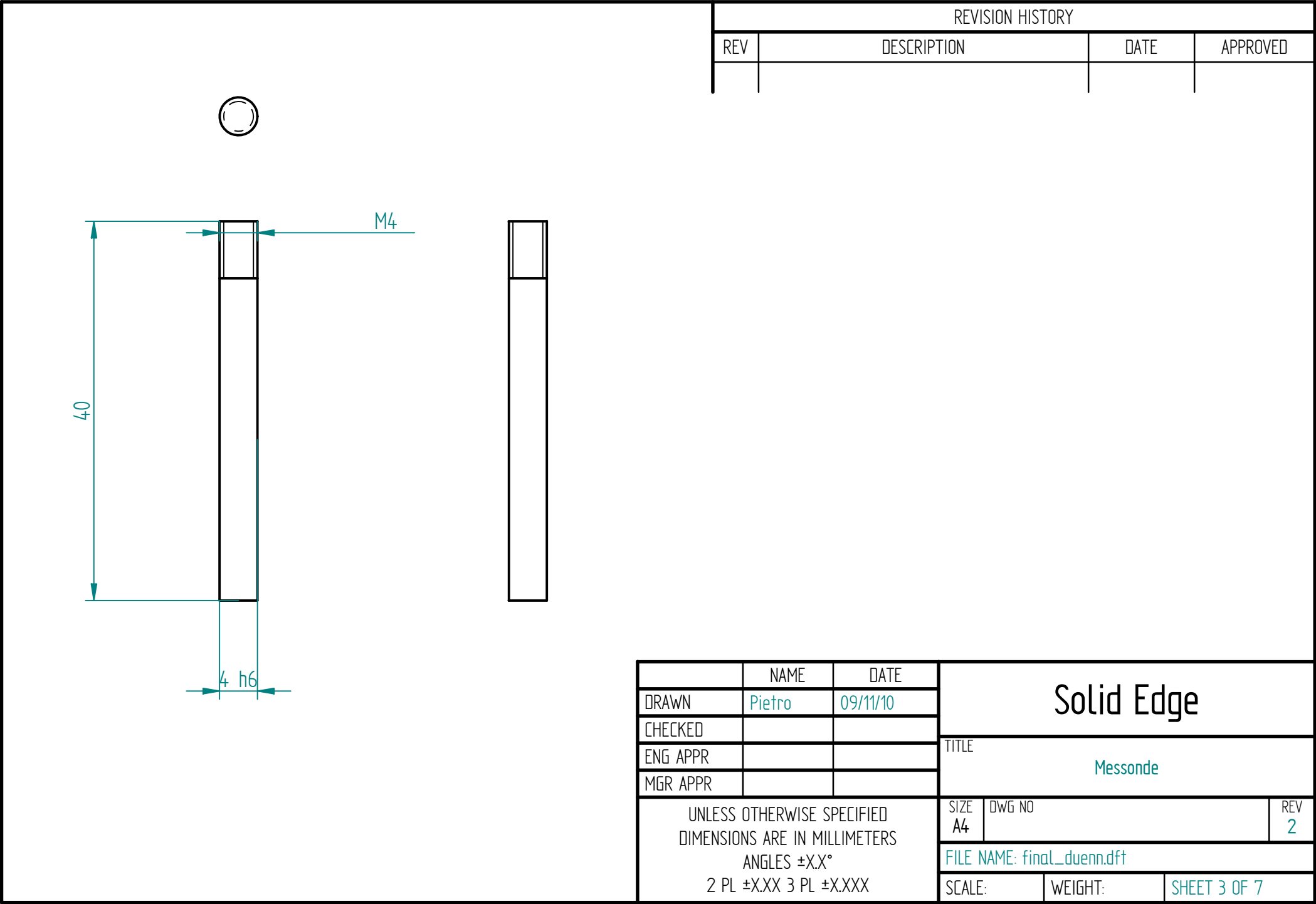


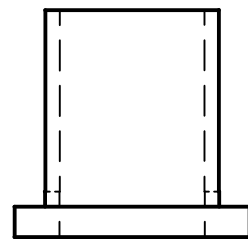
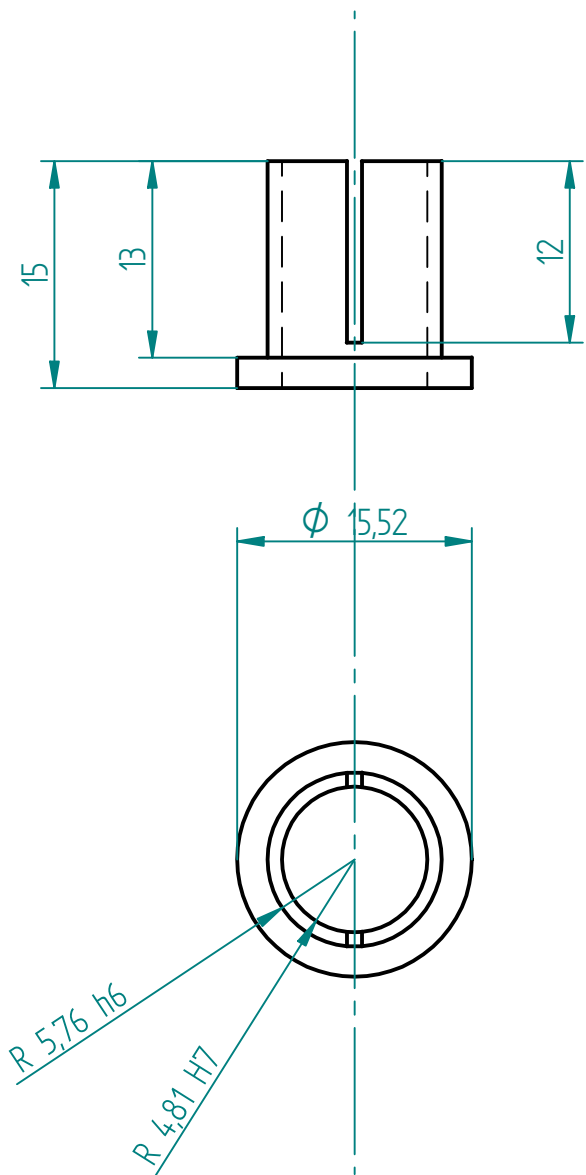
Title	Seite	Anzahl
vordere Scheibe	2	1
Führungsstange	3	3
große Hülse	4	1
geschlitzte Klemmhülse	5	1
Transducergehäuse	6	1
Transducerkopf	7	1

	NAME	DATE	Solid Edge		
DRAWN	Pietro	09/11/10			
CHECKED			TITLE		
ENG APPR					
MGR APPR			Messonde		
UNLESS OTHERWISE SPECIFIED DIMENSIONS ARE IN MILLIMETERS ANGLES ±X.X° 2 PL ±X.XX 3 PL ±X.XXX			SIZE A4	DWG NO	REV 2
			FILE NAME: final_duenn.dft		
			SCALE:	WEIGHT:	SHEET 1 OF 7



	NAME	DATE	Solid Edge		
DRAWN	Pietro	09/11/10			
CHECKED			TITLE		
ENG APPR					
MGR APPR			Messonde		
UNLESS OTHERWISE SPECIFIED DIMENSIONS ARE IN MILLIMETERS ANGLES $\pm X.X^\circ$ 2 PL $\pm X.XX$ 3 PL $\pm X.XXX$			SIZE A4	DWG NO	REV 2
			FILE NAME: final_duenn.dft		
			SCALE:	WEIGHT:	SHEET 2 OF 7



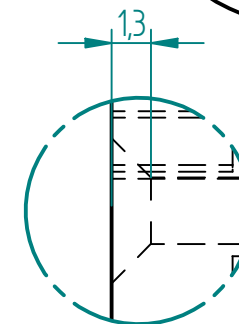
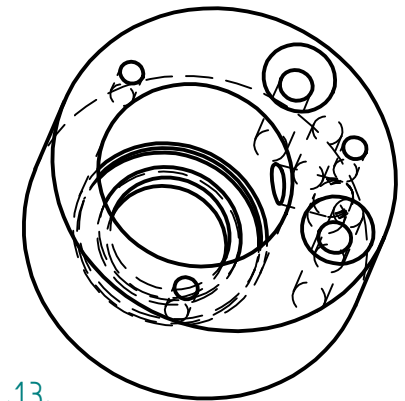
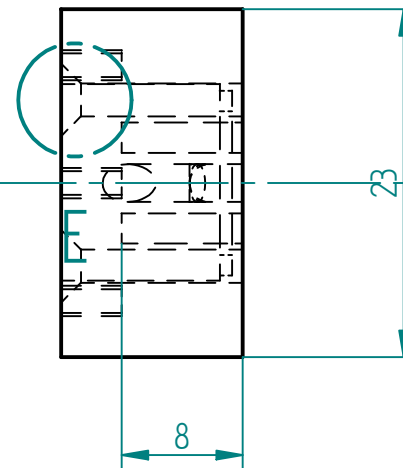
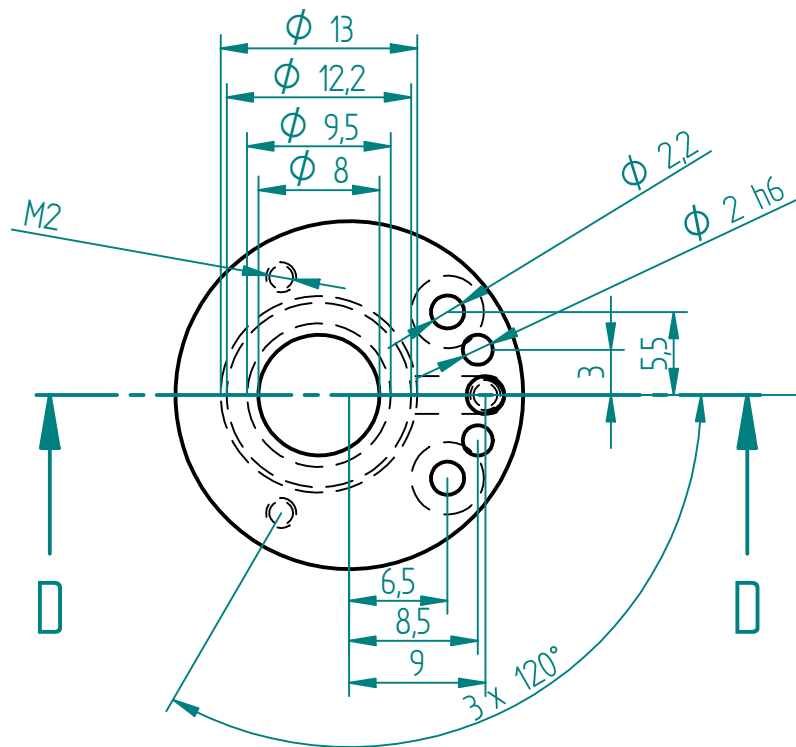


REVISION HISTORY			
REV	DESCRIPTION	DATE	APPROVED

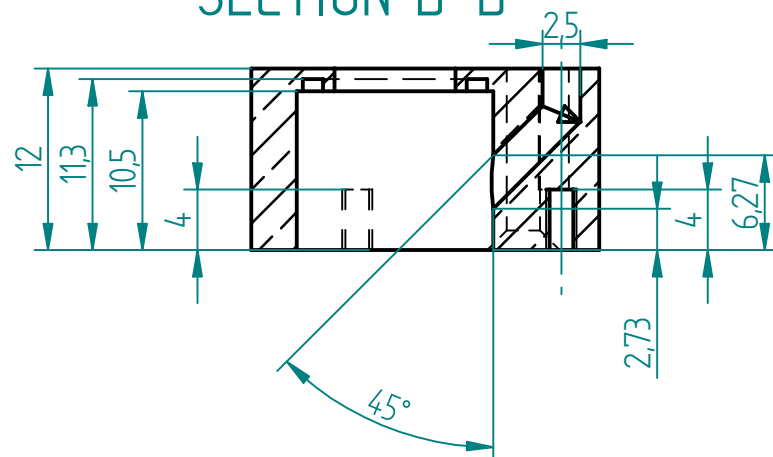
	NAME	DATE	Solid Edge	
DRAWN	Pietro	09/11/10		
CHECKED			Messonde	
ENG APPR				
MGR APPR				
UNLESS OTHERWISE SPECIFIED DIMENSIONS ARE IN MILLIMETERS ANGLES $\pm X.X^\circ$ 2 PL $\pm X.XX$ 3 PL $\pm X.XXX$			SIZE A4	DWG NO
			FILE NAME: final_duenn.dft	
			SCALE:	WEIGHT:
			SHEET 5 OF 7	

REVISION HISTORY

REV	DESCRIPTION	DATE	APPROVED

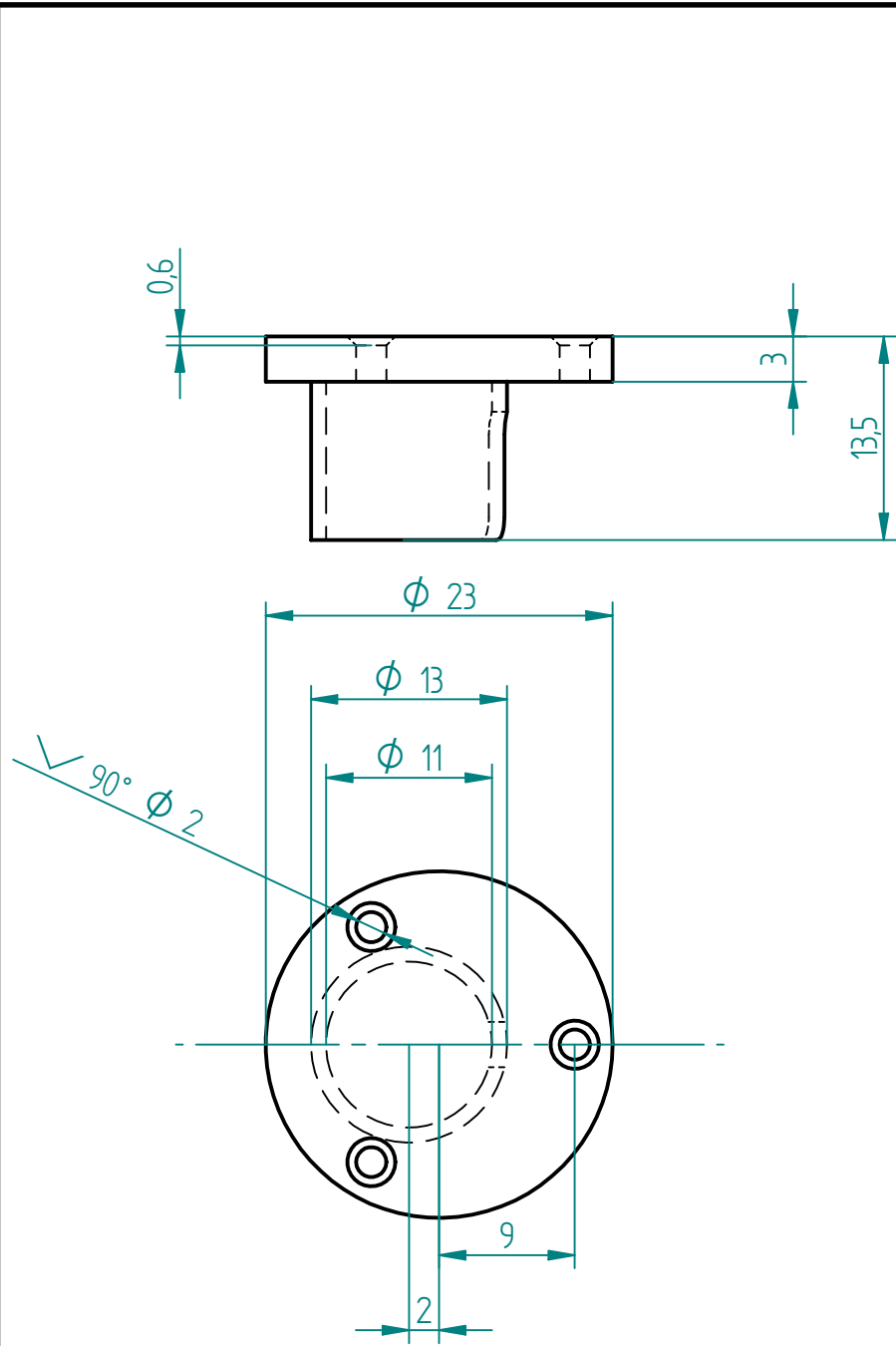


SECTION D-D

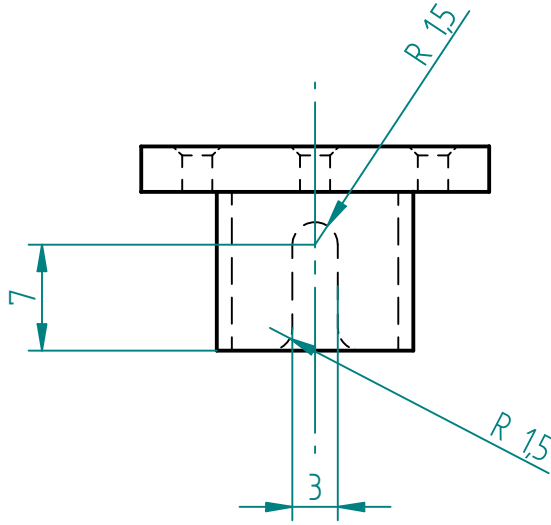


DETAIL E

	NAME	DATE	Solid Edge	
DRAWN	Pietro	09/11/10		
CHECKED			Messonde	
ENG APPR				
MGR APPR			<div> <div>SIZE</div> <div>A4</div> </div> <div> <div>DWG NO</div> <div> </div> </div> <div> <div>REV</div> <div>2</div> </div>	
UNLESS OTHERWISE SPECIFIED DIMENSIONS ARE IN MILLIMETERS ANGLES ±X.X° 2 PL ±X.XX 3 PL ±X.XXX			FILE NAME: final_duenn.dft	
			SCALE:	WEIGHT: SHEET 6 OF 7



REVISION HISTORY			
REV	DESCRIPTION	DATE	APPROVED

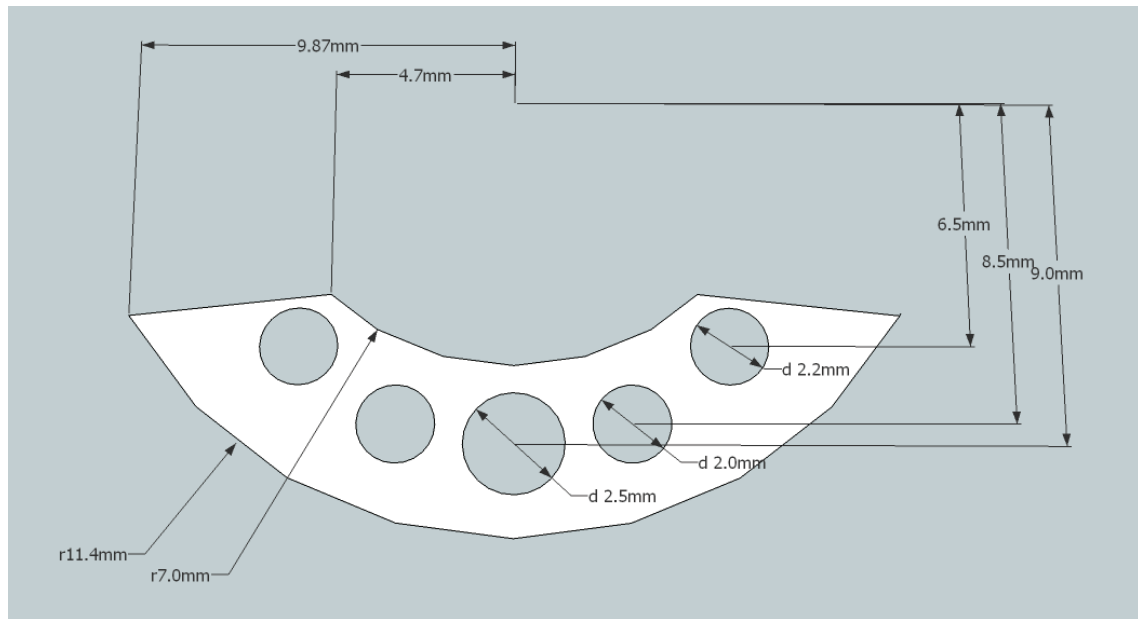


	NAME	DATE	Solid Edge		
DRAWN	Pietro	09/11/10			
CHECKED			Messonde		
ENG APPR					
MGR APPR					
UNLESS OTHERWISE SPECIFIED DIMENSIONS ARE IN MILLIMETERS ANGLES $\pm X.X^\circ$ 2 PL $\pm X.XX$ 3 PL $\pm X.XXX$			SIZE A4	DWG NO	REV 2
			FILE NAME: final_duenn.dft		
			SCALE:	WEIGHT:	SHEET 7 OF 7

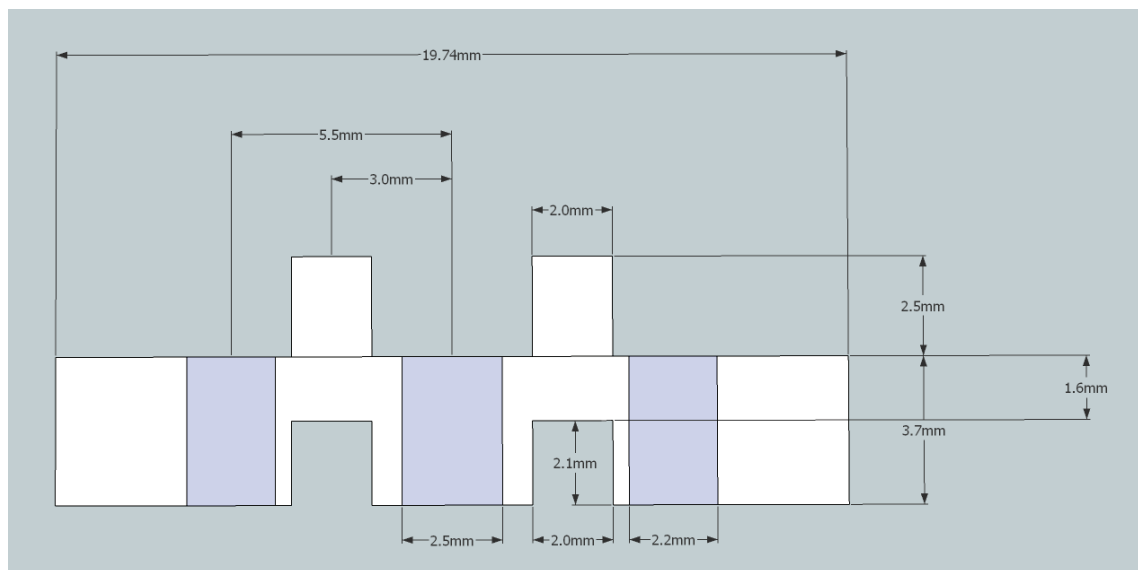
Appendix C

Design and dimensions of the extension for the transducer housing holder.

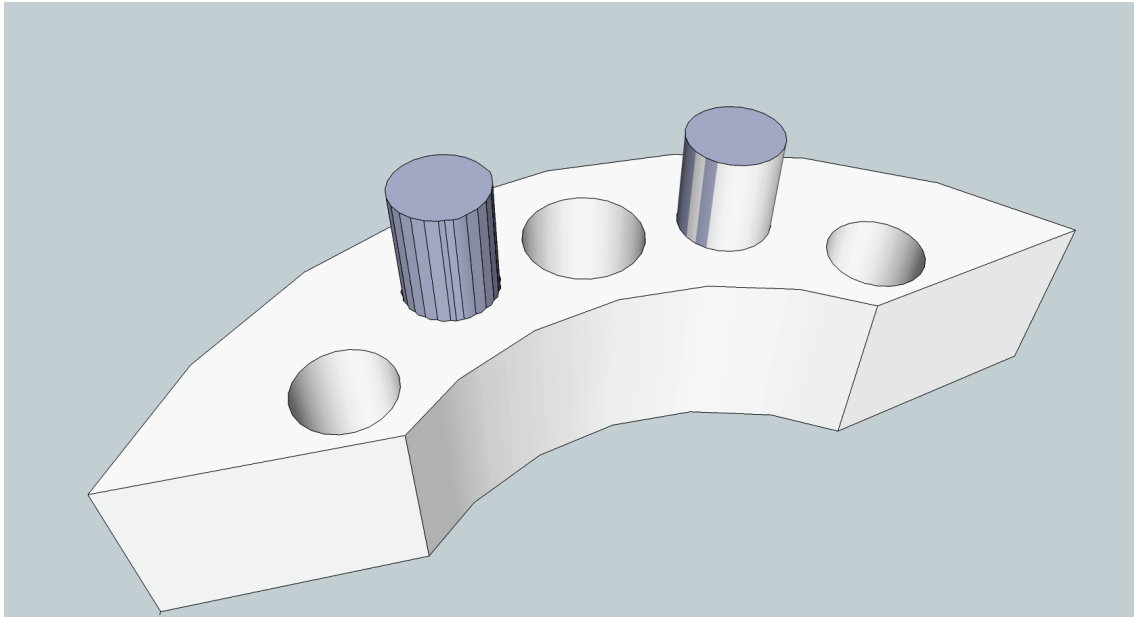
Extension top view:



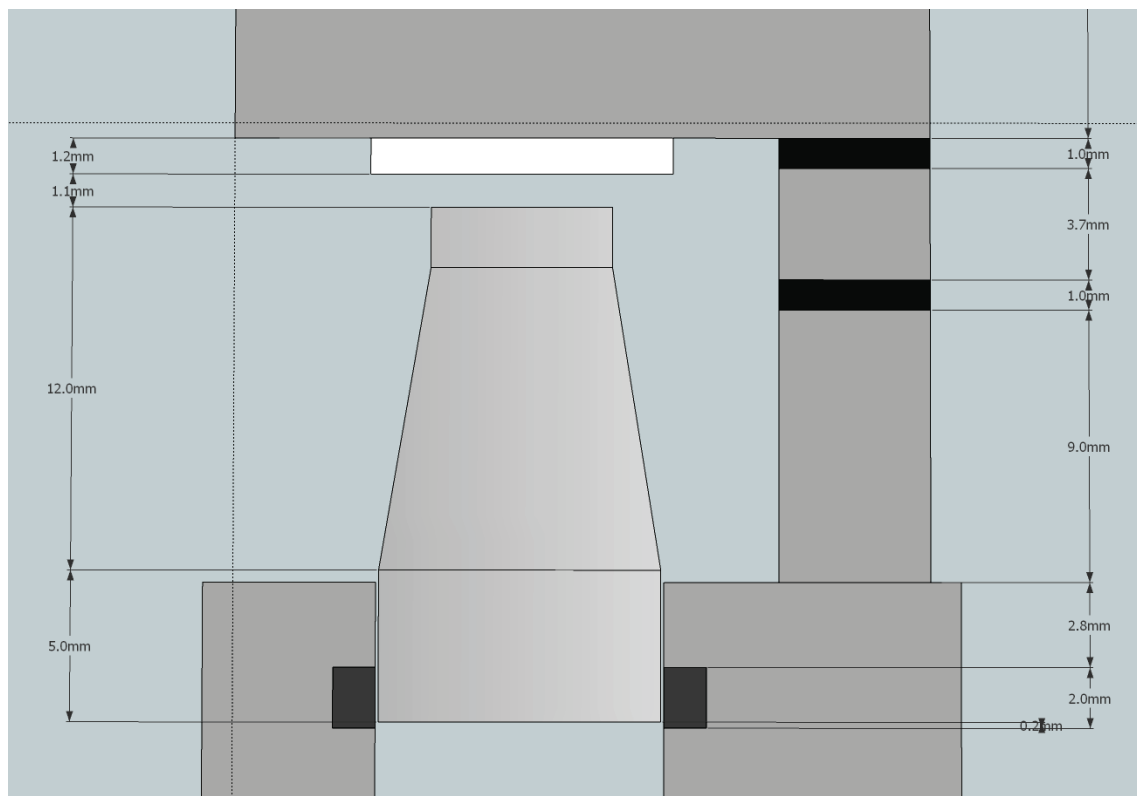
Extension side view:



3D Rendering of the extension:



Cross section of prototype 2 including the extension (resonator length: 1.1 mm):



Appendix D

Curriculum Vitae

DI Cosima Koch

Mostgasse 14/6

1040 Wien, Austria

eMail cosimakoch@gmail.com

Mobile +43-699-19675160

Date of birth: 7.9.1982; Vienna, Austria

Nationality: Austrian

Languages:	German	mother tongue
	English	fluent
	French	fluent
	Spanish	basic

EDUCATION

05/2010 – present	PhD candidate in Technical Chemistry Vienna University of Technology, Austria
10/2000 – 10/2009	Diplom-Ingenieur (M.Sc.) in Technical Physics Vienna University of Technology, Austria
09/2005 – 05/2006	Université de Montréal, Canada Exchange year with Transatlantic Science Student Exchange Programme
10/2004 – 07/2005	Universität Leipzig, Germany ERASMUS exchange year
1992 - 2000	Bundesgymnasium Gänserndorf, Austria Graduation with distinction

SCIENTIFIC WORK

05/2010 – present	Research Assistant (Projektassistentin) Institute of Chemical Technologies and Analytics, Vienna University of Technology, Austria
06/2014 – 08/2015	Local Organizing Committee ICAVS 8 International Congress on Advanced Vibrational Spectroscopy 8 (July 12-17, 2015), Vienna, Austria
10/2009 – 05/2010	Research Assistant (Projektassistentin) University of Natural Resources and Applied Life Sciences (BOKU), Institute for Physics and Material Science, Vienna, Austria
12/2006 – 06/2008	Assistant of the Co-chair ICU 2007 International Congress of Ultrasonics 2007 Vienna, Austria (ICU 2007 Vienna)
10/2007 – 01/2008	Undergraduate teaching assistant Vienna University of Technology, Institute of General Physics
01/2006 – 04/2006	Undergraduate research project Université de Montréal, Department of Physiology, GEPROM, Canada
10/2004 – 7/2005	Undergraduate research project Universität Leipzig, Department of Soft Matter Physics, Germany

AWARDS AND SCHOLARSHIPS

- 2013 The Analyst Poster Award (ICAVS 8)
2013 Best Oral Presentation Award (9. ASAC JunganalytikerInnen Forum, Vienna)
2011 FACSS (Federation of Analytical Chemistry and Spectroscopy Societies) Innovation Award
2011 Marietta Blau TU mobility grant (Vienna University of Technology)
2010 Participation & stay (CISM)
2009 R.W.B. Stephens students prize (ICU 2009)
2007 R.W.B. Stephens students prize "honourable mention" (ICU 2007)
2005 Joint Study scholarship (BMWK)
2005 TOP Scholarship for travelling (Lower Austria)
2004 ERASMUS scholarship
2003 TOP Scholarship (Lower Austria)

ADDITIONAL QUALIFICATIONS

- 10/2013 **Laser Safety Course**
Uvex Academy
02/2012 **Communication & project management course**
science2public, Vienna
07/2011 **ASCOS - Advanced Study Course on Optical Chemical Sensors**
University College Cork, Cork, Ireland
06/2010 **Advanced course on Ultrasound Standing Wave Action on Suspensions and Biosuspensions in Micro- and Macro Fluidic Devices at CISM**
International Centre for Mechanical Sciences, Udine, Italy
09/2008 **Summer School: Electronics for Physiologists**
Medical University of Vienna, Institute of Pharmacology
01 – 06/1998 **Academic Year in America (AYA)**
Burley High School, Idaho, USA

JOURNAL ARTICLES

- C. Koch, A.E. Posch, Ch. Herwig, B. Lendl: *Comparison of fiber optic and conduit attenuated total reflection (ATR) Fourier transform infrared (FT-IR) setup for in-line fermentation monitoring*. Applied Spectroscopy (major revisions under way).
- C. Koch, M. Brandstetter, P. Wechselberger, B. Lorantfy, S. Radel, Ch. Herwig, B. Lendl: *Ultrasound enhanced attenuated total reflection mid-infrared spectroscopy in-line probe – acquisition of cell spectra in a bioreactor*. Analytical Chemistry, 87 (2015), 2314-2320.
- M. Brandstetter, C. Koch, A. Genner, B. Lendl: *Measures for optimizing pulsed EC-QC laser spectroscopy of liquids and application to multi-analyte blood analysis*. Proceedings of SPIE 8993, Quantum Sensing and Nanophotonic Devices XI (2014), 89931U.
- B. Lorantfy, T. Renkecz, C. Koch, G. Horvai, B. Lendl, Ch. Herwig: *Identification of lipophilic bioproduct portfolio from bioreactor samples of extreme halophilic archaea with HPLC-MS/MS*. Analytical and Bioanalytical Chemistry, 406 (9-10) (2014), 2421-2432.
- C. Koch, A.E. Posch, H.C. Goicoechea, Ch. Herwig, B. Lendl: *Multi-analyte quantification in bioprocesses by Fourier-transform-infrared spectroscopy by partial least squares regression and multivariate curve resolution*. Analytica Chimica Acta, 807 (2014), 103-110.

M.R. Plata Torres, C. Koch, P. Wechselberger, Ch. Herwig, B. Lendl: *Determination of carbohydrates present in Saccharomyces cerevisiae using mid-infrared spectroscopy and partial least squares regression*. Analytical and Bioanalytical Chemistry, 405 (25) (2013), 8241-50.

C. Koch, M. Brandstetter, B. Lendl, S. Radel: *Ultrasonic manipulation of yeast cells in suspension for absorption spectroscopy with an immersible mid-infrared fiberoptic probe*. Ultrasound in Medicine and Biology, 39 (6) (2013), 1094-1101.

A.E. Posch, C. Koch, M. Helmel, M. Marchetti-Deschmann, K. Macfelda, B. Lendl, G. Allmaier, Ch. Herwig: *Combining Light Microscopy, Dielectric Spectroscopy, MALDI Intact Cell Mass Spectrometry, FTIR Spectromicroscopy and Multivariate Data Mining for Morphological and Physiological Bioprocess Characterization of Filamentous Organisms*. Fungal Genetics and Biology: 51 (2013), 1-11.

BOOK CHAPTER

S. Radel, C. Koch: *Ecological competence of yeast suspensions in acoustic filters*. p.119-160, Patient - Ultrasound Interaction, Ladislav Doležal and Christian Kollmann (eds.), 2010, Palacky University, ISBN: 978-80-244-2656-3

CONFERENCE CONTRIBUTIONS

Oral Presentations:

C. Koch, M.R. Plata Torres, S. Radel, B. Lorantfy, P. Wechselberger, Ch. Herwig, B. Lendl: *In-line spectroscopy of yeast cells during fermentation using an ultrasound enhanced ATR FT-IR fibre optic probe*. 9. ASAC JunganalytikerInnen Forum, Vienna, Austria, 2013

C. Koch, M.R. Plata Torres, S. Radel, B. Lendl: *Ultrasound enhanced ATR mid-IR fibre optic probe for spectroscopy of particles in suspension*. SciX 2012, Kansas City, MO, USA, 2012 (invited)

C. Koch, M. Brandstetter, S. Radel, B. Lendl: *Ultrasound enhanced ATR mid-IR fibre optic probe for spectroscopy of particles in suspension*. 2011 FACSS conference, Reno, NV, USA, 2011

C. Koch, G. Fritscher, L. Strobl, S. Radel, B. Lendl: *Ultrasonic enhanced mid-infrared spectroscopy for in-line monitoring of cell cultures*. ICU 2011 – International Congress on Ultrasonics, Gdansk, Poland, 2011

C. Koch, P. Palmesi, M. Brandstetter, S. Radel, M. Gröschl, B. Lendl: *Towards ultrasonic enhanced mid-IR fiber optic probes for in-line bioprocess monitoring*. EAA Euroregio 2010, Ljubljana, Slovenia, 2010

C. Koch, S. Radel, M. Gröschl, E. Benes: *Effect of ultrasonic plane wave fields on yeast cultures*. ICU 2009 - International Congress on Ultrasonics, Santiago, Chile, 2009

C. Koch, C. Brunner, A. Ehrlicher, and J. Käs: *Polimerization Forces in Cell-Motility*. 69th Annual Meeting of the Deutsche Physikalische Gesellschaft, Berlin, Germany, 2005

Poster Presentations:

C. Koch, H. Goicoechea, A. Posch, Ch. Herwig, B. Lendl: *ATR FT-IR in-line monitoring of precursor and product in a P. chrysogenum fermentation*. IRDG Christmas Meeting 2014, London, United Kingdom, 2014

C. Koch, M.R. Plata Torres, P. Wechselberger, M. Brandstetter, B. Lorantfy, S. Radel, Ch. Herwig, B. Lendl: *Spectroscopy of yeast cells during fermentation using an in-line ultrasound enhanced ATR FTIR fiber optic probe*. ICAVS 7, Kobe, Japan, 2013

M. Brandstetter, C. Koch, T. Sumalowitsch, A. Genner, V. Fuhrmann, A. Drolz, B. Lendl: *Development and application of a mid-infrared Quantum Cascade Laser based multi-analyte sensor for clinical blood analysis*. ICAVS 7, Kobe, Japan, 2013

C. Koch, B. Lorantfy, M.R. Plata Torres, M. Brandstetter, S. Radel, Ch. Herwig, B. Lendl: *Ultrasound enhanced ATR FTIR spectroscopy – acquiring spectra of cells inline during fermentation*. 200th IRDG Christmas Meeting 2012, London, United Kingdom, 2012

C. Koch, M. Brandstetter, P. Palmesi, S. Radel, B. Lendl: *Ultrasound enhanced fibre optic midIR spectroscopy*. IRDG Christmas Meeting 2010, London, United Kingdom, 2010

M. Brandstetter, C. Koch, B. Zachhuber, S. Radel, J. Schnöller, M. Gröschl, B. Lendl: *Ultrasonic particle manipulation for mid-infrared spectroscopy of suspensions*. CISM Advanced Course on Ultrasound Standing Wave Action on Suspensions and Biosuspensions in Micro- and Macro Fluidic Devices, Udine, Italien, 2010

C. Koch, S. Radel, M. Gröschl, E. Benes: *Bio-suspensions in the ultrasonic h-shape filter*. 7th USWNet Conference, Stockholm, Sweden, 2009

C. Koch, S. Radel, M. Gröschl, E. Benes: *Effect of the ultrasound field in an h-shape filter on yeast cultures*. Regional Biophysics Conference 2009, Linz, Austria, 2009

C. Koch, S. Radel, M. Gröschl, E. Benes: *Yeast cultures affected by ultrasonic plane wave fields*. ICU 2007 – International Congress on Ultrasonics, Vienna, Austria, 2007

C. Koch, S. Radel, M. Gröschl, E. Benes, W.T. Coakley: *Effects of ultrasonic plane wave fields on yeast cultures*. 3rd Congress of the Alps Adria Acoustics Association, Graz, Austria, 2007

Vienna, November 2015